1-2005

Assessment of the Effect of desalination Brine Waste on Marine Water Quality in Ruwais Area: A Numerical Modeling Application

Samer Jouda Al Nahhal

Follow this and additional works at: https://scholarworks.uaeu.ac.ae/all_theses

Part of the Environmental Sciences Commons

United Arab Emirates University

Faculty of Graduate Studies

ASSESSMENT OF THE EFFECT OF DESALINATION BRINE WASTE ON MARINE WATER QUALITY IN RUWAIS AREA: A NUMERICAL MODELING APPLICATION

By

Samer Jouda Al Nahhal

B.Sc. in Civil Engineering

Birzeit University, Palestine (2001)

A Thesis Submitted to the Faculty of Graduate Studies.

United Arab Emirates University in Partial Fulfillment

of the Requirement for the Degree of

Master of Environmental Science

January 2005

United Arab Emirates University

Faculty of Graduate Studies

Thesis Title: **Assessment of the Effect of Desalination Brine Waste on Marine Water Quality in Ruwais Area: A Numerical Modeling Application**

Author's Name: **Samer Jouda Al Nahhal**

Main Supervisor: **Dr. Walid Elshorbagy**
Civil and Environmental Engineering Department
Collage of Engineering, UAE University
Al Ain, UAE

Co-supervisor: **Dr. Waleed Hamza**
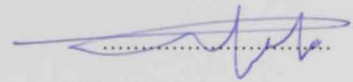Department of Biology
Collage of Science, UAE University
Al Ain, UAE

Assessment of the Effect of Desalination Brine Waste on Marine Water Quality in Ruwais Area: A Numerical Modeling Application

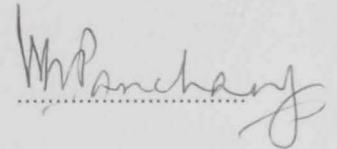A Thesis submitted to the Deanship of Graduate Studies
United Arab Emirates University

In Partial Fulfillment of the Requirements for
M.Sc. Degree in Water Resources

Examination Committee
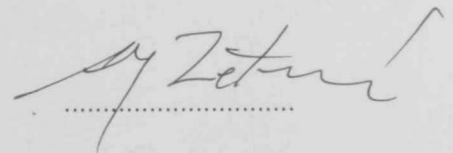
Dr. Walid Elshorbagy, Chair
Civil and Environmental Engineering Department
Collage of Engineering, UAE University
Al Ain, UAE

Prof. Vijay Panchang, External Examiner
Maritime Systems Engineering
Texas A&M University
Texas. USA

Prof. Abdulrazag Zekri, Internal Examiner
Chemical and Petroleum Engineering Department
Collage of Engineering, UAE University
Al Ain, UAE

United Arab Emirates University
January 2005

To All Whom I Love

ACKNOWLEDGEMENTS

ABSTRACT

This thesis aims to investigate the fate and transport of the effluents discharged from the desalination plant as well other facilities located in the Ruwais Industrial Complex (RIC) in the United Arab Emirates. These effluents are discharged into the Ruwais coastal marine waters. The effluents from the desalination plant are characterized by warm water with high salinity, whereas one other effluent is characterized by high nutrient loads. The characterization of the Ruwais environment and such effluents are addressed through comprehensive field surveys of the Ruwais costal water over one full year.

In order to investigate the impacts of such effluents on the coastal marine water quality, a coupled physical-biochemical model is employed to study the hydrodynamics and the water quality of the Ruwais coastal water. Hydrodynamic simulation for the entire basin of the Arabian Gulf is developed as regional model, and the mean currents and the circulation phenomenon in the Gulf is described. Subsequently, a local model for the Ruwais coastal water is nested inside the regional model area with three open boundaries across the Gulf basin, to investigate the mean currents of the coastal area in addition to the spatial and temporal variation of temperature and salinity.

To investigate the quality of the Ruwais coastal waters, the water quality model "EUTROP" is used. This model takes into consideration several water quality compartments, i.e., phytoplankton, zooplankton, particulate organic matter, dissolved organic carbon, phosphate, ammonium, nitrite, nitrate, dissolved oxygen, and chemical oxygen demand. The investigation of water quality covers up to 4 future years and employs two different boundary conditions. The study evaluates the present conditions and the future conditions, where the expansion of existing facilities in the Ruwais area is considered.

It is found that the effects of the effluents in the currents conditions is limited and restricted to the outfall area. It is characterized by slight increase in the temperature and salinity without major problems related to the water quality. Moreover, the influence of the future expansion in connection with increase in temperature and salinity extends up to 10 km offshore without major impacts related to water quality beyond that limit.

TABLE OF CONTENTS

LIST OF TABLES

LIST OF FIGURES

ABBREVIATIONS

20Q-All	Expansion scenario for all facilities by 20 times
20Q-Desal	Expansion scenario for the desalination plant only by 20 times
BC	Boundary Condition
COD	Chemical Oxygen Demand
CTD	Salinity, Temperature, and Density
DO	Dissolved Oxygen
DOC	Dissolved Organic Carbon
HNLC	High Nutrients and Low Chlorophyll/Carbon
IC	Initial Condition
MED	Multi-Effect Desalination
MSF	Multi-Stage Desalination
NH_4	Ammonium concentration
NO_2	Nitrite concentration
NO_3	Nitrate concentration
P	Phytoplankton biomass
PO_4	Phosphate concentration
POC	Particulate Organic Carbon
Q-Base	Base scenario with the original outfalls from the facilities
RIC	Ruwais Industrial Complex
RO	Reverse Osmoses
SQN	Intracellular nitrogen quota of phytoplankton
SQP	Intracellular phosphorous quota of phytoplankton
St. 1	First observation station near to the discharging area

CHAPTER ONE

INTRODUCTION

The marine environment is a primary resource in achieving the social, economic, and strategic objectives of the Arabian Gulf region. The discovery of oil in the region increased the importance of the Gulf due to the dominant economic role of oil all around the world. The fishery industry also represents great social significance for the Gulf people due to the wide diversity of the existing fish species. Nowadays, due to the scarcity of freshwater resources in such arid areas, the Gulf is considered as a main source of water for the desalination plants scattered around its coast that cater to the needs of most of the population and to the industries in the Gulf countries.

The United Arab Emirates (UAE) is a federal country consisting of seven Emirates located along the western coast of the Arabian Gulf. These Emirates are Abu Dhabi, Dubai, Sharjah, Ajman, Um Al-Quwain, Ra's Al-Khaymah and Al-Fujerah. The country has 700 kilometers of coast line, 100 kilometers of which are on the Gulf of Oman and the rest is on the Arabian Gulf. UAE is bounded on the east by the Gulf of Oman and Oman, on the south and west by Saudi Arabia, and on the north by Qatar and the Arabian Gulf. Most of the population in the UAE lives in a few coastal towns or inland oases. The majority of the country's territories are sandy. The climate of the UAE is characterized by extremely hot and humid weather in the summer with average temperature exceeding 40° C, while the winter is mild; the average annual rainfall is very low (78- 152 mm).

The massive development of the UAE and its demographic growth is associated with evolution of desalination technology. Desalinated water has the highest share in the water budget of the country, where the desalination plants supply water for domestic use in addition to industrial and agricultural purposes. The desalination plants supply 98% of the freshwater demand from either seawater or brackish water; for instance, the population of Abu Dhabi, the capital of the UAE, has increased to 2,262,309 in 1997 compared to 200,000 in the early sixties (Sommariva and Syambabu, 2001). In spite of the natural water resources scarcity in the UAE, Abu Dhabi Emirate is considered to have one of the highest per capita water consumptions in the world due to the high standard of life style (Sommariva and Syambabu, 2001). According to Abu Dhabi Water Authority reports, the consumption

per capita exceeds 500 l/d. The supplying of the freshwater from the desalination plants is not limited for the domestic use, but it also extends to the agricultural sector, where the enormous desert greening programmes undertaken by the UAE government increased the agricultural demand of freshwater considerably. In Abu Dhabi Emirate, over 120 million trees have been planted in recent years (Sommariva and Syambabu, 2001); which prompted the government to implement desalination plant projects in a fast track to meet the urgent needs of freshwater.

The robust growth of coastal communities in the UAE is putting a massive stress on the costal marine environment, since all the 7 Emirates of the country along with main cities, ports and most industrial zones are located at the coast.

Ruwais Industrial Complex (RIC) which is the subject of the current study is one of the most important and economical coastal zones as it contains the biggest oil refinery in the UAE and it is considered as the main port for exporting the oil and petrochemical products to the rest of the world. A number of other facilities are also along the coast of Ruwais. This includes a petrochemical factory, a power plant, a fertilization factory, and a gas production plant. A small township is attached to the RIC with amenities and municipal facilities. In order to cater to the needs of the town and these industries, a desalination plant was established.

All of these industrial facilities in addition to the desalination plant discharge their effluents after some treatment to the marine water. These effluents may contain some chemicals, warm waters and a high concentration of brine due to desalination processes. Continuous dumping of such effluents may threaten the ecosystem of the area, and may have many implications on the marine water quality in general and on fauna and flora and eventually the marine life in particular.

Ecologically, marine life in Ruwais coastal area has a wide diversity of marine habitats; i.e. scattered colonies of mangrove in the north along the coast of Sir Bani Yas Island, salt marches in the east and spots of coral reef in the west. This diversified environment is considered as a great wealth for the UAE and the conservation of such resources is of inevitable necessity.

In the present study, a three-dimensional hydrodynamic model is employed to investigate the hydrodynamic conditions of the Ruwais marine waters, and to investigate the fate and transport of the brine discharged from the desalination plant and the warm water released from other facilities. In order to evaluate the brine and the warmer water effects on the marine fauna and flora at the current situation, and for

long term effects, a biochemical three-dimensional model coupled with the hydrodynamic model will be used to simulate the biological and chemical dynamics of the Ruwais coastal water.

1.1 Problem Statement

The desalination plant and cooling lines for other industrial setups in the Ruwais Industrial Complex are generating significant amount of brine and worm waters. Moreover, the effluents from the other facilities have different types and concentrations of chemicals and are also dumped in the coastal water. Continuous discharge of such wastes into the marine environment should have considerable threat to the prevailing balance of the ecosystem, particularly for the protected areas such as Sir Bani Yas Island in the north.

1.2 Objectives

The overall objectives of this thesis can be summarized in the following points:

1. To investigate the fate of the brine water released from the desalination plant located in Ruwais area and to determine the impact of future extensions of these plants on marine environment.

2. To estimate the influence of releasing warmer waters disposed from the desalination plant and the nutrient loads from the other industrial facilities located in the area upon the marine water quality of the Ruwais coast in general and on Sir Bani Yas Island in particular

3. To understand consequent implications of the disposed brine and warmer waters on microbiological community using a system of hydrodynamic and water quality models and thereby predicts the probable consequence on future coastal ecology.

1.3 Study Area

The objective of the study as mentioned before is to investigate the fate transport of brine and warm water on Ruwais coastal marine environment. In order to achieve this goal, the regional modeling for the entire gulf area is performed then a local model for the Ruwais area is nested from the regional gulf. The following section describes the

environment of the Arabian Gulf as well the Ruwais area. A more detailed description of the water quality and ecological conditions is further presented in Chapter 4.

1.4 Physical Description of the Arabian Gulf

As the modeling work of Ruwais coastal area is based and nested from the Arabian Gulf, this section briefly describes the physical environment of the Arabian Gulf as well the Ruwais area.

The Arabian Gulf is considered as one of the most important water bodies in the world due to its strategic location. It overlooks many countries including United Arab Emirates, Qatar, Bahrain, Saudi Arabia, Kuwait, Iraq, Iran and Oman. These eight states sit atop the largest hydrocarbon reservoirs on earth, with about 76 billion metric tons of recoverable oil distributed over the gulf. The natural gas reservation is about 32.4 trillion cubic meters (Reynolds, 1993).

Other than the significance of the Arabian Gulf as the main way to export the oil and gas production to the world, it has a special significance for all Arabian Gulf countries as it is considered as the main source of the distilled water for these counties, due to lack of the rainfall and other water resources in the area.

Bathymetry

The Arabian Gulf is located between latitudes 24° N and 30° N and longitudes 48° E and 57°E (Fig. 1.1). It is a semi-enclosed sea, stretches 1,000 kilometers from the Shatt Al-Arab waterway in the southern Iraq to the Strait of Hormuz, and varies in width from 75 to 350 kilometers. It is bordered by the Arab Peninsula in the south (United Arab Emirates, Qatar, Saudi Arabia, and Kuwait), by Iraq in the north, and by Iran on the east. The gulf extends over an area of about 239,000 km² with an average depth of about 36 meters. The maximum depth is about 100 m along its axis, and the average volume is about 8630 km³ (Reynolds, 1993).

The Gulf has a northwest-southeast axis. It connects with the Gulf of Oman and the Arabian Sea from the east by a waterway called Strait of Hormuz. The strait touches Iran in the north and Oman in the south. Its length is about 280 km, and the width is only 56 km at its smallest level, while the average depth is about 100 m. The Strait of Hormuz has a great strategic importance, as it is the only sea route through which oil from Kuwait, Iraq, Iran, Saudi Arabia, Bahrain, Qatar, as well as most of

United Arab Emirates can be transported. From hydrological point of view, it is a unique path for the water exchange between the Arabian Gulf and the Gulf of Oman. This process keeps the salinity level of the gulf almost constant over the years. This phenomenon was studied by several scientists, among which Hughes and Hunter (1979) and Hunter (1983) who estimated the residence time of the Arabian Gulf basin to be 2 to 5 years, while John and Olson (1998) proved by their measurements that the residence time ranges between 350 to 500 days. The complex circulation pattern prevailing in the Gulf (to be discussed later) makes the calculation of the residence time difficult and explains the large discrepancy in its estimation by different studies.

The Arabian Gulf bathymetry is characterized by an increasing depth from south to north. A shallower shelf extends in front of United Arab Emirates coast; where the average depth is about (20 m). The depth increases toward the Iranian coast where the maximum depth there is about (80 m).

Rivers

Most of the river discharges into the Arabian Gulf concentrate at the northern part; primarily from Iraq and Iran. Shatt Al-Arab is considered as a confluence of three major rivers: Tigris, Euphrates and Karun. The annual average flow of Tigris and Euphrates is 708 $m^3.s^{-1}$, and the Karun outflow is 748 $m^3.s^{-1}$. Ninety percent of the Tigris and Euphrates rivers' flow is lost in evaporation and agricultural activities. Hence, the main discharge into the Gulf comes from Karun River. Some recent investigations estimated the outfall into the Shatt Al-Arab approximetly 1000 $m\ y^{-1}$. Other major rivers discharge into the Arabian Gulf are; the Hendijan (203 $m^3.s^{-1}$), the Hilleh (444 $m^3.s^{-1}$) and the Mand (1387 $m^3.s^{-1}$). The sum of these averages amounts to an annual runoff of 110 km^3y^{-1} (Britannica.com, 2001).

Climate

The climate components are considered the main driving forces in the hydrodynamic processes. The gulf region and the Arabian Peninsula are known to be one of the hottest areas in the world (ROPME, 1999). The main reason of the dryness of the area is due to the coastal mountain series that separating the Arab Peninsula from the sea. The eastern zones of the gulf are an exception to these conditions, where they are affected by the Indian Ocean monsoon causing some sparse rainfalls.
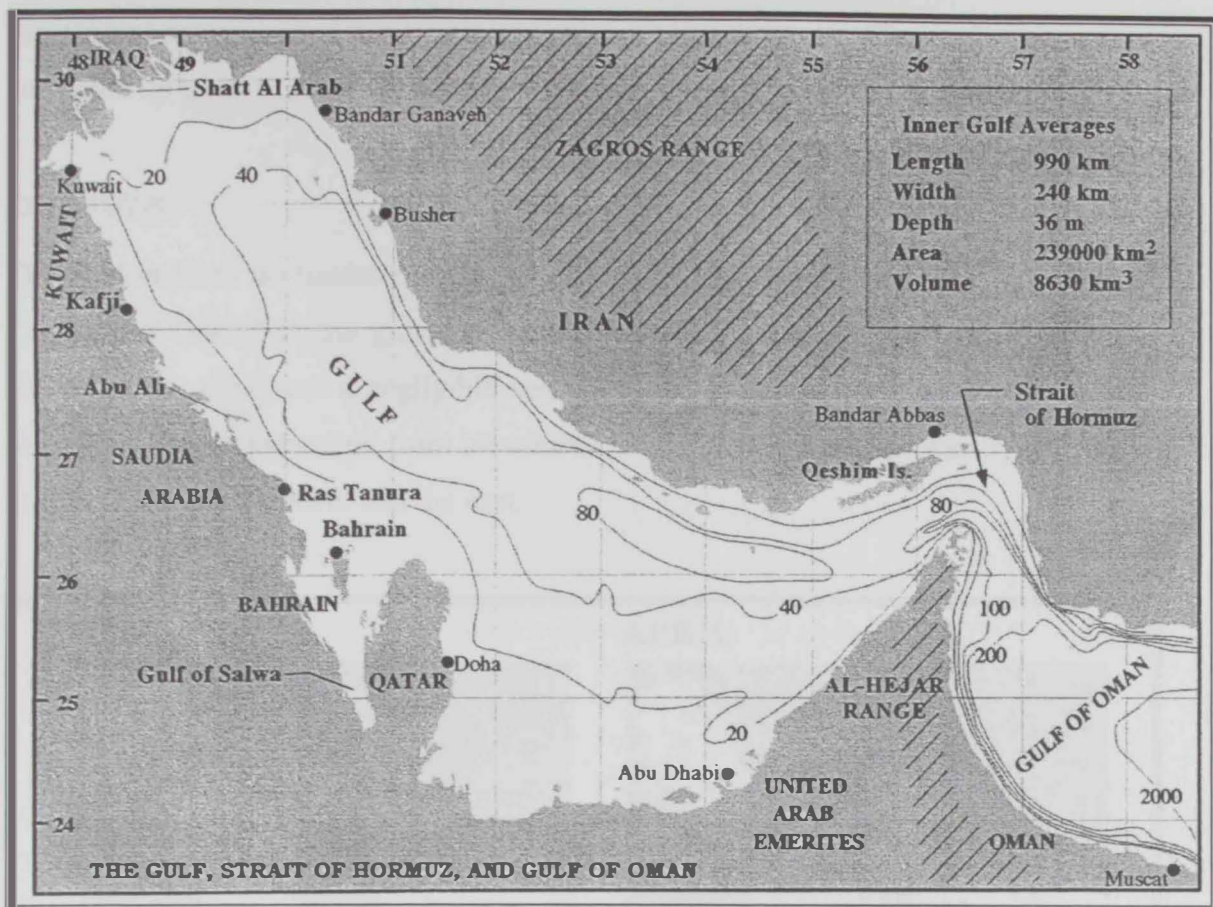
Figure 1.1: Topography and bathymetry of the Arabian Gulf, Strait of Hormuz and Gulf of Oman

Wind

The winds have a great influence on mixing and circulation of the Arabian Gulf. As the Gulf region is located between latitude 24- 30° N, this zone is classified as north-temperate tropical margin. Most of the world's deserts lie in this area. The Gulf is situated between the tropical trade-wind circulation and the synoptic weather system of mid-latitudes, where the sinking dry air produces a clear skies and arid conditions (Perrone, 1979).

The "Shamal" winds blow from the northwest during the year. They have a clear effect at the gulf area. In summer it is occasionally calm and rarely becomes strong (Murty and El-Sabh, 1984); while in winter, it abruptly blows with high speed reaching up to 10 m.s^{-1} once or twice a year. They are accompanied by strong winds and produce the highest waves of the season (Fig. 1.2).

The Arabian Peninsula coast line is exposed to strong sea breeze. During the day time, the intense heating of the land relative to the water leads the air to rise up, so the sea breeze blows toward the beach; while during the night, when the land cools,

the process reverses; and the land breeze blows toward the sea. The sea breeze speed can reach up to 10 m.s⁻¹, while the land breeze does not exceed 2 m.s⁻¹.

Precipitation

The Arabian Gulf is characterized by low rainfall and is categorized as an arid region. The annual rainfall in the gulf area varies between 78 mm and 152 mm (ROPME, 1999), which represents a negligible amount in the freshwater budget of the area. In the winter season extending from November to March, the rainfall intensity generally increases toward the north and the east.
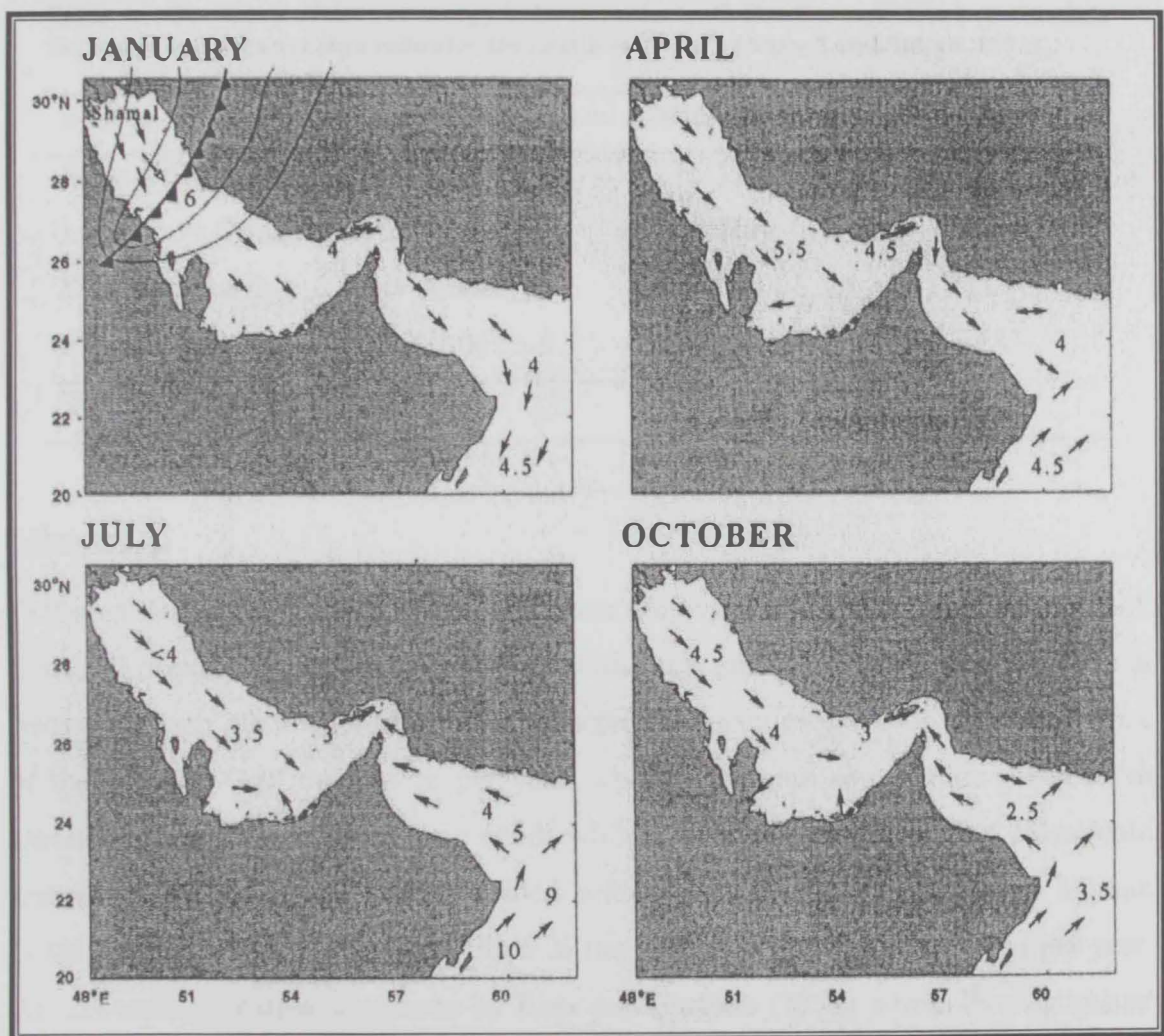
Figure 1.2: Typical wind pattern in the Gulf region all around the year. The arrows and the numbers indicate the direction and the speed of the winds respectively. The Shamal winds pattern is represented for the month of January (Reynolds, 1993).

Radiation

The intense evaporation over the Arabian Gulf surface leads to highly saline water in the basin. Increasing the salinity of the Gulf causes the surface water to be denser hence to sink in the bottom of the gulf, and move toward the Strait of Hormuz to exit from the bottom. Less saline water enters from the Arabian Sea to the Gulf from the top of Strait of Hormuz to compensate for the evaporated and the exited part of the Gulf water.

The annual net heat loss over the entire Gulf is about 21 $W.m^{-3}$ (Table 1.1) (Ahmed and Sultan, 1991).

Table 1.1: Summary of the net energy balance in the Gulf. Positive indicates heat flux into the water and negative sign indicates the heat loss ($W.m^{-3}$) (Ahmed and Sultan, 1991).

Source	Max/Month	Min/Month	Mean
Solar radiation	275/ June	136/ December	212
Long wave (heat)	-92/ January	-42/ May	-66
Sensible heat flux	-30/ January	42/ June	1
Evaporative	-299/ July	-85/ February	-168
Total			-21

Evaporation

Different studies were carried out to estimate the evaporation from the Arabian Gulf. Some of these studies were in harmony with each other and some of them were at odds with each other. Privett (1959) estimated the mean evaporation in open surface of the Arabian Gulf by 1.44 m per year, where maximum evaporation occurred in December as a result of the strong winds while the minimum was in May. Hastenrath and Lamb (1979) estimation coincided with Privett's trend. Meshal and Hassan (1986) estimated the mean evaporation in the coast of the Gulf around 2 m per year. An extreme estimation was done by Ross and Stoffers (1978) where they estimated the evaporation as 5 m per year.

Salinity and temperature

Many studies were conducted to estimate the salinity and the temperature of the Arabian Gulf. Emery (1956) and Dryssen (1985) made some efforts in this field, as

Emery studied the summer time and Dryssen investigated the winter time. More comprehensive study was achieved later by Reynolds (1993). Reynolds utilized the data from NOAA vessel Mt Mitchel to carry out his study. These data were acquired using several types of measurements such as, CTD measurements, current meter mooring, buoy tracking and observation of metrological and oceanographic variables. The period of the study was 4 months, extended from the end of winter to the early summer in year 1992. The results for salinity and temperature for both summer and winter are presented in Figure 1.3. A recent study (Elshorbagy *et al.*, 2004a) provided the missing salinity and temperature data in the southern shelf of the Arabian Gulf.

The temperature maps show that the temperature of the northern parts of the Arabian Gulf is usually cooler than the southern parts in both summer and winter. The average temperature in summer reaches up to 35° C and decreases in the winter up to 15°C. Through the Strait of Hormuz, warmer waters enter to the Gulf during the winter season to compensate the evaporated water and to preserve the energy balance as mentioned before, which keeps the temperature of the strait almost unchanged.

a: summer time   b: winter time
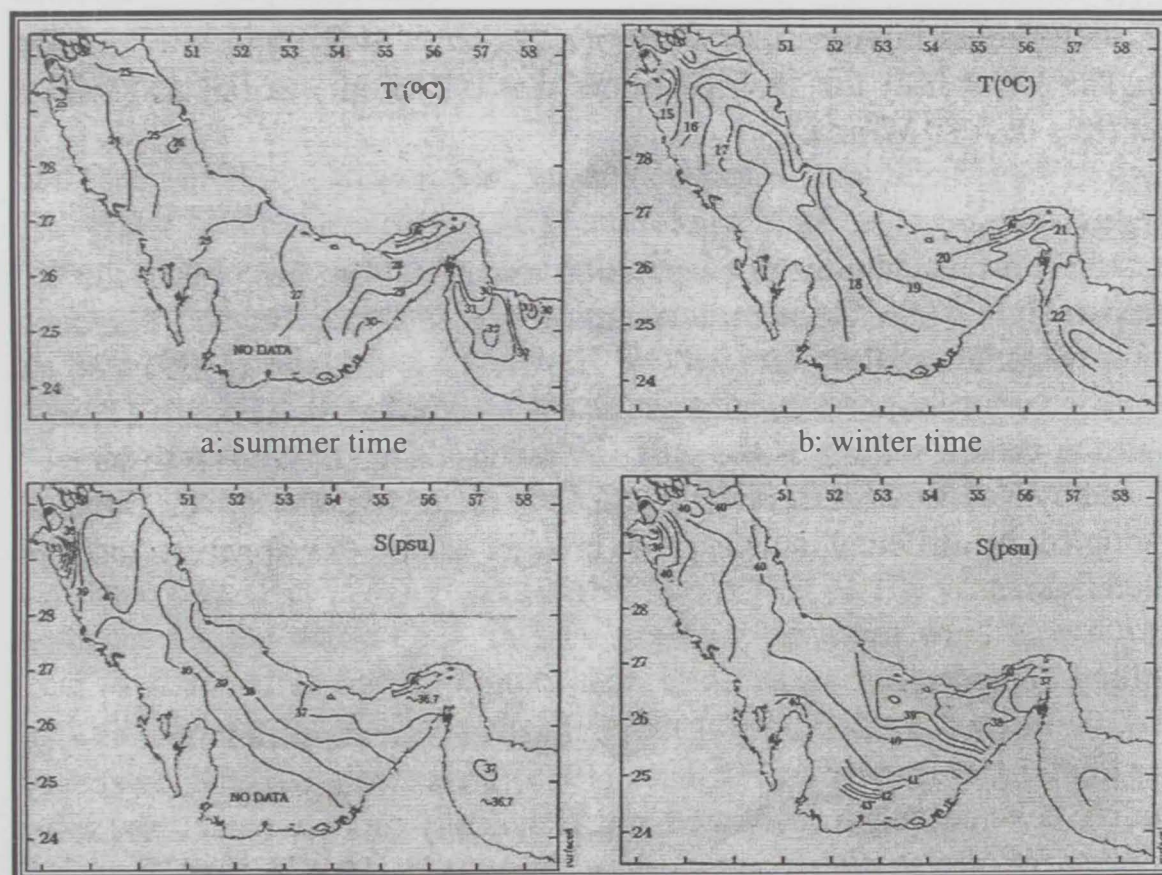
Figure 1.3: Distribution of salinity and temperature in the surface water of the Arabian Gulf in summer and winter (Reynolds, 1993)

Ruwais industrial complex officially inaugurated in 1982. It has been developed to be a major contributor to the national economy of the UAE. It is located along the coast of the UAE, 240 kilometers west of the capital Abu Dhabi (Fig. 1.4).

The complex comprises the most important petrochemical industries in the UAE (www.takreer.com, 2004). The refinery plant is the major establishment there. Several petrochemical utilities integrated with it; mainly, the fertilizer manufacturers. The refinery plant and the other facilities discharge their effluent after some treatment to the nearing coastal water. The effluents can possibly carry high chemical concentrations, in addition to warmer water. To cover the need of freshwater for the manufacturing activities and municipal use, a multi-stage flash desalination plant is present with a capacity of 150,000 m^3/d. A large amount of residual brine and worm water is continuously discharged into the marine water by the plant. The effluent water temperature from the plant reaches up to 45° C, and its salinity around 70 ppt. (Elshorbagy *et al.*, 2004b). These values are somewhat high compared to the ambient coastal waters, and may threaten the water quality of the area. This will be investigated in the present study
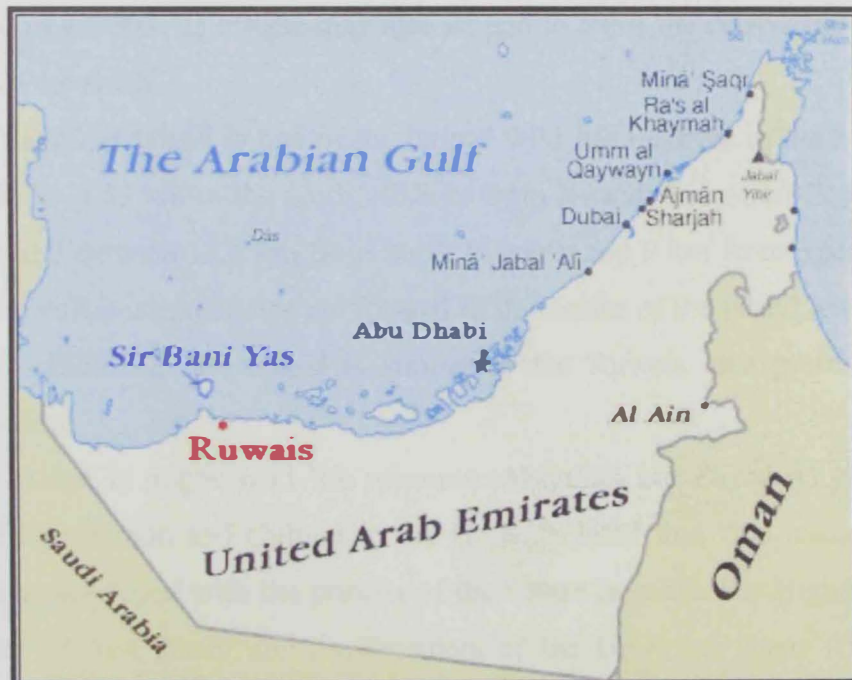
Figure 1.4: Locations of Ruwais Area and Sir Bani Yas Island along the UAE Coast.

The average daytime temperature in the summer within the Ruwais area exceeds 41° C, with extreme maximum reaching up to 50° C. In the winter months, the lowest daytime mean temperature does not usually go below 20° C. The relative humidity is

high throughout the year, averaging about 70% and reaching 95% or more in the early morning hours and late night in the summer. In winter, the relative humidity may temporarily fall below 50% during the Shamal winds (Shamal wind occurs in June-July). The rainfall at Ruwais is not accurately known; but ranges approximately between 0 to 100 millimeters, averaging around 20 millimeters per year (Elshorbagy *et al.*, 2004a). Most of the rainfalls occur during the period of November to March in the form of showers or thunderstorms. In an average year, measurable rain may fall on about 10 - 15 days.

The coastal water of Ruwais is characterized by high temperature and salinity all around the year. In the summer, the water temperature rises up to $35^{\circ}C$, while in winter it decreases up to $20^{\circ}C$. The surface salinity has slight variation over the year, where it fluctuates between 45 and 46 ppt. (Elshorbagy *et al.*, 2004a).

The Ruwais port is one of the most vital ports in the UAE due to its import-export activities of oil and other petrochemical products. The movement of ships and tankers is continuous day and night, all around the year. Loading and unloading activities of oil and petrochemical products may produce some oil spilling and other wastes. Such contaminants move with the currents and may damage the marine environment in the Ruwais area in general. Its effects may also extend to harm the ecosystem at Sir Bani Yas Island in the north.

Sir Bani Yas Island is one of the largest wild life reserves in the Middle East (Vine, 1999). It is 15 km in the north offshore from Ruwais Industrial Complex (Fig. 1.4). The island extends 17.5 km from north to south and 9 km from east to west. A range of bare volcanic mountains are located in the center of the island with height of 148 m. The climate in the island is similar to the Ruwais area presented in the previous section.

The island is major wild life resource. Abdullah bin Zayed Al Nahyan, the Minister of Information and Culture in the UAE declared that "the island, Sir Bani Yas, has been developed with the priority of the nature in mind. His Highness Sheikh Zayed, Ruler of Abu Dhabi and the President of the UAE, has made it a personal mission to rescue as much as possible of Arabian's wild life as well as threatened species from Africa and Asia, and to provide them with a secure and peaceful home. The success of this project is immediately evident to everyone who visits the island." (Vine, 1999)

In the last two decades, most of the lands in Sir Bani Yas Island have been planted with different types of fruits and wild trees. 200,000 fruit trees were planted there (Vine, 1999). The eastern coast of the island has been planted with the mangrove. The coastline of Sir Bani Yas has been transformed by landfill operation and dredging ever since 1981, and the earlier maps no longer reflect the present geographic reality (King, 1998).

The marine life around the island is widely diversified. The rich and secure environment attracts several kinds of marine creatures to seek shelter in it. The most important marine species which stamp the marine ecology of Sir Bani Yas shore line are the colonies of coral reefs spreading along the southern east of the island. There are less than 20 km away from the disposal outlets of the Ruwais Industrial Complex. Coral reefs have a fiscal and biological value, where they are important for fishery and nursery. Moreover, the commercial types of them can potentially contribute to the national income in addition to their tourism significance. As the coral reefs sensitivity to temperature and salinity of the surrounding environment is very high, it is very crucial to investigate the effect of the effluents disposed from the Ruwais compound on the ambient water.

1.5 Methodology

In order to study the current and future impact assessment of the brine discharging from the desalination plant and the warm water effluents from other facilities located in the Ruwais coastal area upon the marine water, two numerical models are employed. The first is a 3-D hydrodynamic model and the second is a 3-D ecological model coupled with the hydrodynamic one.

Study of the hydrodynamics of Ruwais coastal water is conducted using a three dimensional multi-level rectilinear grid model called "COSMOS". This model was used by Elshorbagy et al. (2004a) to study the hydrodynamic characterization of the Arabian Gulf, and was used again by Elshorbagy et al. (2004d) to study the salinity and temperature for Ruwais coast. In the current work the model used to study the dynamics of currents in the Ruwais marine water, in addition to the spatial and temporal distribution of the salinity and temperature. In order to simulate of the Ruwais area, the hydrodynamic model is first run for the entire Arabian Gulf as a regional model to simulate the different hydrodynamic conditions and to provide such conditions at the boundary of the local Ruwais model to be nested inside the regional

model with finer grid size. Several types of data have been collected for the regional model. The bathymetry of the Gulf and the tidal constituents for the considered boundary are obtained from the Admiralty Tide Tables (ATT, 2001). The salinity and the temperature for the boundary as well as for the whole model at time = 0 (initial condition) are based on the data of Mt Mitchell's campaign (Reynolds, 1993). The wind conditions are based on Hellarman monthly wind data and records from three offshore metrological stations in the southern part of the UAE coast. Other model parameters were turned via comparison with some cited measurements to be performed later. The simulation has been done for the whole year by considering the change of solar radiation and variation of wind pattern in summer and winter seasons. After that, the boundary conditions for the local model are extracted and the model is run again with a finer grid size considering the effluents from the different sources located along the Ruwais coast. The simulation is also done over one whole year with the same previous considerations.

In order to simulate the water quality conditions of the Ruwais coastal water, three-dimensional biological model called "EUTROP" is used. This model has been used in different studies; Nakata and Taguchi (1982), Nakata et al. (1983, 1985), Taguchi and Nakata (1998), Taguchi et al. (1999) and Elshorbagy et al. (2004b). The model used advection-dispersion scheme to simulate the lower-trophic ecological processes in the physically active regime. Information on all possible potential sources of nutrient disposed into the sea and other biological parameters of the Ruwais marine ecosystem are obtained from Elshorbagy et al. (2004b). Elshorbagy's data mainly consisted of four groups of survey covering the summer and winter seasons in the years 2003 and 2004. It included phytoplankton biomass (P), zooplankton biomass (Z), particulate organic mater (POC), dissolved organic matter (DOC), phosphate concentration (P), Ammonium concentration (NH4), nitrite concentration (NO2), nitrate concentration (NO3), dissolved oxygen concentration (DO) and chemical oxygen demand concentration (COD). The model employs and considers the temperature, salinity, and flow dynamic data provided by the resolved hydrodynamic model. In the beginning, the model compartment parameters are stabilized in order to match the observed and calculated values of the different compartments. After that, the model is run to simulate the current situation for one whole year by considering the summer and winter variations. After that, the model is run for several years to predict the effects of the future expansions of the desalination

plant and the other facilities upon the water quality of the Ruwais as well on the aquatic life. Figure 1.5 shows a simplified diagram of the modeling process along with the different types of involved data.

Data Required	Hydrodynamic Model
Geographical data: Location, Topographic data (bathymetry and land boundary)	**Grid Generation:** Making rectiliniear grid data
Metrological Data: Wind (speed & direction), Solar radiation, Humidity, Cloud cover, Precipitation, Evaporation	**Depth Generation:** Making bathymetry data on the grid
Hydrographic Data: Water Temp., Salinity, Tides, Density, Inflow rivers (Quantity, Temp., Salinity)	**COSMOS:** Hydrodynamic calculations
Water Quality Data: Zooplankton biomass, Phytoplankton Biomass, NO$_2$, NO$_3$, NH$_4$, PO$_4$, POC, DOC, DO, COD.	**Water Quality Model "EUTROP"**

Figure 1.5: Simplified diagram showing the steps of water quality modeling process.

CHAPTER TWO

LITERATURE REVIEW

Arabian Gulf represents the main artery for its encompassing countries. It is considered as their window to the rest of the world to share civilization and prosperity. Beneath it, huge reservoirs of oil exist, and inside it, enormous wealth of fishes lives. Most capitals and vital cities of the Arabian Peninsulas' countries are located along its coasts. Moreover, each country has several ports and industrial areas on the shore, aside from the recreational and tourism areas that spread along the coast. Over and above, the Gulf importance extends to be the major source of the desalinated fresh water in these arid regions.

United Arab Emirates is one of countries that overlook the Arabia Gulf. Expanding and developing of communities in the UAE coast increased the pressure on the coastal marine environment due to major industrial zones mostly constructed on the coastal line. Most of these zones discharge their effluents into the coastal water increasing the nutrient supply in the marine water. Moreover, the oil import/export petrochemical activities in the different ports of the country produce a lot of pollutants which may deteriorate the water quality of the coast. In addition to the desalination and power plants which are scattered on the UAE coast discharge huge quantities of hyper saline and warm water increasing the salinity and temperature of the coastal waters; as may severely threat the fauna and flora of the UAE marine ecosystem.

In the current chapter, an intensive literature preview will be performed in order to address the main topics discussed in this thesis. These topics will cover the importance of the desalination as the main source of the fresh water in the UAE, the brine and thermal discharged effluents from the desalination plants. Different types of models utilized to assess these pollutants in the world in general and in the UAE in particular will be briefly survey, and finally the impact assessment of such contaminants on the marine biota will be discussed.

2.1 Desalination in the UAE

Water is a limited finite resource. It is essential for the life existence on the planet. Moreover, it is required to satisfy the economic and social development for the mankind. Water is becoming scarce commodity due the population growth and the change of lifestyle (Tsiourtis, 2001). Desalination of seawater is considered a suitable solution to meet the deficit of the potable water both at the present and in the future (Einav *et al.*, 2002). Desalination is used on a large scale in many arid regions in the world where the rainfall and the fresh water resources are limited (Morton *et al.* 1996). The growing technology of desalination is currently providing enormous quantities of water to meet the escalating needs for domestic and industrial sectors in many water scarce countries (Al-Weshah, 2002).

UAE is an arid country. Its natural water resources of the fresh water are very limited. It is considered as one of the most dependent countries on the desalinated water because it has the second rank of utilizing the desalinated water in the Arab countries after the Saudi Arabia (ACSAD, 1997; ESCWA, 1999; Khouri, 2002). 98% of the country's supply comes from the desalination of seawater or brackish water (Sommariva and Syambabu, 2001).

There are three main techniques of desalination; multi-stage flash desalination (MSF), multi-effect desalination (MED), and membrane processes mainly reverse osmoses (RO); (Semait, 2000).

The MSF procedure is the most common technique used in the Arabian Gulf region (Awerbuch, 1997). It requires large amounts of energy, so it is suitable for the areas that are rich in cheap fuel (Einav *et al.*, 2002). All large size desalination plants (above 5 MIGD) in the UAE are based on MSF technology (Sommariva and Syambabu, 2001). MSF desalination plant requires an input of seawater around 8 to 10 times the production of its fresh water for cooling and feed backup (Morton at al., 1996).

The MED technique has a limited usage in the world. Even though it produces a good water quality, it mostly used for the remote area, resort locations, islands, etc. (Semait, 2000). MED technology has been applied in some of the UAE projects, where two units of Umm Al Nar desalination plant in Abu Dhabi Emirate were constructed and being used since the year 2000 (Sommariva and Syambabu, 2001).

The RO technology is widely used nowadays and it is considered as the fastest developing technique in the water desalination (Semait, 2000). It is considered as the most efficient desalination process both in terms of energy and costs (Winston and Sirkar, 1992; Altman, 2000). RO desalination plants are used to serve small and large communities in the UAE (Ahmed *et al.*, 2001). RO desalination plant requires seawater feeding about 2.5 to 3 times its fresh water production (Morton at al., 1996).

MSF desalination plant has been constructed in the RIC to cater to the need of fresh water for the population, manufacturing, and the agricultural purposes. It produces 15,000 m^3/ day. The aim of the current work is to study the effluent impacts of the Ruwais desalination plant and the other facilities; mainly the brine and temperature on the Ruwais marine water quality. In the beginning, a brief description of MSF desalination process will be introduced; later most of the effluent components from the MSF desalination plants will be addressed. The hydrodynamic models as a tool to investigate the temperature and salinity dispersion in the marine coastal water will be presented. Moreover, the effect of the brine and warm water on the marine ecology will be discussed.

2.2 Multi-Stage Flash (MSF) Desalination Plant

Semait (2000) stated that "The MSF distillation is currently the most common and simple technique in use". Commercially, the MSF has operated since 30 years ago (Awerbuch, 1997). Figure 2.1 shows a simple schematic diagram showing the main part of the MSF desalination plant. The seawater is fed into the system under high pressure passing through closed pipes to exchange the heat with vapor, it also be used to condense the vapor in the upper section of flash chambers. The seawater water is heated to a certain initial temperature to be flushed along the lower part of the chambers under low pressure. The seawater transforms to a vapor state. This vapor passes from chamber to another, through that, it passes through a mist eliminator to condense over the condensing tubes in the upper part of chambers. The heat of this vapor transfers to the feed from the seawater to be heated before entering the steam heater, so a part of energy is saved. The condensate drips into collectors and pumped out as distilled water. The brine water in the lower part of chambers pumped again into the system to increase the water recovery. After that, the exhausted brine with high salt concentration is rejected out to dump into the sea after some treatment to

reduce its salinity and temperature. The energy consumption by this technique is very high, so increasing the energy efficiency can be achieved by increasing the number of stages (chambers), raising the temperature of the preheated seawater, enhancing the heat transfer at the condensing vapor, utilization the heat rejected by the distilled water product and the disposed brine, and other factors (Semait, 2000).
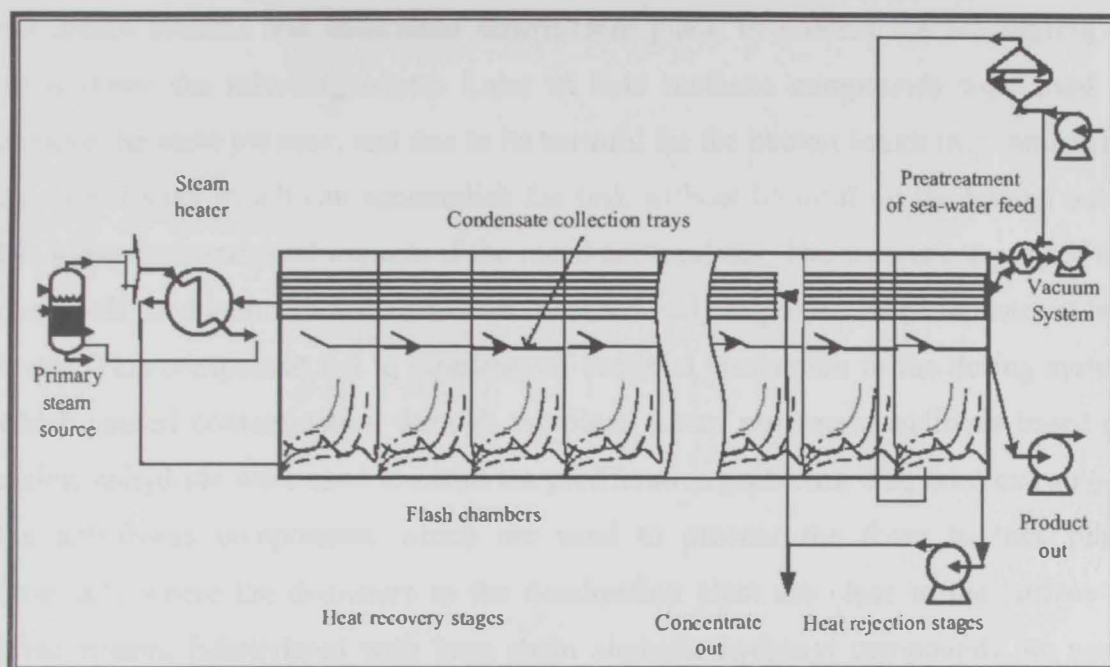
Figure 2.1: Schematic diagram of a Multi-Stage Flash desalination plant (Semiat, 2000)

2.2.1 Disposals from the MSF Desalination Plants

Several studies were conducted to investigate the effluent characteristics of the MSF desalination plants. Most of these studied concentrated on the brine and thermal discharging as the most important components of such effluents.

ESCWA (1993) reported that the cost is the main key in disposal method selection, where the disposal cost ranges from 5% to 33% of the total cost of desalination. Many factors are controlling the disposal cost, such as, the characteristics of the rejected brine, the level of treatment before disposals, means of disposal, volume of disposed brine, and the nature of the disposed area.

Ahmed *et al.* (2001) mentioned that all the desalination plants in the UAE dispose their effluents in the sea, although some of them discharge their effluent in nearby creeks linking to the sea.

The Ruwais desalination plant is one of such plants disposes its effluents directly to the coastal water after some treatments (Elshorbagy *et al*. 2004).

Morton *et al*. (1996) reported that the most important effluents discharging from the MSF desalination plants are the concentrated brine with high temperature, in addition to some chemicals which can be grouped into three main categories; biocides which is used for disinfection. Traditionally chlorine compounds are used to disinfect the intake systems and associated downstream plant, to prevent the bio fouling or settle down the microorganisms. Later tri halo methane compounds were used to achieve the same purpose, and due to its harmful for the human health they replaced it by copper salts which can accomplish the task without harmful on the human but it has some environmental impacts if the metal accumulates. The second category of the chemicals used is the scale control which is used early as polymeric phosphates at low levels. This component led to problems of bacterial production in the dosing system which caused contamination through the plant. Later, polymeric additives based on maleic anhydride were used to avoid the proliferation problems. The third category is the anti-foams components which are used to prevent the foam to take place especially where the demisters in the desalination plant are close to the surface of brine stream. Ethoxylated with long chain aliphatic hydroxyl compounds are used, where their discharging into the sea have negligible effects on the environment.

In the current study, not all the discharging components will be taken in consideration, because some of them can not be calculated by the water quality model used in the study, even due to their slight effects or their impacts are taking place on very long period which not be easily to be recognized by the model. The main components which were taken in consideration in the hydrodynamic model were the brine disposal and the temperature increments due to the different discharges, whilst, phosphate (PO_4), nitrite (NO_2), nitrate (NO_3), ammonium (NH_4), dissolved organic matter (DOC), particulate organic carbon (POC), and chemical oxygen demand (COD) were taken in account for the water quality model as discussed in details later in chapters 5 and 6.

2.3 Hydrodynamic Models

Al Hajri (1990) reported that, every 6 minutes, one ship passes the Strait of Hormuz, and 60% of the worlds' marine transports come from this area.

In spite of the economical and strategic importance of the Gulf itself, in addition to the incredible development of the coastal communities in the Gulf area, the oceanographic observations from this region is very scarce, and most of them were carried out by individual efforts of few countries (Reynolds, 1993).

Since the last two decades, the oceanographic hydrodynamic models have been widely used to simulate the Arabian Gulf. Two types of modeling are common, tidal models and circulation models. Several studies were carried out to identify the tides in the Arabian Gulf (e.g. Lardner *et al.*, 1982; Galt, 1983; Galt *et al.*, 1983; Blain, 1998; Blain *et al.*, 2002). Others separate studies investigated the circulation in the Gulf (e.g. Lardner *et al.*, 1987; Lardner *et al.*, 1988; Lardner *et al.*, 1991; Horton *et al.*, 1992; Lardner *et al.*, 1993; Reynolds, 1993; Proctor *et al.*, 1994; Azzam *et al.*, 2004). The third group of studies discussed both tides and circulation (e.g. Chao et al., 1992; Elshorbagy *et al.*, 2004a).

As a general idea, numerical computational models in the past were based on two dimensional (2-D) and depth-averaged equations (Cheong *et al.*, 1992; Shankar *et al.*, 1997). In these 2-D models, the velocities of the currents at different depths are unified and the average value is considered. These calculations gave misleading values for the current velocity, as the current velocity at the surface layers differs from its velocity at the bottom layer due to friction force at the seabed. Moreover, in order to track the oil spill and the fate transport of the contaminants, the vertical distribution of the currents have to be well defined (Zhang and Gin, 2000). Therefore, a three dimensional (3-D) hydrodynamic model became a necessity for realistic simulation of the flow field.

There are two main categories of 3-D hydrodynamic models; multi-layer and multi-level ones. The difference between these two types refers to the construction of the interference layer. In a multi-layer model, the interfacial layers deals independently, without mass transport across the layers and can be displaced vertically to maintain continuity. However, the multi-level model assumes that the interfacial layers are fixed in space and continuity is maintained through the vertical transport between layers (Zhang and Gin, 2000).

2.4 Water Quality Models

In this part of the study, a brief literature will be introduced to describe miscellaneous three-dimensional water quality models which are used in different parts of the world in general and in the Arabian Gulf region in particular.

Three-dimensional ecological modeling has been used when the computer power has been developed enough to recognize the complex finite element processes; hence a desired combination of spatial and temporal resolution with the necessary trophic resolution could be perform (Moll and Radach, 2003). The first appearance of three-dimensional ecological models was in Japan and USA in about 1986, where the large scale ecological models were utilized to deal with dynamics and circulation of the oceans (Maier-Reimer and Bacastow, 1990). They have been used to investigate the climate change problems. Whereas, most of the shelf seas ecological models were used to investigate the eutrophication problems (Zevenboom, 1994).

Several three-dimensional ecological models were used around the world. Earlier, the models addressed pelagic habitats only (Skogen, 1993). After that, they included a simple bottom detritus compartments (Moll, 1995). Later, more sophisticated models were developed to treat all chemical and biological compartments at once (Baretta *et al.*, 1995). The following paragraphs describe some of these ecological models.

NORWECOM (Norwegian Ecological Model System) is a three-dimensional model. It was developed in 1993 by Skogen (Skogen, 1993). The first use of the model was documented by Aksnes (1995) when he simulated the mesocosm experiments in the North Sea. Then it was widely used by several scientists to assess different water quality parameters (Eriksord and Svendsen, 1997; Skogen *et al.*, 1995; Skogen *et al.*, 1998; Moll, 2000).

ERSEM (European Regional Seas Ecosystem Model) is considered as one of the most famous ecological models in the world. The model was developed within a MAST project over 7 years (1990- 1996). Several studies where carried out in Europe by using ERSEM model. Varela *et al.* (1995) and Ebenhöh *et al.* (1997) utilized the model to calculate the primary production in the North Sea. A microbial dynamics with carbon assimilation and nutrient uptake were simulated by using a modified version of the model (ERSEM-II) by Baretta *et al.* (1997). The dynamics of the North Sea meso-zooplankton was modeled by Broek-Huizen *et al.* (1995). Blackford (1997)

modeled the benthic biological dynamics in the North Sea, whereas, Bryant *et al.* (1995) modeled the production, predation and growth of fish. Patsch and Radach (1997) used ERSEM model for long-term simulation to cover the period 1955-1993 in order to study the effects of eutrophication on the North Sea. Moreover, the model was used by Radach and Ruardij (1997) and Lenhart (1999) to investigate reduced nutrient loads from the major rivers around the North Sea with different scenarios.

POL3dERSEM (Proudman Oceanographic Laboratory 3d ERSEM Model) was utilized by Allen *et al.* (2001) to simulate the North Sea ecosystem. It is considered as advanced extension for ERSEM and ERSEM-II models, where it could use finer grid size hence, it gave more accurate results for modeling north coast European continental shelf to investigate the spatial and temporal variation of physical and chemical factors which cause the spring blooms in the North Sea.

FINEST is a three-dimensional coupled hydro-ecosystem model. It was used by Tamsalu and Ennet to simulate the Gulf of Finland. Later, some tunings were done to be valid to use in the Mediterranean Sea, so it was utilized by Hamza *et al.* (2004) to simulate the Egyptian coastal ecosystem functions. In both cases, the model gave acceptable results.

EUTROP is Japanese water quality simulation software. It uses a three-dimensional coupled physical and biological model. It specialized to quantify and evaluate the physical and biological interactions in an estuarine lower-trophic ecosystem in terms of the cycles of carbon, nitrogen, phosphorous and oxygen. It takes in consideration twelve compartments, among which two living compartments; phytoplankton and zooplankton. It was used by Nakata and Taguchi (1982), Nakata *et al.* (1983, 1985), Taguchi and Nakata (1998), and Taguchi *et al.* (1999) to simulate different water bodies in Japan coastal marine water and lakes. EUTROP was modified and stabilized to be valid for using in the Arabian Gulf region. Elshorbagy *et al.* (2004b) used the model to simulate the ecology of the Ruwais marine water in the UAE coast.

Taguchi and Nakata (1998) utilized the EUTROP water quality model to study the mechanism of water pollution in Japanese Hamana Lake which is considered one of highly eutrophicated semi-enclosed estuarine. They adopted chemical oxygen demand (COD) as a water quality index. COD average concentration of summer in the period between 1988 and 1991 was simulated. They concluded that COD flux due to the primary production is 10 times larger than the external loading flux. Moreover,

they verified that the phosphorous is the limiting nutrient in the lake, and the benthic generation is the major source of it in the estuarine.

Elshorbagy *et al*. 2004b also employed the EUTROP water quality model to investigate the impact of the effluents discharging from the Ruwais Industrial Complex (RIC) on the Ruwais costal water in the UAE in both summer and winter seasons. The model was used after some calibration for the parameters of the compartments was done to be adapted for simulating such subtropical regions like the Arabian Gulf. Elshorbagy reported that the Ruwais water characterized by NHLC (High nutrients-low chlorophyll) condition, which was caused due to the excessive discharging of the nitrogen nutrients (NH_4, NO_2, and NO_3) from the different facilities locating at the coast and lacking in the phosphate (PO_4) which was considered as a limiting nutrient in the area. He concluded also that the harsh environment at such area mainly the high pollution due to oil and industrial activities reduced considerably the zooplankton biomass. Where the pollution is considered as one of the main factors reduce the zooplankton biomass in the coastal waters (Uriate and Villate, 2004).

2.5 Effects of the MSF Desalination Plants on the Marine Ecosystem

There are many impacts associated with the MSF desalination processes on the marine ecosystem. Theses impacts are mainly caused by the elevated temperature and high concentration of brine disposing into the coastal water (Morton *et al*., 1996). Many studies dealt with these issues to explain the influence of such effluents on the marine ecology and habitats.

Morton *et al* 1996 mentioned that the typical recovery effluent based on feed is 10 %. That means the salinity of the effluent is 1.1 times the salinity of raw seawater, while the actual discharge salinity from the RO desalination plants range from 1.3 to 1.7 and from MSF desalination plants decreases to be from 1.1 to 1.5 times the salinity of the feed water. Whereas, Hoepner 1999 remarked that the effluent of brine is usually diluted twice with cooling water before being discharged, so the concentration factor becomes 1.05 times the salinity of the raw seawater.

Ecologically, it is widely accepted that the marine biocoenosis tolerates the salinity variation of plus/minus 1 ppt, so a conservative discharge recommendation follow this line (Del Bene *et al*., 1994).

Semait (2000) mentioned that the brine disposal problem is mild in small operation scales, and there is no serious damage may occur for the marine

environment, whereas, at large scale operations the problem becomes little more severe. He suggested dilution and spreading of such brine plumes to overcome such problem.

Einav *et al*. (2002) declared that the main effects of salinity increase on marine biota occur near the discharge pipe, where increasing salinity may influence the benthic and planktonic organisms by different ratios. So, she suggested 4 alternatives of discharging techniques, which are; discharging the brine by long pipe far into the sea, discharging the brine directly to the coastal line after good treatment, discharging the brine through the outlet of the attached power station, and sending the brine directly to a salt production plant. And she commented that the sensitivity to increase in salinity varies from species to other. Some species like planktonic algae can tolerate to variations in salinity, another can tolerate the raising of salinity after a period of acclimatization, whereas most of the species may die.

Einav and Lokiec (2003) indicated according to Dawes (1998) and Levinton (1995) as professional studies that there is no specified salinity limit above which definite damage will occur to benthic population. They also mentioned also that the effects of high salinity discharge are limited to the local environment of the discharging area and it has no accumulated damage of the sea.

Hoepner (1999) mentioned that in the hot and arid regions, the extensive evaporation of the seawater produces variation difference in salinity exceeds plus/minus 1 ppt, that referring to the bathymetry of the region, solar radiation, wind, tidal regime, water exchange between shallow and offshore waters and other influences. So he suggested studying such those zones regarding to their local conditions. He claimed also that the effluent effects on the coastal water are usually little or even absent.

Hoepner and Windelberg (1996) argued that, for the Gulf entire basin, brine discharge is absolutely intangible because the natural evaporation is by magnitudes higher. This conclusion is valid also regionally since the salinity increases by evaporation are highest with in the shallow coastal zones where the brine discharge takes place.

Hoepner (1999) stated that "Thermal desalination plants discharge the concentrate usually with a temperature 10 to 15 °C above ambient seawater temperature." He elaborated according to Altayran and Madany (1992) investigations about the thermal effects of some desalination plant in Bahrain that in shallow water

regions with hot climate, the spatial and temporal variation of temperature is usual and often exceeds the effluents effects by far, so he concluded that the effluent temperature is a minor problem in the southern part of the Arabian Gulf.

Generally, Morton *et al.* (1996) reported that increasing the seawater temperature and salinity due to desalination schemes, power stations, and industrial facilities reduces the overall concentration of the dissolved oxygen in the water, which restricts the life forms to those able to live in low oxygen levels. This phenomenon becomes more pronounced if residual chemical concentrations that are used for de-aeration are present such as sodium metabisulphite. Moreover, at the level of the individual organisms, extreme temperature may result in death, whereas, sub lethal temperature may influence the biological rates of the different processes in the organisms such as the movement, the onset of maturity, life stage development, growth and size. At the species level, excessive temperature may influence the individual abundance and population diversity. Moreover, the desalination process has a potential thread on the phytoplankton and zooplankton due to pass concomitant with the inflow of seawater into pretreatment processes which usually use a chlorination method for disinfection which almost causes a complete death for all the biological activities in such inflow waters. The temperature differentials across the distiller in addition to the shear stresses and rapid pressure throughout the system enhance significantly the disinfection and prevent most of the biological organism to keep alive.

CHAPTER THREE

PHYSICAL SIMULATION

The United Arab Emirates (UAE) is located in the northeastern part of the Arabian Peninsula. It has 600 kilometers of coastline on the Arabian Gulf. Rapid development during the last two decades; propagated the need for evaluating the marine hydrodynamics, the ecosystem, and the fate transport of oil and other contaminants dumped at the Arabian Gulf water. In order to do that, different studies were achieved, among which Azzam *et al.*, 2004.

In the present study, a sophisticated three dimensional multi-level rectilinear grid model "COSMOS" was employed to simulate the hydrodynamics of Arabian Gulf as a regional model, and then a local model was nested for the Ruwais area in the UAE coastal waters. This hydrodynamic model was developed and used by Nakata and Taguchi (1983), Nakata *et al.* (1983, 1985), Taguchi and Nakata (1998) and Taguchi *et al.* (1999) in order to simulate the Japanese coastal waters. COSMOS hydrodynamic model was developed to simulate the hydrodynamic processes in the estuaries and coastal bays, especially for mesoscale (1-100 km) semi enclosed regions.

The hydrodynamic investigations of the Arabian Gulf were restricted to study water currents in the basin, with brief description about its general pattern of circulation. The present study is based on a comprehensive field survey of the Ruwais area to identify the effect of the local discharge effluents from the RIC on the coastal water temperature and salinity. Then 3-D physical model and a biological model "EUTROP" are employed together to investigate the water quality of the Ruwais coastal area, as will be discussed in chapter 6.

3.1 Theoretical Background

3.1.1 The Model Features

COSMOS employs a series of equations which describe the fluid motion, flow continuity, sea surface fluctuation, heat and salt transfer, in conjunction with equation of state. The driving forces of the flow field are tide, river discharge, sea surface wind, heat exchange with the atmosphere and horizontal density gradient. The sea water is considered as incompressible fluid, and the Coriolis parameters which govern the motion of the current due to earth rotation are considered as constant over the entire simulation region.

According to the previous conditions, the main basic equations of the numerical model are shortly listed as follows with respect to the Cartesian coordinate system shown in Figure 3.1:

Horizontal Fluid Motion

In x-direction

$$\frac{\partial u}{\partial t} + \frac{\partial}{\partial x}(uu) + \frac{\partial}{\partial y}(vu) + \frac{\partial}{\partial z}(wu) = -f_0 \cdot v - g \cdot \frac{\partial \zeta}{\partial x} - \frac{g}{\rho}\int_z^0 \frac{\partial \rho}{\partial x}\,dz - \frac{1}{\rho}\frac{\partial P_a}{\partial x}$$

$$+ \frac{\partial}{\partial x}\left(A_x \frac{\partial u}{\partial x}\right) + \frac{\partial}{\partial y}\left(A_y \frac{\partial u}{\partial y}\right) + \frac{\partial}{\partial z}\left(A_z \frac{\partial u}{\partial z}\right) \tag{1}$$

In y-direction

$$\frac{\partial v}{\partial t} + \frac{\partial}{\partial x}(uv) + \frac{\partial}{\partial y}(vv) + \frac{\partial}{\partial z}(wv) = f_0 \cdot u - g \cdot \frac{\partial \zeta}{\partial y} - \frac{g}{\rho}\int_z^0 \frac{\partial \rho}{\partial y}\,dz - \frac{1}{\rho}\frac{\partial P_a}{\partial y}$$

$$+ \frac{\partial}{\partial x}\left(A_x \frac{\partial v}{\partial x}\right) + \frac{\partial}{\partial y}\left(A_y \frac{\partial v}{\partial y}\right) + \frac{\partial}{\partial z}\left(A_z \frac{\partial v}{\partial z}\right) \tag{2}$$

Flow Continuity

$$\frac{\partial u}{\partial x} + \frac{\partial v}{\partial y} + \frac{\partial w}{\partial z} = 0 \tag{3}$$

$$\frac{\partial \zeta}{\partial t} = -\frac{\partial}{\partial x}\left(\int_{H}^{\zeta} u\ dz\right) + \frac{\partial}{\partial y}\left(\int_{H}^{\zeta} v\ dz\right) \qquad (4)$$

Conservation of Heat and Salt

$$\frac{\partial T}{\partial t} + \frac{\partial}{\partial x}(uT) + \frac{\partial}{\partial y}(vT) + \frac{\partial}{\partial z}(wT) = \frac{\partial}{\partial x}\left(K_x \frac{\partial T}{\partial x}\right) + \frac{\partial}{\partial y}\left(K_y \frac{\partial T}{\partial y}\right) + \frac{\partial}{\partial z}\left(K_z \frac{\partial T}{\partial z}\right) \quad (5)$$

$$\frac{\partial S}{\partial t} + \frac{\partial}{\partial x}(uS) + \frac{\partial}{\partial y}(vS) + \frac{\partial}{\partial z}(wS) = \frac{\partial}{\partial x}\left(K_x \frac{\partial S}{\partial x}\right) + \frac{\partial}{\partial y}\left(K_y \frac{\partial S}{\partial y}\right) + \frac{\partial}{\partial z}\left(K_z \frac{\partial S}{\partial z}\right)$$

(6)

Figure 3.1: Coordinate system of the estuarine hydrodynamic model

Equation of State

$$\rho = \rho(S, T) \qquad (7)$$

Where, the right hand side was described by the Knudsen's expression that relates seawater density to water temperature and salinity:

$$\rho = \frac{\sigma_t}{1000} + 1 \quad (g \cdot cm^{-3}) \tag{8}$$

$$\sigma_t = \Sigma_t + (\sigma_0 + 0.1324) \cdot \{1 - A_t + B_t (\sigma_0 - 0.1324)\} \tag{9}$$

$$\Sigma_t = \frac{(T - 3.98)^2}{503.570} \cdot \frac{T + 283.0}{T + 67.26} \tag{10}$$

$$\sigma_0 = -0.069 + 1.4708 \cdot Cl - 0.001570 \cdot Cl^2 + 0.0000398 \cdot Cl^3 \tag{11}$$

$$A_t = T \cdot (4.7869 - 0.098185 \cdot T + 0.0010843 \cdot T^2) \times 10^{-3} \tag{12}$$

$$B_t = T \cdot (18.030 - 0.8164 \cdot T + 0.01667 \cdot T^2) \times 10^{-6} \tag{13}$$

In the previous equations, u, v and w are the velocity components ($cm \cdot s^{-1}$) in the x, y and z direction, respectively, ζ the sea-surface level (cm), H the still-water depth (cm), ρ the seawater density ($g \cdot cm^{-3}$), f_0 the Colioris parameter (s^{-1}) which is given as $f_0 = 2 \cdot \omega \cdot \sin \varphi_0$ with the angular velocity ω (s^{-1}) of the earth rotation and the mean latitude φ_0 of the estuary, g the gravitational acceleration (980 $cm \cdot s^{-2}$) and P_a the atmospheric pressure ($g \cdot cm^{-2} \cdot s^{-1}$). T and S denote water temperature (^{o}C) and salinity (ppt), respectively; but here chlorinity Cl (‰) is adopted as the state variable instead of salinity. A_x, A_y and A_z represent the coefficient of eddy viscosity ($cm^2 \cdot s^{-2}$) in the x, y and z directions, respectively, and similarly K_x, K_y and K_z stand for the coefficients of eddy diffusivity ($cm^2 \cdot s^{-2}$).

Depth Integration

As shown in Figure 3.1, the water column is divided into K number of computational levels, where h_k represents the thickness of each level k, and the level boundary is defined from z = -H_{k-1} to z = -H_k; i.e. $h_k = H_k - H_{k-1}$. The depth-integrated velocity components are described as:

$$M_k \equiv \int_k u \, dz \,, N_k \equiv \int_k v \, dz \quad (k=1,2, \ldots, K) \tag{14}$$

The basic equations from (1 to 8) are vertically integrated within each level in the model as the following regime.

Equation of Motion in the X-Direction

$$\frac{\partial M_k}{\partial t} + \frac{\partial}{\partial x}(M_k u_k) + \frac{\partial}{\partial y}(M_k v_k) - (uw)\Big|_{-H_{k-1}} + (uw)\Big|_{-H_k} = f_0 N_k + \frac{h_k}{\rho_k}\left\{\left[\widetilde{P}_x\right]_k - \frac{1}{2}g \cdot h_k \frac{\partial \rho_k}{\partial x}\right\}$$

$$+ \frac{\partial}{\partial x}\left(A_x \frac{\partial M_k}{\partial x}\right) + \frac{\partial}{\partial y}\left(A_y \frac{M_k}{\partial y}\right) + \frac{1}{\rho} \cdot \tau_x^{k-1,k} - \frac{1}{\rho} \cdot \tau_x^{k,k+1} \tag{15}$$

Equation of Motion in the Y-Direction

$$\frac{\partial N_k}{\partial t} + \frac{\partial}{\partial x}(N_k u_k) + \frac{\partial}{\partial y}(N_k v_k) - (vw)\Big|_{-H_{k-1}} + (vw)\Big|_{-H_k} = -f_0 M_k + \frac{h_k}{\rho_k}\left\{\left[\widetilde{P}_y\right]_k - \frac{1}{2}g \cdot h_k \frac{\partial \rho_k}{\partial y}\right\}$$

$$+ \frac{\partial}{\partial x}\left(A_x \frac{\partial N_k}{\partial x}\right) + \frac{\partial}{\partial y}\left(A_y \frac{\partial N_k}{\partial y}\right) + \frac{1}{\rho} \cdot \tau_y^{k-1,k} - \frac{1}{\rho} \cdot \tau_y^{k,k+1} \tag{16}$$

Equation of Continuity

For the top-level ($k=1$), depth integration of the flow distribution of equation (3) becomes:

$$\int_1 \left\{\frac{\partial u}{\partial x} + \frac{\partial v}{\partial y} + \frac{\partial w}{\partial z}\right\} dz = \frac{\partial}{\partial x}\left(\int_1 u\ dz\right) + \frac{\partial}{\partial y}\left(\int_1 v\ dz\right) - u\Big|_\varsigma \frac{\partial \varsigma}{\partial x} - v\Big|_\varsigma \frac{\partial \varsigma}{\partial y} + w\Big|_\varsigma - w\Big|_{-H_1}$$

$$= \frac{\partial M_1}{\partial x} + \frac{\partial N_1}{\partial y} + \frac{\partial \varsigma}{\partial t} - (v_P - v_E) - w\Big|_{-H_1} \tag{17}$$

$w\Big|_\varsigma$, is precipitation rate v_P and the evaporation rate v_E for the vertical flow velocity at the sea surface. Moreover, the depth integration for the inter-layer k ($2<k<K$) represented as:

$$\int_k \left\{\frac{\partial u}{\partial x} + \frac{\partial v}{\partial y} + \frac{\partial w}{\partial z}\right\} dz = \frac{\partial M_k}{\partial x} + \frac{\partial N_k}{\partial y} + w\Big|_{-H_{k-1}} - w\Big|_{-H_k} \tag{18}$$

And for the bottom level ($k=K$), becomes:

$$\int_K \left\{ \frac{\partial u}{\partial x} + \frac{\partial v}{\partial y} + \frac{\partial w}{\partial z} \right\} dz = \frac{\partial M_K}{\partial x} + \frac{\partial N_K}{\partial y} + w \bigg|_{-H_{K-1}} \tag{19}$$

Equation of Heat Transport

For the top-level ($k=1$), the local change and the advection terms of the heat transport equation (5) are integrated as:

$$\frac{\partial}{\partial t}(h_1 T_1) + \frac{\partial}{\partial x}(M_1 T_1) + \frac{\partial}{\partial y}(N_1 T_1) - (wT)\bigg|_\varsigma$$

$$= \frac{\partial}{\partial x}\left(h_1 K_x \frac{\partial T_1}{\partial x}\right) + \frac{\partial}{\partial y}\left(h_1 K_y \frac{\partial T_1}{\partial y}\right) - \frac{Q_s}{\rho \cdot c_v} - \left(K_z \frac{\partial T}{\partial z}\right)\bigg|_{-H_1} \tag{20}$$

And for the level k ($2 < k < K$) the equation becomes:

$$\frac{\partial}{\partial t}(h_k T_k) + \frac{\partial}{\partial x}(M_k T_k) + \frac{\partial}{\partial y}(N_k T_k) + (wT)\bigg|_{-H_{k-1}} - (wT)\bigg|_{-H_k}$$

$$= \frac{\partial}{\partial x}\left(h_k K_x \frac{\partial T_k}{\partial x}\right) + \frac{\partial}{\partial y}\left(h_k K_y \frac{\partial T_k}{\partial y}\right) + \left(K_z \frac{\partial T}{\partial z}\right)\bigg|_{-H_{k-1}} - \left(K_z \frac{\partial T}{\partial z}\right)\bigg|_{-H_k} \tag{21}$$

Where T_1 represents the mean water temperature defined by $T_1 = \int_K T \, dz$, and Q_s represents the heat exchange flux with the atmosphere.

Equation of Salt Transport

The depth integration equation for salt transport does not account for the exchange flux with the atmosphere through sea surface but the change in the surface water volume is taken into account through the processes of precipitation and evaporation. The integration expression ends up as follows for any level k:

$$\frac{\partial}{\partial t}(h_k S_k) + \frac{\partial}{\partial x}(M_k S_k) + \frac{\partial}{\partial y}(N_k S_k) + (wS)\bigg|_{-H_{k-1}} - (wS)\bigg|_{-H_k}$$

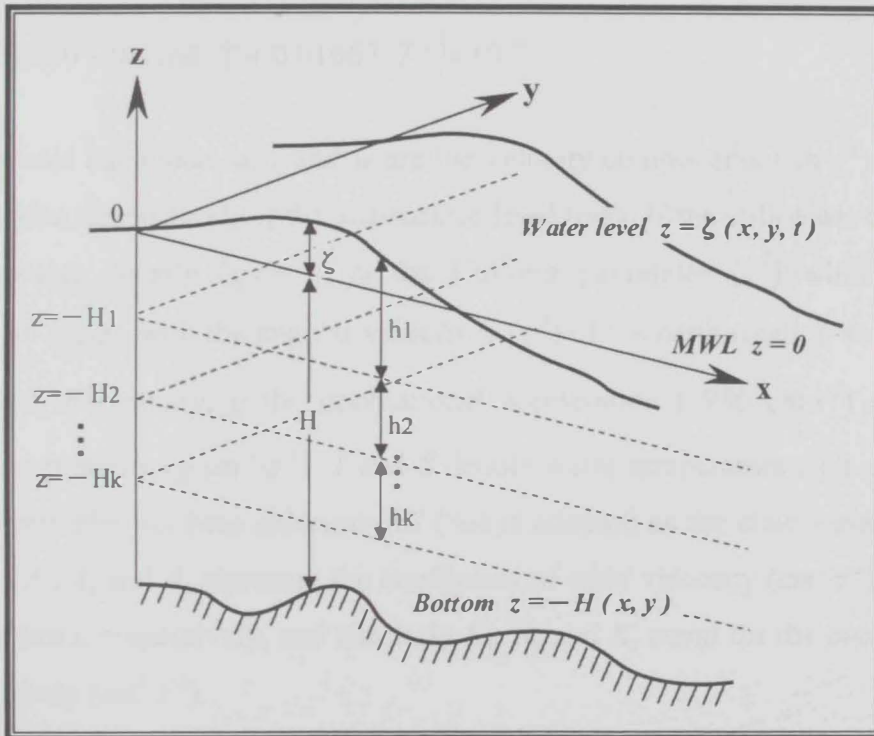$$= \frac{\partial}{\partial x}\left(h_k K_x \frac{\partial S_k}{\partial x}\right) + \frac{\partial}{\partial y}\left(h_k K_y \frac{\partial S_k}{\partial y}\right) + \left(K_z \frac{\partial S}{\partial z}\right)\bigg|_{-H_{k-1}} - \left(K_z \frac{\partial S}{\partial z}\right)\bigg|_{-H_k} \tag{22}$$

3.2 Regional Model (Arabian Gulf)

3.2.1 Model Setup

The hydrodynamic model "COSMOS" was employed to simulate the entire basin of the Arabian Gulf as a regional model. The area of simulation is shown in Figure 3.2. The computational conditions of the model are summarized in Table 3.1, where, the grid interval is 5 km, with model size 123 x 214 grid steps. The vertical dimension of the model is dividing the water column into 6 layers; 4, 6, 10, 20, 30, and 40m from the top to the bottom respectively. Four main rivers are taken into consideration (Fig. 3.2). These rivers are Shat Al-Arab rivers (Tigris and Euphrates), Hindijan, Hilleh and Manad, those have different flows, but same temperature and salinity as listed in Table 3.1. The boundary conditions of the model are at the Strait of Hormuz. The tidal constituents for the boundary are collected from the Admiralty Tide Tables (ATT, 2001), while, the salinity and the temperature for them are based on the data of Mt Mitchell's campaign (Reynolds, 1993). The wind conditions are based on Hellarman monthly wind data and records from three offshore metrological stations in the southern part of the UAE coast. Other model parameters are identical to those used in the model employed by Elshorbagy *et al.* (2004a).

Due to the wide difference of the metrological conditions for the summer and winter in the Gulf region, the model is run for two separate periods, summer and winter, each covered 60 days. The data of the metrological conditions are shown in Table 3.1 too.
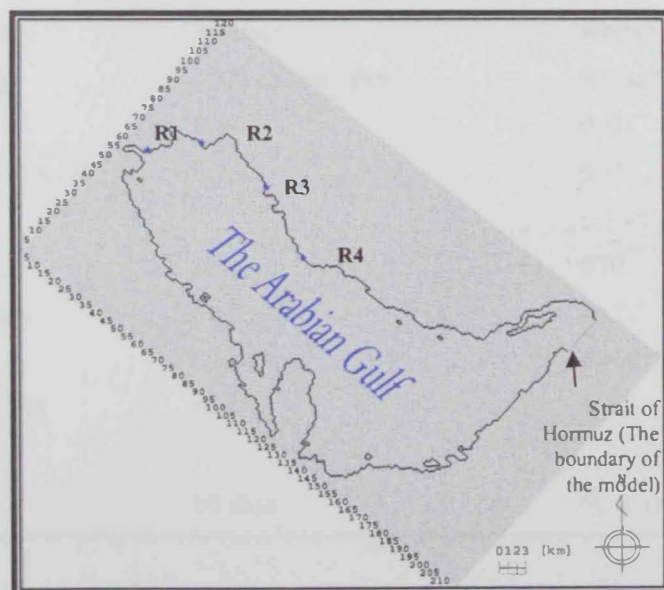
Figure 3.2: The simulated regional model, (★) indicates the rivers location.

Table 3.1: Computational conditions of the hydrodynamic model for the Arabian Gulf

Parameter	Selected value	
Area	Entire basin of the Arabian Gulf (Fig. 3.2).	
Grid size	5 km	
Number of horizontal meshes	123 (north-south) x 216 (east-west)	
Vertical layer locations	*6 vertical layers*	
	Level 1: from surface to -4, Level 2: from -4 to -10	
	Level 3: from -10 to -20 , Level 4: from -20 to -40	
	Level 5: from -40 to -70 , Level 6: from -70 to the bottom	
River conditions	*4 rivers at the north (Fig. 3.2)*	
	River 1: Q= $1.26 * 10^8$ m^3.day^{-1}, T = 15°C, Salinity = 0 ppt	
	River 2: Q= $1.75 * 10^7$ m^3.day^{-1}, T = 15°C, Salinity = 0 ppt	
	River 3: Q= $3.84 * 10^7$ m^3.day^{-1}, T = 15°C, Salinity = 0 ppt	
	River 4: Q= $1.20 * 10^7$ m^3.day^{-1}, T = 15°C, Salinity = 0 ppt	
Tidal constituents for the boundary conditions at Strait of Hormuz	M2, S2, K1, O1; obtained from Admiralty Tide Table (ATT, 2001)	
Temperature and Salinity for the boundary at Strait of Hormuz	Collected from Mt Mitchell data (Reynolds, 1993)	
Wind condition	Records from three offshore metrological stations in the UAE	
Model parameters		
Coriolis parameter	$6.376 * 10^{-5}$ s^{-1}	
Friction coefficient for seabed	0.0026 (assumed)	
Wind friction coefficient at the sea surface	0.001	
Horizontal and vertical eddy viscosity and diffusivity	$1.98 * 10^6$ m^2.s^{-1}	
Metrological conditions	*Summer*	*Winter*
Global solar radiation	1500 cal.cm^{-2}.day^{-1}	970 cal.cm^{-2}.day^{-1}
Day length	0.57	0.50
Empirical coefficient of solar altitude reflection	0.35	0.35
Cloudiness	0.01	0.01
Daily mean temperature	30 °C	20 °C
Relative humidity	53 %	60 %
Empirical constant of the cloudiness reflection	0.65	0.65
Calculated period	60 days	60 days

3.2.2 Model Development

To run the COSMOS model, some data files have to be prepared in a special digital format. This can be done by using number of subroutines included in the CENESIS suite. The procedure is summarized in the following three steps:

1) A rectilinear grid is developed for the study area. This is done by tracing a digitized map prepared earlier by a digitizer. Such grid generation process is carried out by using GUI software titled "GRDGNR". The grid size and the depth levels are determined in this step and used as a part of the control data for COSMOS.

2) The next step is to create the model bathymetry. "DEPGNR", is software used along with grid information to interpolate the depth data in three dimensional schemes. In this process, the depth of each point of the grid is determined. The output files obtained are used as input conditions for COSMOS.

3) Having developed the grid and bathymetry for the model, the next step is to develop the initial and boundary conditions. Two small softwares are used to create the initial and boundary conditions for COSMOS, they are "CSMINT" and "CSMBND" respectively.

3.2.3 Results and Discussion

The main goal of the regional hydrodynamic model is to study the current dynamics across the Gulf basin, hence to extract the boundary condition for the local Ruwais model. As a result, the regional Gulf model was run for 60 days period to simulate both summer and winter hydrodynamics. The model was fairly calibrated in a similar way to the study made by Elshorbagy *et al*. (2004a) and the simulated water level is compared with the same field measurements. The water level measurements are collected at three stations at UAE coast; Abu Dhabi, Dubai and Ruwais. Comparison the measured and calculated results show a good agreement with slight mismatch for the amplitude at Abu Dhabi during the spring tide as shown in Figure 3.3.

Figure 3.4 shows the time-average currents for the summer season at the surface layer. It is obvious that the dominating residual currents directed southward perpendicular to the gulf axis. At the UAE eastern coast in the south, the currents are stronger and tended to be eastward parallel to the coast while the currents circulate

counterclockwise around Bahrain Island. At Strait of Hormuz, the currents tend to be inward the Gulf basin.

In winter (Fig. 3.5), the current flow patterns in the center of the Gulf tend to be perpendicular to the Gulf axis toward the south. At the Iranian and Arabian Peninsulas' coasts, the currents direct toward the southern east. At the eastern southern part of the Gulf, the currents incline toward the northeast heading to the Strait of Hormuz as they exit to the Oman Gulf.
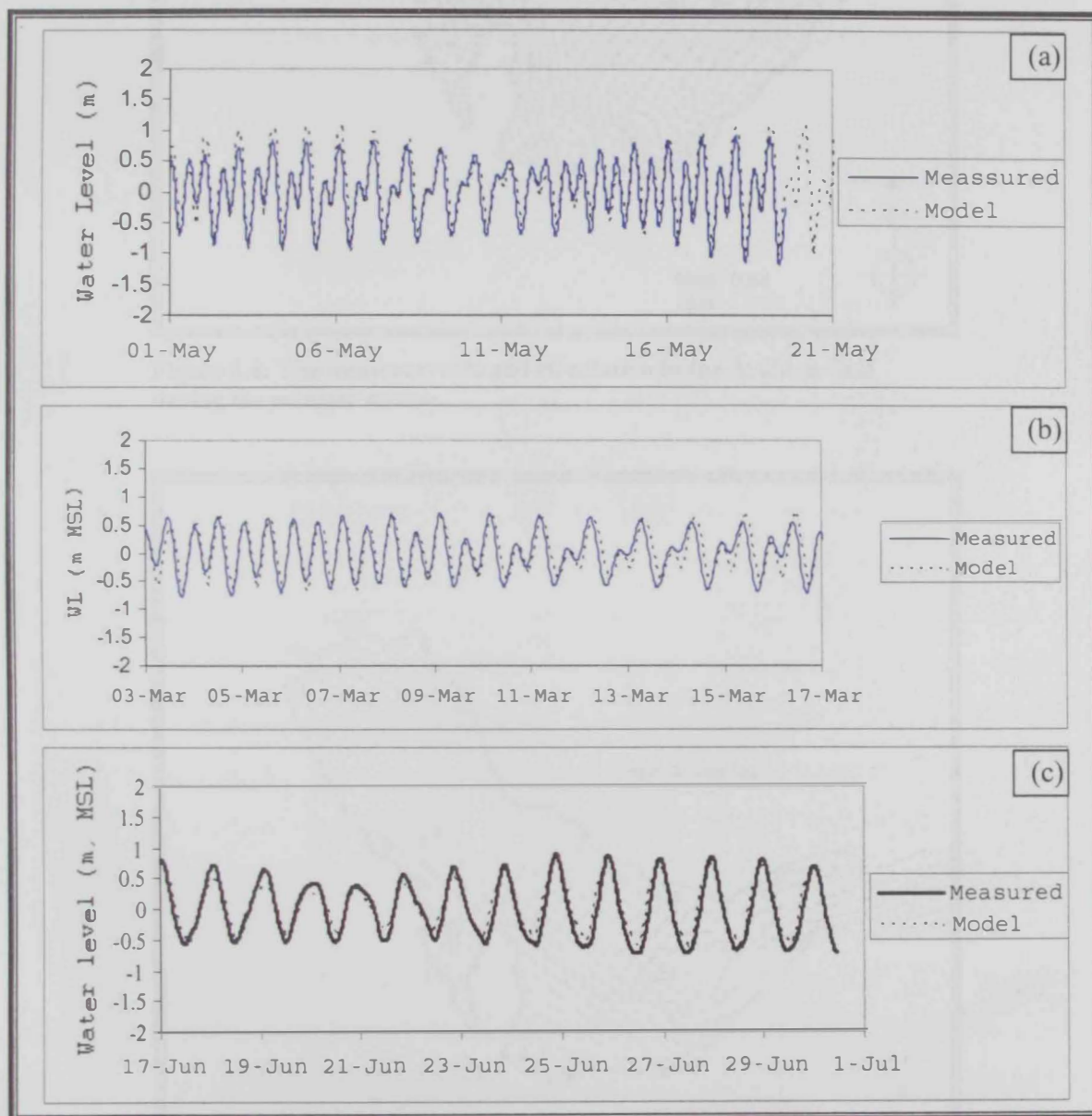
Figure 3.3: Comparison of predicted and simulated water levels at (a) Abu Dhabi (b) Dubai and (c) Ruwais (Elshorbagy, 2004a)
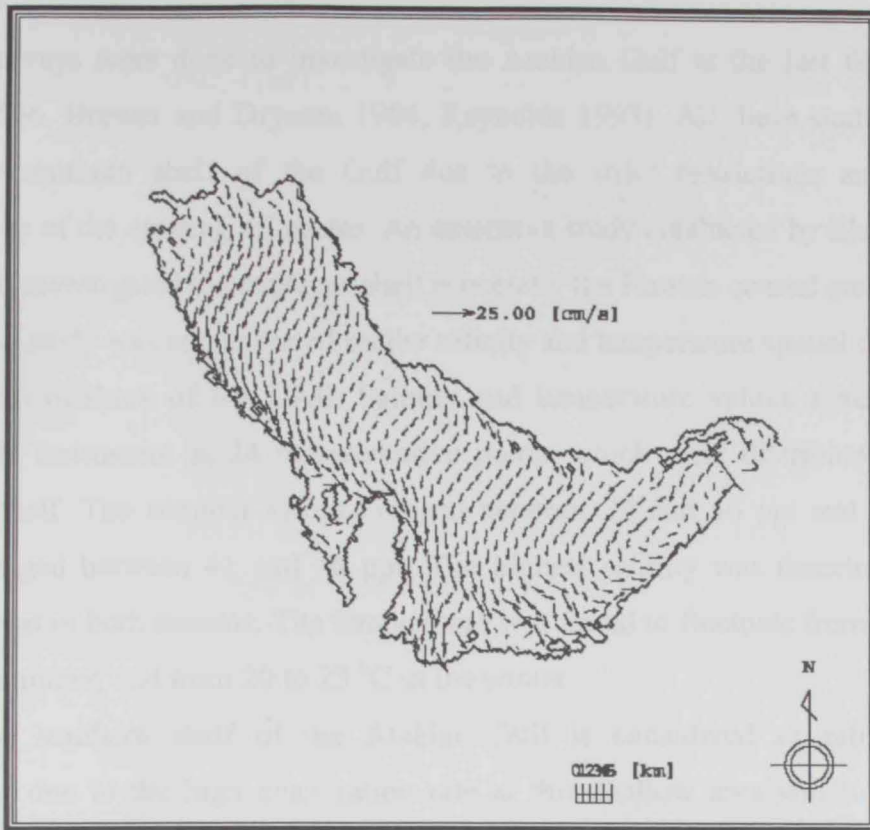
Figure 3.4: The mean currents and circulation in the Arabian Gulf during the summer season.
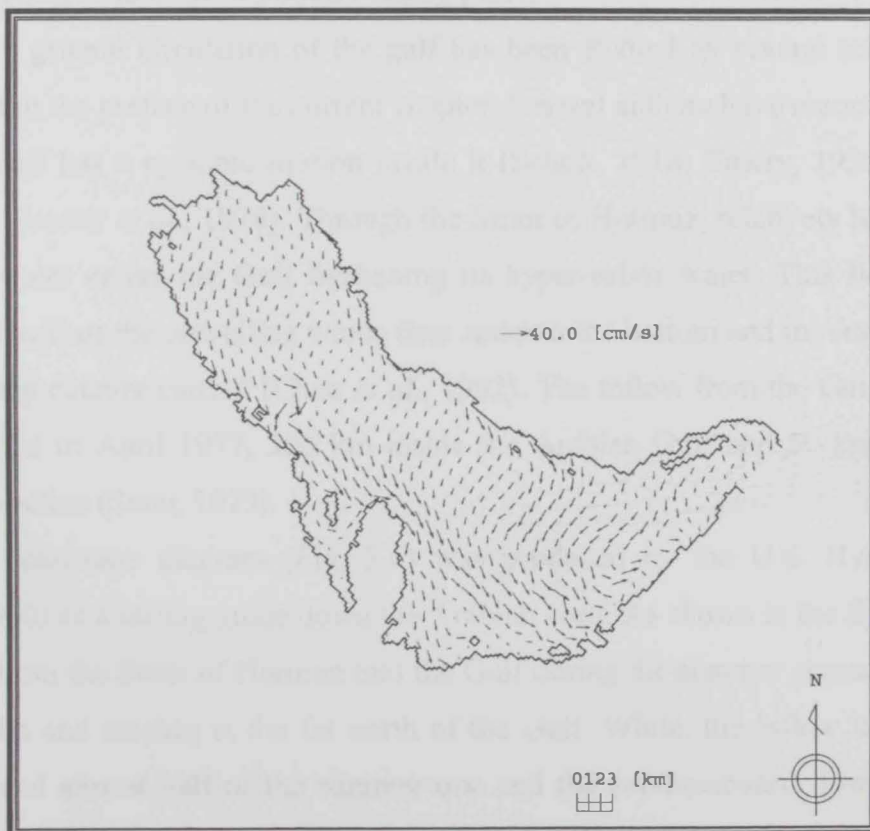
Figure 3.5: The mean currents and circulation in the Arabian Gulf during the winter season.

Several surveys were done to investigate the Arabian Gulf at the last few decades (Emery 1956, Brewer and Dryssen 1984, Reynolds 1993). All these studies did not cover the southern shelf of the Gulf due to the strict restrictions and security implications of the existing oil routes. An extensive study conducted by Elshorbagy *et al.* (2004d) investigated the southern shelf especially the Ruwais coastal area.

The study was concentrated on the salinity and temperature spatial distribution over 80 km offshore of the UAE. Salinity and temperature values were measured using CTD instrument at 24 representative points which were distributed over the southern shelf. The summer salinity ranged between 39 and 46 ppt and the winter salinity ranged between 41 and 46 ppt. The highest salinity was detected near the Ruwais coast in both seasons. The temperature was found to fluctuate from 31 to 32.5 °C in the summer, and from 20 to 23 °C in the winter.

The southern shelf of the Arabian Gulf is considered as salinity water generation, due to the high evaporation rate at this shallow area which makes the coastal water more saline. This water sinks to the bottom thereafter to exit from the Strait of Hormuz, and less saline water enters from the Strait to substitute this water and keep the circulation continuously taking place.

The general circulation of the gulf has been studied by several scientists, as mentioned in the preface of the current chapter. Several authors have reported that the Arabian Gulf has a cyclonic motion inside it (Schott, 1918; Emery, 1956; Sugden, 1972; and Brewer *et al.*, 1978). Through the Strait of Hormuz, relatively low-salinity and cool water enters the Gulf freshening its hyper-saline water. This flow moves northward against the prevailing winds then sinks to the bottom and moves out of the Gulf as deep counter current (Chao *et al.*, 1992). The inflow from the Gulf of Oman was detected in April 1977, 200 km inside the Arabian Gulf and 50 km from the Iranian shoreline (Sonu, 1979).

A schematic diagram (Fig. 3.6) was produced by the U.S. Hydrographic Office (1960) as a sailing guide down the Arabian Gulf. As shown in the figure, there is inflow from the Strait of Hormuz into the Gulf during the summer characterized by broad width and reaches at the far north of the Gulf. While, the inflow in winter is narrower and almost half of the summer one and the southeastward flow along the Arabian coast is wider.

A more comprehensive study about the circulation in the gulf was achieved by RSMAS (2000). The study classified the Arabian Gulf into two regimes; northern and southern or eastern. The northern regime is governed by the winds which blow to the south along the Gulf axis and with the fresh waters discharged from the rivers at Shatt Al-Arab in the head of the Gulf (Tigris and Euphrates) and at high land of Iran (the Hindijan, Hilleh and Manad), (Fig. 3.7). The downwind flow in the Gulf is a result of the low pressure field at the southern part. This produces down-willing at the western coast and upwelling on the coast of Iran (Reynolds, 1993).

The flow along the Kuwait and Saudi Arabia coast in northern regime is increased by the rivers inflow from Shatt Al-Arab and Iran. The center of the northern Gulf appears to be fairly stagnant (Reynolds, 1993). In the southern regime, the down flow along the Iranian coast continues along the coast to reach the Strait of Hormuz. The northern and southern regimes are singled out by a front that is found off Qatar (Fig. 3.7). This front is characterized by the highest surface temperature in summer and lowest in the late of winter and spring. The location of the front associates with fresh water inflow into the Gulf from the Strait of Hormuz. Most of this inflow ends in a counter-clockwise cyclonic flow to the coast of mid-Gulf front (Fig. 3.7). The intensive evaporation over the Gulf causes an inverse circulation with hyper-saline water leaves the Gulf through the Strait. The High salinity water zones extend from Qatar to the Emirates coast (the hatched region in Figure 3.7). The salinity of water in this region may reach up to (>42 ppt) (RSMAS, 2000).
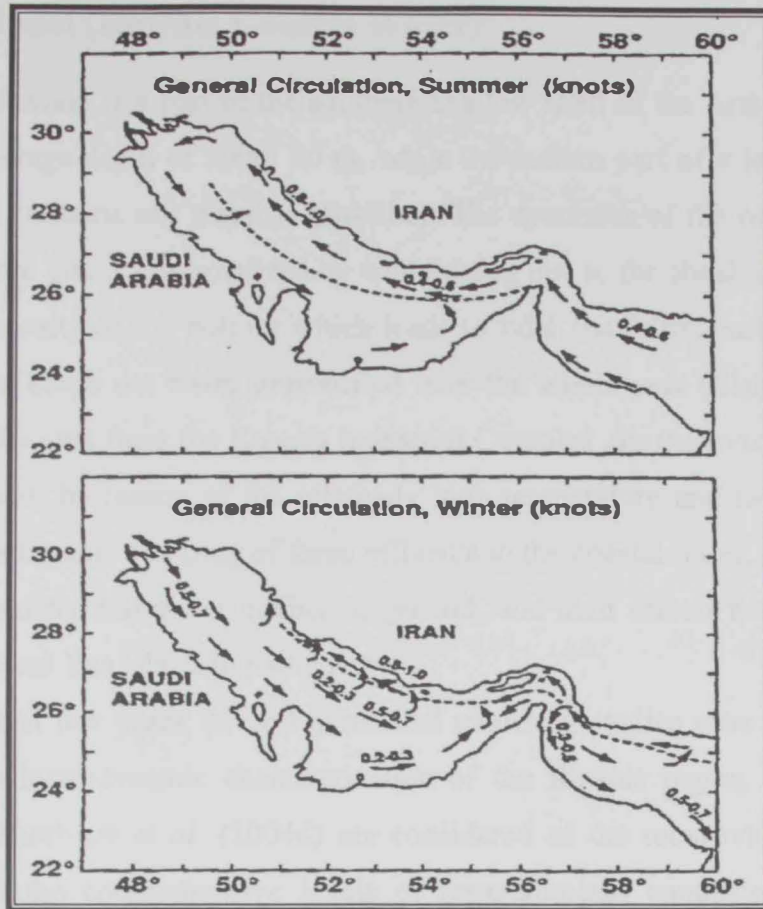
Figure 3.6: A schematic illustration of the general circulation in the Arabian Gulf and vicinity. The top panel is for summer and the bottom is for winter. (The U.S. Hydrographic Office, 1960)
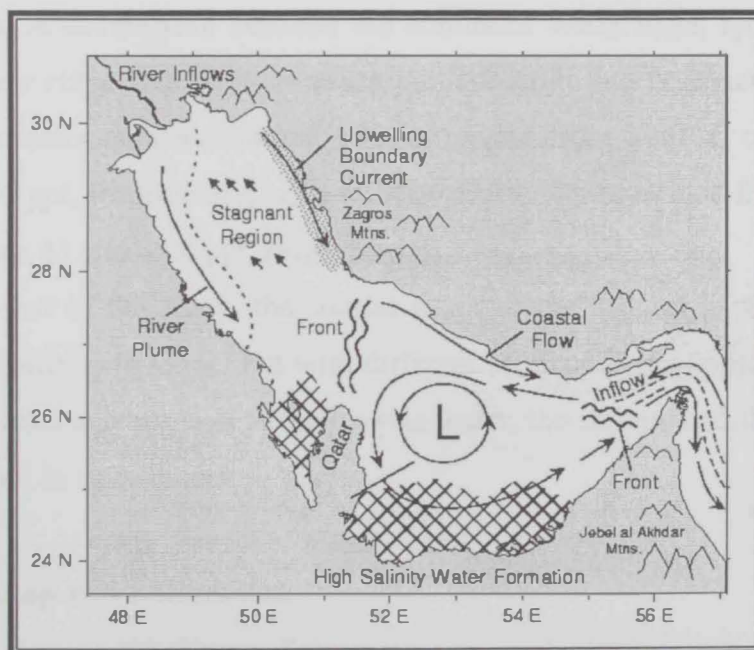
Figure 3.7: Circulation schematic for the Arabian Gulf (RSMAS, 2000)

3.3 Local Model (Ruwais Coastal Water)

Ruwais coastal water is a part of the southern shallow shelf of the Arabian Gulf. The area has an average depth of about 20 m, while the eastern part of it is shallow (less than 2 m) and contains salt marshes (Sabkha). The dynamics of the coastal water in the Ruwais shore line is characterized by well mixing due to the shoal of the region in addition to sinuosity of the bottom which leads to tidal flat in the eastern side. This mixing process keeps the water unstratified over the whole year (Elshorbagy *et al.*, 2004c). The effluents from the Ruwais Industrial Complex are the most influential at the coastal water, by reason of the relatively high temperature and salinity of these discharges. Continuous dumping of these effluents in the coastal water, may threat the marine biochemistry and water quality in general, and their effects may extend to a cultivated Sir Bani Yas Island in particular.

In the last few years, several numerical modeling studies were carried out to investigate the hydrodynamic characterization of the Ruwais region. Azzam *et al.* (2004) and Elshorbagy *et al.* (2004d) are considered as the most relevant of these studies due to the comprehensive levels of measurements conducted and results obtained. The studies produced considerable detail about the bathymetry, tides, temperature and salinity of the region. They used the Japanese modeling software mentioned earlier (COSMOS) with a resolution of 200m x 200m to resolve the area hydrodynamics. A comparison between the simulated water level, temperature, and salinity and their respective measurements produced fair and reasonable agreement. The average summer temperature and salinity ranged from 32.0 $^{\circ}$C to 32.7 $^{\circ}$C and from 45.5 to 46 ppt, respectively, whereas, the winter values ranged from 20.5 $^{\circ}$C to 21.2 $^{\circ}$C and from 45.5 to 46.0 ppt, respectively.

In this part of the study, the coastal water of the Ruwais is simulated using COSMOS hydrodynamic model but with different setup specifications. In addition to discussing the tides and currents at the Ruwais water, the salinity and the temperature will be addressed in more detail.

3.3.1 Model Setup and Calibration

The numerical model of the Ruwais is nested inside the regional model of the entire Arabian Gulf to adopt the boundary flow data. The regional model has its boundary at the Strait of Hormuz. The grid size of the local model was selected to be 1km, so that

long term ecological simulations can be conducted using the same model within reasonable times. The sea surface area used in the local modeling is 374 km^2. The horizontal distributions of the grids are 26 east-west and 22 north-south grid steps (Fig.3.8). The water column consists of 6 layers having the same distribution used in the regional model, i.e. 4, 6, 10, 20, and 30m. Tidal constituents, temperature and salinity for the three open boundaries are nested from the regional Gulf model using the sub-model software, COSBND while the initial values of same variables are nested using the sub-model software, COSINIT. Other computational conditions used in the modeling are also listed in Table 3.3.

Since the outfalls of these facilities are close to each other, they are categorized into three outlets. Outfall (1) includes an oil refinery and gas production plant. Outfall (2) includes desalination plant, power plant, sulfur and fertilization units. Outfall (3) includes only the effluent of the petrochemical factory (Borooj). Each group of these discharge sources has different flow rates with different temperature and salinity values as summarized in Table 3.2.
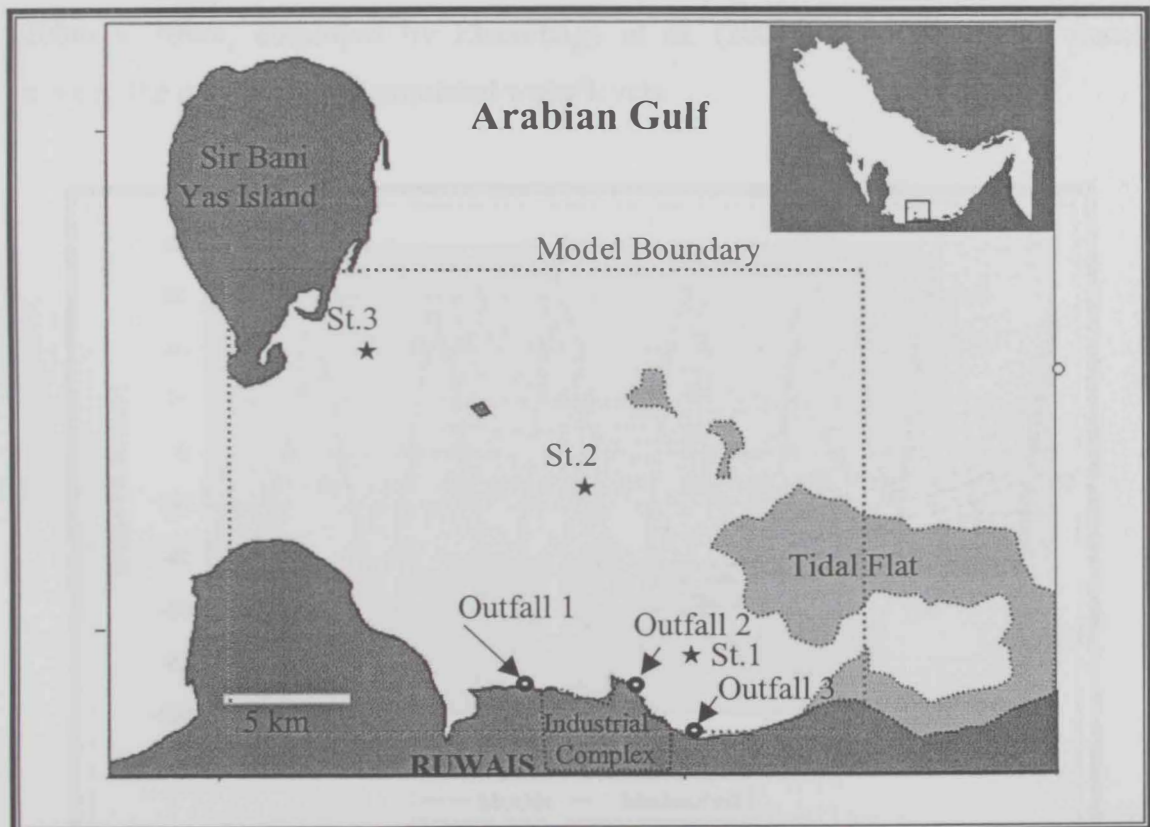
Figure 3.8: Map of Ruwais coast. The dotted line shows the model boundary and the stars (★) indicates the location of the observation stations.

Table 3.2: Inflow sources in the Ruwais costal water

	Utility	Q $(m^3.day^{-1})$	T Summer (° C)	T Winter (° C)	Salinity (ppt)
Outfall 1	Oil Refinery (TAKREER)	243600	30.0	23.0	46.0
	Gas Production Plant (GAZCO)	600000	45.0	35.0	46.0
	Total	*843600*	*40.7*	*31.5*	*46.0*
Outfall 2	Desalination and Power Plant	192000	45.0	40.0	70.0
	Fertilization Factory	120000	40.0	35.0	46.0
	Total	*312000*	*43.1*	*38.1*	*60.8*
Outfall 3	Petrochemical Factory (Borooj)	*840000*	*45.0*	*35.0*	*50.0*

The local model of Ruwais is calibrated using the measurements of the water level conducted near Sir Bani Yas Island during the period between June, 23rd, 2003 and June, 29th, 2003. Figure 3.9 shows a comparison of the measured and the simulated values. It shows fair agreement in the amplitude and the phase during the considered period with some deviations in the amplitude at the first few days within the neap-tide period. This may be due to the coarse grid used in the model, where the finer grid (200m x 200m) employed by Elshorbagy *et al.* (2004d) produced better match between the measured and simulated water levels.
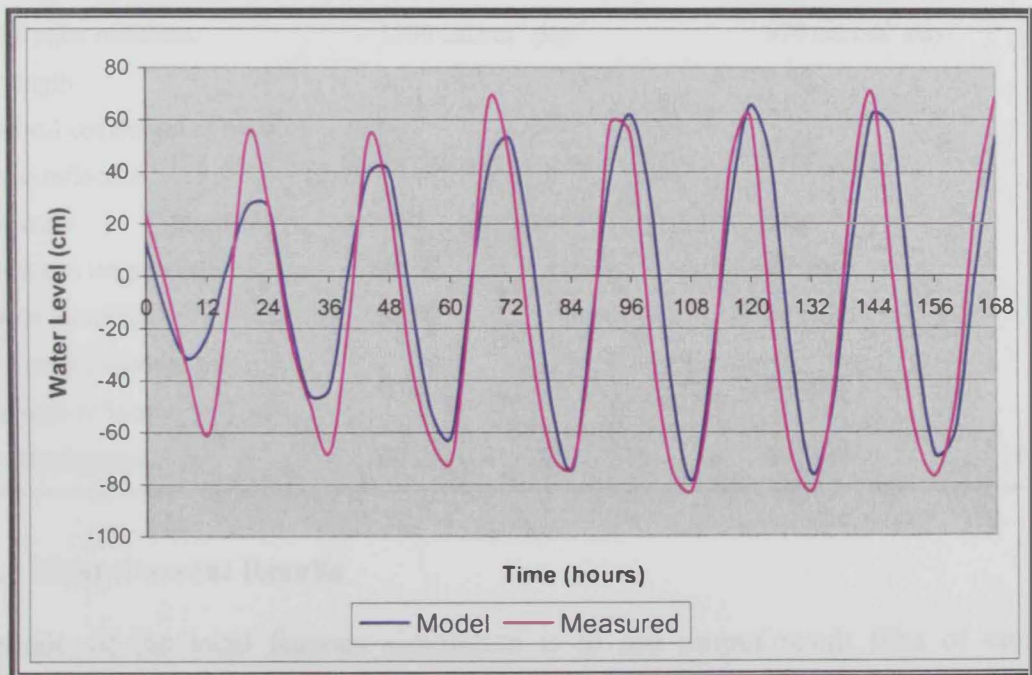
Figure 3.9: Comparison of measured and simulated water levels at Sir Bani Yas Island at the period from 23rd, June, 2003 to 29th, June 2003.

Table 3.3: Computational conditions of the hydrodynamic model for the Ruwais coastal water

Parameter	Selected value	
Area	Ruwais coastal water with sea surface area= 374 km^2 (Fig. 1).	
Grid size	1 km	
Number of horizontal meshes	26 (east-west) x 22 (north-south)	
Vertical layer locations	*6 vertical layers*	
	Level 1: from surface to -4, Level 2: from -4 to -10	
	Level 3: from -10 to -20 , Level 4: from -20 to -40	
	Level 5: from -40 to -70 , Level 6: from -70 to the bottom	
Inflow conditions	Three inflow sources at the south, they are listed in Table 3.2	
Tidal constituents for the boundary conditions	Nested from the regional Gulf model	
Temperature and Salinity for the boundary	Nested from the regional Gulf model	
Wind condition	Records from offshore metrological station in the Ruwais	
Model parameters		
Coriolis parameter	$6.376 * 10^{-5}$ s^{-1}	
Friction coefficient for seabed	0.0026 (assumed)	
Wind friction coefficient at the sea surface	0.001	
Horizontal and vertical eddy viscosity and diffusivity	$1.98 * 10^6$ m^2.s^{-1}	
Metrological conditions	*Summer*	*Winter*
Global solar radiation	1500 cal.cm^{-2}.day^{-1}	970 cal.cm^{-2}.day^{-1}
Day length	0.57	0.50
Empirical coefficient of solar altitude reflection	0.35	0.35
Cloudiness	0.01	0.01
Daily mean temperature	30 °C	20 °C
Relative humidity	53 %	60 %
Empirical constant of the cloudiness reflection	0.65	0.65
Calculated period	60 days	60 days

3.3.2 Mean Current Results

The aim of the local Ruwais simulation is to use output result files of currents, temperature and salinity spatial distribution as initial conditions to the water quality numerical model (EUTROP). This should allow studying the effect of temperature

and salinity on the coastal water at present time and its long term impacts in the future.

Figure 3.10 shows the mean currents calculated over the 2-months of summer simulation period. The mean currents are very week in the southern part of the Ruwais coast (<3 cm/s), as the water there is almost stagnant whereas relatively strong currents exist at the northern eastern side of the area and move outside the model boundary as the velocity may exceed 7 cm/s. In general, the water enters the area from the western boundary and the northern part of the eastern boundary while flow exchange (inflow/ outflow) takes place at the northern boundary. The mean flow field produced from the winter simulation is fairly close to the summer one.
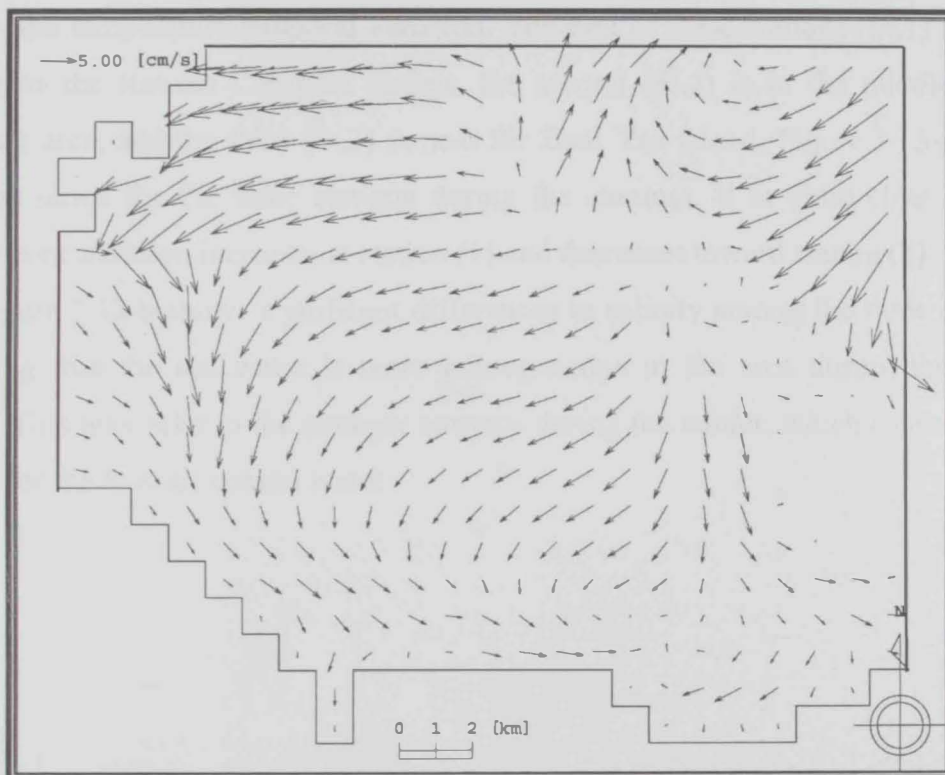
Figure 3.10: Mean currents in the Ruwais coastal water during the summer season.

3.3.3 Salinity and temperature horizontal distributions

Salinity Distributions

As shown in Figure 3.11, the salinity values range between 44.5 to 46.3 ppt during the summer season. Such distribution is attained at the end of 2-month simulation over the period of June 1st to August 1st, 2003. It's noticeable that the salinity increases toward the shoreline, this refers to shoal of the water at the shore, which causes more

evaporation, hence higher salinity. The most saline zone concentrates near the outlets of the Ruwais Industrial Complex, where the salinity there reaches up to 46.3 ppt; this refers to the high saline water which discharges from the desalination plant increasing the salinity of water near the outlet area. The salinity near Sir Bani Yas Island is about 45.0 ppt, this value coincides with other investigations (Elshorbagy *et al.*, 2004c). The dark blue areas with zero salinity value at the figures refer to tidal flat zones.

During winter season (Fig. 3.12), salinity distribution is almost similar to summer trend where the salinity increases toward the shoreline and decreases offshore. The salinity ranges between 43 to 45.3 ppt. Also, the most saline water concentrates near the Ruwais outlets, where the salinity reaches up to 45.3 ppt. Three stations were selected on the modeled area; St.1, St.2, and St.3 (Fig. 3.8), to trace the salinity and temperature temporal variation. The first of these stations (St.1) is in the vicinity to the Ruwais Complex outlets, the second (St.2) is in the middle of the modeling area, and the third (St.3) is near Sir Bani Yas Island. Figure 3.13-a shows the time series for the three stations during the summer. It is quite clear that the salinity concentration increases at station (1) and decreases toward station (3).

Figure 3.13-b shows significant differences in salinity among the three stations, indicating that the sea water is more homogeneous in the area during the winter season. This may refer to the stronger currents during the winter, which causes higher mixing for the Ruwais coastal water.
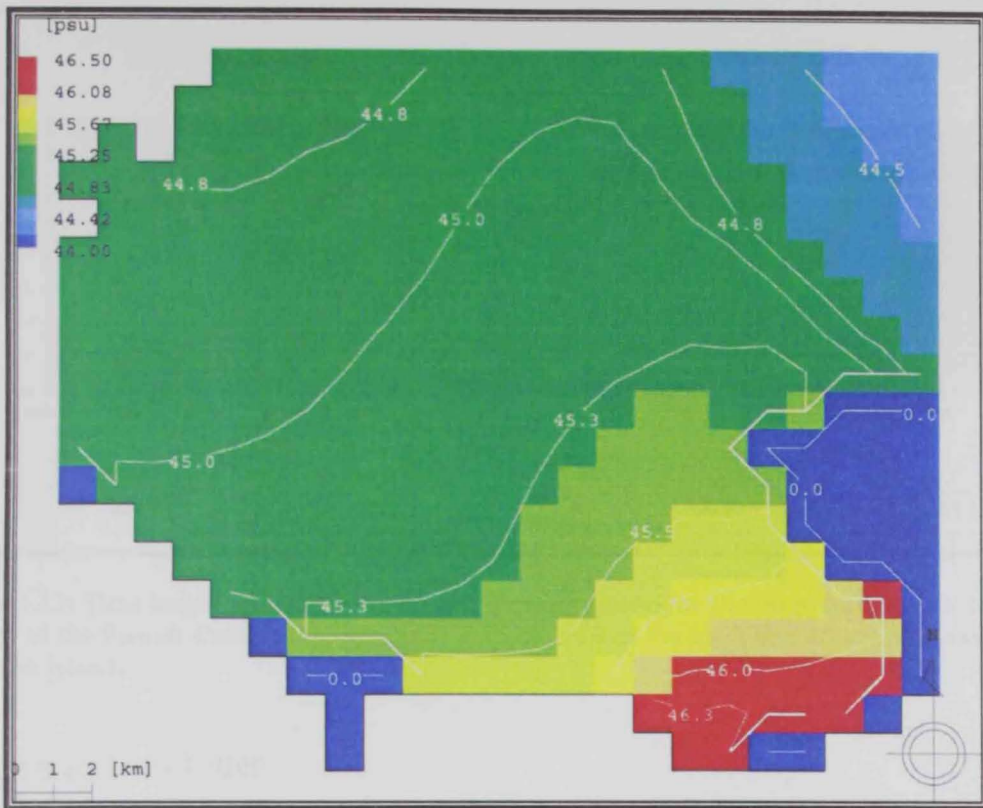
Figure 3.11: Salinity spatial distribution during the summer season.
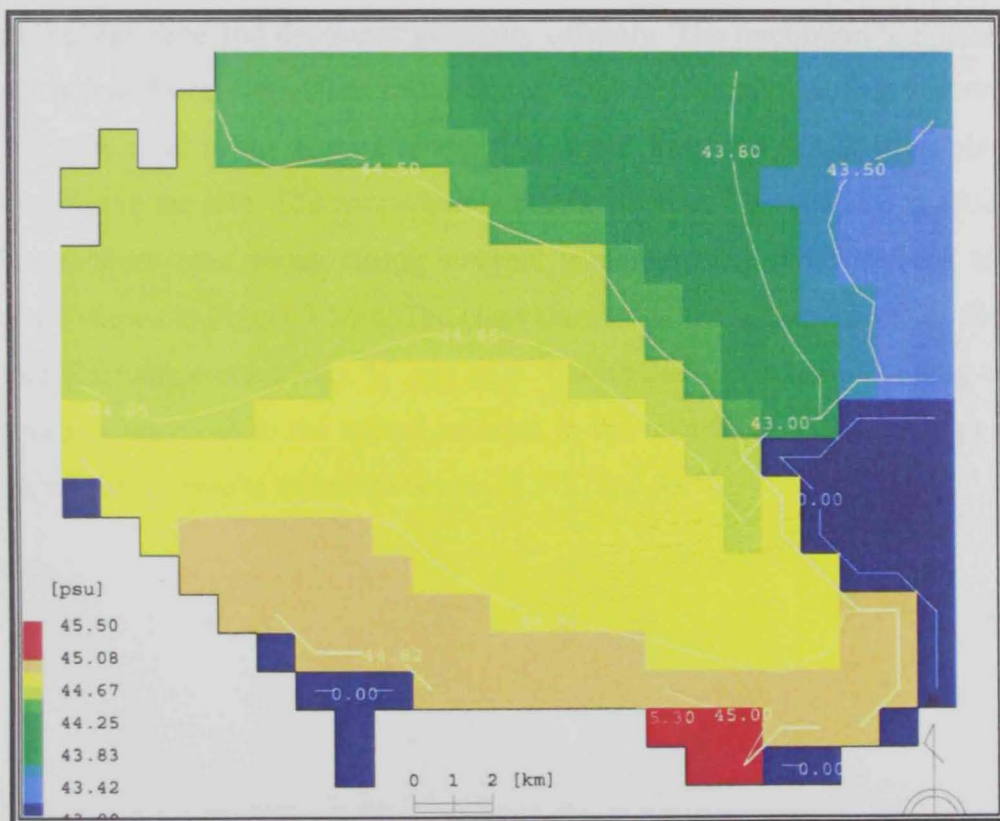
Figure 3.12: Salinity spatial distribution during the winter season.
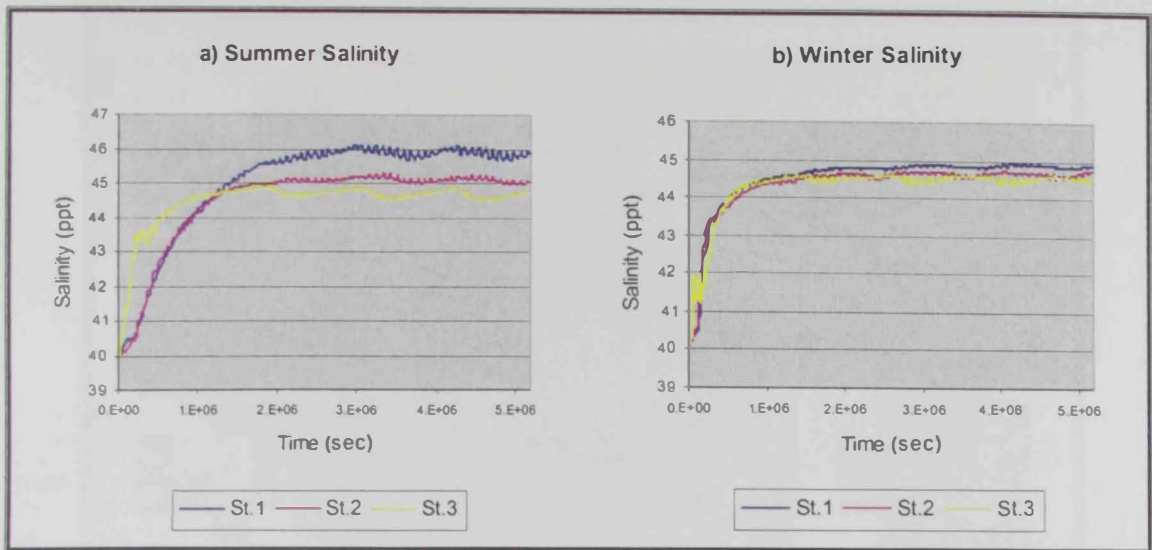
Figure 3.13: Time series for salinity during the summer season for the three stations, (St.1: in the vicinity of the Ruwais Complex outlets. St.2: in the middle of the modeling area. St.3: near Sir Bani Yas Island).

Temperature Distribution

Distribution of the summer temperature in the surface Ruwais coastal water is shown in Figure 3.14. The temperature ranges between 31.5 °C to 33.4 °C, where it increases toward the shoreline and decreases gradually offshore. The maximum temperature in summer is found near the outlets of the Ruwais Industrial Complex that is about 33.4 °C. This may refer to the wormer water discharged form the desalination plant and other utilities in the area. The temperature near the Sir Bani Yas Island was about 33.2 °C. Temperature time series during summer season for the three stations selected earlier are shown in Figure 3.16-a. The chart shows that the temperatures for the three locations fluctuate around 33.3 °C and 33.8 °C with the maximum prevailing at St.1. These values are close to the values reported in the other studies (Elshorbagy *et al.*, 2004c), where the results ranged between 30.5 °C and 33 °C.
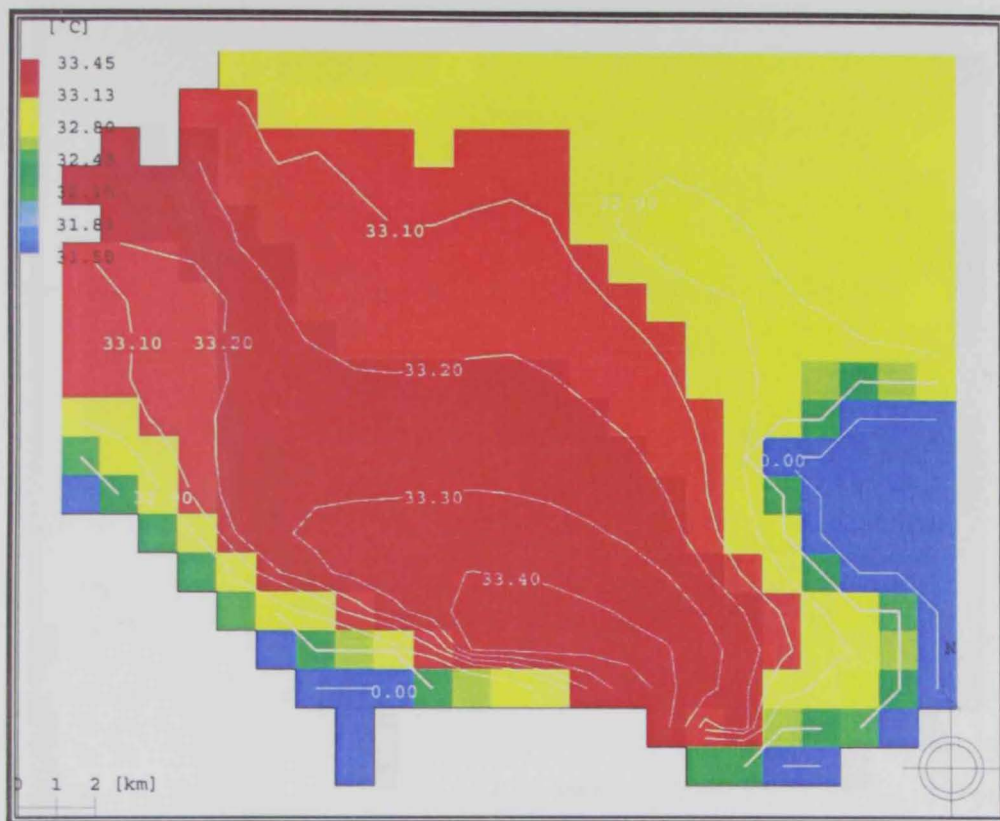
Figure 3.14: Temperature spatial distribution during the summer season.

Figure 3.15 shows the distribution of the temperature for the Ruwais area during winter season. The temperature ranges between 21 to 22 °C. The narrow range of the surface temperature variation for the area shows that the temperature distribution is quite homogenous over the modeled zone. It is worth mentioning that the highest water temperature is near the outlets of the Ruwais Industrial Complex, where the temperature there reaches up to 21.7°C. Figure 3.16-b shows the temperature time series for the three stations during winter where it shows a very slight difference with temperature variation at the stations.

Table 3.4 summarizes the average temperature and salinity for the three observation stations. It shows that there are about 12 °C differences between summer and winter seasons, and about 0.5 ppt. differences for the salinity.
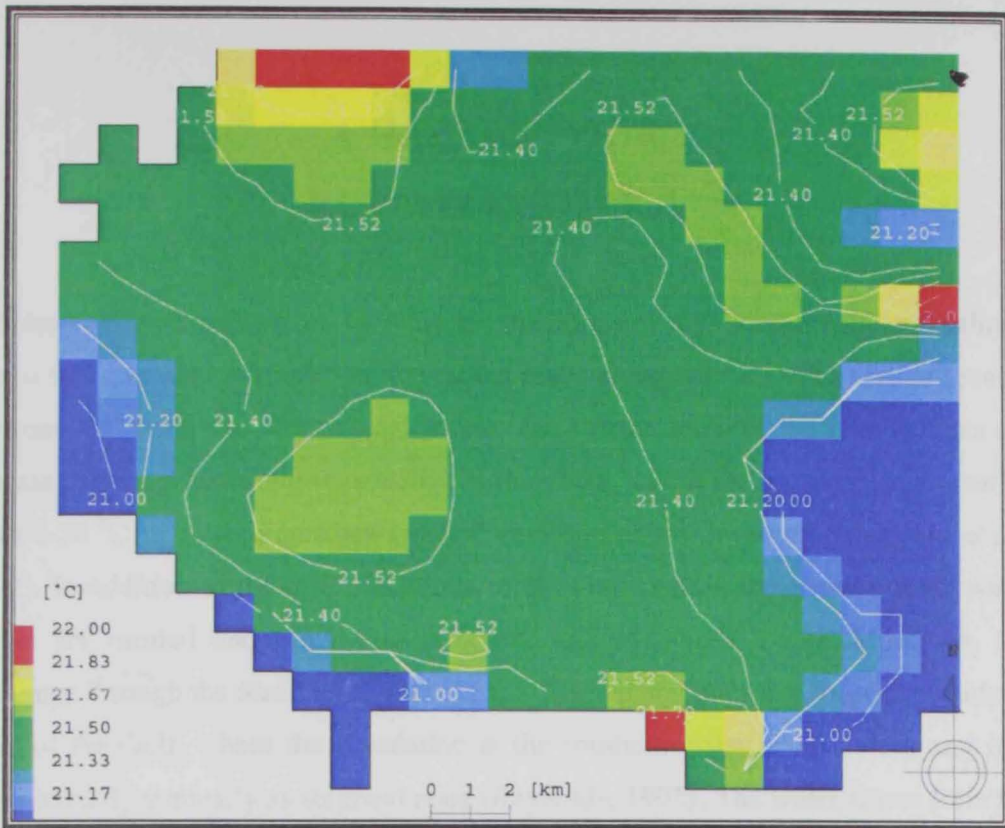
Figure 3.15: Temperature spatial distribution during the winter season.
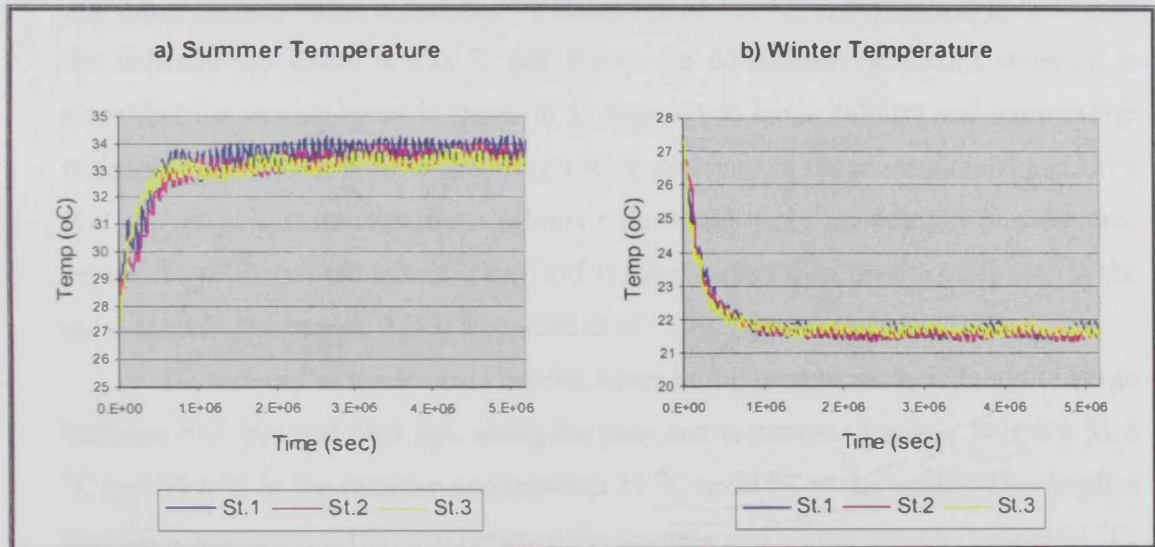
Figure 3.16: Temperature temporal variation during the summer and the winter seasons, (St.1: in the vicinity of the Ruwais Complex outlets. St.2: in the middle of the modeling area. St.3: near Sir Bani Yas Island).

Table 3.4: Average temperature and salinity in summer and winter at the three selected stations.

	Summer		Winter	
	Temperature (°C)	Salinity (ppt.)	Temperature (°C)	Salinity (ppt.)
Station 1	33.78	45.83	21.66	44.86
Station 2	33.39	45.00	21.51	44.68
Station 3	33.25	44.71	21.6	44.50

CHAPTER FOUR
RUWAIS ECOLOGY

Arabian Gulf is characterized by extreme conditions of high temperature and salinity due to the extensive evaporation rate taking place along the year. The Gulf is located between the temperate and tropical zones. The marine biota of the Gulf reflects the climate pattern with strong seasonality in the north, where the air temperature varies from 0-50 °C to a more constant tropical environment in the south (Sheppard *et al.*, 1992). In addition to the arid conditions of the Gulf region, the riverine fresh water inputs are limited and the evaporation rate exceeds these inputs. Moreover, the exchange through the Strait of Hormuz is also limited and does not cover the southern shelf of the Gulf, where the circulation at the southern coast is very weak and it is considered dynamically as stagnant zone (Reynolds, 1993). The water enters from the Strait of Hormuz with a salinity ranged between 36.5 ppt to 37.0 ppt (Sheppard *et al.*, 1992), where the salinity reaches 42 ppt at the Bahraini coast in the west and the maximum salinity value is detected by Basson *et al.* (1977) in the Gulf of Salwah near the Bahraini too where it was 70 ppt. Given the conditions introduced above, it is clear that the marine biota in the Gulf is exposed to harsh salinity and temperature regimes. This type of regime produces a wide diversity of the marine fauna and flora that can adapt with such extreme salinity values and water temperature fluctuations; hence, the primary production in the Gulf is often higher than for the other seas in the same latitude (Sheppard, 1993; Sheppard *et al,*. 1992; Price *et al.*, 1993).

The salinity in the Ruwais marine water in the present study is found to range between 43.0 ppt and 46.3 ppt. along the year and temperature ranges between 31.5 °C and 33.4 °C in the summer and between 21 °C to 22 °C in the winter. This implies that the temperature difference between the summer and winter season is about 11 °C.

In order to use the water quality modeling software "EUTROP", different water quality parameters from the Ruwais marine water are needed. These data include phytoplankton biomass (mgC/m³), zooplankton biomass (mgC/m³), particulate organic mater (POC), dissolved organic matter (DOC), phosphate concentration (PO_4), ammonium concentration (NH_4), nitrite concentration (NO_2), nitrate concentration (NO_3), dissolved oxygen concentration (DO) and chemical oxygen demand concentration (COD). The model employs the temperature, salinity,

and flow dynamic data provided by the hydrodynamic model resolved earlier. In the present chapter, the field sampling and in situ measurements are briefly described, followed by the laboratory analysis methods employed to quantify the different parameters. The second part of the chapter will describe the marine ecology of the Ruwais in the light of the measurements and the experimental results. It is worth mentioning that the ecological description here will be only limited to lower trophic level in the water column as it will be the case for the numerical simulation introduced later.

4.1 Field Sampling

Observation of coastal water quality in the Ruwais marine water was performed from June 2003 to January 2004. Sampling campaigns were carried out by a team from the UAE University using different boats provided by the local marine authorities. The work was part of an externally funded research project conducted in the UAE University. The water quality and ecological data described here are all obtained from scientific papers that are now revised and processed by international journals after received the necessary approval and publication release from relevant sponsors; mainly TAKREER oil company. Four field sampling expeditions were done. Three of them were at the beginning of spring, summer and autumn season (June, August and November, respectively), and the last one at the end of winter (January).

Water sampling and in situ measurements were done at 10 selected locations scattering near the coastal line in the Ruwais study area. Figure 4.1 shows the station locations numerated from S1 to S10. In situ measurements carried out for salinity and temperature whereas the water samples for phytoplankton, zooplankton, dissolved oxygen (DO), nutrients (Nitrate, Nitrite, Ammonia, and Phosphate), total organic carbon (TOC), and dissolved organic carbon (DOC) were collected, preserved and later sent back to the laboratories of UAE University for analysis. The sampling methods employed during the field work can be summarized as the following.
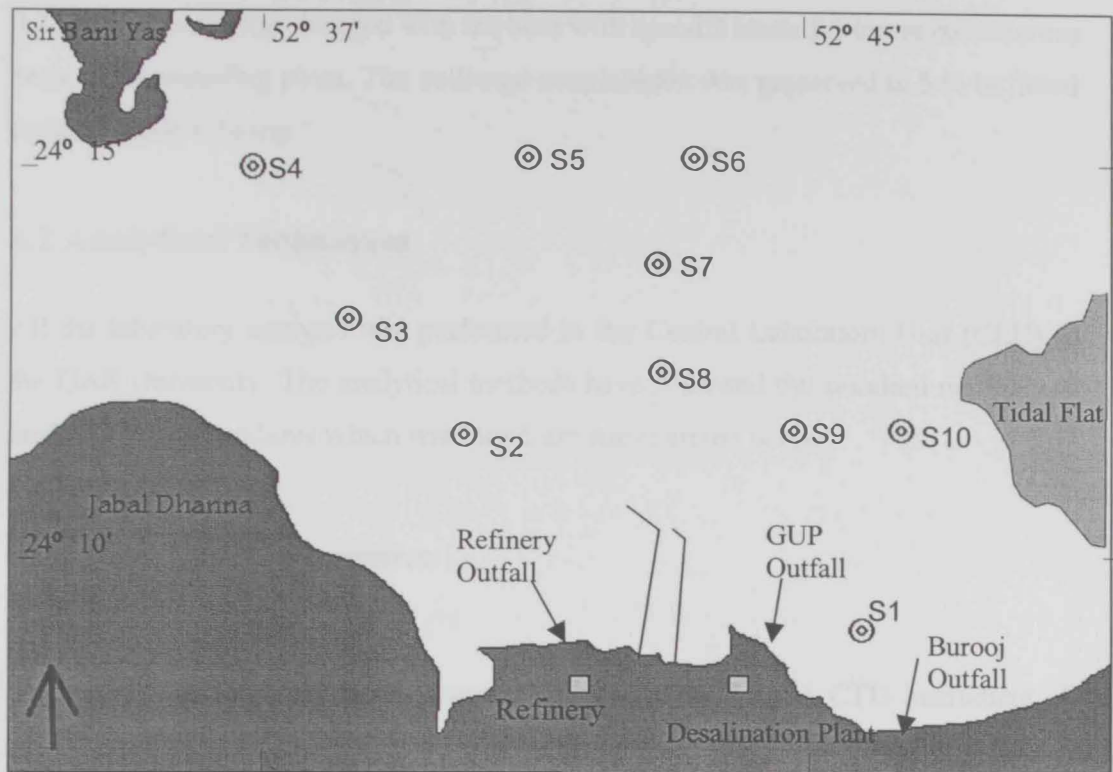
Figure 4.1: Ruwais coast and locations of measurement stations (⊚) (Elshorbagy *et al.*, 2004d)

4.1.1 Water Quality Sampling

For nutrients, TOC and DOC analysis, three water samples for each analysis were collected in every station at three depths; surface, middle and bottom. The sampling was done using a Niskin water sampler with closing mechanism. Samples for TOC and DOC were filled in a dark glass bottles and preserved in ice after lowering its pH to less than 2.0 using Hydrochloric acid, whereas the nutrient samples were collected in clean glass bottles and preserved in ice too.

4.1.2 Biological Sampling

Sampling for phytoplankton pigments and community structure was done by Niskin water sampler at three levels; surface middle and near bottom. Samples for phytoplankton cell count were preserved by adding a calculated amount of Lugol's solution to the samples. Whereas, samples for phytoplankton pigment estimation were preserved in ice boxes to be transported later to the laboratories.

        Sampling for zooplankton was carried out by collecting zooplanktons by oblique hauls using a Horon Tranter net (mesh size 300 microns and mouth area of

0.25 m^2). The net was dragged with the boat with speed 2 knots for ten minutes across each of the sampling point. The collected zooplankton was preserved in 5 % buffered formaldehyde solution.

4.2 Analytical Techniques

All the laboratory analysis was performed in the Central Laboratory Unit (CLU) in the UAE University. The analytical methods have followed the standard methods of analysis. The procedures which were used are summarized below.

4.2.1 Water Quality Parameters

Temperature and Salinity

Temperature and salinity were measured in the field by using CTD instrument. A heavy weight was tied with the CTD sensor to keep the cable almost vertically; hence the measured depths are around the actual depths mentioned at Admiralty charts. Temperature and salinity were recorded at three levels; surface, middle and bottom.

Dissolved Oxygen

DO was determined using Winkler methods described in Standard Methods, 1995, APHA. Many measurements were also made in-site using DO probe and cross-checked with the analytical results

Nutrients

The nutrients which are, Nitrate-nitrogen, Nitrite-nitrogen and Ammonia-nitrogen were estimated by using HACH DR/4000 spectrophotometer in the light of the instrument manual procedures (HACH company, 1999) and Phosphate-phosphorus is measured by using ICP equipment in the Central Laboratory Unit (CLU) of UAE University.

TOC and DOC

In order to measure the organic carbon (TOC) concentration in sea water, total organic carbon analyzer (Shimadzu V$_{chs}$) was used. It was used to measure the total

carbon (TC) first and then the inorganic carbon (IC). The difference between them is called total organic carbon (TOC). The measurement procedure by using total organic carbon analyzer (TOC-V$_{chs}$) can be summarized as the following:

- Five standard solutions were prepared with different known TC and IC concentrations (100 ppm, 50 ppm, 20 ppm, 10 ppm, and 5 ppm) per each.
- The calibration curve was constructed at the instrument (TOC-V$_{chs}$) using the solutions mentioned in step 1.
- After the calibration curve was prepared, the measurement of the samples was made. The results obtained were TOC values which were (TC –IC) in ppm.
- To measure dissolved organic carbon (DOC), the same procedure was followed as step 1 and 2 but the samples were pre-filtered using glass filter papers (GF 6, Glasfaser Rundfilter, Dia 70 mm) soaked in deionized zero-organic water for 48 hours.

4.2.2 Biological Parameters

Phytoplankton Pigments

Absorbance of acetone extract at wavelength 665 and 750 nm method was used to determine phytoplankton pigments (Chlorophyll-a). The sample was treated earlier by 0.1N HCL acid (Standard Methods, 1995, APHA).

Zooplankton

Displacement method was utilized to determine zooplankton biomass. 300 micron filter nylon plankton net was used to filter the sample. The animals retained on the net were measured by displacement of same amounts of water. To estimate zooplankton population, the sample was washed off excess formaldehyde, sub sampled and stereo microscope was used to estimate the population qualifiedly and quantatively (Standard Methods, 1995, APHA).

4.3 Ecological Description of Ruwais Area

The study area, Ruwais costal water, is characterized by well mixing conditions so; the stratification phenomenon is not a common feature in the region. This well mixed water column is attributed to several reasons, such as, the shallowness of the area, the wide tidal flat zone which is located at the east in addition to sinusoidal nature of the seas bed at the area which helps the mixing process to take place in an efficient way. Elshorbagy *et al.* (2004e) reported that over a 12-hour of the spring tide; the influx volume is equal to one third of the entire basin volume. This shows that on the average, one third of the basin volume (shifted to the west and north) is renewed each 12 hours. This refreshing allows to the northern western part of the area to mix with the Gulf water, hence to dilute the concentration of the pollutants which is emitted from the oil tankers and oil pipelines located in the area. On the other hand, the eastern and southern parts of the study area are exposed to weak water currents with average ranges from 5 to 20 cm/s. These delicate currents enhance stagnancy conditions of the eastern and southern sides, hence the flushing process is weak so that pollutant concentrations build up continuously causing adverse effects on the water quality and the marine ecology of the area.

In this part of the study, the ecological characteristics of the Ruwais marine water is discussed on the light of the environmental data obtained from a previous study done by Elshorbagy *et al.*, 2004d. Measurements of water quality and biological parameters are averaged over the ten selected sampling stations and tabulated in Table 4.1. The measurements include the results for the four trips June 03, August 03, November 03, and January 04. These parameters include phytoplankton biomass, zooplankton biomass, particulate organic carbon (POC), dissolved organic carbon (DOC), nitrite (NO_2-N), nitrate (NO_3-N), ammonium (NH_4-N), phosphate (PO_4-P), chemical oxygen demand (COD) and dissolved oxygen (DO).

This results interpretation will be the onset for the water quality modeling interpretation in the following chapters, and it will illustrate the relation among the different water quality parameters, and how they interact with each other.

Table 4.1: Monthly average variation of measured parameters at surface layer

	Phytoplankton (mgC/m³)	Zooplankton (mgC/m³)	POC (mg/m³)	DOC (mg/m³)	PO_4-P (µM)	NO_3-N (µM)	NH_4-N (µM)	NO_2-N (µM)	COD (mg/l)	DO (mg/l)
Jun. 03	0.78	0.74	3206.9	1592.2	0.88	68.6	1.8	0.30	10.1	5.75
Aug. 03	4.42	0.93	525.1	2131.4	1.08	71.4	2.7	0.23	13.5	5.95
Nov. 03	7.25	1.92	869.7	3407.2	0.62	77.4	1.6	0.36	21.6	3.59
Jan. 04	3.83	0.56	309.5	2630.1	1.18	64.8	1.4	0.34	16.7	6.55

4.3.1 Biological Productivity

<u>Phytoplankton</u>

In the present study, phytoplankton term refers to micro-phytoplankton species with size larger than 20 microns.

Information regarding phytoplankton densities in the Arabian Gulf is very rare (Elshorbagy *et al.*, 2004e). Table 4.2 lists some counts reported in the Arabian Gulf and other near water bodies.

Table 4.2: Phytoplankton counts in different coastal waters.

Counting location	Phytoplankton counts per liter	Reference
Ruwais coastal water	15.4×10^3	Elshorbagy *et al.*, 2004e
Dubai offshore	$135.8 - 245.2 \times 10^3$	Dubai Municipality, 1996
Dubai Greek Lagoon	$7828 - 8444.7 \times 10^3$	Dubai Municipality, 1996
Goa coastal water	30.0×10^3	Qasim, 1979

The table shows that the phytoplankton counts in the Ruwais coastal water is very low compared with the other counts even in the UAE coast. The count in Goa is more closer to the Ruwais count, while the values in Dubai offshore is significantly greater than the Ruwais counts, whereas, Dubai Creek Lagoon undergoes a eutrophication conditions, so the counts there is extremely high.

The low values of phytoplankton counts in the Ruwais coastal waters may be due to several reasons, the most important of which is the overwhelming dosing of

chlorine at the intake of different facilities spreading along the coast. This practice has taken place in the area for so many years to kill jelly fish and large fishes to prevent them from entering with the influent water to avoid pump damages. Chlorine is added in many cases in an uncontrolled manner so that a reasonable estimation of its level becomes infeasible. Another reason of low phytoplankton biomass is the high levels of hydrocarbon components which are produced from the oil activities in the region such as filling tankers with oil, evacuation of ballast water from tankers in the Ruwais basin, some oil spill accidents, in addition to the effluent discharging from the different utilities in the Ruwais Industrial Complex. All of these activities produce high amounts of hydrocarbon components which may have hazardous effects on the phytoplankton biomass. Other reason is related to higher salinity concentration in the water (45- 46 ppt) in the Ruwais area. Limitation of some nutrients such as Phosphate (to be discussed later), may be also one of the reasons.

Phytoplankton Pigments

Chlorophyll-a concentration in the coastal water is considered as an effective method to measure the amount of phytoplankton in the marine water, whereas the existence of photosynthetic pigments in the sea grass is sufficient indication for the primary production. The availability of the pigments in the sea water may color it and eventually affect its transparency. As a result, the amount of light penetrating the sea surface may be reduced and the photosynthesis process is decreased causing a depletion of the dissolved oxygen that can affect most of the aquatic life. The measured values of chlorophyll-a concentration in the area ranged from 0.83 to 1.39 mg/m^3. The estimation of chlorophyll-a via satellite images is a primary tool to determine the eutrophication state of the estuaries and lakes and to assess their water quality conditions. Figure 4.2 shows a satellite image for the chlorophyll-a concentration at the UAE costal water. The Ruwais area marked with blue box in the west, is characterized by low productivity due to low concentration of chlorophyll-a, as the pigments concentration ranged between 0.5 to 1.5 mg/m^3. The image supports the findings of low primary production reported by the considered measurements in the Ruwais basin.
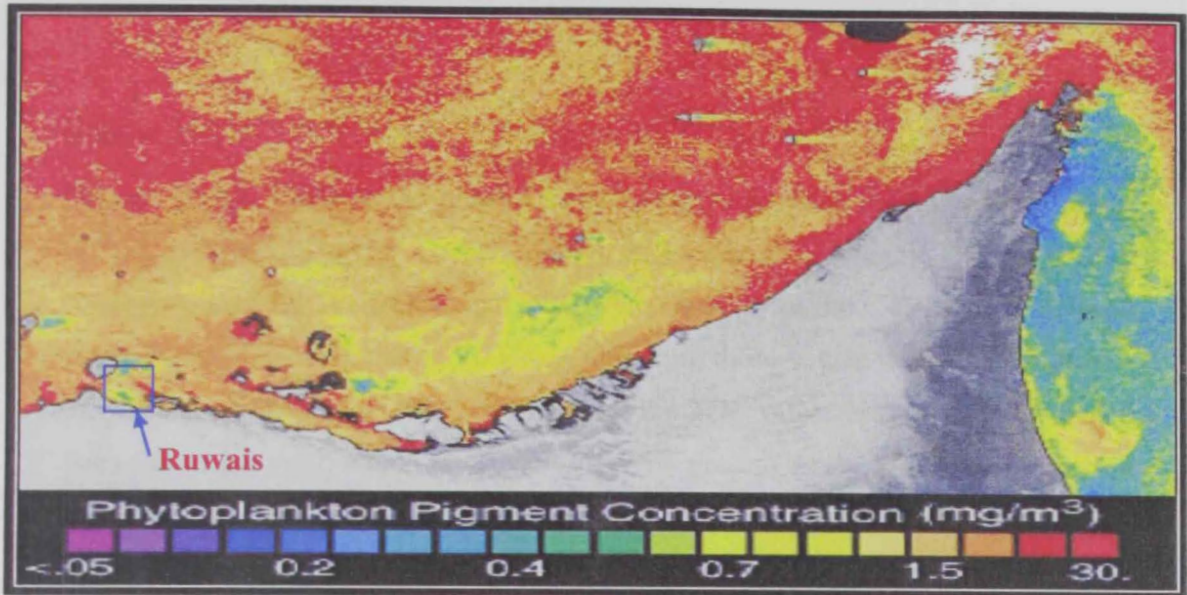
Figure 4.2: Satellite image of phytoplankton pigment concentration in UAE coastal water (NASA, 1989)

Phytoplankton Biomass

Phytoplankton biomass is represented by the mass of carbon which forms the phytoplankton cells. The units of phytoplankton biomass expressed as milligram carbon per cubic meter is the suitable form to use in the water quality numerical model "EUTROP". Raymont's approach (Raymont, 1983) which depends on the average Carbon/ Chlorophyll-a ratio of 15.3 (Cushing, 1958) is utilized in the current work to determine the phytoplankton carbon biomass. The average calculated values of phytoplankton biomass in the study area ranged from 0.26 to 10.9 mgC/m^3, where some reported values in the Arabian Gulf measure to be > 4 gC/m^3 and reach 15-18.9 gC/m^3 at the northern areas if the Gulf (Al-Yamani et $al.,$ 1997a, 1997b).

Figure 4.3 shows the variation of the phytoplankton biomass over the four sampled months during the current work. It is noticeable that there is an increasing trend of phytoplankton biomass in the summer months that may refer to rising of the water temperature. Whereas, the biomass decreases in the winter season related to decrease in the temperature as the temperature is one of the main parameters affecting the growth rate of the phytoplankton.

Organic Matter

Organic matter (OM) in the present study is represented as Total Organic Carbon (TOC), Dissolved Organic Carbon (DOC), and Particulate Organic Carbon (POC). Average values for TOC, DOC and POC were found to be 3.67, 2.44, and 1.23 mg/l respectively (Elshorbagy *et al.* 2004e). Comparing these values with other studies in the Arabian Gulf, Emara (1998) reported that the TOC values near UAE coast ranged from 0.8 to 3.9 mg/l, which is very close to the present work. Whereas comparison with other oceanographic literatures (Starikova, 1970 and Williams, 1975) showed that TOC at the UAE coastal water is higher than those in the other parts of the world. This may refer to excessive activities of oil and petrochemical industries in the region, which produce a lot of hydrocarbon compounds due to oil spill and effluent discharging from refineries. Referring to Table 4.1, it's noticed that POC level was much higher in June 2003 than other months, apparently caused by the turbulence in the water column caused by the prevailing strong wind conditions during the sampling time. On the other hand, DOC level was higher in November than the other months. This refers to an oil spill accident associated with a fracturing of oil line occurring toward the end of October 2003, so its effects extended up to November 2003.

Chemical oxygen demand (COD) levels in the Ruwais coastal water ranged between 8.5 to 25.2 mg/l. These values are higher than values in most of the world (Elshorbagy *et al.*, 2004e) oceans. This may again refer to high hydrocarbon levels in the water due to oil pollution and petrochemical activities.

Carbon/Chlorophyll-a Ratio

Carbon/Chlorophyll-a ratio in the present study ranged from 0.98 to 7.55, while Cushing (1958) suggested this ratio to be in the range of 13.6 to 17.3. This wide deviation may refer to uncounted species of smaller size cells of phytoplankton such as nanoflagillates, naked dinoflagellates, and picoplankton where as mentioned earlier; the counted species covered only the phytoplankton sizes larger than 20μm. Taking the small-size species into account can potentially raise the calculated ratio of carbon/Chlorophyll-a, where several recent studies reported that the picoplankton, for example, can significantly contribute to the primary production in some coastal waters (Estrada, 1985; Kimor *et al.*, 1987; Abdel-Moati, 1990). Due to limitation in

experimental and analytical resources in addition to restricted time for the current study, such species were not taken into account. Thus, the numerical simulation introduced later calculates the phytoplankton biomass for cells larger than $20\mu m$ only.
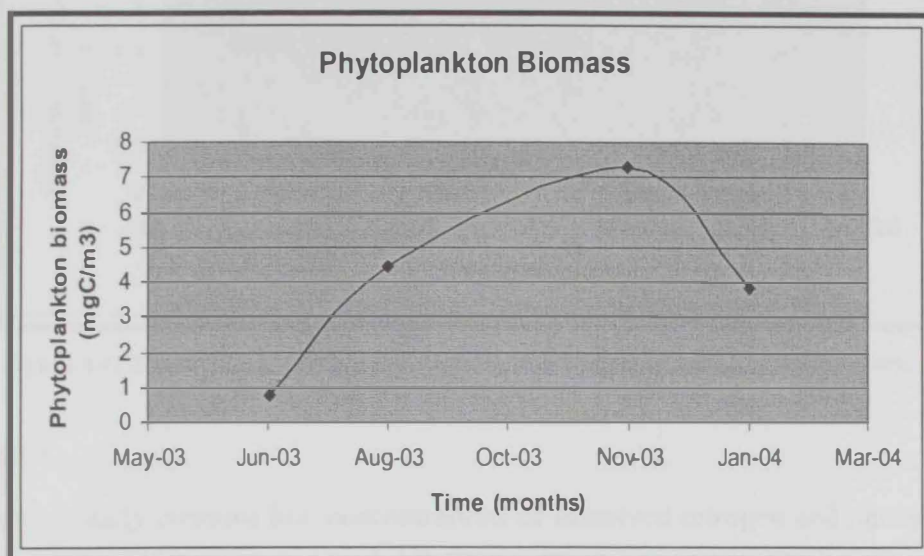
Figure 4.3: Phytoplankton biomass expressed in (mgC/m^3) during the sampling work.

Zooplankton

Zooplankton is considered as a secondary producer and also as a primary consumer on phytoplankton species. Surveying the Ruwais costal water gave rise to poor zooplankton biomass condition in the area. Elshorbagy *et al.* (2004e) reported that the average zooplankton biomass in the Ruwais marine water is 1.03 mgC/m^3, whereas comparable studies show much higher values in different zones in the Arabian Gulf, where 104- 407 mgC/m^3 was reported by Michel *et al.* (1986a). This poor productivity in the Ruwais water may be due to several reasons; one of them is the low productivity of phytoplankton as a primary producer which consequently affects the growth rate of zooplankton as the primary consumer.

Figure 4.4 shows the zooplankton biomass variation during the sampling period. The general trend is consistent with phytoplankton biomass one, where the zooplankton increases during the summer period from June to November and decreases in the winter season. This matching between zooplankton and phytoplankton biomasses gives a logical interpretation for the food web interaction in a lower tropic level.
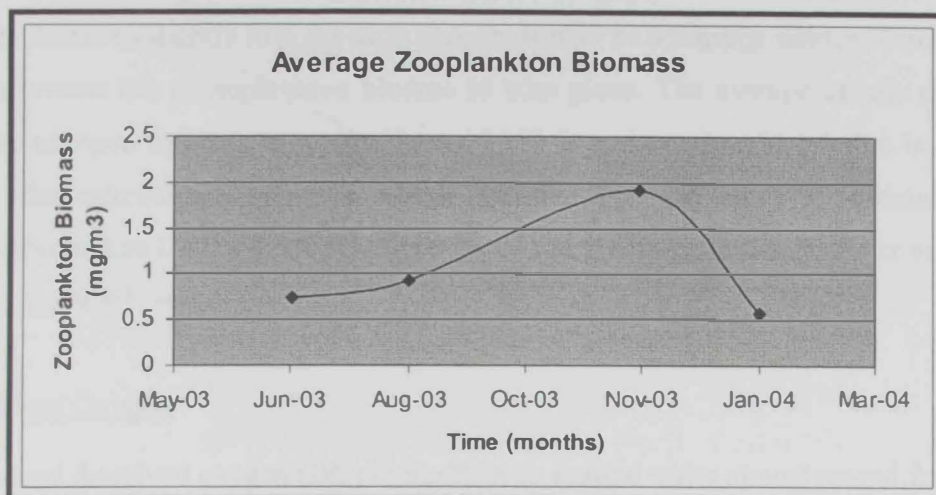
Figure 4.4: Zooplankton biomass expressed in (mgC/m³) during the sampling work.

Nutrients

Seawater usually contains low concentrations of dissolved nitrogen and phosphorous compounds. They are usually considered as limiting factors for phytoplankton population growth. Inorganic Nitrogen exists in seawater in different forms, i.e.; nitrate, nitrite and ammonium, while, the inorganic phosphorous exists as phosphate. Nutrient measurements for the sampled locations at different times are listed in Table 4.1. Inspection of these values indicates that most of nutrient measurements in the Ruwais coastal water are low to moderate, while Nitrates (NO_3-N) which ranges between 64 to 78 μM is considered to be extremely high when compared with Dubai and Abu Dhabi Creeks; 0.5- 23.79 μM and 0.08- 18.72 μM, respectively (Abu Hilal and Adam, 1995). This high concentration of Nitrates may refer to effluents from the fertilization plant and petrochemical industries located in the area.

The PO_4-P levels ranged from 0.5 to 1.4 μM. These values are less than values estimated in Dubai Creek (0.8- 28.8 μM) and in Abu Dhabi Creek (0.02- 4.53 μM), while they are close to the values in Kuwait (0.14- 0.18 μM), Saudi Arabia (0.0- 0.34 μM) and Qatar (0.2- 0.88 μM).

NOAA/EPA, 1988 reported that the nitrogen levels in healthy coastal system should range from 6.7 to 67.5 μM while the phosphorous concentration should range from 0.3 to 3.2 μM. Higher concentrations of both can lead to less diversity and/or eutrophication conditions.

In the present study, the nitrogen levels are very high whereas the phosphate levels are moderate to slightly low. As such phosphate may be a limiting nutrient constituent that prevents the phytoplankton blooms to take place. The average atomic ratio of nitrate-nitrogen to phosphate-phosphorus (N:P) is estimated at 74.1:1 that is higher than other estimations in the area, where, Shriadha and Al-Ghais (1999) estimated the N:P ratio in Abu Dhabi, Umm Al-Quwain and Ras Al-Khayma coastal water as 9.5:1, 8.9:1, and 9.8:1, respectively.

Dissolved Oxygen

Measured dissolved oxygen (DO) in the Ruwais marine water almost ranged from 5.2 to 6.7 mg/l for most of the samples, whereas during November sampling their average dropped to 3.4 mg/l. sudden depletion of dissolved oxygen may refer to the oil accident which occurred in October and mentioned earlier. The DO ranges in the Ruwais are comparable with other study carried out by Banat *et al.*, 1993, where they reported that the DO levels in Abu Dhabi costal water ranged from 6.1 to 6.7 mg/l.

4.4 Conclusion

The introduced coverage of different measurements reveals that the study area can be classified as HNLC, i.e., high nutrients and low chlorophyll/carbon. Even though the nutrients are abundant and available, primary as well as secondary producers are extremely limited. This phenomenon is likely related to inhibitory factors such as harsh environment; in particular the high salinity and the high contents of hydrocarbons associated with oil contamination. The high chlorine dosing taking place at the intakes does indeed contribute to such phenomena especially close to the shoreline. These conditions, however indicate that the area is ecologically unstable and changes in effluent levels and qualities may give rise to blooming condition; i.e., red-tide. It is, therefore recommended to establish a monitoring program that targets observing the effluent quantities as well as the water quality of the coastal basin in general.

CHAPTER FIVE
EUTROP SIMULATION MODEL

In the current study, a water quality simulation software "EUTROP" is employed to investigate the fate transport and the effect of brine and warm water discharge from Ruwais desalination and other existing coastal facilities on the water quality of the Ruwais. EUTROP is one of the suit software CENSIS; that is a three dimensional coupled physical and biochemical model. It is used in the second stage of the modeling process after performing the hydrodynamic simulation using COSMOS model, where the COSMOS output files are used as an input files in the water quality simulation process.

This chapter presents a brief description of the numerical scheme and theoretical background of the EUTROP model. The model parameters are then tuned against the gathered field data.

5.1 EUTROP Theoretical Background

EUTROP model contains twelve state variable referred to as compartments. Four compartments are expressed as carbon stock; phytoplankton, zooplankton, detritus and dissolved organic matter. Other two intercellular nutrients of phytoplankton; nitrogen quota and phosphorous quota are also expressed. Moreover, four nutrients such as ammonium, nitrite, nitrate, and phosphate are included. Two oxygen parameters; dissolved oxygen and chemical oxygen demand. Table 5.1 shows the twelve compartments and their units. These compartments are considered as the main variables in the system that interact with each other as a basic present for the biochemical processes taking place in the real situation. Such biochemical processes among different compartments are illustrated in Figure 5.1. The description of the governing equations introduced in the current section is mostly adapted from the user guide of CENSIS Model (CENSIS user guide, Chuden CTI, 2004).

Table 5.1: Compartments of the biochemical coupled EUTROP model

No	Symbol	Definition	Unit
1	P	Phytoplankton biomass	mgC/m^3
2	SQP	Intracellular phosphorous quota of phytoplankton	$\mu g\text{-}atmP/l$
3	SQN	Intracellular nitrogen quota of phytoplankton	$\mu g\text{-}atmN/l$
4	Z	Zooplankton biomass	mgC/m^3
5	POC	Particulate (Detrital) organic matter	mgC/m^3
6	DOC	Dissolved organic matter	$\mu g\text{-}atmP/l$
7	PO_4	Phosphate concentration	$\mu g\text{-}atmN/l$
8	NH_4	Ammonium concentration	$\mu g\text{-}atmN/l$
9	NO_2	Nitrite concentration	$\mu g\text{-}atmN/l$
10	N_3	Nitrate concentration	$\mu g\text{-}atmN/l$
11	DO	Dissolved oxygen concentration	mgO_2/l
12	COD	Chemical oxygen demand concentration	mg/l

Surface

Gas Exchange

Gas Exchange

B3

Dissolved Organic Matter

Phytoplankton

Extracellular Release

Mineralization   Photosynthesis

Respiration

Mineralizati

B5   B1

B6

Growth

Mortality   B14

B13

Grazing   B2

Nutrient Uptake

Biodegradation   Mineralization

B4

Respiration

Dissolved Oxygen

Respiration   Diel Migration

Oxidati

B8 , B10

Egestion, Death

Zooplankton   B11

Detritus

B7 Feeding

Respiration
B9

Mineralization

Sinking

B12

Phosphate   Carbonat

Sinking

Ammoniu   B15   Nitrite   B16   Nitrate   B18

Denitrification

Nitrification   Nitrification

B17   Deoxidization

B19   B20   Benthic Consumption

Bottom   Benthic Regeneration

Figure 5.1: Schematic diagram of an estuarine ecosystem EUTROP model

The general equation describing the coupled physical and biological model is expressed as the following:

$$\frac{\partial B}{\partial t} + (v \cdot \nabla)B + (w + w_P)\frac{\partial B}{\partial z} = [\nabla \cdot (K_H \nabla)]B + \frac{\partial}{\partial z}\left(K_z \frac{\partial B}{\partial z}\right) + \left(\frac{dB}{dt}\right) + q \qquad (5.1)$$

Where

B: the concentration of an arbitrary compartment

$v = (u, v)$: the horizontal component of flow velocity

$\nabla = (\partial / \partial x, \partial / \partial y)$: is the horizontal gradient operator

w : the vertical velocity component

w_P: is the sinking rate for a particulate organic compartment

K_H, K_z: is the horizontal and the vertical component of eddy diffusivity respectively

dB/dt: is the local change in standing stock according to the biochemical processes

q: is the fluxes due to external source

The following subsections will describe briefly the major equations controlling the model biochemical processes with association with the model compartments.

5.1.1 Phytoplankton

Let N_p be the number of phytoplankton categories and P_j be biomass of each category j. The main equation which describes the change of the biomass of phytoplankton by biological processes can be formulated as:

$$\left(\frac{dP_j}{dt}\right) = Photosynthetic\ growth\ (B_1) - Extracellular\ release\ (B_3) - Respiration\ (B_5)$$
$$- Grazing\ by\ zooplankton\ (B_4) - Natural\ mortality\ (B_6) \qquad (5.2)$$

In previous equation, each term will be interpreted separately to clear the whole processes which are related to phytoplankton biomass, as the following:

Photosynthetic Growth

$$B_1 = v_1(T) \cdot \mu_1(P_j, SQN_j, SQP_j) \cdot \mu_2(I, P_j) \cdot P_j \tag{5.3}$$

The notations, $v(\ )$, $\mu(\ )$ in the equations hereinafter denote physiological rate coefficient and degree of limitation to the physiological rate, respectively.

The term $v_1(T)$ is the maximal growth rate of the phytoplankton, it can be formulated as:

$$v_1 \equiv v_1(T) = \alpha_1 \cdot \exp(\beta_1 \cdot T) \tag{5.4}$$

where α_1 is the maximal growth rate at 0 °C and β_1 is the temperature coefficient (°C $^{-1}$, $\beta_1 = \ln Q_{10}/10$).

The term $\mu_1(P, SQN, SQP)$ represents the growth limitation by cellular pools. In the model, the cell quota works as the limiting factor for the growth rate of phytoplankton, where the growth of the phytoplankton continues due to the nutrient intracelular quota even though the ambient nutrient is went out. Nitrogen quota and phosphorous quota are considered as the main nutrients affecting the growth rate, and the most limiting nutrient is determined based on Liebig's low of minimum. The model expression for the limiting nutrient is formulated as:

$$\mu_1(P, SQN, SQP) = \min\left\{\frac{SQN}{SQN + [N:C]_p \cdot P}, \frac{SQP}{SQP + [P:C]_p \cdot P}\right\} \tag{5.5}$$

where $[N:C]_p$ and $[P:C]_p$ are the ratio of nitrogen and phosphorous pools to carbon stock in the cell substrate; namely, the inverses of C/N, C/P ratios, respectively.

The term $\mu_2(I, P_j)$ is related to instantaneous photosynthetic growth rate which is mainly affected by light intensity (I). The model adopts a combination of Monod equation for enzymatic reaction and Steel (1962) equation to represent the photosynthetic light response as the following:

$$\mu_2 = \frac{I}{I_{opt}} \cdot \exp\left(1 - \frac{I}{I_{opt}}\right) \tag{5.6}$$

where I_{opt} is the light optimum for photosynthetic process, it has a constant value.

Due to the water turbidity, an attenuation of the light intensity may occur, this prohibits the light to reach to the deep part of the estuarine, so the photosynthesis process may be affected severely or it may even stop completely. This phenomenon was described by the well known Lambert-Beer law:

$$I_z = I_0 \cdot \exp(-k \cdot z) \tag{5.7}$$

where I_z is the light intensity at the depth z, I_0 is the sea-surface light intensity and k is the light extinction coefficient in the water.

The diurnal variation in sea-surface solar radiation may affect the photosynthesis process. A cubic sinusoidal light scheme was introduced by Ikushima (1967) as the following:

$$I_0 \equiv I_0(t) = I_{max} \cdot \sin^3\left(\frac{\pi}{DL}t\right) \tag{5.8}$$

where I_{max} is the diurnal maximum of the sea-surface light intensity at the highest solar altitude, DL is the daylight length from sunrise to sunset.

Extracellular Release

$$B_3 = \mu_3(P_j) \cdot P_j \tag{5.9}$$

A part of photosynthetic product in phytoplankton is released in dissolved organic form. This physiological process is called extracellular release or excretion. Almost 15% of the total carbon fixed by phytoplankton is released as excretion Watt (1966). Approved through laboratory work that there is a relation between the extracellular release and chlorophyll-a content (Chl a in mg/m³), the empirical expression which formulate this relation can be expressed as:

$$\ln\left(\%\beta\right) = \ln 13.5 - 0.00201 \cdot Chla \tag{5.10}$$

This equation is substituted in the model as:

$$\mu_3\left(P\right) = \beta_0 \cdot \exp\left\{-\gamma \cdot \left[Chla:C\right] \cdot P\right\} \tag{5.11}$$

where P is the phytoplankton carbon biomass (mgC/m^3), β_0 is the maximal fractional release rate (0.135 in the equation (5.10)), γ is the chlorophyll-a coefficient (0.00201 m^3/mgChla in the equation (5.10)), $\left[Chla:C\right]$ is the chlorophyll-a/carbon ratio (mg Chl $\underline{a}$ / mg C).

Respiration

$$B_5 = v_5\left(T\right) \cdot P_j \tag{5.12}$$

Respiration in the phytoplankton consumes a part of the photosynthesis process product. The respiration rate follows an exponential trend with temperature degree as the following:

$$v_5\left(T\right) = \alpha_5 \cdot \exp\left(\beta_5 \cdot T\right) \tag{5.13}$$

where α_5 is the respiration rate at 0 °C day^{-1} and β_5 is the temperature coefficient (°C^{-1}).

Natural Mortality

The model does not take in account the grazing of phytoplankton by higher-trophic level organisms. Decreasing of the phytoplankton cells in the model refers to two factors; grazing by zooplankton in a lower-trophic level and the natural mortality, where the phytoplankton loss turned into the detritus compartment. The natural mortality of phytoplankton is controlled by the Steele and Henderson (1992) quadratic formula which is:

$$B_6 = v_6\left(T\right) \cdot P_j^2 \qquad (j=1, 2, ..., N_P) \tag{5.14}$$

where v_6, represents the temperature-dependent mortality rate. In this model, the function v_6 is formulated as:

$$v_6(T) = \alpha_6 \cdot \exp(\beta_6 \cdot T) \tag{5.15}$$

where α_6 is the mortality rate at 0 °C (in $(mgC/m^3)^{-1} \cdot day^{-1}$) and β_6 is the temperature coefficient (°C^{-1}).

Grazing by zooplankton (B4) term will be discussed later in section 5.1.3.

5.1.2 Phytoplankton Cell Quota

The dynamics of the intracellular quota of the phytoplankton cells can be described in the model as:

Phosphorous Quota

$$\left(\frac{dSQP}{dt}\right) = Phosphorous\ uptake - Utilization\ by\ photosynthetic\ growth - Grazing$$

$$loss - Release\ due\ to\ mortality - Sinking\ loss$$

$$= B_2^P - [P:C]_P \cdot B_1 - (B_4 + B_6) \cdot \frac{SQP}{P} - w_P \cdot \frac{\partial}{\partial z}(SQP) \tag{5.16}$$

The phosphorous uptake by the phytoplankton cells is expressed as:

$$B_2^P = v_0^P(PO_4) \cdot [P:C]_p \cdot P \tag{5.17}$$

$$v_0^P(PO_4) = UP_{max} \cdot \frac{PO_4}{K_P + PO_4} \cdot \mu_7(P, SQP) \tag{5.18}$$

$$\mu_7(P, SQP) = \left\{ PQP_{max} - \frac{[P:C]_P \cdot P + SQP}{[P:C]_P \cdot P} \right\} \Big/ (PQP_{max} - 1) \tag{5.19}$$

where UP_{max} is the maximal uptake rate for phosphate, PO_4 the phosphate concentration, K_P a half-saturation constant, P the phytoplankton carbon biomass, SQP the intracellular phosphorous quota, PQP_{max} the maximal specific phosphorous

quota (ratio of maximal quota to subsistent quota), $[P:C]_P$ is a P/C composition of cell substrate, and w_P is the sinking rate of phytoplankton living cell (in $m.day^{-1}$).

Nitrogen Quota

$$\left(\frac{dSQN}{dt}\right) = Nitrogen\ uptake - Utilization\ by\ photosynthetic\ growth - Grazing\ loss$$
$$- Release\ due\ to\ mortality - Sinking\ loss$$

$$= B_2^N - [N:C]_P \cdot B_1 - (B_4 + B_6) \cdot \frac{SQN}{P} - w_P \cdot \frac{\partial}{\partial z}(SQN) \tag{5.20}$$

It's worth mentioning that in the existence of all nitrogen nutrients; ammonium, nitrate and nitrite, the model select even ammonium or nitrate to be uptaken by the phytoplankton neglecting the intermediate form of the nitrogen nutrient which is the nitrite. Moreover, Wrobleweski (1977) proved that when the ammonium and the nitrate are abundant in the ambient, the phytoplankton prefer to uptake the ammonium to nitrate. This phenomenon is taken also in consideration in this model so the nitrogen uptake by the phytoplankton cells is expressed as:

$$B_2^N = v_0^N (NH_4, NO_3) \cdot [N:C]_P \cdot P \tag{5.21}$$

$$v_0^N (NH_4, NO_3) = UN_{max} \cdot \left\{ \frac{NH_4}{K_{NH4} + NH_4} + \frac{NO_3}{K_{NO3} + NO_3} \cdot e^{-\Psi \cdot NH_4} \right\} \cdot \mu_6 (P, SQN) \tag{5.22}$$

$$\mu_6 (P, SQN) = \left\{ PQN_{max} - \frac{[N:C]_P \cdot P + SQN}{[N:C]_P \cdot P} \right\} / (PQN_{max} - 1) \tag{5.23}$$

where UN_{max} is the maximal uptake rate for nitrogen, K_{NH4} and K_{NO3} are half-saturation constants for ammonium (NH_4) and nitrate (NO_3), respectively, SQN is the nitrogen quota, PQN_{max} the maximal specific nitrogen quota, $[N:C]_P$ is a tissue N/C composition, and ψ is the ammonium inhabitation factor for nitrate uptake (in $l. \mu M^{-1}$).

5.1.3 Zooplankton

Let N_Z be the number of zooplankton categories and Z_j be biomass of each category j. The main equation which describes the change of the biomass of zooplankton by biological processes can be formulated as the following:

$$\left(\frac{dZ_j}{dt}\right) = Grazing\ (B_4) + Detritus\ feeding\ (B_7) - Egestion\ (B_8) - Respiration\ (B_9)$$

$$- Natural\ mortality\ (B_{10}) \pm Diel\ vertical\ migration\ (B_{11}) \tag{5.24}$$

In previous equation, each term will be discussed separately to clear the whole processes which are related to zooplankton biomass, as the following:

Feeding (Grazing)

$$B_4 = \mu_7(P, POC) \cdot v_4^j(T; P, POC) \cdot Z_j \tag{5.25}$$

Several studies approved that there is a lower threshold for food density, below which the feeding process no longer takes place (Parsons *et al.*, 1967). Ivlev (1945) proposed an equation to describe the grazing process of the zooplankton as the following:

$$R = R_{max} \cdot \left[1 - \exp\left\{-\lambda \cdot \left(\Pi - \Pi^*\right)\right\}\right] \cdot Z \tag{5.26}$$

where R denotes feeding amount (ration) of zooplankton at the food density Π, Z the zooplankton biomass, R_{max} the maximal feeding rate, λ is a constant and Π^* stands for lower threshold for feeding activity and it is expressed in the model as a constant value.

The maximum feeding rate (R_{max}) follows an exponential temperature response and expressed as:

$$R_{max} = \alpha_4 \cdot \exp(\beta_4 \cdot T) \tag{5.27}$$

where α_4 is the maximal feeding rate at 0 °C and β_4 is the temperature coefficient. In the model, it is considered that there are two forms of particulate organic matters which can be grazed by zooplankton; phytoplankton and detritus. These foods can be expressed numerically as:

Phytoplankton category j; $\mu_7^j(P, POC) = \dfrac{P_j}{\left(\sum\limits_{n=1}^{N_P} P_n\right) + POC}$ ($j=1,2, …, N_P$) (5.28)

Total phytoplankton; $\mu_7(P, POC) = \sum\limits_{j=1}^{N_P} \mu_7^j(P, POC)$ (5.29)

Detritus; $1 - \mu_7(P, POC) = \dfrac{POC}{\left(\sum\limits_{n=1}^{N_P} P_n\right) + POC}$ (5.30)

$\Pi = \sum\limits_{j}^{N_P} P_j + POC$; (j = 1, 2, …, N_p) (5.31)

The final formula of the feeding rate of zooplankton (in day^{-1}) can be expressed by substitution of the equations (5.27) and (5.31) into equation (5.26) to become:

$$v_4(T; P, POC) = \alpha_4 \cdot \exp(\beta_4 \cdot T) \cdot \left[1 - \exp\left\{-\lambda \cdot \left(\sum\limits_{j}^{N_P} P_j + POC - \Pi^*\right)\right\}\right]$$ (5.32)

Detritus feeding by zooplankton is expressed as:

$$B_7 = \left[1 - \mu_7(P, POC)\right] \cdot v_4^j(T; P, POC) \cdot Z_j$$ (5.33)

Egestion

The excretion process from zooplankton is called egestion. It is calculated in the model as:

$$B_8 = (1 - e) \cdot v_4(T; P, POC) \cdot Z$$ (5.34)

where (e) is the assimilation efficiency in the zooplankton.

Respiration

$$B_9 = v_9^j(T; P, POC) \cdot Z_j \tag{5.35}$$

The respiration process in the zooplankton is divided into two types; stationary respiration which is produced of the basic metabolism and active respiration which is produced due to the energy expenditure during the feeding activities. The stationary respiration is expressed as:

$$v_s = \alpha_3 \cdot \exp(\beta_3 \cdot T) \tag{5.36}$$

where α_3 is the basic metabolic rate at 0 °C and β_3 is the temperature coefficient. Whereas, the active respiration is expressed as:

$$v_a = \eta \cdot v_4(T; P, POC) \tag{5.37}$$

where η is a proportional constant ($0 < \eta < 1$) and v_4 is the feeding rate described by equation (5.32). So, the total respiration loss is considered as the sum of stationary and active respiration and it can be described as:

$$v_9(T; P, POC) \equiv v_s + v_a = \alpha_3 \cdot \exp(\beta_3 \cdot T) + \eta \cdot v_4(T; P, POC) \tag{5.38}$$

Natural Mortality

The loss of zooplankton biomass is referred to natural mortality and feeding by carnivorous animals. As mentioned before, the model is taking in consideration the lower trophic level, so all the losses of zooplankton will be considered as related to the mortality and it is expressed in a quadratic form as the following:

$$B_{10} = v_{10}(T) \cdot Z^2 \tag{5.39}$$

where v_{10} represents the temperature-dependent mortality rate, which is formulated as:

$$v_{10}(T) = \alpha_{10} \cdot \exp(\beta_{10} \cdot T) \tag{5.40}$$

where α_{10} is the mortality rate at $0\ ^{\circ}\text{C}$ (in $(\text{mgC/m}^3)^{-1}\cdot\text{day}^{-1}$) and β_{10} is the temperature coefficient.

<u>Diel Migration</u>

$$B_{11} = w_z(t) \cdot \frac{\partial Z_j}{\partial z} ; \quad (j=1,2,\ ...,\ N_Z) \tag{5.41}$$

Diel vertical migration phenomenon is referred to ascending of zooplankton community to upper layer in the night time and descending to the lower layers in the daytime. This can be described in the model as a sinusoidal function with time and the day length.

Ascending rate is expressed as:

$$w_z(t) = w_{up} \cdot \sin\left\{\frac{\pi}{1-DL}(t-DL)\right\} ; (DL \le t \le 1) \tag{5.42}$$

where w_{up} represents the maximal nocturnal ascending rate (in m/s), and DL id the functional daytime length.

Descending rate is expressed as:

$$w_z(t) = -w_{down} \cdot \sin\left(\frac{\pi}{DL}t\right) ; (0 \le t \le DL) \tag{5.43}$$

where w_{down} is the maximal diurnal descending rate (in m/s) here w_{down} is the maximal diurnal descending rate (in m/s).

5.1.4 Detritus

The particulate organic matter in the model represents dead phytoplankton and zooplankton in addition to non-biological components. Other particulate organic carbon is excluded from the detritus term. Biological change in the standing sock is given as:

$$\left(\frac{dPOC}{dt}\right) = \textit{Phytoplankton mortality } (B_6) + \textit{Zooplankton mortality } (B_{10})$$

$$+ \textit{Egestion by zooplankton } (B_8) - \textit{Feeding by zooplankton } (B_7)$$

$$- \textit{Mineralization } (B_{12}) - \textit{Biodegradation } (B_{13})$$

$$= \sum_{j=1}^{N_P} B_6^j + \sum_{j=1}^{N_z} \left(B_{10}^j + B_8^j - B_7^j\right) - B_{12} - B_{13} \tag{5.44}$$

where B6, B10, B8 and B7 terms are discussed in earlier sections in the current chapter, and can be reformatting as the following:

$$B_6^j = v_6^j(T) \cdot P_j^2 \qquad (j=1,2,\ldots,N_P) \tag{5.45}$$

$$B_{10}^j = v_{10}^j(T) \cdot Z_j^2 \qquad (j=1,2,\ldots,N_z) \tag{5.46}$$

$$B_8^j = (1-e) \cdot v_4^j(T;P,POC) \cdot Z_j \qquad (j=1,2,\ldots,z) \tag{5.47}$$

$$B_7^j = \frac{POC}{\left(\sum P_i\right) + POC} \cdot v_4^j(T;P,POC) \cdot Z_j \qquad (j=1,2,\ldots,N_z) \tag{5.48}$$

The other two terms B_{12} and B_{13} are related to bacterial decomposition, where the bacteria decomposes the most of organic parts of detritus and transfers them to dissolved inorganic matter in a process called mineralization. The infrangibly fraction of detritus remains in organic form for long time. According to the notations in the model, the part of detritus which is subjected to bacterial decomposition (mineralization) can be expressed as the following:

$$B_{12} = (1-\kappa) \cdot v_{12}(T;DO) \cdot POC \tag{5.49}$$

where κ represents the infrangibly fraction, κ ($0<\kappa<1$) The mineralization of the detritus responses to Monod equation, where:

$$v_{12}(T,DO) = \alpha_{12} \cdot \exp(\beta_{12} \cdot T) \cdot \frac{DO}{DO_1 + DO} \tag{5.50}$$

where α_{12} is the apparent decomposition rate at 0 °C, β_{12} the temperature coefficient, and DO_1 the half-saturated oxygen concentration that reflects limitation of dissolved oxygen to bacterial decomposition.

The infrangibly fraction of detritus is expressed in the model as:

$$B_{13} = \kappa \cdot v_{12}(T;DO) \cdot POC \tag{5.51}$$

5.1.5 Dissolved Organic Matter (DOC)

As mentioned in the previous section (5.1.4), the particulate organic matter (detritus) is referred to died phytoplankton and zooplankton in addition to non-biological components. The reminder part of organic matter is considered as dissolved organic matter and it is expressed as carbon stock. The biological change in the dissolved organic matter is expressed in the model as the following:

$$\left(\frac{dDOC}{dt}\right) = \textit{Extracellular release by phytoplankton } (B_3) + \textit{Biodegradation of detritus}$$
$$(B_{13}) - \textit{Bacterial decomposition } (B_{14})$$

$$= \sum_{j=1}^{N_P} B_3^j + B_{13} - B_{14} \tag{5.52}$$

where the first two terms (B_3) and (B_{13}) are discussed in previous section and they can be reformatting:

$$B_3^j = \left\{1 - \mu_3(P_j)\right\} \cdot B_1^j \quad (j=1,2, \dots, N_P) \tag{5.53}$$

$$B_1^j = v_1^j(T) \cdot \mu_1(P_j, SQN_j, SQP_j) \cdot \mu_2(I, P_j) \cdot P_j \tag{5.54}$$

whereas the bacterial decomposition term can be expressed as the following:

$$B_{14} = v_{14}(T, DO) \cdot DOC \tag{5.55}$$

where the dissolved organic matter has an exponential temperature response along with a hyperbolic oxygen response as the following:

$$v_{14}(T,DO) = \alpha_{14} \cdot \exp(\beta_{14} \cdot T) \cdot \frac{DO}{DO_2 + DO} \qquad (5.56)$$

where α_{14} is the decomposition (mineralization) rate at $0\ ^{\circ}C$ (day^{-1}), β_{14} is the temperature coefficient ($^{\circ}C^{-1}$), DO_2 is the half-saturated oxygen concentration (mgO_2/l) standing for limitation by dissolved oxygen.

5.1.6 Phosphate

The nutrient part of the model comprises of four main nutrients which are, Phosphate, ammonium, nitrite and nitrate. The biochemical change in phosphate concentration is given as follows:

$$\left(\frac{dPO4}{dt} \right) = - \text{Uptake by phytoplankton (B}_2\text{)} + \text{Excretion by zooplankton (B}_9\text{)}$$

$$+ \text{Mineralization of detritus (B}_{12}\text{)} + \text{Mineralization of dissolved organic}$$
$$\text{matter (B}_{14}\text{)} + \text{Benthic regeneration (B}_{19}\text{)}$$

$$= -\sum_{j=1}^{N_P} B_{2P}^j + \sum_{j=1}^{N_Z} [P:C]_Z^j \cdot B_9^j + [P:C]_{POM} \cdot B_{12} + [P:C]_{DOM} \cdot B_{14} + B_{19} \qquad (5.57)$$

where the first four terms (B$_2$), (B$_9$), (B$_{12}$) and (B$_{14}$) are discussed earlier in the previous sections, and they can be reformatting as the following:

$$B_{2P}^j = v_{2P}^j(PO_4) \cdot [P:C]_P^j \cdot P_j \qquad (j=1,2, \ldots, N_P) \qquad (5.58)$$

$$B_9^j = v_9^j(T;P,POC) \cdot Z_j \qquad (j=1,2, \ldots, N_Z) \qquad (5.59)$$

The last term of equation (5.57) is represents the benthic regeneration of phosphorus which is regulated by physical diffusion and metabolic processes of the benthic community, and it is expressed as:

$$B_{19} = v_{19}(T,DO) \qquad (5.60)$$

Where

$$v_{19}(T,DO) = \alpha_{19} \cdot \exp(\beta_{19} \cdot T - \gamma_P \cdot DO) \qquad (5.61)$$

In the equation, T represents the water temperature ($^{\circ}$C) and DO represents he dissolved oxygen concentration (mgO_2/l) just above the seabed. α_{19} is the phosphorous regeneration rate at 0 $^{\circ}$C ($mgP \cdot m^{-2} \cdot day^{-1}$), β_{19} is the temperature coefficient ($^{\circ}C^{-1}$) and γ_P is a parameter (l/mgO_2) that represents inhibition of phosphorous regeneration by dissolved oxygen.

5.1.7 Ammonium, Nitrite and Nitrate

In the model, the dissolved inorganic nitrogen is distinguished into three forms; ammonium, nitrite and nitrate. Biochemical changes in concentration of these constituents are described as follows:

<u>Ammonium</u>

$$\left(\frac{dNH_4}{dt}\right) = - \textit{Uptake by phytoplankton} (B_2) + \textit{Excretion by zooplankton} (B_9)$$

$$+ \textit{Mineralization of detritus} (B_{12}) + \textit{Mineralization of dissolved organic}$$
$$\textit{matter} (B_{14}) - \textit{Nitrification} (B_{15}) + \textit{Deoxidization of nitrate} (B_{17})$$
$$+ \textit{Benthic regeneration} (B_{20})$$

$$= - \sum_{j=1}^{N_P} B_{2,NH4}^j + \sum_{j=1}^{N_Z} [N:C]_Z^j \cdot B_9^j + [N:C]_{POM} \cdot B_{12} + [N:C]_{DOM} \cdot B_{14}$$

$$- B_{15} + B_{17} + B_{20} \tag{5.62}$$

Where

$$B_{2,NH4}^j = v_{2,NH4}^j (NH_4, P, SQN) \cdot [N:C]_P^j \cdot P_j \qquad (j=1,2, \dots, N_P) \tag{5.63}$$

$$v_{2,NH4}(NH_4, P, SQN) = UN_{max} \cdot \frac{NH_4}{K_{NH4} + NH_4} \cdot \mu_6(P, SQN) \tag{5.64}$$

$$\mu_6(P, SQN) = \left\{ PQN_{max} - \frac{[N:C]_P \cdot P + SQN}{[N:C]_P \cdot P} \right\} \Big/ (PQN_{max} - 1) \tag{5.65}$$

$$B_9^j = v_9^j(T; P, POC) \cdot Z, \qquad (j=1,2, \dots, N_Z) \tag{5.66}$$

$$B_{15} = v_{15}(T, DO) \cdot NH_4 \tag{5.67}$$

$$B_{17} = v_{17}(T, DO) \cdot NO_3 \tag{5.68}$$

$$B_{20} = v_{20}(T, DO) \tag{5.69}$$

<u>Nitrite</u>

$$\left(\frac{dNO_2}{dt}\right) = Oxidization\ of\ ammonium\ (1^{st}\ Nitrification;\ B_{15}) - Oxidization\ of\ nitrite$$

$$Nitrification\ (2^{nd}\ Nitrification;\ B_{16})$$

$$= B_{15} - B_{16} \tag{5.70}$$

Where

$$B_{15} = v_{15}(T,DO) \cdot NH_4 \tag{5.71}$$

$$B_{16} = v_{16}(T,DO) \cdot NO_2 \tag{5.72}$$

Note that the nitrification corresponds to ammonium transfer to NO_2 while the 2nd nitrification corresponds to NO_2 transfer to NO_3.

<u>Nitrate</u>

$$\left(\frac{dNO_3}{dt}\right) = - Uptake\ by\ phytoplankton\ (B_2) + Nitrification\ (B_{16})$$

$$- Deoxidization\ (B_{17}) - Denitrification\ (B_{18})$$

$$= -\sum_{j=1}^{N_P} B_{2,NO3}^{j} + B_{16} - B_{17} - B_{18} \tag{5.73}$$

Where

$$B_{2,NO3}^{j} = v_{2,NO3}^{j}(NH_4, NO_3, P, SQN) \cdot [N:C]_P^{j} \cdot P_j \qquad (j=1,2, ..., N_P) \tag{5.74}$$

$$v_2^{N}(NH_4, NO_3) = UN_{max} \cdot \frac{NO_3}{K_{NO3} + NO_3} \cdot e^{-\Psi \cdot NH_4} \cdot \mu_6(P, SQN) \tag{5.75}$$

$$\mu_6(P, SQN) = \left\{ PQN_{max} - \frac{[N:C]_P \cdot P + SQN}{[N:C]_P \cdot P} \right\} \Big/ (PQN_{max} - 1) \tag{5.76}$$

$$B_{16} = v_{16}(T,DO) \cdot NO_2 \tag{5.77}$$

$$B_{18} = v_{18}(T) \cdot NO_3 \tag{5.78}$$

Nitrification

The oxidation process of nitrogen is called nitrification. In model the rate of

nitrification process depends on the nitrifying bacteria activity as follows:

$$\frac{dNH_4}{dt} = -k_{NH4} \cdot NH_4 \qquad (5.79)$$

$$\frac{dNO_2}{dt} = +k_{NH4} \cdot NH_4 - k_{NO2} \cdot NO_2 \qquad (5.80)$$

where k_{NH4} and k_{NO2} denote the nitrification rates of ammonium and nitrite, respectively.

The nitrifying rates are expressed in the model as the following:

$$k_{NH4} \equiv v_{15}(T, DO) = \alpha_{15} \cdot \exp(\beta_{15} \cdot T) \cdot \frac{DO}{DO_{NH4} + DO} \qquad (5.81)$$

$$k_{NO2} \equiv v_{16}(T, DO) = \alpha_{16} \cdot \exp(\beta_{16} \cdot T) \cdot \frac{DO}{DO_{NO2} + DO} \qquad (5.82)$$

where α_{15} and α_{16} are the nitrification rates (in day^{-1}) of ammonium and nitrite, respectively, at $0\,^{\circ}\text{C}$ and without oxygen limitation, β_{15}, β_{16} are the corresponding temperature coefficients ($^{\circ}\text{C}^{-1}$, $\ln Q_{10}/10$), and DO_{NH4}, DO_{NO2} are the half-saturated oxygen concentration (mgO_2/l) standing for limitation by dissolved oxygen.

Deoxidization and Denitrification

In the model it is assumed that the deoxidizing reaction of nitrate-nitrogen toward ammonium-nitrogen takes place under the anaerobic condition and follows the exponential temperature response. The expression is given as:

$$v_{17}(T, DO) = \alpha_{17} \cdot \exp(\beta_{17} \cdot T) \cdot \mu_{17}(DO) \qquad (5.83)$$

$$\mu_{17}(DO) = \begin{cases} 0 & (DO \geq DO_{NO3}) \\ 1 & (DO \leq DO_{NO3}) \end{cases} \qquad (5.84)$$

where α_{17} is the deoxidization rate (in day^{-1}) of nitrate at 0 °C and β_{17} is the temperature coefficient (°C^{-1}). The function μ_{17} reflects the upper threshold of dissolved oxygen, DO_{NO3} (in mgO_2/l), above which the deoxidizing reaction no longer proceeds.

Denitrification process is the inverse of the nitrification one. It is expressed in the model as:

$$B_{18} = v_{18}(T) \cdot NO_3, v_{18}(T) = \alpha_{18} \cdot \exp(\beta_{18} \cdot T) \tag{5.85}$$

where α_{18} is the overall denitrification rate day^{-1} at 0 °C and β_{18} is the temperature coefficient (°C^{-1}).

Benthic Nitrogen Regeneration

Benthic nitrogen regeneration is related only to the ammonium compartment. It is expressed in the model as:

$$v_{20}(T, DO) = \alpha_{20} \cdot \exp(\beta_{20} \cdot T - \gamma_N \cdot DO) \tag{5.86}$$

where α_{20} represents the nitrogen regeneration flux at 0°C and zero oxygen concentration ($mgN \cdot m^{-2} \cdot day^{-1}$), β_{20} is the temperature coefficient ($^{o}C^{-1}$) and γ_N is an oxygen inhibition parameter (l/mgO_2).

5.1.8 Dissolved Oxygen (DO)

Dissolved oxygen is one of the most important parameters in the biochemical model, where it plays main rule in oxidizing and nitrifying of the other compartments. The biochemical change in dissolved oxygen concentration is given as follows:

$$\left(\frac{dDO}{dt}\right) = Photosynthetic\ supply\ (D_1) - Respiratory\ loss\ by\ phytoplankton\ (D_2)$$

$$- Respiratory\ loss\ by\ zooplankton\ (D_3) - Loss\ due\ to\ bacterial$$

$$decomposition\ of\ detritus\ (D_4) - Loss\ due\ to\ mineralization\ of\ DOM\ (D_5)$$
$$-Oxidation\ of\ ammonium\ (D_6) - Oxidation\ of\ nitrite\ (D_7) - Consumption\ by$$
$$sediment\ (D_8) \pm aeration\ (D_9)$$

$$= \sum_{j=1}^{N_P} [TOD:C]_P^j \cdot \left(B_1^j - B_5^j\right) - \sum_{j=1}^{N_Z} [TOD:C]_Z^j \cdot B_9^j - [TOD:C]_{POM} \cdot B_{12} - [TOD:C]_{DOM} \cdot B_{14}$$
$$-0.048 \cdot B_{15} - 0.016 \cdot B_{16} - F_{DO}(T) + k_a \cdot (DO_S - DO) \tag{5.87}$$

Where

$$B_1^j = v_1^j(T) \cdot \mu_1(P_j, SQN_j, SQP_j) \cdot \mu_2(I, P_j) \cdot P_j \qquad (j=1,2,\ ...,\ N_P) \tag{5.88}$$

$$B_5^j = v_5^j(T) \cdot P_j \quad (j=1,2,\ ...,\ N_P) \tag{5.89}$$

$$B_9^j = v_9^j(T; P, POC) \cdot Z_j \qquad (j=1,2,\ ...,\ N_Z) \tag{5.90}$$

$$B_{12} = (1 - \kappa) \cdot v_{12}(T; DO) \cdot POC \tag{5.91}$$

$$B_{14} = v_{14}(T, DO) \cdot DOC \tag{5.92}$$

$$B_{15} = v_{15}(T, DO) \cdot NH_4 \tag{5.93}$$

$$B_{16} = v_{16}(T, DO) \cdot NO_2 \tag{5.94}$$

It is clear that all biochemical processes which are related to dissolved oxygen are converted from carbon fluxes to oxygen fluxes are expressed in oxygen/ carbon ratio [TOD: C] as shown in equation (5.87). The main oxidation and deoxidaton processes in the model will be discussed below in a brief manner.

Photosynthetic Supply

Referring to section 5.1.1, the carbon flux photosynthetically assimilated by each phytoplankton category is given as:

$$B_1^j = v_1^j(T) \cdot \mu_1(P_j, SQN_j, SQP_j) \cdot \mu_2(I, P_j) \cdot P_j ; (mgC \cdot m^{-3} \cdot day^{-1}; j=1,2, , N_P) \tag{5.95}$$

By converting to oxygen flux by specific [TOD: C] ratio, the photosynthetic oxygen supply can be expressed as follows:

$$D_1 = \sum_{j=1}^{N_P} [TOD:C]_P^j \cdot B_1^j \quad (mgO_2 \cdot l^{-1} \cdot day^{-1}) \tag{5.96}$$

Respiratory Losses by Plankton

The respiratory oxygen losses by phytoplankton and by zooplankton, they can be calculated as follows:

$$D_2 = \sum_{j=1}^{N_P} [TOD:C]_P^j \cdot B_5^j \quad (mgO_2 \cdot l^{-1} \cdot day^{-1}) \tag{5.97}$$

$$D_3 = \sum_{j=1}^{N_Z} [TOD:C]_Z^j \cdot B_9^j \quad (mgO_2 \cdot l^{-1} \cdot day^{-1}) \tag{5.98}$$

Consumption through Bacterial Decomposition

A part of dissolved oxygen is consumed by respiration activities which take place by bacteria during decomposing of particular organic matter. This part of dissolved oxygen is expressed in the model as:

$$D_4 + D_5 = [TOD:C]_{POM} \cdot B_{12} + [TOD:C]_{DOM} \cdot B_{14} \quad (mgO_2 \cdot l^{-1} \cdot day^{-1}) \tag{5.99}$$

Oxygen Consumption through Nitrification

The nitrification process of ammonium-nitrogen to nitrite-nitrogen and nitrite-nitrogen into nitrate-nitrogen by nitrification bacteria consumes a part of dissolved oxygen. It is expressed respectively in the model as:

$$D_6 = 0.048 \cdot B_{15} = 0.048 \cdot v_{15}(T, DO) \cdot NH_4 \quad (mgO_2 \cdot l^{-1} \cdot day^{-1}) \tag{5.100}$$

$$D_7 = 0.016 \cdot B_{16} = 0.016 \cdot v_{16}(T, DO) \cdot NO_2 \quad (mgO_2 \cdot l^{-1} \cdot day^{-1}) \tag{5.101}$$

Consumption by Sediment

Consumption of dissolved oxygen due to benthic sediments is related to physicochemical and biological processes which take place in the sediment, such as, bacterial decomposition, respiration by benthic organisms, nitrification in the surface mud, etc. All these types of consumptions are expressed in the model as:

$$D_8 = \alpha_{DO} \cdot \exp\left(\beta_{DO} \cdot T^*\right) \cdot h_B \cdot DO, T^* = \max\left\{\ 0, T - T_B\ \right\} \tag{5.102}$$

where T and DO denote water temperature ($^o C$) and dissolved oxygen concentration (mgO_2/l) just above the seabed, respectively, T_B is the lower temperature threshold ($^o C$) above which the oxygen consumption takes place, α_{DO} gives the consumption rate (day^{-1}) at $T = T_B$, β_{DO} the temperature coefficient ($^o C^{-1}$), and h_B the height of the benthic water column (length from the seabed to the center of bottom level).

Aeration

The sea-surface aeration is expressed in the model as:

$$D_9 = k_a \cdot \left(DO_s - DO\right) \tag{5.103}$$

where DO and DO_s are respectively the dissolved oxygen concentration and the saturated oxygen concentration in the surface layer (both in mgO_2/l), k_a is the aeration rate (day^{-1}).

The aeration rate is a function of the wind velocity (m/s) and it is formulated in the model as:

$$k_a = \frac{1}{\zeta + 0.5 \cdot h_1} \cdot \begin{cases} 0.13 \times W & (W \le 3.6) \\ 2.2 \times (W - 3.39) & (3.6 \le W \le 13) \\ 4.3 \times (W - 8.36) & (13 \le W) \end{cases} \tag{5.104}$$

where ζ is the tide level and h_1 is the thickness of the top level (both in m).

5.1.9 Chemical Oxygen Demand (COD)

Chemical oxygen demand (COD) in the model is a parameter associated with the fragile fraction of organic matter, which includes phytoplankton, zooplankton, detritus and dissolved organic matter. COD is expressed in the mode as follows:

$$COD = \sum_{j=1}^{N_P} \lambda_P^j \cdot P_j + \sum_{j=1}^{N_Z} \lambda_Z^j \cdot Z_j + \lambda_{POM} \cdot POC + \lambda_{DOM} \cdot DOC \qquad (5.105)$$

Where, λ stands for the COD/C ratio of each organic compartment, which is closely related to the tissue composition of total oxygen demand (TOD) vs. carbon.

5.2 Calibration of Model Parameters

Marine ecological models have a large numbers of water quality parameters which control the behavior of the model compartments as well as the biochemical processes among them. Some of these parameters may differ greatly from one region to another around the world due to the peculiar physical, biological, chemical and physiological characteristics of each environment especially in the lower-trophic level where, biochemical processes are imbricate and complicated. Most of the biological parameters need laboratory experiments to determine their values.

An important step of any water quality modeling process is to stabilize the model results via adjusting these parameters. In other words, to validate the model to be used for predictive process, some parameters have to be justified to adapt the ambient conditions for the study area, hence to get reasonable results. The stabilization process involves tuning a selected number of the model parameters and the model is run until the computed values match the field-observed values with an acceptable level of accuracy. In the current study, due to resources and time limitation, many of these parameters are determining according different related literatures, while other parameters are tuned many times to get the best results as described earlier.

It should be noted that EUTROP water quality model is run using the same grid regime employed in the flow model, so that the simulated temperature, salinity, tides, current velocities, and vertical eddy diffusivity are readily accommodated in the ecological simulation.

In the present work, there are four sets of data. Due to the large variation of the summer and winter climate conditions in the gulf area, these sets are classified into two major groups, one is for the summer condition (June 2003 and August 2003) and the other is for winter condition (November 2003 and January 2004). As

mentioned earlier (chapter 4), each set of data comprised 30 field measurements from 10 stations taken at three different levels, surface, middle and bottom.

Here, the main considered component which will be investigated is the desalination plant located in the RIC. It is worth mentioning that the desalination plant is not the only component which may deteriorate the coastal water quality of the Ruwais. That is because several other facilities are located in the same area as mentioned in chapter 4. Most of these facilities dispose their effluents in the Ruwais coastal water. But the desalination plant can be distinguished as a higher concentration brine disposal and one of the major sources of the temperature increment in the Ruwais waters. Whereas, the effluents of the other facilities have ambient physical and nutrient conditions with the exception of fertile factory (Table 5.2).

Summer parameter stabilization is performed over two month period between the two observed summer sets; June 2003 and August 2003. The field measurements of June 2003 are considered as initial conditions and the calculated values at the end of two-month period are compared with the field observed values of August 2003. An extensive effort was done to stabilize the compartment parameters, where the model was run several times, in each run, one of these parameters was tuned until reasonable match between the observed and the calculated values is achieved. Figure 5.2 shows a comparison between the observed and the calculated values for the summer condition.

The stabilization process is repeated for winter condition where the initial conditions are taken as the data set of November 2003 and the model calculated results are compared with the field-observed data at January 2004. Figure 5.3 shows the calculated values of various compartments versus the field observed data for the winter condition. The calculated and measured compartment values are distributed almost symmetrically indicating fair agreement similar to the summer results with a better match obtained in case of NO_2 results.

It is worth mentioning for both Figures 5.2 and 5.3, the model calculated values in summer and winter seasons are distributed in a horizontal fashion with a narrow range of variation, whereas, the field-observed values distribute over a wider range and scattered randomly around the ideal trend line. This shows clearly that the output results of the water quality model are more homogenous than the field-observed data. This may refer to several reasons. One of them is the high influence of the model boundary results. As the most of the observed compartments close to the

boundary showed less variation, the variation in the output results over the entire area became small. Other local reason may also arise, which is related to the uncounted petrochemical and oil amounts which pollute the marine water in the Ruwais area due to the continuous movement of the tankers and in accidental oil spill at the existing SPMs (Single Point Mooring). This can potentially contribute to the erratic and non-homogeneity nature of the field-observed data especially DOC and COD.

The stabilized parameters of the model compartments for summer and winter seasons are listed in Table 5.3. Many of the physiological parameters of the model plankton are employed from another study (Taguchi and Nakata, 1998).

Brief comments are presented below about selected compartments in light of the conducted stabilization process parameter values (Table 5.3) and their relevant theoretical aspects.

Table 5.2: Chemical and nutrient loads into the modeled area

	Utility	Q $(m^3.day^{-1})$	NO_2 $(kg.day^{-1})$	NO_3 $(kg.day^{-1})$	NH_4 $(kg.day^{-1})$	PO_4 $(kg.day^{-1})$	COD $(kg.day^{-1})$	DOC $(kg.day^{-1})$
Outfall 1	Oil Refinery (TAKREER)	243600	194.88	316.70	0.00	19.49	19488.00	974.40
	Gas Production Plant (GAZCO)	600000	300.00	600.00	10.00	1.40	36000.00	2400.00
	Total	*843600*	*494.90*	*916.70*	*10.00*	*20.90*	*5548.00*	*3374.40*
Outfall 2	Desalination and Power Plant	192000	19.20	192.00	0.00	15.36	9600.00	768.00
	Fertilization Factory	120000	12.00	120.00	60.00	9.60	6000.00	480.00
	Total	*312000*	*31.20*	*312.00*	*60.00*	*24.96*	*15600.00*	*1248.00*
Outfall 3	Petrochemical Factory (Borooj)	*840000*	*420.00*	*480.00*	*100.00*	*84.00*	*33600.00*	*12600.00*

Figure 5.2: Parameter-stabilization results based on the summer data at three different levels; surface, middle and bottom (● Surface, ■ Middle, ▲ Bottom), ------ and - - - are representing both upper and lower hourly fluctuation respectively of different compartments.
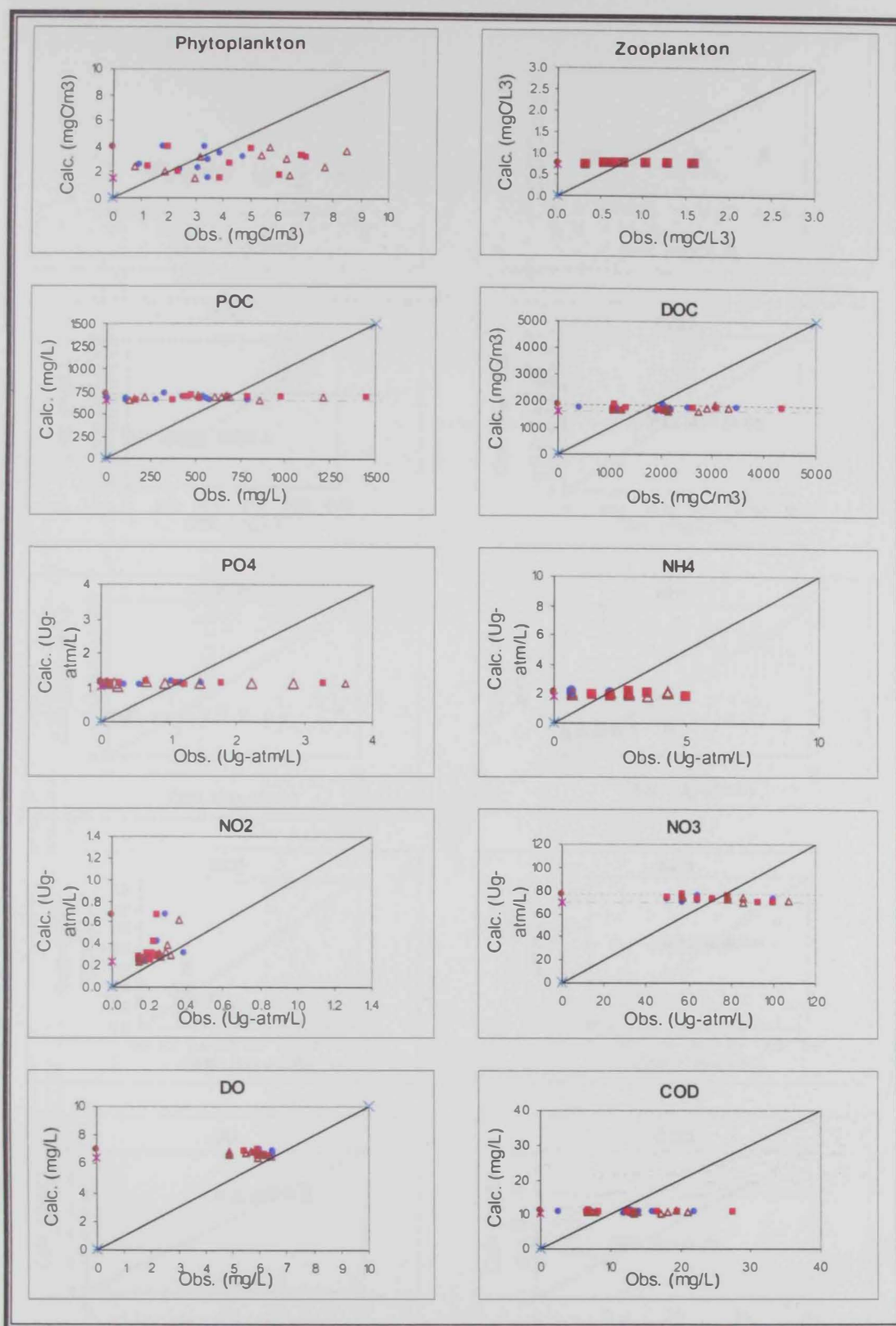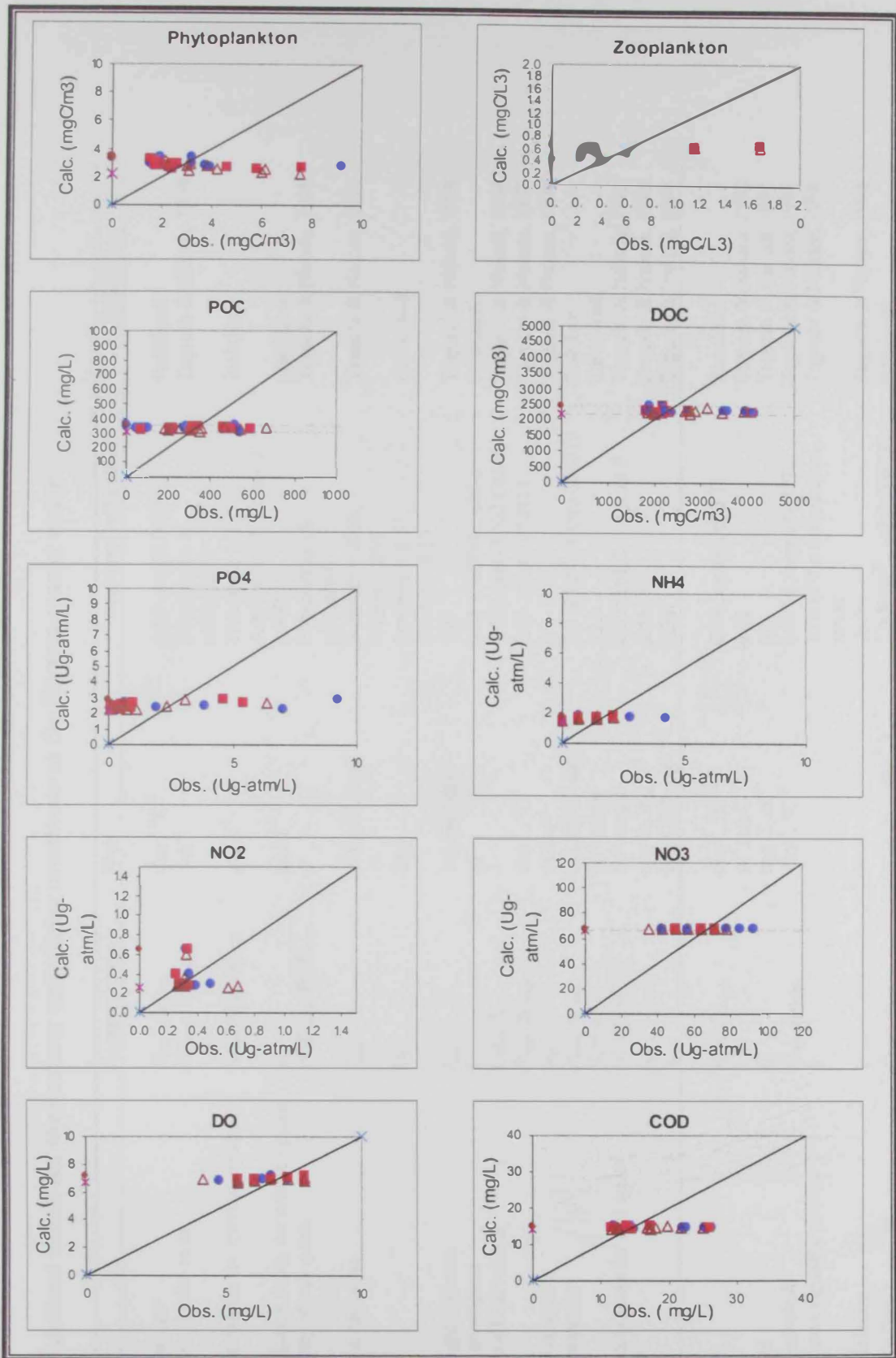
Figure 5.3: Parameter-stabilization results based on the winter data at three different levels; surface, middle and bottom (• Surface, ■ Middle, ▲ Bottom), ------ and ------ are representing both upper and lower hourly fluctuation respectively of different compartments.

Table 5.3: Final stabilized values for the summer and winter conditions at the Ruwais coastal water.

Parameter	Nomenclature	Unit	Arabian Gulf values	Reference
Phytoplankton				
Maximum growth rate	G_{max}, $\beta_{G\ max}$	day^{-1}, $^{\circ}C^{-1}$	$0.50 \cdot exp(0.0633T)$	Stabilized
Maximum nutrient uptake rates	UP_{max}, UN_{max}	day^{-1}	Phosphorus 36, nitrogen 12	Taguchi & Nakata, 1998
Half saturation constants for nutrient uptake	K_{PO4}, K_{NH4}, K_{NO3}	$\mu M.l^{-1}$	Phosphate 1.0, Ammonium 1, nitrate 2	Stabilized
Ammonium inhibition factor for nitrate uptake	ψ	$\mu M.l^{-1}$	1.462	Stabilized
Maximum capacity of cell quota	PQP_{max}, PQN_{max}	-	Phosphorus 16, nitrogen 8	Taguchi & Nakata, 1998
Maximum surface radiation	I_{max}	$cal.cm^{-2} \cdot day^{-1}$	Summer = 2000, Winter = 800	Taguchi & Nakata, 1998
Daytime length	DL	Day	Summer = 0.57, Winter = 0.53	Calculated
Photosynthetic light optimum	I_{opt}	$cal.cm^{-2}.day^{-1}$	150	Taguchi & Nakata, 1998
Light extinction coefficient	k	m^{-1}	$0.21 + 0.0088 \cdot Chl\text{-}a$	Stabilized
Fraction of extracellular release	Ext_0, β_{Ext}	-	$0.135.exp(-0.002.Chl\text{-}a)$	Taguchi & Nakata, 1998
Respiration rate	P_{resp}, $\beta_{P\ resp}$	day^{-1}, $^{\circ}C^{-1}$	$0.03 \cdot exp(0.0524T)$	Taguchi & Nakata, 1998
Sinking rate of living cells	w_p	$m.day^{-1}$	0.2	Taguchi & Nakata, 1998
Rate of natural mortality	P_{mot}, $\beta_{P\ mot}$	$m^3.mg\ C^{-1}.day^{-1}$, $^{\circ}C^{-1}$	$2.0 \times 10^{-2} \cdot exp(0.0693T)$	Stabilized
C /Chl-a ratio	[Chl-a:C]	by weight	15.3	Calculated
C/P, C/N ratios (except for cell quota)	$[C:P]$, $[C:N]$	by weight	C/P 161.3, C/N 15.9	Taguchi & Nakata, 1998
O / C ratio	λ_p	$mg\ O_2.mg\ C^{-1}$	3.41	Taguchi & Nakata, 1998
COD / C ratio	γ_p	$Mg\ COD.mg\ C^{-1}$	1.38	Taguchi & Nakata, 1998
Zooplankton				
Maximum ration	R_{max}, $\beta_{R\ max}$	day^{-1}, $^{\circ}C^{-1}$	$0.18 \cdot exp(0.0693\ T)$	Stabilized
Ivlev's constant	λ	$m^3.mg\ C^{-1}$	0.01	Taguchi & Nakata, 1998
Feeding threshold	Π	$mg\ C.\ m^{-3}$	0.0	Taguchi & Nakata, 1998
Rate of basic metabolism	Z_{resp}, β_{Zresp}	day^{-1}, $^{\circ}C^{-1}$	$0.0214 \cdot exp(0.0637T)$	Taguchi & Nakata, 1998
Energy expenditure in grazing activity	η	-	30% of the daily carbon ration	Taguchi & Nakata, 1998
Assimilation efficiency	e	%	70.0	Taguchi & Nakata, 1998
Rate of natural mortality	Z_{mot}, β_{Zmot}	$m^3.mgC^{-1}.day^{-1}$, $^{\circ}C^{-1}$	$5.0 \times 10^{-2} \cdot exp(0.0693T)$	Stabilized

C/P, C/N ratios	$[C:P],[C:N]$	by weight	C/P 50.0, C/N 6.0	Taguchi & Nakata, 1998
O/C ratio	λ_z	Mg O_2.mg C^{-1}	3.31	Taguchi & Nakata, 1998
COD / C ratio	γ_z	mg COD.mg C^{-1}	1.46	Taguchi & Nakata, 1998
Detrital carbon				
Mineralization rate	V_{POC}, β_{POC}	day^{-1},$^{o}C^{-1}$	0.0015. exp(0.0693T)	Stabilized
Oxygen limitation	DO_{POC}	mg O_2 .l^{-1}	0.5	Taguchi & Nakata, 1998
Fraction of biodegradation	κ	-	25% of mineralization	Assumed
C/P, C/N ratios	$[C:P],[C:N]$	by weight	C/P 63.9, C/N 7.2	Taguchi & Nakata, 1998
O/C ratio	λ_{POC}	mg O_2.mgC^{-1}	3.31	Taguchi & Nakata, 1998
COD / C ratio	γ_{POC}	mg COD.mg C^{-1}	1.46	Taguchi & Nakata, 1998
Sinking rate	w_{POC}	m.day^{-1}	0.5	Taguchi & Nakata, 1998
Dissolved organic carbon				
Mineralization rate	V_{DOC}, β_{DOC}	day^{-1},$^{o}C^{-1}$	0.001 . exp(0.0693T)	Stabilized
Oxygen limitation	DO_{DOC}	mg O_2.l^{-1}	0.5	Taguchi & Nakata, 1998
C/P, C/N ratios	$[C:P],[C:N]$	by weight	C/P 124.98, C/N 10	Taguchi & Nakata, 1998
O/C ratio	λ_{DOC}	mg O_2.mg C^{-1}	2.82	Taguchi & Nakata, 1998
COD / C ratio	γ_{DOC}	mg COD.mg C^{-1}	1.38	Taguchi & Nakata, 1998
Others				
Nitrification rate of ammonium	k_{NH4}, β_{NH4}	day^{-1},$^{o}C^{-1}$	0.01 . exp(0.0693T)	Stabilized
Oxygen limitation	DO_{NH4}	mg O_2.l^{-1}	0.5	Taguchi & Nakata, 1998
Nitrification rate of nitrite	k_{NO2}, β_{NO2}	day^{-1},$^{o}C^{-1}$	0.1 . exp(0.0693T)	Stabilized
Oxygen limitation	DO_{NO2}	mg O_2 .l^{-1}	0.5	Taguchi & Nakata, 1998
Aeration rate	k_a	day^{-1}	0.5	Stabilized

5.2.1 Phytoplankton

Phytoplankton is considered as the most important compartment in the model, where it affects and is affected by many other model compartments. As some parameters have a distinct effect on the phytoplankton, other parameters have a slight or even null effect as follows:

Maximum growth rates of phytoplankton "G_{max}" the most effective parameters on its biomass. Increasing "G_{max}" by 40% tends to increase the phytoplankton biomass by 59%., whereas there is a slight increase (5%) of the particular organic matter (POC). Referring to equation (5.44), this slight increase of (POC) may be due to the increased mortality of phytoplankton associated with the high growth rate. It is worth mentioning that even with high growth rate of phytoplankton biomass, the zooplankton biomass was not affected, this may refer to scarcity of zooplankton species in the Ruwais coastal water as the amounts of phytoplankton do not contribute to their grazing. So excess amount of phytoplankton may not be grazed, and is may cause red tides and push toward the eutrophication conditions.

Rate of natural mortality "P_{mot}" has an essential effect on the phytoplankton biomass, where increasing "P_{mot}" by 90% tends to decrease the phytoplankton biomass to 76% without any change on the other compartments.

Some other parameters are used to make fine tuning of the phytoplankton compartment, where changing their values have a slight effect on the phytoplankton results. These parameters are; half saturation constants for nutrient uptake (KPO_4, KNH_4, KNO_3), ammonium inhibition factor for nitrate uptake (ψ), and light extinction coefficient (k).

5.2.2 Zooplankton

Zooplankton has complex relations with the other model compartments through different parameters as follows:

Maximum ration "R_{max}" has a crucial role in controlling the zooplankton biomass, where increasing "R_{max}" by 90% tends to increase the zooplankton biomass by 370%. This result has many effects on most of the model compartments, where phytoplankton biomass decreases by 9.2%. This indicates that even with the tremendous increase of zooplankton, phytoplankton is not severely affected. This refers to the very few number of zooplankton species which originally exist.

Moreover, "R_{max}" increasing causes (POC) to decrease by 7.8%. Referring to equation (5.44), this may be occurred due to high feeding rate of zooplankton on the detritus. Also, increasing "R_{max}" by 90% tends to increase (PO_4) by 6.2% due to the excretion of zooplankton; according to equation (5.57). This similarly increases (NH_4) by 15.6% due to the same reason; equation (5.62).

Rate of natural mortality "Z_{mot}" is the second parameter that affects the zooplankton biomass, where increasing "Z_{mot}" by 90% causes a decrease of zooplankton biomass by 5.5% as reflected by equation (5.24).

5.2.3 Detritus

As mentioned in the previous section (5.1.4), detritus is related to dead phytoplankton, zooplankton and non-biological components. In the model, detritus is affected by several factors. Mineralization rate of detritus (α_{12}) was used to stabilize the (POC) compartment. It was found that increasing (α_{12}) by 90%, POC compartment increases by 3.9%, NH_4 increases by 5% which causes an increase in the nitrification processes rate so, NO_2 increases by 3.6% as can be seen from equations (5.44), (5.62), and (5.70) respectively.

5.2.4 Dissolved Organic Matter

Increasing the mineralization rate of bacterial decomposition (α_{14}) by 100% yields an increase of (NH_4), (NO_2), and (PO_4) compartments by 7.1%, 5%, and 1.68% as reflected in equations (5.62), (5.70), and (5.57), respectively. Whereas, a decreasing by 2% and 0.63% occurs for (DOC) and (DO) compartments corresponding to equations (5.52) and (5.87) respectively.

5.2.5 Ammonium and Nitrite

To stabilize the nitrogen-related nutrients, nitrification rate of ammonium (K_{NH4}) and nitrification rate of nitrite (K_{NO2}) were tuned to get the desirable trend of results. It was found that increasing (K_{NH4}) by 100% tend to decrease (NH_4) by 9.1% and increase (NO_2) by 1.7%. These are corresponding to equation (5.62) and 5.70) respectively. Whereas, increasing (K_{NO2}) by 100% produces an increase of 10.6% for (NO_2) compartment.

The remaining compartments such as (PO_4), (DO), and (COD) are stabilized implicitly during tuning of other compartments as shown in equations (5.57), (5.87), and (5.105).

5.3 Aerial Distribution of Simulated Results

This section presents the simulated results and describes their aerial distribution.

Figures from 5.4 to 5.13 show the surface spatial distribution of different compartments in summer season. Due to homogeneity of the water column in the area as mentioned before, the compartments have slight difference in their values in the three depths; surface, middle and bottom. Hence, the surface layer is used herein to explain the general trend for the different compartments in the Ruwais coastal area.

Figure 5.4 shows the phytoplankton distribution in the area. It is noted that its value fluctuates almost from 2 to 5 mg/m^3. The value of phytoplankton biomass is higher in the south due to high nutrient rates corresponding to the RIC effluents which dump high quantities of the nutrients in the coastal water, whereas its values decreases southward and westward.

Figure 5.5 shows that the zooplankton biomass varies from 0.6 to 1.3 mg/m^3. It is clear that the distribution of the zooplankton have a trend contrasting with phytoplankton distribution, where the zooplankton biomass is lower in south and higher in the north in spite of the abundance of the phytoplankton in south. This may be attributed to high pollution due to the effluents from the RIC in addition to the petrochemical contaminants due to oil activates in the port of Ruwais which may threaten the zooplankton biomass and diminish its growth.

Figure 5.6 shows that the particulate organic matter (POC) is varying from 300 to 700 mg/m^3. The values decreases eastward and northward and increases southward and westward.

The dissolved organic matter (Fig. 5.7) is high in the south due to the RIC effluents which contribute to raise the DOC concentration in the southern area up to 2400 mgC/m^3, and it reduces toward the east to around 1200 mgC/m^3 due to mixing with the eastern boundary with the Gulf water that causes a dilution for the DOC concentration.

Figure 5.8 shows the phosphate (PO_4) spatial distribution that varies from 0.3 to 1.0 µmol/L, and it increases eastward. At the effluent area, it is noticeable that the

phosphate concentration increases due to the nutrient discharges from the industrial complex.

The distribution of ammonia (NH_4) which is shown in Figure 5.9 indicates high concentrations near the open boundary and vicinity to the effluent area reach up to 2.66 $\mu mol/L$, whereas values the middle area fluctuate around 2.3 $\mu mol/L$.

Figure 5.10 illustrates the nitrite (NO_2) distribution as its values increase toward the shore line and decrease offshore. Its value varies from 0.3 to 2 $\mu mol/L$ with the high concentration around the effluent area due to the industrial complex discharging.

The nitrate NO_3 (Fig. 5.11) has a general increasing trend eastward, and its values vary from 59 to 87 $\mu mol/L$.

Figure 5.12 shows the dissolved oxygen (DO) distribution. DO varies between 5 to 10 mg/L, and it decreases toward the shoreline. This decrease may refer to high petrochemical pollutants that lead to more oxygen consumption by the bacteria for their decomposition.

Figure 5.13 shows the surface distribution of the chemical oxygen demand (COD). It is clear that the COD decreases eastward and it varies from 5 to 13 mg/L. At the effluent points, DOC has high levels in association with high the bacterial decomposing activities.
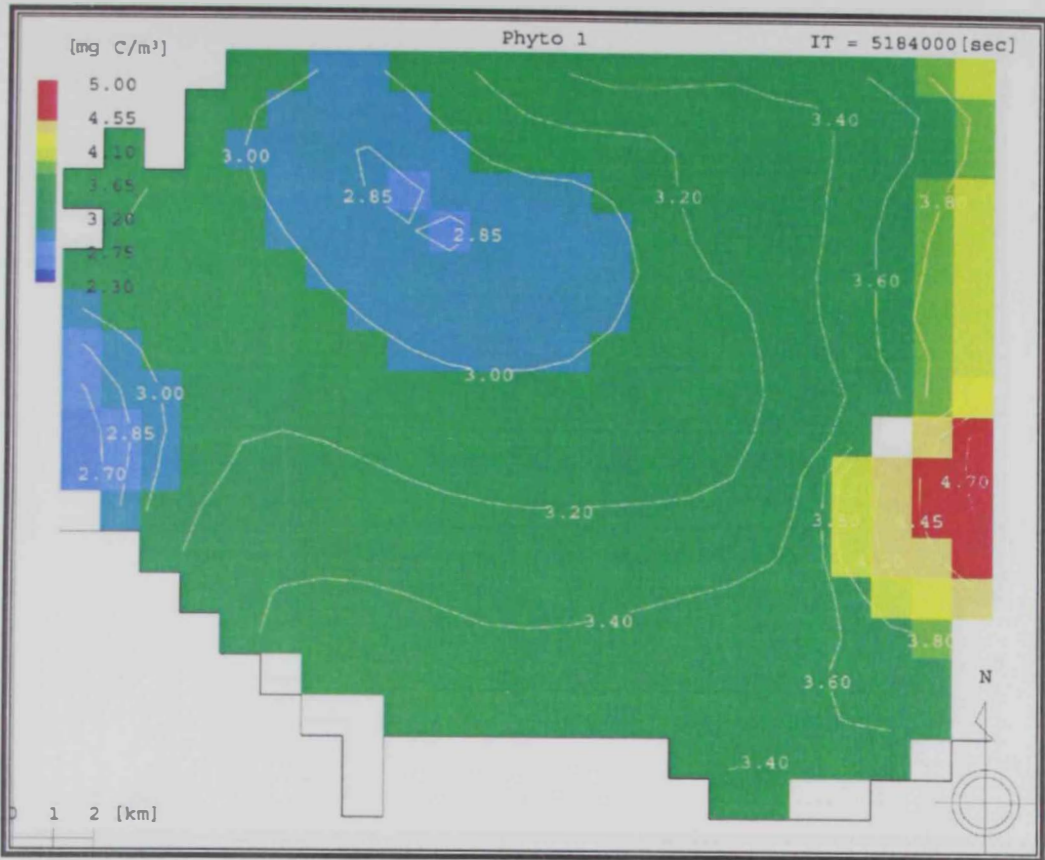
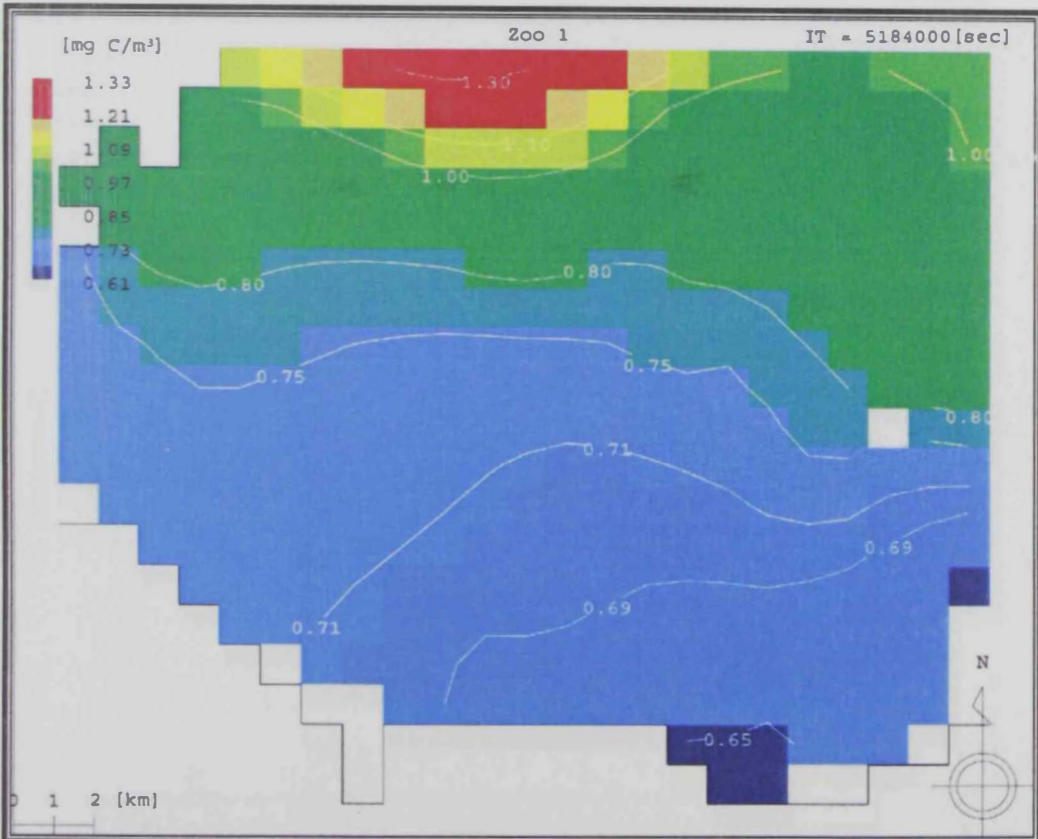Figure 5.4: Surface spatial distribution of phytoplankton in summer season

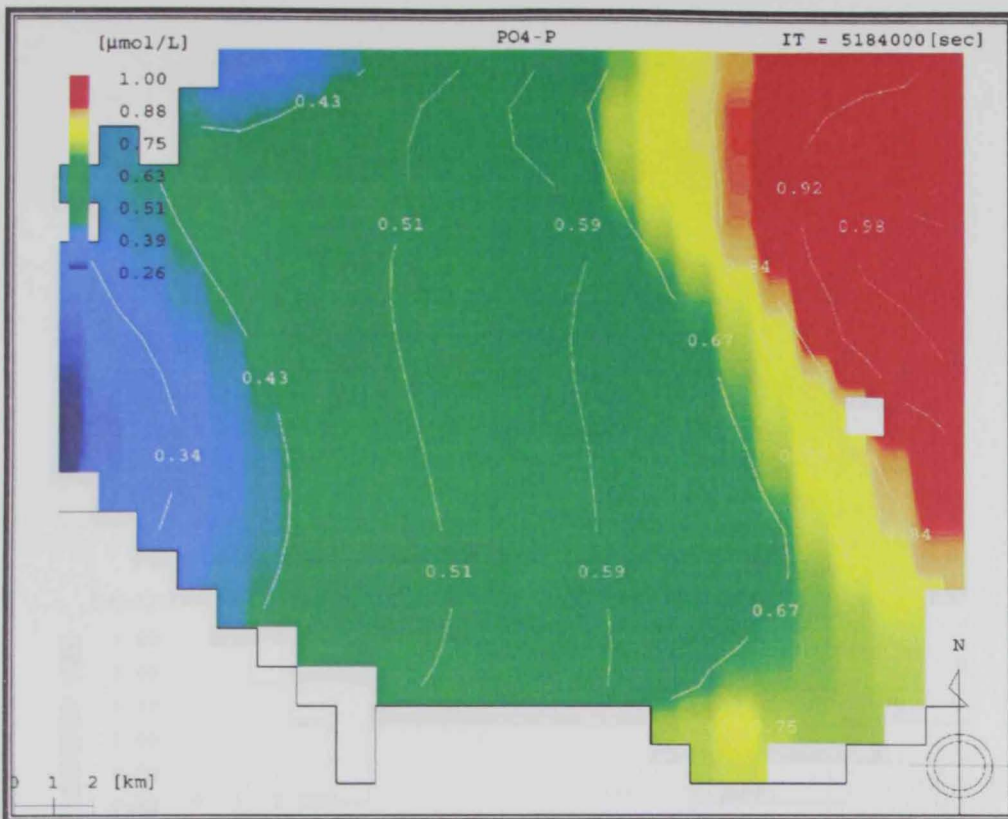Figure 5.5: Surface spatial distribution of zooplankton in summer season

Figure 5.6: Surface spatial distribution of POC in summer season

Figure 5.7: Surface spatial distribution of DOC in summer season

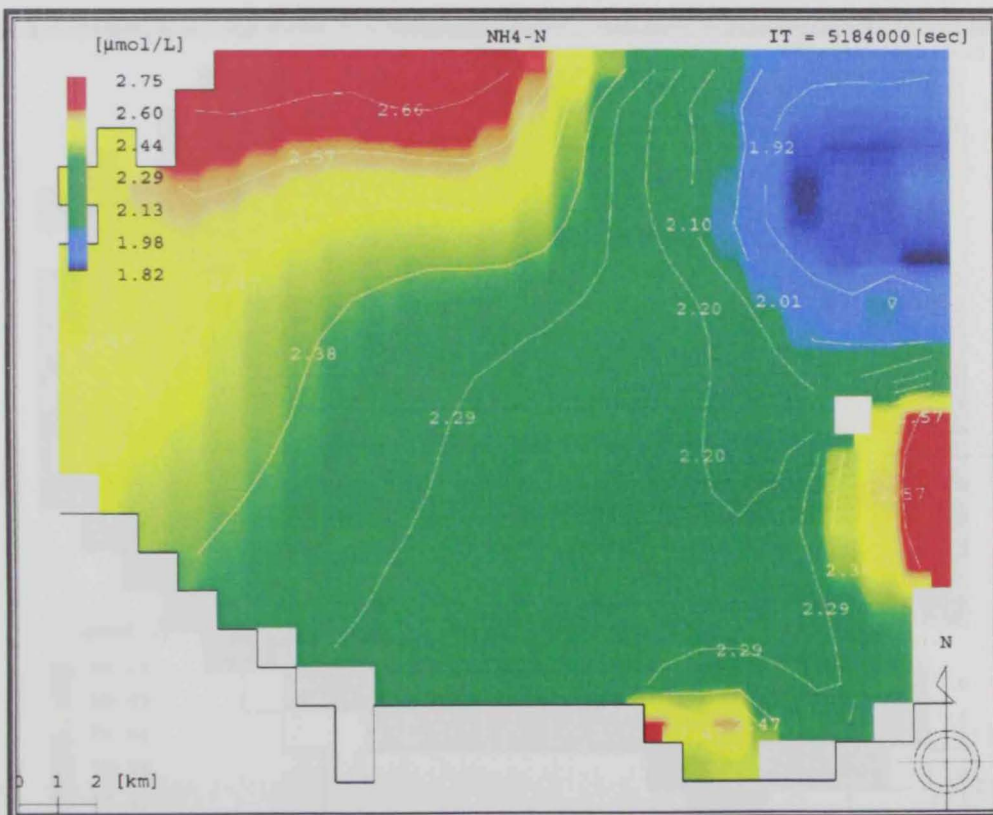Figure 5.8: Surface spatial distribution of PO₄ in summer season

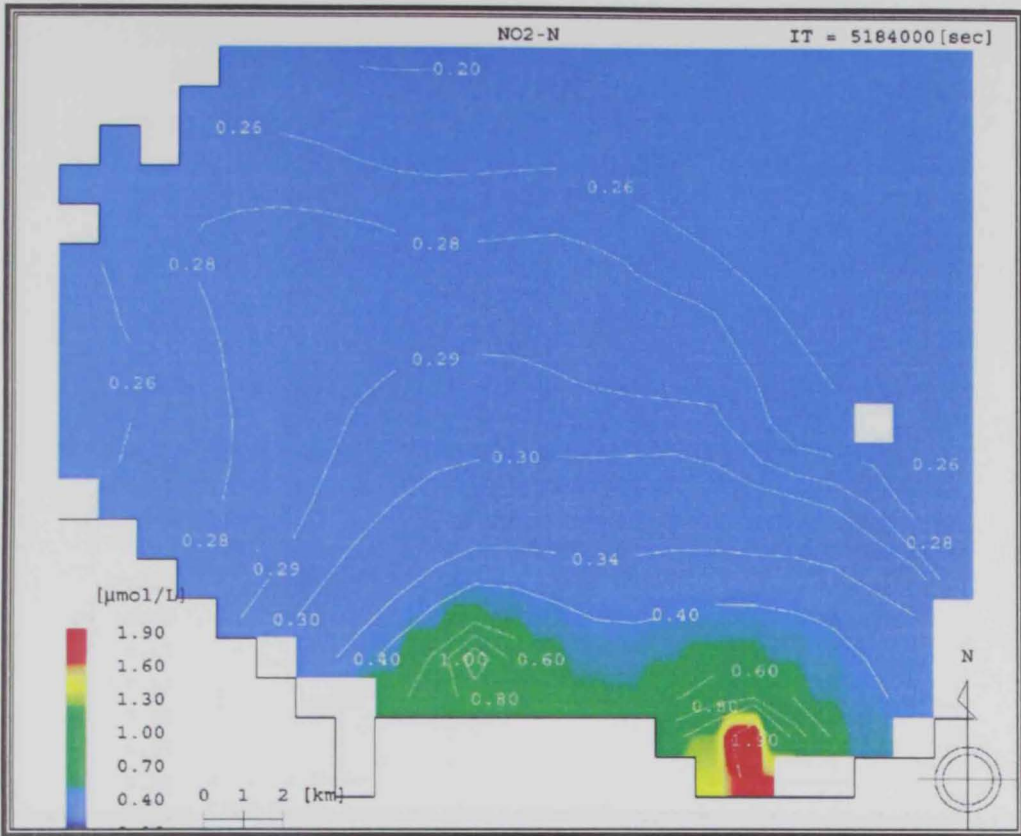Figure 5.9: Surface spatial distribution of NH₄ in summer season

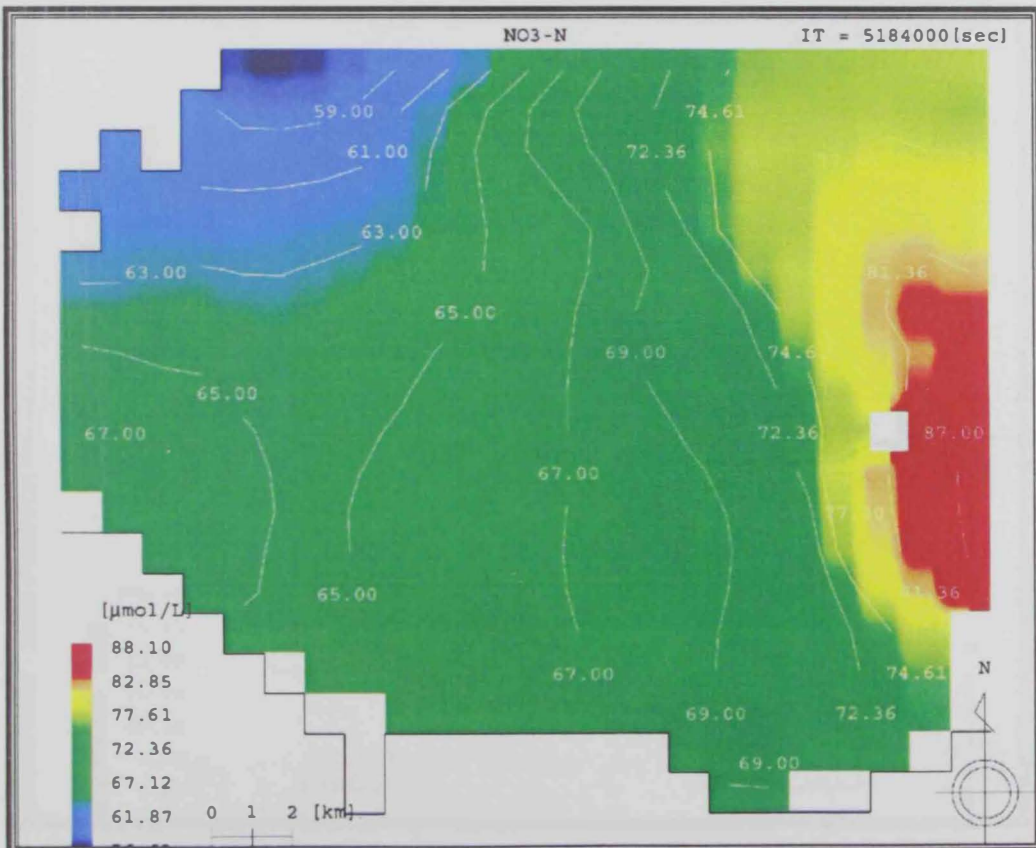Figure 5.10: Surface spatial distribution of NO₂ in summer season

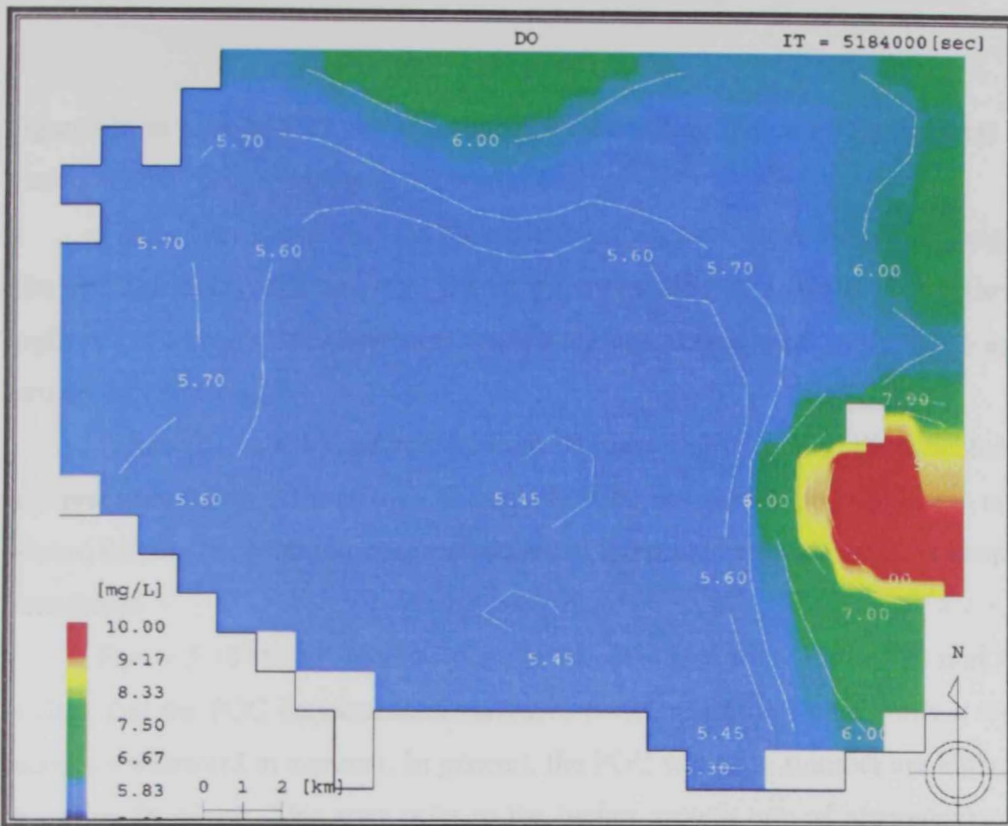Figure 5.11: Surface spatial distribution of NO₃ in summer season

Figure 5.12: Surface spatial distribution of DO in summer season
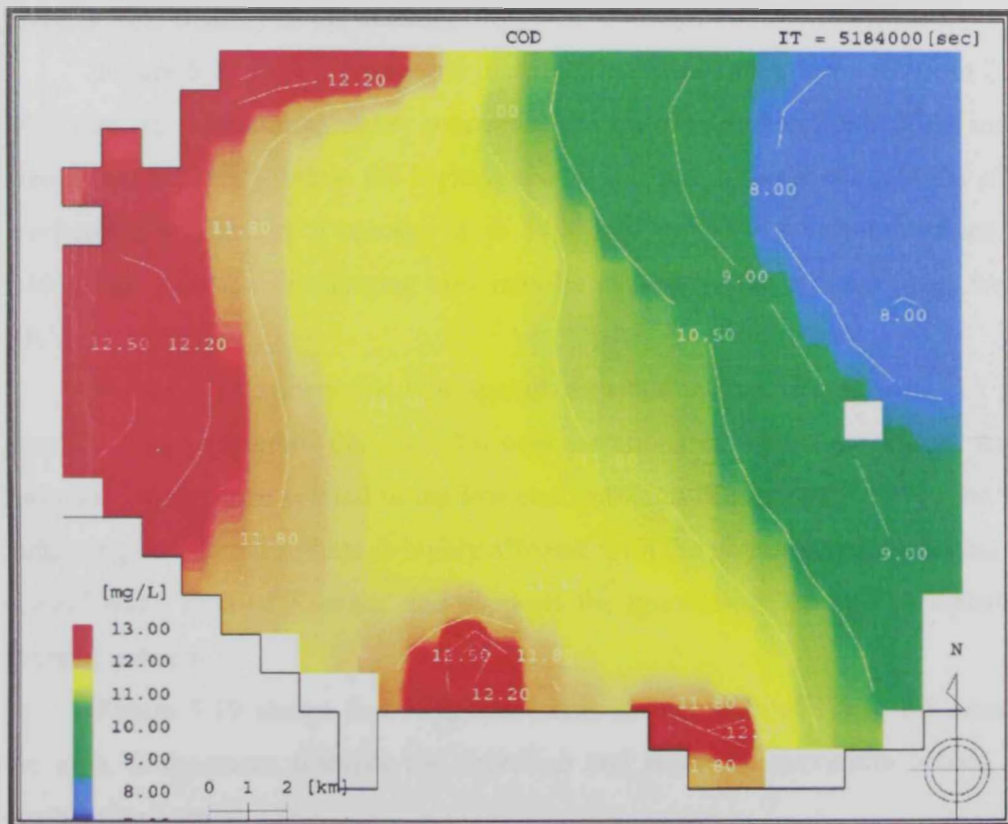

Figure 5.13: Surface spatial distribution of DOC in summer season

Figures from 5.14 to 5.23 show the surface spatial distribution of the different water quality model compartments in the winter season.

Figure 5.14 shows that the phytoplankton biomass varies from 2 to 5 mgC/m^3. The RIC effluent zone has the lowest phytoplankton biomass concentration (2.5 mgC/m^3), whereas values increases toward the open boundaries in the north and the east up to 5 mgC/m^3.

Figure 5.15 shows the zooplankton biomass distribution in the modeled area. It varies from 0.8 to 1.3 mgC/m^3. The zooplankton has similar phytoplankton trend in winter; i.e., the concentration decreases toward the shore line and increases toward the boundaries.

Figure 5.16 shows the POC distribution. It ranges from 350 to 730 mgC/m^3. It is clear that the POC concentration increases eastward in the winter while it tends to increases westward in summer. In general, the POC values in summer are higher than its values in winter. This may refer to the higher growth rate of phytoplankton and zooplankton in summer than in winter, which produces higher mortality rates. It may be also attributed to increased levels of oil contamination as the tanker activities increase significantly in the summer.

Figure 5.17 shows the spatial distribution of the DOC. It ranges from 2500 to 3400 mgC/m^3. Generally, higher concentrations are toward the middle of the modeled area (3000 mgC/m^3), while the highest spot is located in the south near the effluent discharging area where it reaches up to 3400 mgC/m^3. These extreme values at the middle and near the discharging area may be caused by the effluent loads from the RIC.

Figure 5.18 shows the PO$_4$ spatial distribution that ranges from 0.5 to 2.0 μmol/L. It is noticeable that the PO$_4$ concentrations in winter are higher than the summer. This may be related to the low concentration of phytoplankton in the winter indicating that the phosphate is highly affected with the phytoplankton biomass in the coastal water area of Ruwais, and supports the speculation that the phosphate is a limiting nutrient.

Figure 5.19 shows that NH$_4$ concentration ranges from 1.5 to 2.5 μmol/L in the area. It increases towards the shoreline and reach its maximum values at the discharging area.

Figure 5.24 shows the NO_2 spatial distribution that ranges from 0.5 to 1.8 µmol/L and increases toward the shoreline. It is clear that there is no large difference in the summer and winter values of NO_2.

Figure 5.25 shows that NO_3 concentration varies from 63 to 76 µmol/L as it increases south-western ward in contrast with the summer trend.

Figure 5.22 shows that the DO varies from 5.5 to 10 mg/L. It increases toward the south-east. This may be attributed to high rate of aeration of the water due to the tanker and ships movement in that area where the port is located.

Figure 5.23 shows that COD ranges from 13 to 22 mg/L. The higher concentration values are located in the middle of the modeled area. This may relate to high DOC values in that area. Generally, COD in winter is higher than in summer due to higher values of DOC in winter than in summer.

Figure 5.14: Surface spatial distribution of Phytoplankton for winter season

Figure 5.15: Surface spatial distribution of Zooplankton for winter season

Figure 5.16: Surface spatial distribution of POC for winter season

Figure 5.17: Surface spatial distribution of DOC for winter season

Figure 5.18: Surface spatial distribution of PO₄ for winter season

Figure 5.19: Surface spatial distribution of NH₄ for winter season

Figure 5.20: Surface spatial distribution of NO₂ for winter season

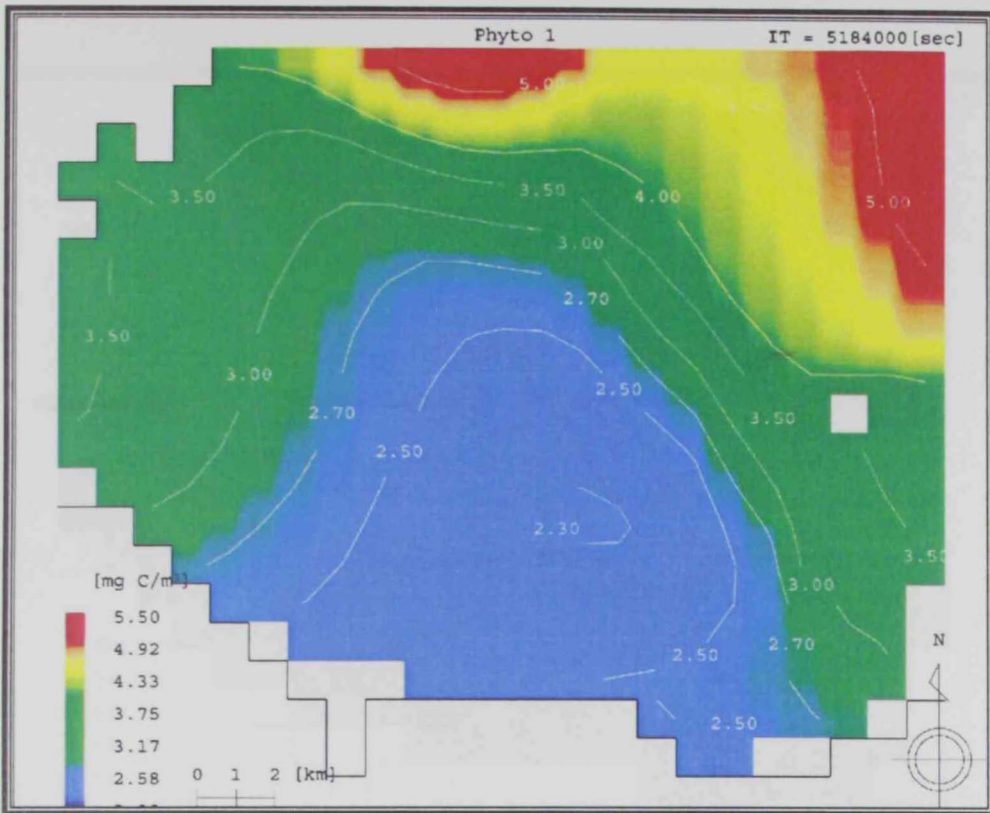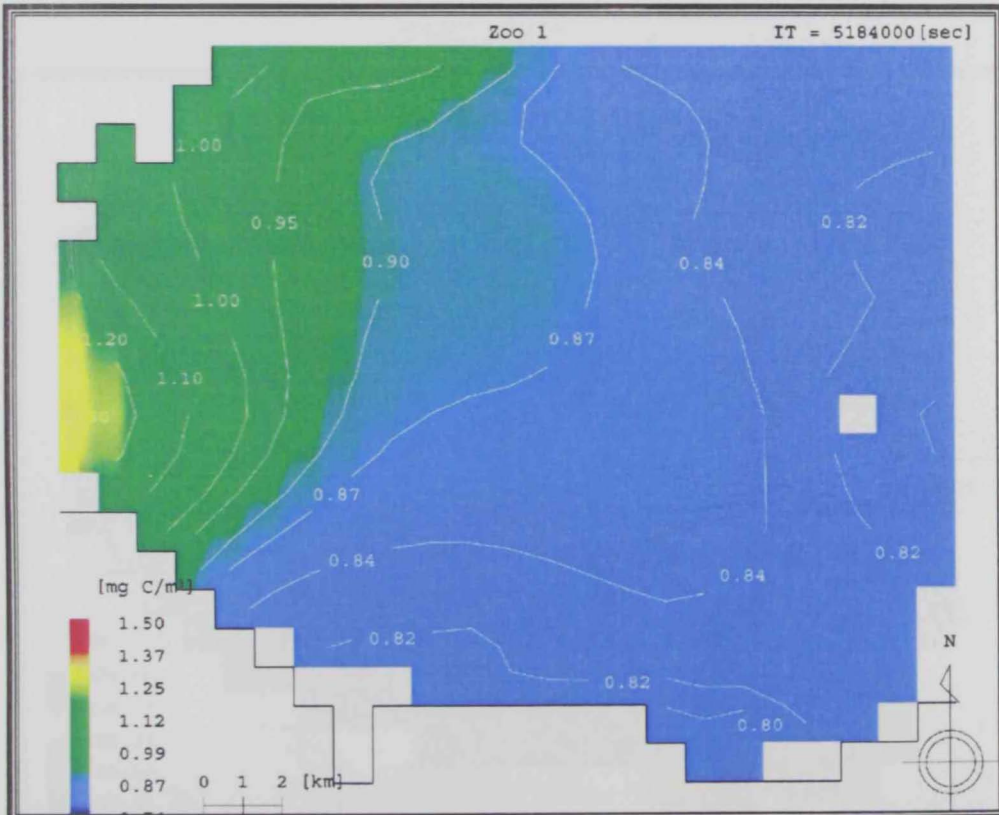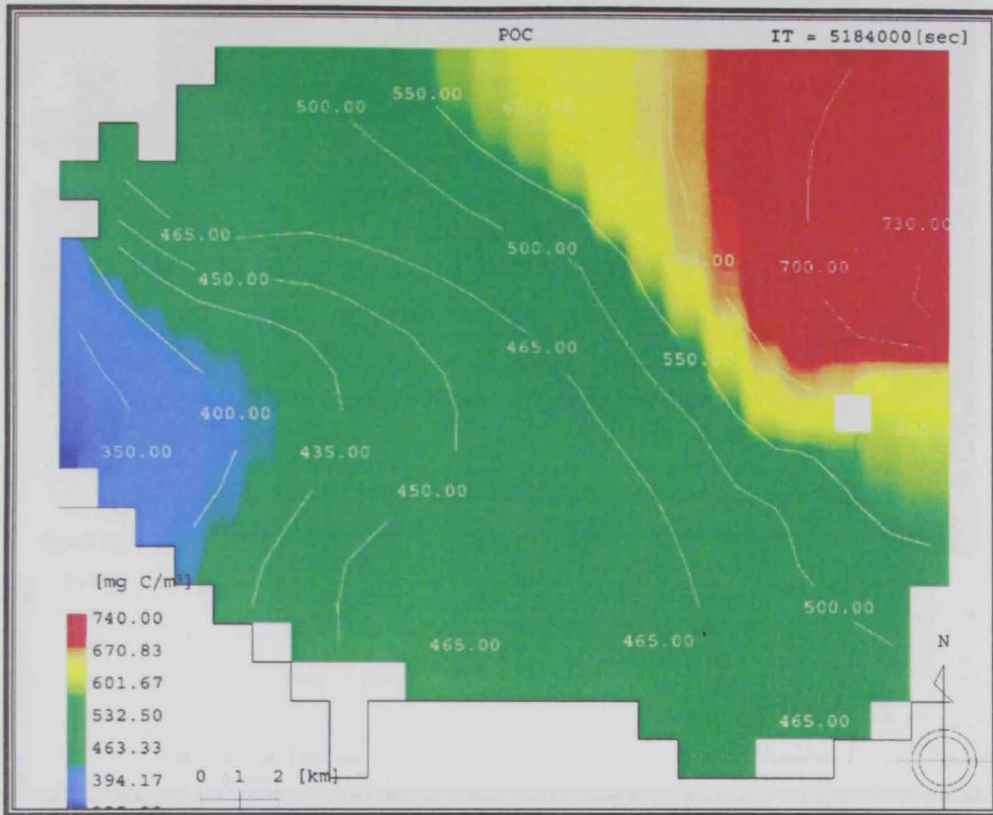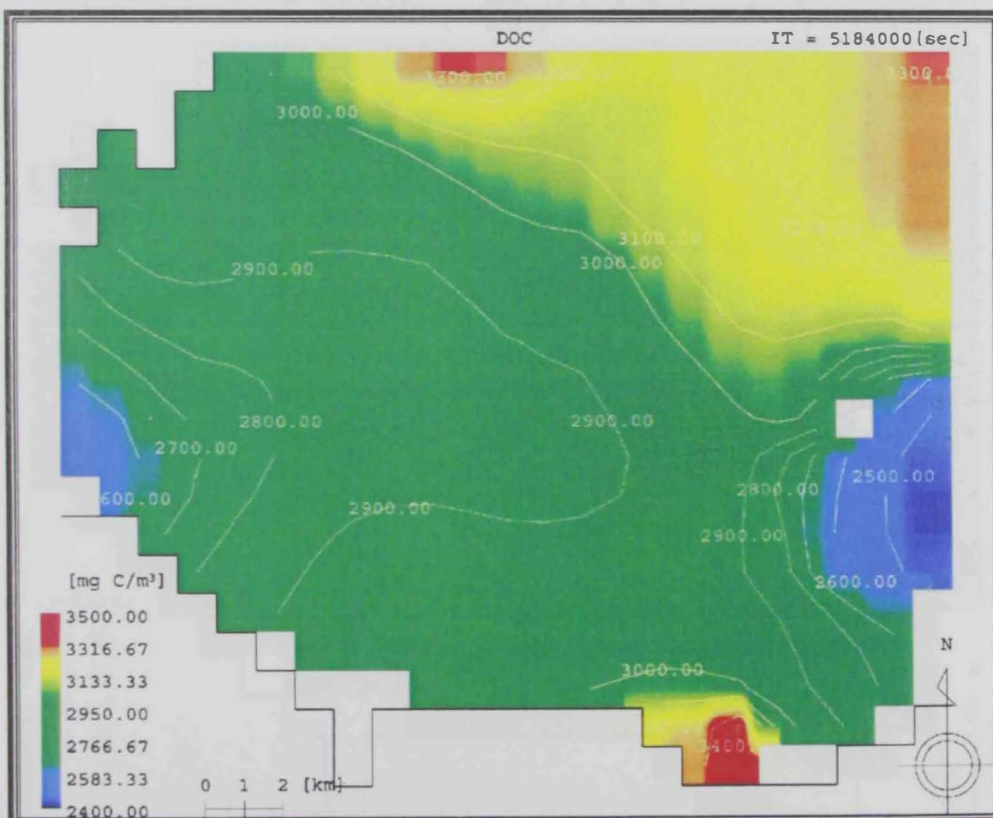
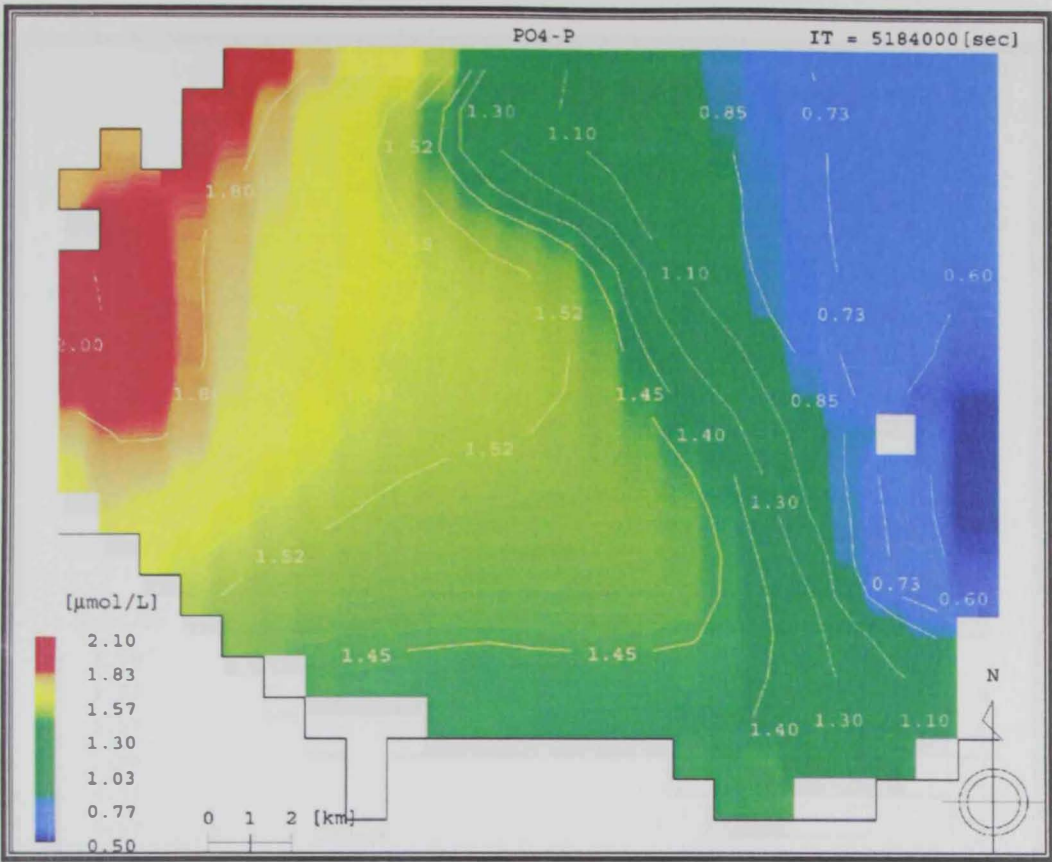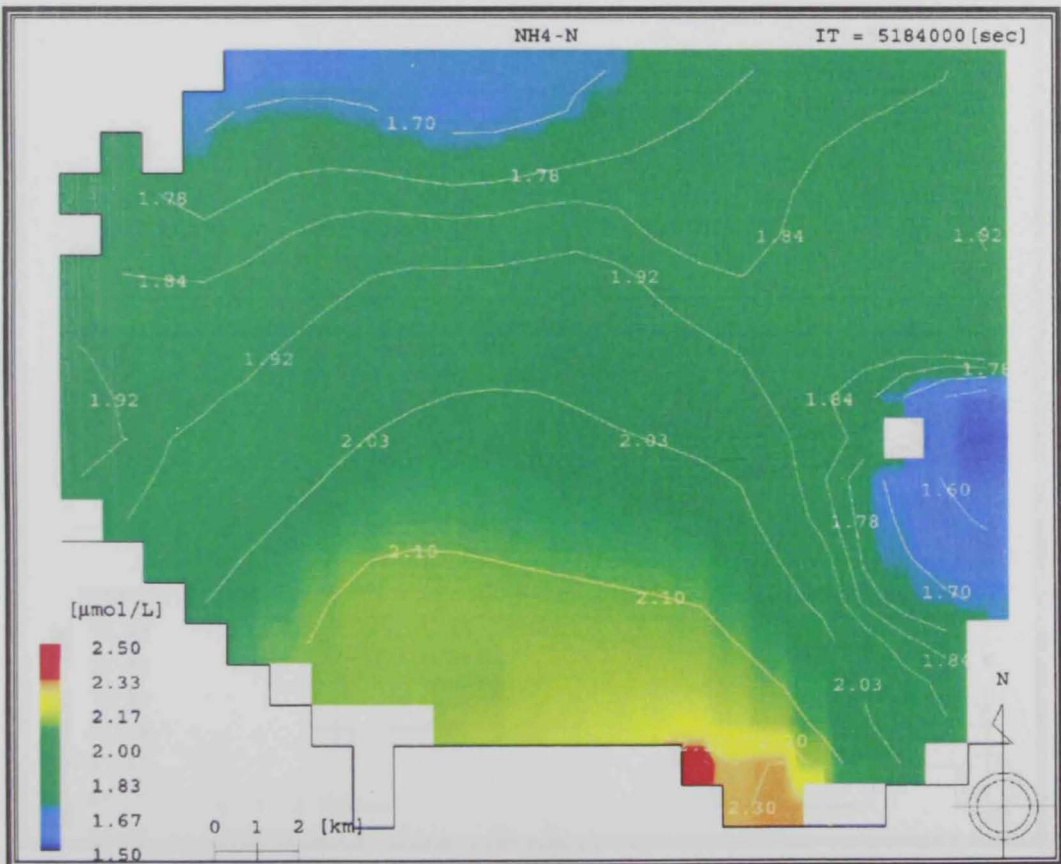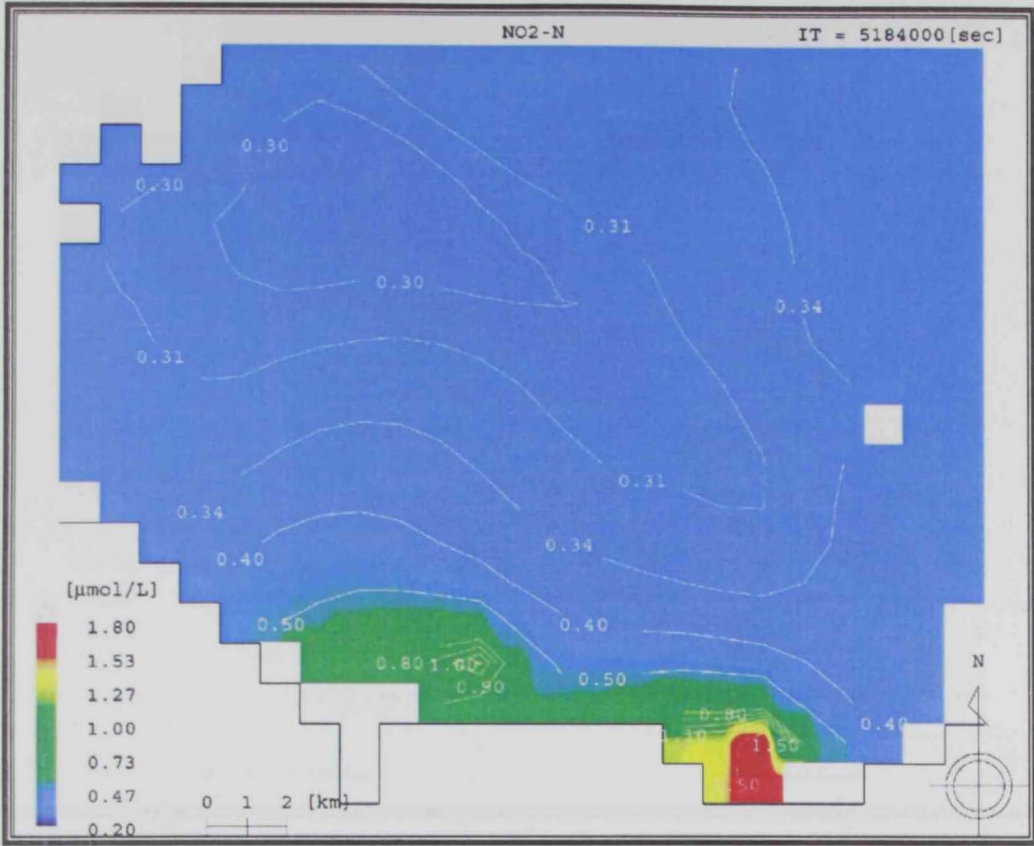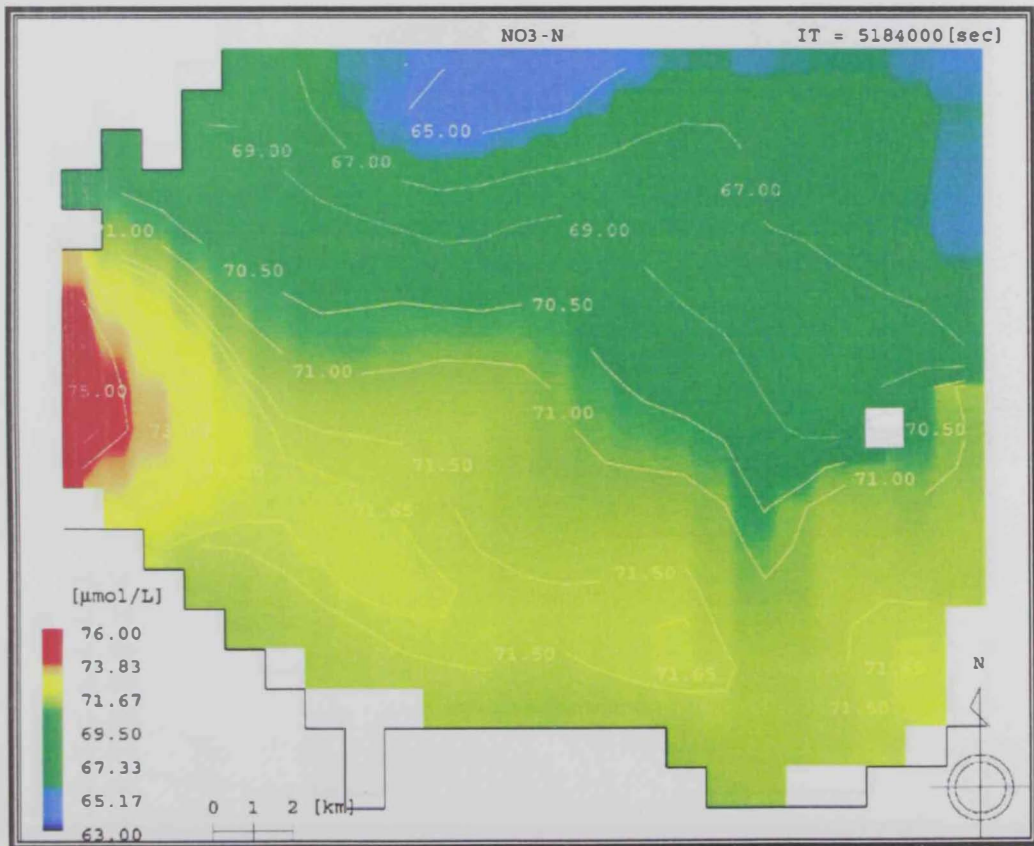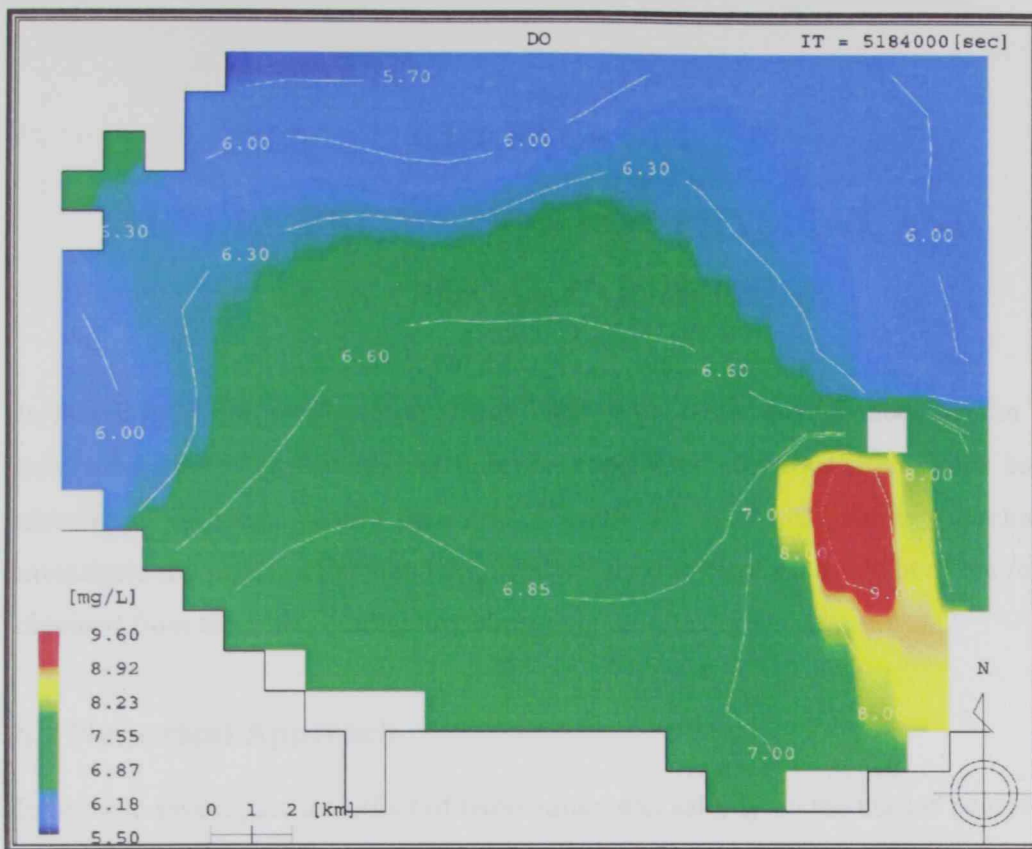Figure 5.21: Surface spatial distribution of NO₃ for winter season

Figure 5.22: Surface spatial distribution of DO for winter season
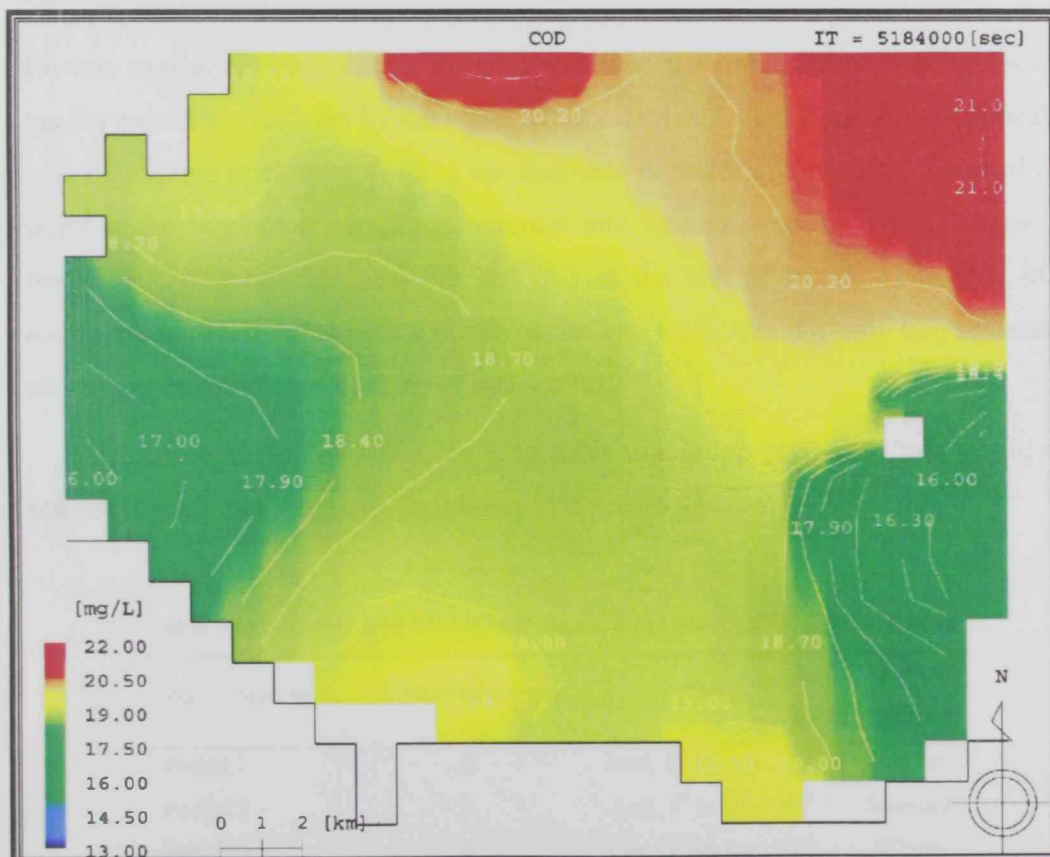
Figure 5.23: Surface spatial distribution of COD for winter season

CHAPTER SIX
FUTURE PREDICTION FOR PHYSICAL AND ECOLOGICAL CONDITIONS

In this chapter, the numerical approach used in the water quality modeling for long term prediction is explained, and then the considered scenarios used in the impact assessment investigation are presented. Results of the hydrodynamic modeling to investigate the future salinity and temperature are discussed on the light of the results obtained from the water quality modeling.

6.1 Numerical Approach

In order to investigate the effect of temperature and salinity on the marine ecosystem, the 1 km coarse grid model developed earlier for the Ruwais coastal area is nested with the regional model of the entire Arabian Gulf basin. The local nested model is employed in the simulation of both hydrodynamic and biological features of the Ruwais coastal environment. In the present study, the simulated periods by the water quality model are dictated by the water quality data collected from site of application. . As mentioned in chapter 4, there are four sets of water quality data. Three of them were at the beginning of spring, summer and autumn seasons (June, August and November, respectively), and the last one at the end of winter (January). In the numerical simulation for both hydrodynamic and water quality, only two seasons are taken in consideration; i.e. summer and winter.

The time domain considered in long term simulation is divided into years; each year is divided into 4 periods as follows in Table (6.1).

Table 6.1: Summer and winter months used for the local model simulation

Period Number	Number of months	Time	Season condition
Period 1	2	June, 1st to July., 31st	Summer
Period 2	2	Aug.,1st to Sep. 30th	Summer
Period 3	4	Oct., 1st.to Jan., 31st	Winter
Period 4	4	Feb., 1st to May, 31st	Summer

To accommodate the proposed periods with the available data set in the first year, an approximation is made in which the needed data for October is considered equivalent to the available November data, while the needed data for February is considered equivalent to the available January data set.

6.1.1 Hydrodynamic Modeling Numerical Approach

Due to the lack of data for regional boundary conditions at Strait of Hormuz for future years, the hydrodynamic model is run for one full year in four separate runs considering the four proposed periods in Table 6.1. Thus, the successive iterations for the water quality future simulation are modeled over the same regime of hydrodynamic conditions that take into account the differences between both summer and winter seasons but repeated in typical annual cycles.

The four separate runs of hydrodynamic modeling conducted to cover one full year are described here. First, the boundary condition files of the four simulation periods for different model parameters are prepared using auxiliary software as mentioned in chapter 4. The data used for such files are the field measured data. In the first run for the period 1, the field measured values on June 1st are employed as initial conditions along with summer set of model parameters listed in Table 3.3. The output files of the previous simulation process are used as initial condition files for the second simulation period 2, again along with summer set of model parameters. Then, the output file produced from the second period is used as initial condition file for the third simulation period 3 with winter set of model parameters listed in Table 3.3. Finally, the output of the third simulation period is considered as initial condition for the last simulation period 4 with summer set of model parameters.

6.1.2 Water Quality Numerical Modeling Approach

Water quality data available for ecological modeling is also limited to one year similar to the hydrodynamic data. The difference here is that the water quality model "EUTROP" is run for several future years utilizing one-year data set only; where the open boundary conditions for the successive years are recreated from the previous years.

The simulation process of the first year starts from the first of June and extend to 31st of May of the next year. Initial and boundary conditions of the water quality

model for the first year are illustrated in Figure 6.1. It is shown that the initial condition used in the first year is the observed data of June 2003. These data and August 2003 observed data are both used to create the boundary condition for the first period. This is accomplished by extrapolating each data set to approximate the boundary data in June and August. The two extrapolated sets are then utilized to produce linear time-dependent boundary condition over the period in question. The model is run considering summer condition, and the results for different compartments are obtained for August 2003. For each compartment, the average of the obtained result and the observed data is considered as initial conditions for the second simulation period. Moreover, this averaged file is used with October observed data set to create the boundary condition for the second simulation period. The process of creating such initial and boundary conditions continues similarly for the whole first year taking into consideration the proper set of model parameters, i.e. summer and winter.

In order to proceed with the simulation for the second and further extended years, the process of creating the boundary condition is different due to the absence of data for the next years. So, two different approaches are used to achieve this task.

Approach 1: Boundary conditions based on the previous year results

This approach is illustrated in Figure 6.2. For the simulation of the first period in the second year starting at the first of June 2004, the result files obtained from the last simulation of the fist year (June 2004 results) are used as initial conditions and it is also used with the average results of August 2003 to create the boundary conditions for the first simulation period (June, 1st to July., 31st). For the second simulation period, the result file of the previous simulation is used as an initial condition and it is also used with results of October 2003 to create the boundary condition of the second period, and so on. In Figure 6.2, the boxes which have the same color indicate that they have the same data sets.

The reason for using such technique for creating boundary conditions for the second year periods is referring to the speculation that the effect of the first year condition vanishes gradually in the second year and almost disappears with extended periods. This approach is consistent with the initial condition assumption where its effect normally disappears after certain period of time. The disadvantage of such

technique is the new simulations are always restrained by the previous year results. The second approach is used to overcome this limitation.

Approach 2: Constant Boundary Conditions

This approach is simpler and straightforward as it tends to avoid the influence of the previous year conditions on the future simulations. Figure 6.3 illustrates the procedure of dealing with boundary conditions for further year simulations. As shown in the figure, the starting point is similar to the previous approach (Result June, 2004). This result set is used as an initial condition for the first period of simulation in the second year (June, 1st to July, 31st). Moreover, the same set is used to generate the boundary condition for that period, so the boundary conditions are considered constant over the simulation period. Then, the results of previous simulation is used as an initial condition for the next period and also used to create the boundary condition of the same period (Aug., 1st to Sep., 30th), and the process goes on for other periods of following years. In Figure 6.3, the boxes which have the same color indicate that they have the same data sets. The results of using such approaches are discussed in detail later in the current chapter.
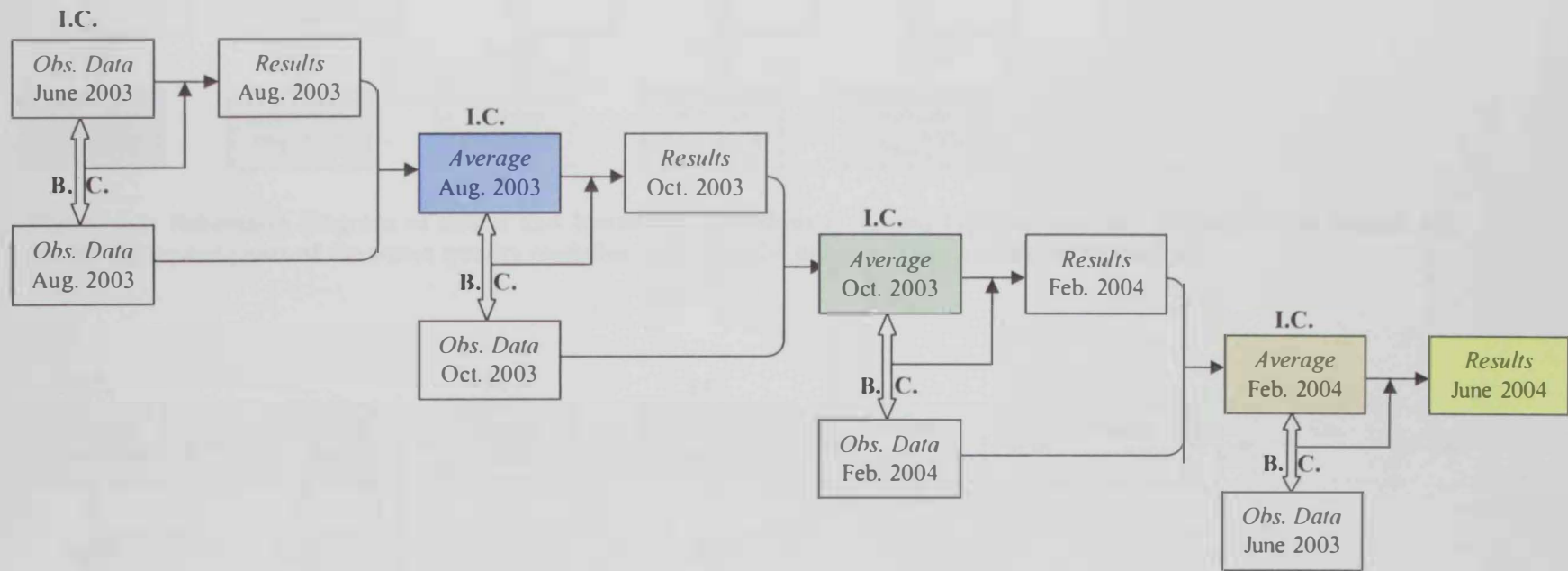
Figure 6.1: Schematic diagram of initial and boundary conditions (I.C, and B.C respectively) utilized in the first year of the water quality modeling.

Figure 6.2: Schematic diagram of initial and boundary conditions (I.C, and B.C respectively) utilized in the second and further extended years of the water quality modeling based on the previous year results (Approach 1).

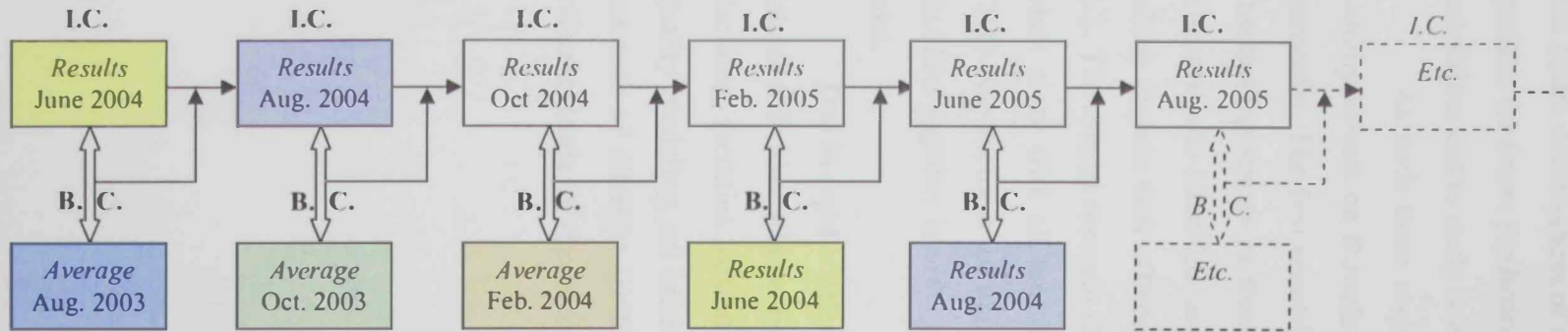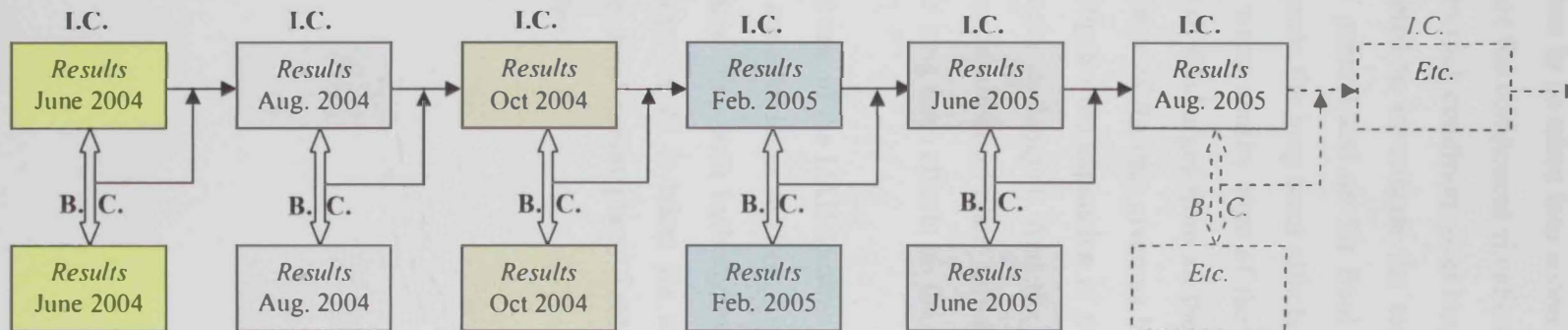**Figure 6.3:** Schematic diagram of initial and boundary conditions (I.C, and B.C respectively) utilized in the second and further extended years of the water quality modeling based on constant B.C's, (Approach 2).

6.2 Considered Modeling Scenarios

In order to model environmental and/or ecological component for long term changes, the future development of such component has to be taken into account. Assessment process for future prediction has to investigate the component situation in the current conditions and to study how it may respond to such conditions over long time period.

As such three scenarios are considered to investigate the temperature and salinity effects on Ruwais water quality in general and on Sir Bani Yas Island in particular. The first scenario (Q-Base) examines the long term effects of the current discharging situations from the RIC on the water quality state of the Ruwais coast. This scenario takes into account the amount of discharges from all the RIC facilities which dispose their effluent at the coastal water of Ruwais given as before in Table 5.2. The second scenario (20Q-Desal.) investigates the expansion of the desalination plant alone with all the other facilities remain unchanged. And the third scenario (20Q-All) explores the expansion of both the desalination plant as well as the other facilities together in order to investigate their long term effects on the ecology of the area.

Due to rapid accelerated development rate of the UAE coast as well as the oil related activities, a large expansion factor is considered for the desalination plant and the other facilities located in the Ruwais area. For both hydrodynamic and water quality modeling, an enhancement by a factor of 20 is taken for all the effluent amounts of different facilities including the desalination plant. Table 6.2 lists the effluents loads for the three considered sections.

6.3 Temperature-Salinity Simulation

In order to investigate the long term effects of salinity and temperature for the present and future expansion of the RIC facilities on the Ruwais ecosystem; hydrodynamic modeling for the Ruwais costal water is run for a full year over the four successive time periods proposed earlier. The simulation is conducted for the three different scenarios discussed in the previous section (Q-Base, 20Q-Desal., and 20Q-All).

Effluent flows, temperature, and salinity values for both summer and winter conditions for the three different scenarios are shown in Table 6.2. The salinity and the temperature values for each outfall are calculated using a weighted average method as follows:

$$T = \frac{\sum_{i=1}^{n}(Q_i.T_i)}{\sum_{i=1}^{n}Q_i}, \ (i = 1, 2, 3, ..., n) \tag{6.1}$$

$$S = \frac{\sum_{i=1}^{n}(Q_i.S_i)}{\sum_{i=1}^{n}Q_i}, \ (i = 1, 2, 3, ..., n) \tag{6.2}$$

Where Q_i (m^3/day) is the flow rate of the effluent source and T_i (^oC), S_i (*ppt*) are the temperature and salinity values for the effluent source, respectively.

In the current section, the salinity and temperature for both summer and winter seasons are spatially and temporally investigated in the modeled area for different scenarios. The same selected observation points; S1, S2, and S3 used in chapter 3 (Figure 3.8) are used here too.

The figures hereinafter show the temperature and salinity for the surface layer. As mentioned before the water column in the modeled area is homogeneous, so the other layers have the same spatial and temporal distributions of as surface layer.

Table 6.2: Discharge loads scenarios and some of their physical properties in summer and winter seasons

	Utility	Q (m³.day⁻¹)	T Summer (°C)	T Winter (°C)	Salinity (ppt)
Scenario 1(Q-Base): Base conditions					
Outfall 1	Oil Refinery (TAKREER)	243600	30.0	23.0	46.0
	Gas Production Plant (GAZCO)	600000	45.0	35.0	46.0
	Total	*843600*	*40.7*	*31.5*	*46.0*
Outfall 2	Desalination and Power Plant	192000	45.0	40.0	70.0
	Fertilization Factory	120000	40.0	35.0	46.0
	Total	*312000*	*43.1*	*38.1*	*60.8*
Outfall 3	Petrochemical Factory (Borooj)	*840000*	*45.0*	*35.0*	*50.0*
Scenario 2 (20Q-Desal.): Expansion for desalination plant only					
Outfall 1	Oil Refinery (TAKREER)	243600	30.0	23.0	46.0
	Gas Production Plant (GAZCO)	600000	45.0	35.0	46.0
	Total	*843600*	*40.7*	*31.5*	*46.0*
Outfall 2	Desalination and Power Plant	3840000	45.0	40.0	70.0
	Fertilization Factory	120000	40.0	35.0	46.0
	Total	*3960000*	*44.8*	*39.8*	*69.3*
Outfall 3	Petrochemical Factory (Borooj)	*840000*	*45.0*	*35.0*	*50.0*
Scenario 3 (20Q-All): Expansion for all facilities including the desalination plant					
Outfall 1	Oil Refinery (TAKREER)	4872000	30	23	46.0
	Gas Production Plant (GAZCO)	12000000	45	35	46.0
	Total	*16872000*	*40.7*	*31.5*	*46.0*
Outfall 2	Desalination and Power Plant	3840000	45	40	70.0
	Fertilization Factory	2400000	40	35	46.0
	Total	*6240000*	*43.1*	*38.1*	*60.8*
Outfall 3	Petrochemical Factory (Borooj)	*16800000*	*45*	*35*	*50.0*

6.3.1 Temperature Simulation

Figure 6.4 shows a comparison of the temperature temporal variation at the three observation points (St.1, St.2, and St.3) for the three different scenarios. The two-months period (June, 1st to July, 31st) is selected to display the summer results, and the two-months (Oct.,1st to Nov.,30th) is selected for winter results.

It is quite noticeable that a tangible effect of the disposed warm water from the desalination plant and other facilities is taking place in the vicinity of the discharging

zone. These discharges increase the water temperature in the discharging area represented by Station 1. The temperature at that station are 33.78 °C, 34.16 °C and 36.07 °C for the Q-Base, 20Q-Desal., and 20Q-ALL scenarios, respectively (Table 6.3). This indicates that there is around 0.38 °C average temperature increment in case of expanding the desalination plant only (20Q-Desal.) and is around 2.29 °C average temperature increment in case of expanding all facilities twenty times (20Q-All) in summer, and about 0.46 °C, 3.18 °C temperature increase in winter, respectively. This indicates that the desalination expansion by itself (20Q-Desal.) does not greatly affect the coastal temperature, whereas the expansion of all facilities (20Q-All) causes a pronounced increase in the coastal temperature due to the high temperature effluent released from the other facilities especially from Borooj outfall; where the quantity of the disposed effluents from that outfall is about 4 times higher than the effluents of the desalination plant itself. Moreover, the water temperature of this effluent is higher than the desalination plant effluent by around 1.9 °C (Table 3.2), which mainly causes high jump of the coastal water temperature in scenario 3.

Station 2 is located in the middle of the modeling area, around 10 km away from the discharging zone. As shown in Figure 6.4, there is a light temperature increase due to expansion of the desalination plant (20Q-Desal.) and the other facilities (20Q-All) relative to the base condition (Q-Base) as shown in Table 6.3. This is around 0.02 °C, 0.31 °C in summer and 0.07 °C , 0.71 °C in winter, respectively. This temperature variation is considered low with respect to the daily or seasonally temperature variation, so such expansions have limited influences on the coastal water temperature and their influences constrained to some kilometers around the outfalls (< 10 km).

At station 3, near Sir Bani Yas Island, it is clear from Figure 6.4 that there are no temperature effects due to discharging from the RIC facilities on the coastal water of the island in all scenarios. As mentioned earlier, this is due to the large distance separating the island from the discharging zone (around 20 km). Over that distance, currents, tides, and water exchanging through the model boundaries contribute effectively to vanish the thermal effects of such effluents over long distances like the Bani Yas Island.

Incremental increases of temperature for the three scenarios at the three stations are little higher than the case of summer with a maximum of 3.18 °C for the 20Q-All scenario at station 1.

Spatial distribution of the temperature due to the different scenarios in both summer and winter are shown in the Figures from 6.5 to 6.10. Generally, the temperature increases toward the shoreline and decreases toward the model boundaries. The general trend of temperature increment in south is referred to the shoal of such areas which is influenced directly by the land temperature. On the other hand, the zone near the RIC outfalls is highly influenced by the warm discharges from the different facilities. The effect of such discharges decreases toward the model boundaries (Gulf ward) and disappears after several kilometers (<10 km) as discussed above.

Table 6.3: Average temperature at the observation stations in mid of summer and winter

Scenarios	Q-Base	20Q- Desal.		20Q- All	
	(1) Value	(2) Value	(2) – (1) Δ	(3) Value	(3) – (1) Δ
Summer Average Temperature (°C)					
Station 1	33.78	34.16	0.38	36.07	2.29
Station 2	33.42	33.44	0.02	33.73	0.31
Station 3	33.25	33.25	0	33.30	0.05
Winter Average Temperature (°C)					
Station 1	21.66	22.12	0.46	24.84	3.18
Station 2	21.49	21.56	0.07	22.20	0.71
Station 3	21.56	21.56	0	21.62	0.06
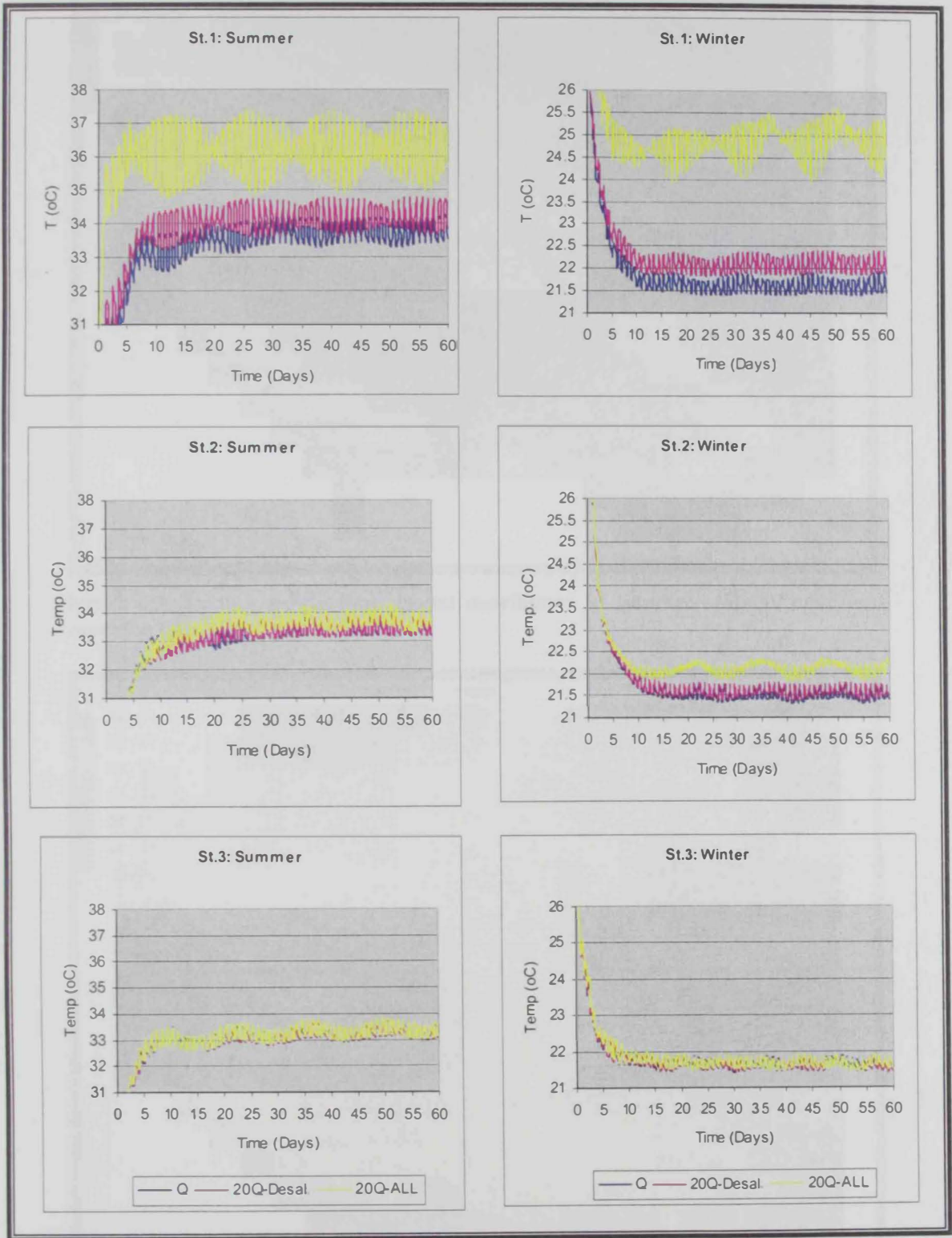
Figure 6.4: Temperature time series at the three selected observation stations (St.1, St.2, and St.3) in summer and winter seasons.
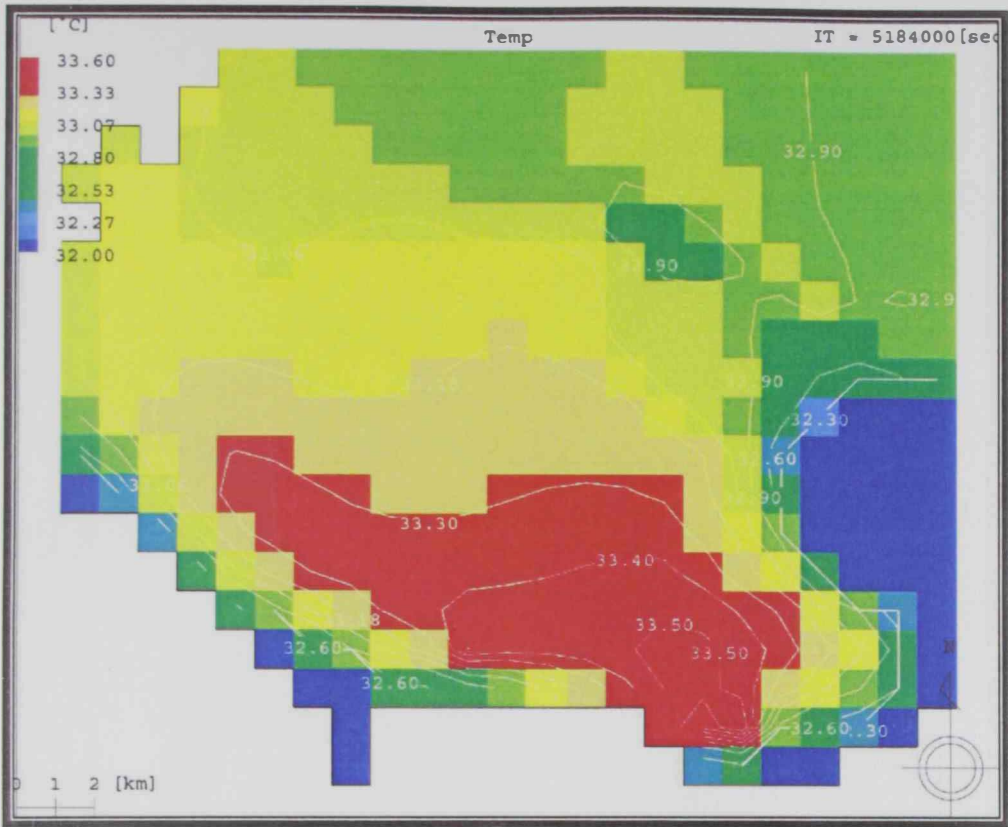
Figure 6.5: Surface temperature spatial distribution at summer (July.31ˢᵗ) for base condition (Q).
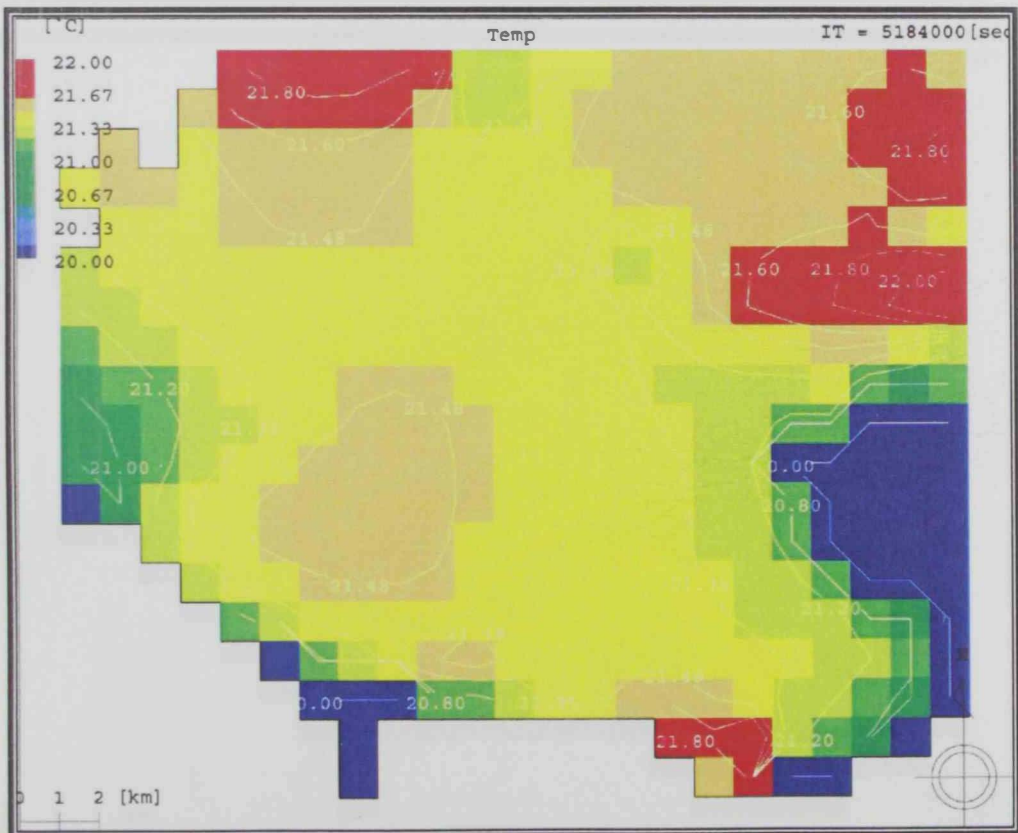
Figure 6.6: Surface temperature spatial distribution at winter (Nov.,30ᵗʰ) for base condition (Q).

Figure 6.7: Surface temperature spatial distribution at summer (July.31ˢᵗ) for expansion of desalination plant only (20Q-Desal.).

Figure 6.8: Surface temperature spatial distribution at winter (Nov.,30ᵗʰ) for expansion of desalination plant only (20Q-Desal.).

Figure 6.9: Surface temperature spatial distribution at summer (July.31ˢᵗ) for expansion of all facilities (20Q-All).

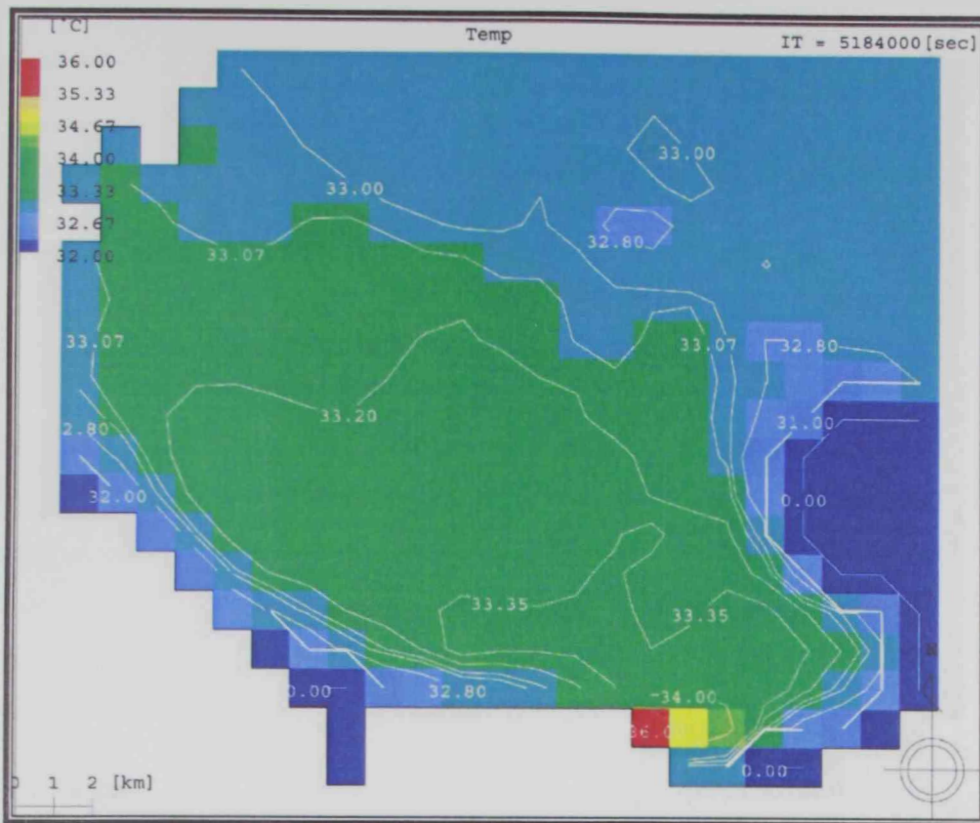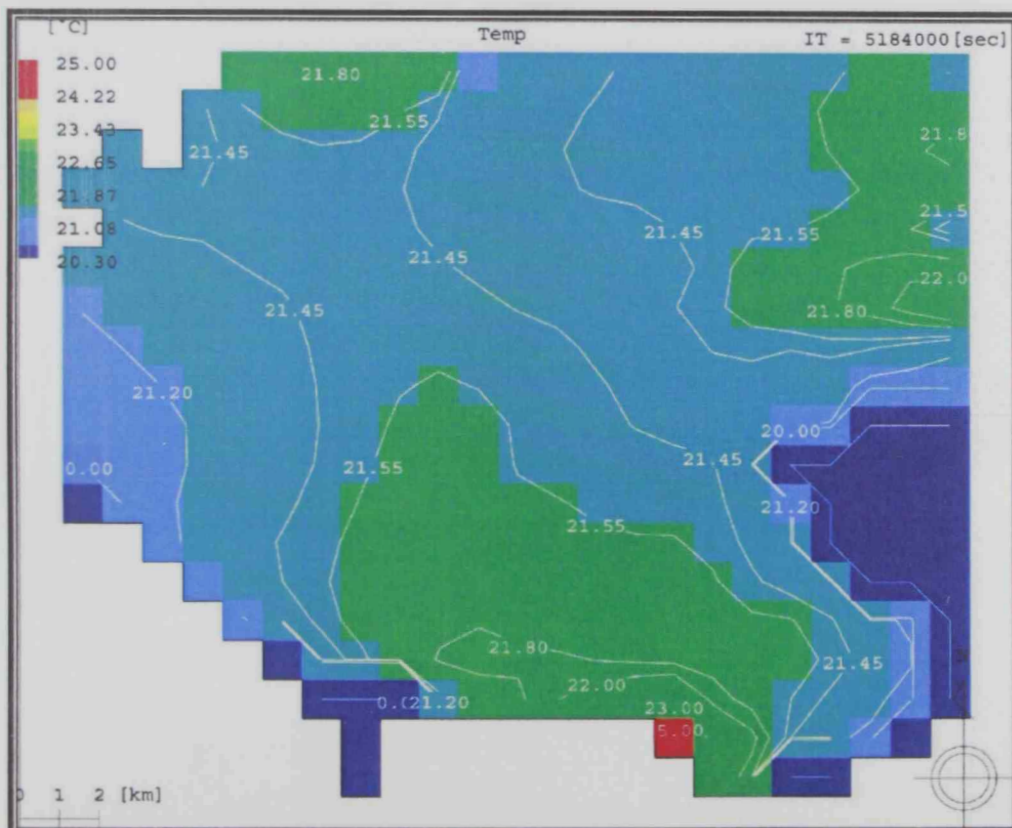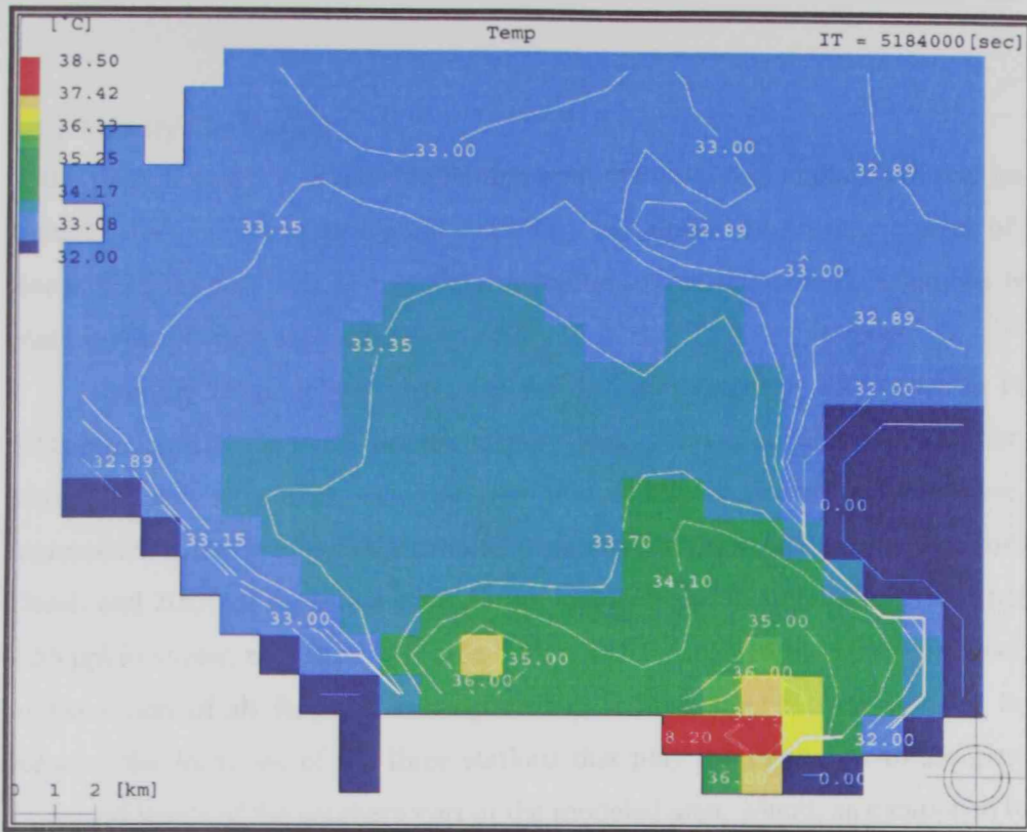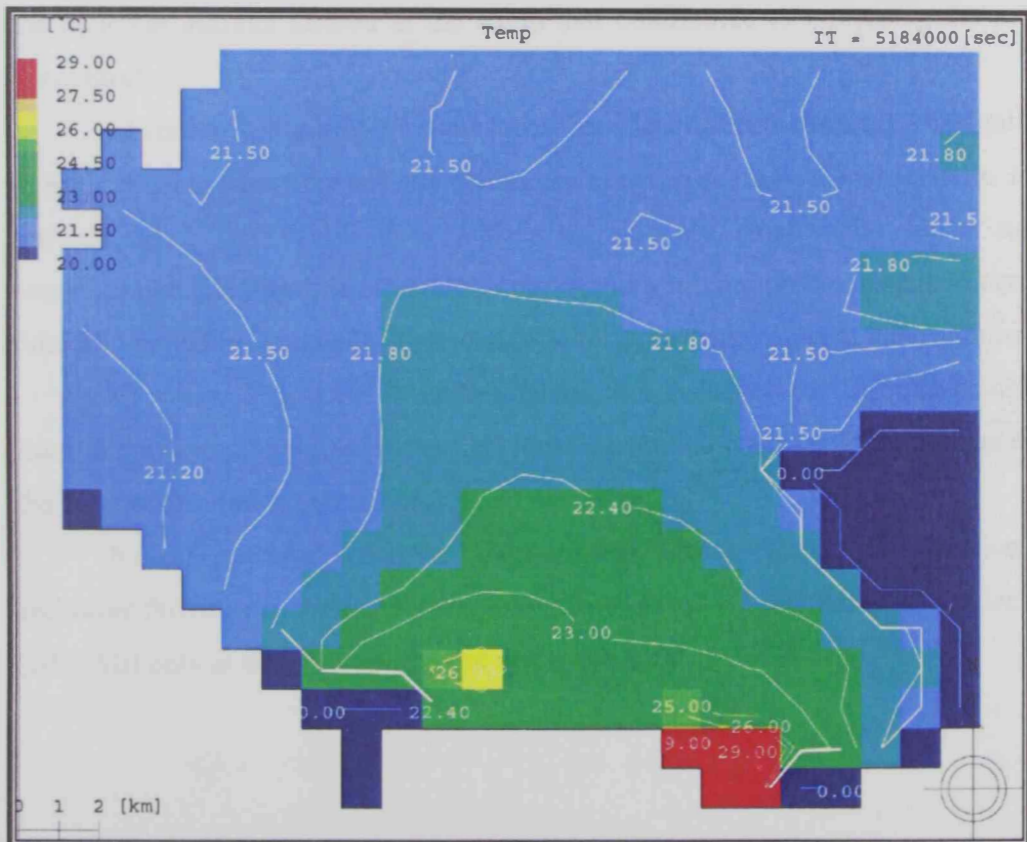**Figure 6.10: Surface temperature spatial distribution at winter (Nov.,30ᵗʰ) for expansion of all facilities (20Q-All).**

6.3.2 Salinity Simulation

In the present study, it is remarkable that with the desalination plant effluent has the highest salinity concentration of the outfalls; it has almost the smallest volume of flow discharge. This note will be beneficial hereafter to interpret some phenomena taking place in the different scenarios.

Salinity temporal variations for the different scenarios are shown in Figure 6.11. It is clearly observed that the salinity concentration at station 1 is higher than station 2 and 3 in both summer and winter for all scenarios. Moreover, the incremental increase of average salinity at station 1 over the Q-Base scenario for 20Q-Desal. and 20Q-All scenarios are 1.53 ppt and 2.19 ppt in summer and 1.21 ppt and 2.56 ppt in winter, respectively (Table 6.4), which means that the salinity increase due to expansion of all facilities is tangible and is more tangible and referred to two reasons; the locations of the three stations that play the main rule to the generally increased levels of the southern part of the modeled area, where, as mentioned before that the high temperate of the southern part causes more evaporation that leads to higher salinity. The other reason is referred to as the influence of brine disposal from the different outfalls located at the south that contributes to increasing the salinity concentration.

At station 2, Figure 6.11 shows that the effect of brine disposal is insignificant in all scenarios, where the salinity difference between scenario 1 and scenario 2 does not exceed 1 ppt (Table 6.4) which is relatively small. The lower salinity concentration Gulf-ward is referring to the exposed mixing processes due to currents, tides and boundary exchanges that tend to reduce the brine disposal concentration.

At station 3 near Sir Bani Yas Island, the influence of the brine discharged from the different facilities of the RIC for all scenarios completely disappears due to the large separation (about 20 km).

It can be concluded that the effect of brine disposal from the desalination plant and other facilities as well has a tangible effect in case of expanding all the facilities (20Q-All) only at station 1 nearby the discharge area.
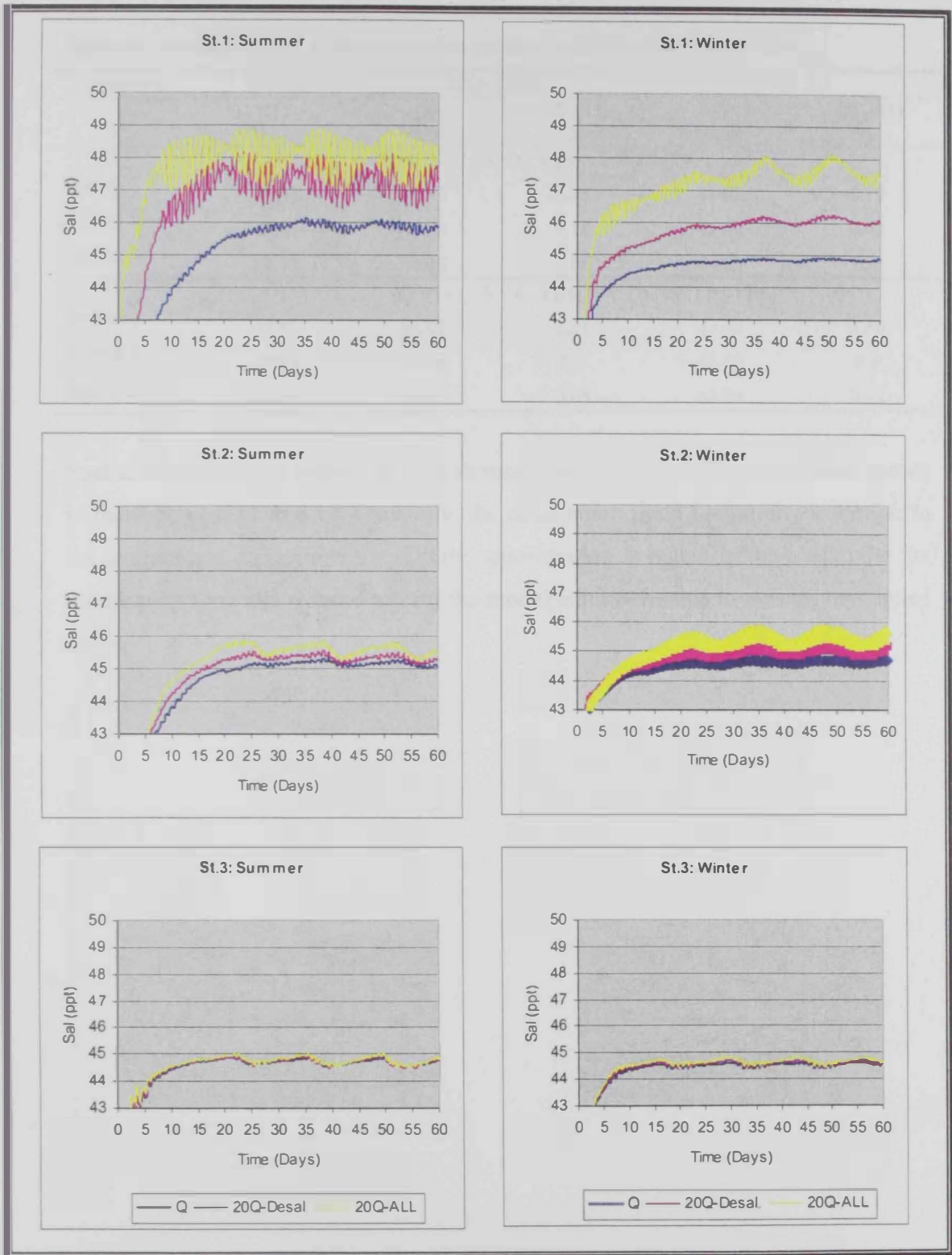
Figure 6.11: Salinity time series at the three selected observation stations of summer and winter seasons.

Table 6.4: Average salinity at the observation stations in mid of summer and winter

Scenarios	Q-Base	20Q- Desal.		20Q- All	
	(1) Value	(2) Value	(2) – (1) Δ	(3) Value	(3) – (1) Δ
	Summer Average Salinity (ppt)				
Station 1	45.83	47.36	1.53	48.02	2.19
Station 2	45.07	45.26	0.19	45.49	0.42
Station 3	44.73	44.76	0.03	44.83	0.1
	Winter Average Salinity (ppt)				
Station 1	44.86	46.07	1.21	47.42	2.56
Station 2	44.69	45.09	0.4	45.59	0.9
Station 3	44.52	44.57	0.05	44.64	0.12

Spatial distribution of salinity in both summer and winter for all scenarios are shown in the Figures 6.12 to 6.17. Generally, the distribution trend for salinity is similar to the temperature one, where the salinity concentration is higher in the south near the discharging zone and reduces toward the model boundaries due to reasons mentioned earlier.
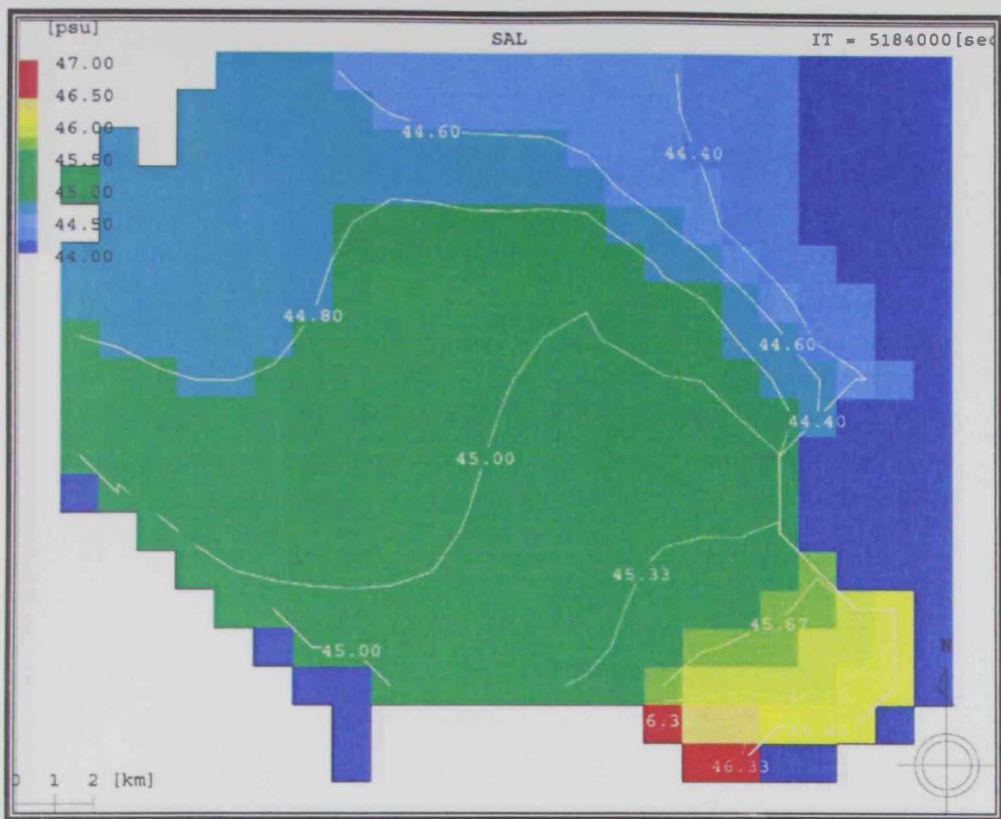
Figure 6.12: Surface salinity spatial distribution at summer (July.31st) for base condition (Q).
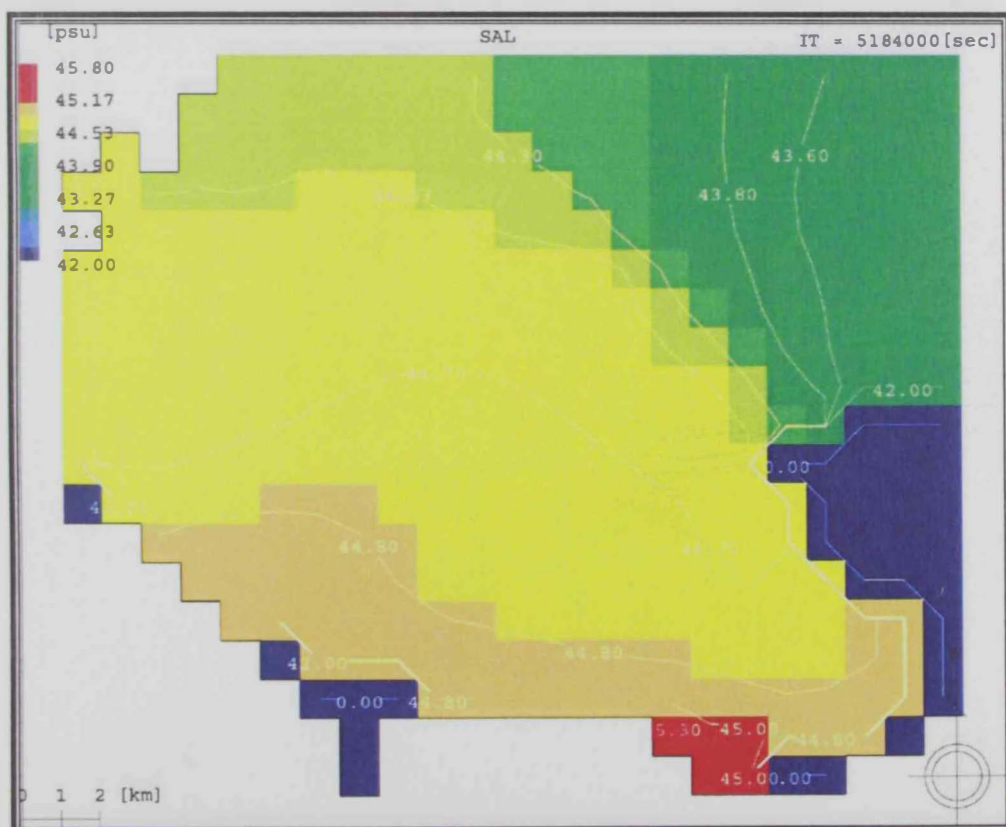
Figure 6.13: Surface salinity spatial distribution at winter (Nov..30th) for base condition (Q).

Figure 6.14: Surface salinity spatial distribution at summer (July.31st) for expansion of desalination plant only (20Q-Desal.).

Figure 6.15: Surface salinity spatial distribution at winter (Nov.,30th) for expansion of desalination plant only (20Q-Desal.).
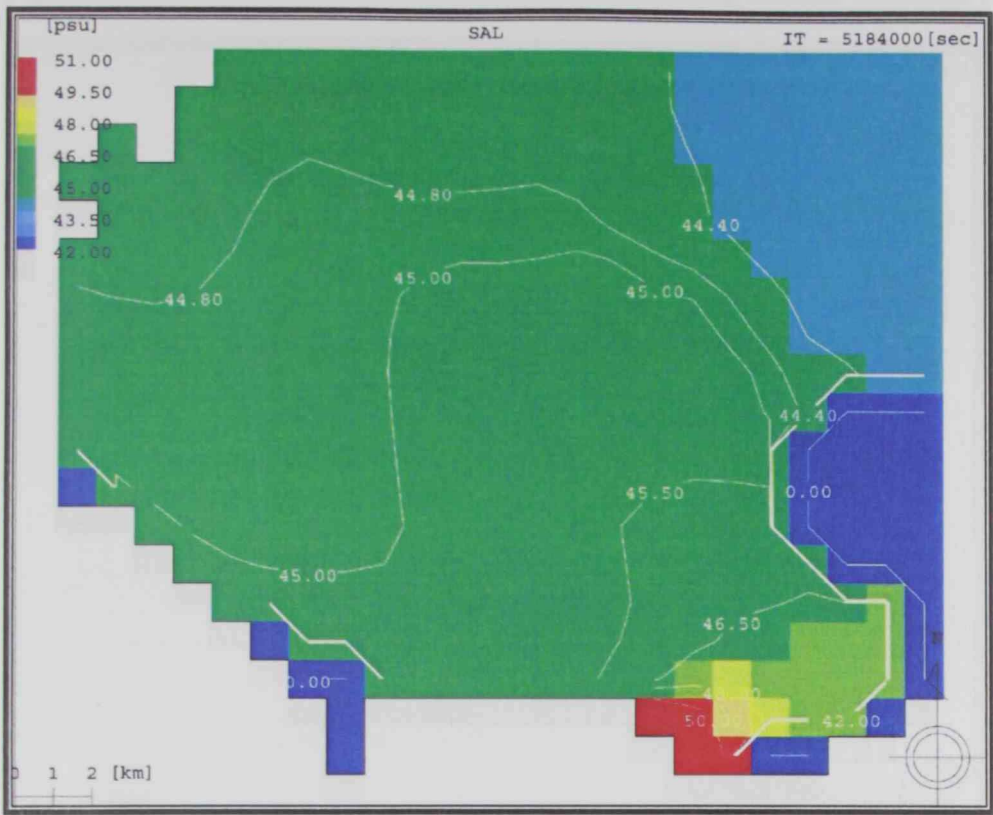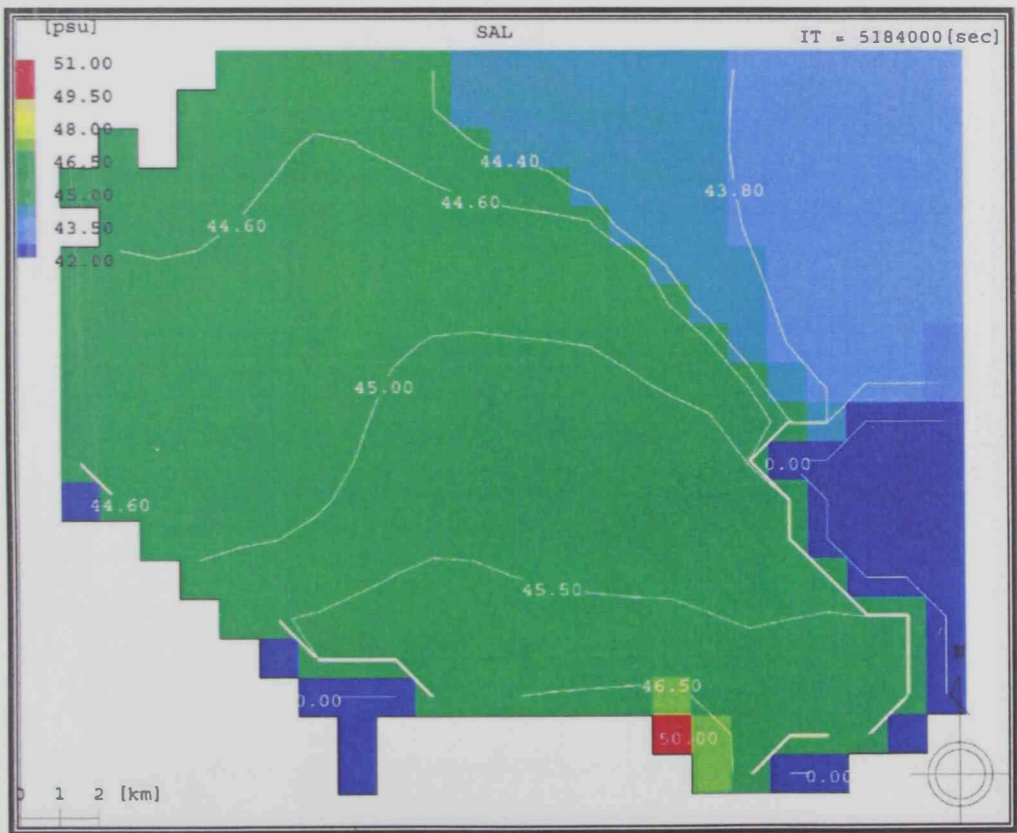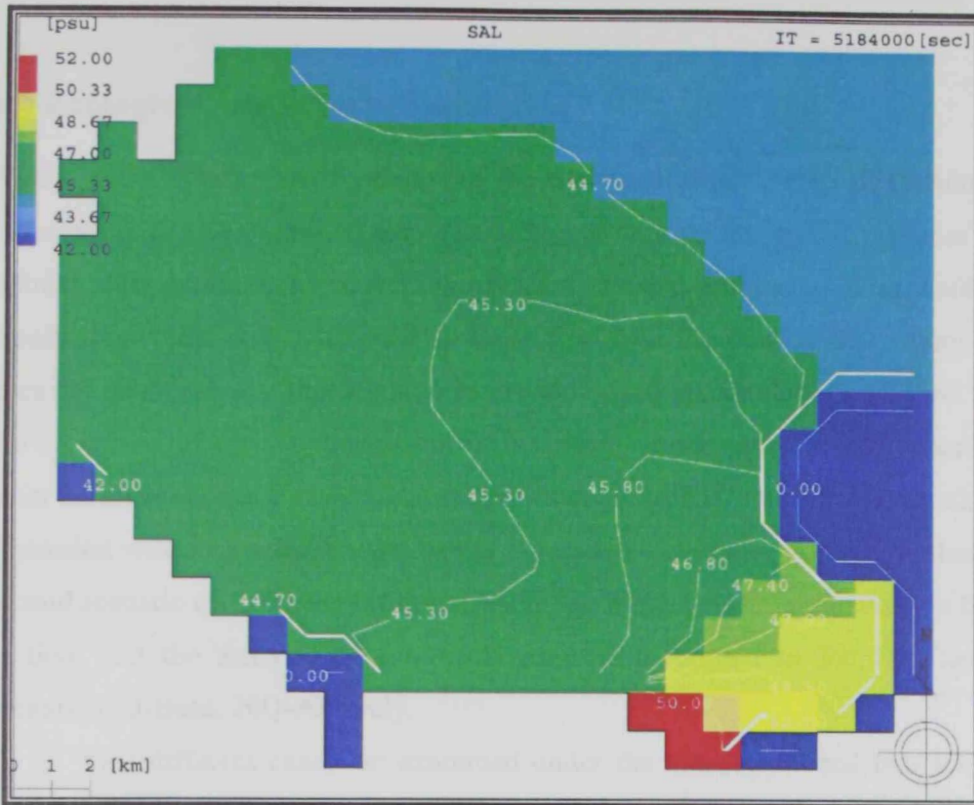
Figure 6.16: Surface salinity spatial distribution at summer (July.31st) for expansion
of all facilities (20Q-All).
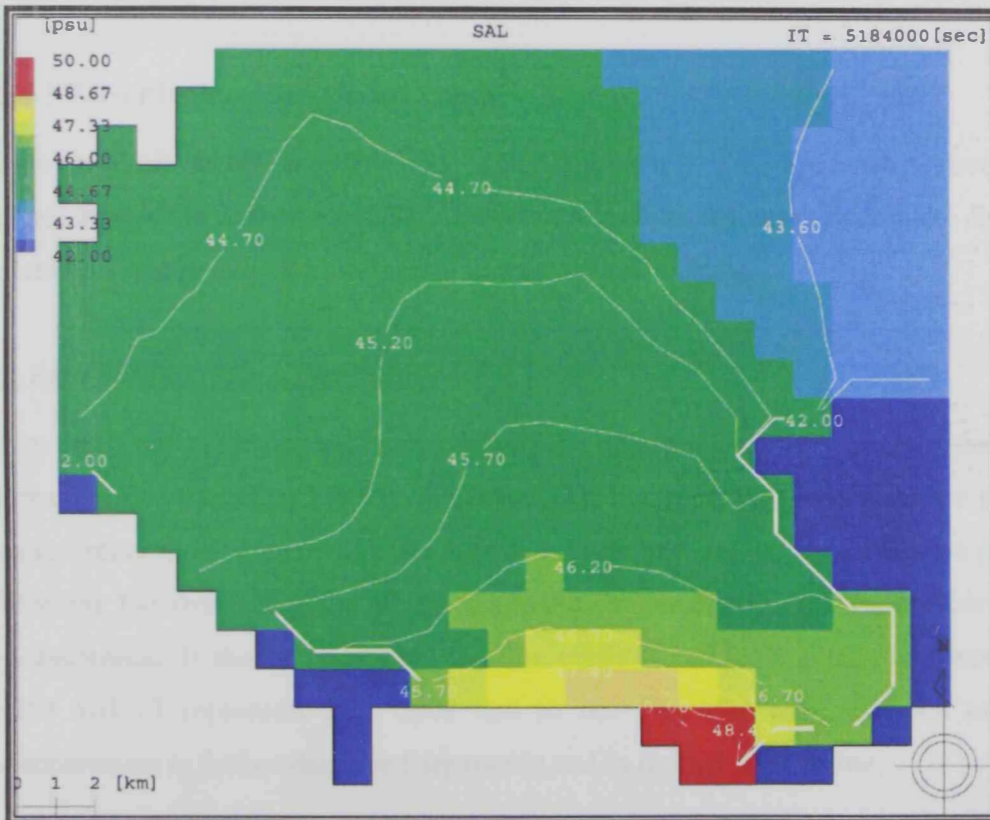
Figure 6.17: Surface salinity spatial distribution at summer (July.31st) for expansion of
all facilities (20Q-All).

6.4 Ecological Long-Term Simulation

Based on the biochemical processes of the ecological model, most of the biological processes have an exponential response to temperature values, and no response for the salinity concentration. Moreover, the limited thermal influence of expanding the desalination plant only (Scenario 2, 20Q-Desal.) on the coastal water temperature does not qualify to test this scenario in the ecological assessment. In addition to that, the expansion of the desalination plant is directly proportional to the expansion of other facilities, as the Ruwais plant mostly cater to the RIC industrial demands, so its expansion will be a natural result of the expansion of the other facilities. Hence, the second scenario (20Q-Desal.) is discarded in the water quality simulations in the next section, and the analysis of ecological impacts is limited to the first and third scenarios (Q-Base, 20Q-All) only.

Two different cases are examined under the aforementioned two scenarios; zero plankton in the effluent loads and non-zero plankton in the effluent loads to represent the uncontrolled chlorination practical at the intakes yield erratic plankton loads ranging from zero to ambient levels from time to another.

6.4.1 Zero Plankton in Effluent Loads

Two sets of results are obtained using approach 1 and approach 2 boundary conditions of the further years. This situation resembles the case of complete death of planktons due to intense chlorination practiced at all intakes.

Q-Base Scenario Using Approach 1

Time series of the major ten compartments are obtained over three years at the same three stations considered before (Figure 6.18). For each year, 4 values are plotted representing the average compartment value in the last day of the simulation period. Whereas the first value for all the compartments represents the field observation measurement. It should be noticed that the origin (0) of these plots represents June 2003 and 12 represents June 2004 and so on. The long term variation of each compartment is further discussed separately and in more details below.

Phytoplankton Biomass

As shown in Figure 6.18, phytoplankton biomass concentration fluctuates temporally through the years in a cyclic manner keeping identical values over the corresponding periods of each year for all the observation stations. It attains maximum values in August, after which it decreases slightly in October then it dramatically decreases to the lowest concentration value in February. The main reason for such behavior is the temperature variation through the years as shown in Figure 6.19. It is clearly noticed that the phytoplankton trend in all stations follow the temperature variation trend that is considered as the dominant factor of phytoplankton fluctuation.

Other factor may have an influence in such trend is the light intensity which varies from one season to another. Light intensity value is much higher in the summer than the winter due to the clear sky and larger radiation on the water. This increases the photosynthesis process hence increases the phytoplankton biomass.

Spatially, phytoplankton varies in a tangible way, where its concentration at station 1 is higher than the other stations, whereas the concentration at station 3 is higher than station 2. Due to slight difference in the temperature among the three stations all over the year, temperature effect can be discarded as a variation factor. According to Figure 6.18, the nutrients (PO_4, NH_4, NO_2, and NO_3) are seen to dominate in such spatial distribution of the phytoplankton. In this scenario, the effect of NO_2 can be neglected due to its low concentration (less than 0.8 $\mu mol/L$) while the inhabitation factor (Ψ) for the nitrogen nutrients is taken as 1.462 $\mu mol/L$, (Table 5.3). NH_4 and NO_3 trends follow the phytoplankton trends, increase in summer and decrease in winter, so it is clear that there are abundant of such these nutrients in the coastal water, hence PO_4 can be considered as a limiting nutrient in the modeled region. This can be noticed by the inverse relation between the phytoplankton growth and PO_4 concentration.
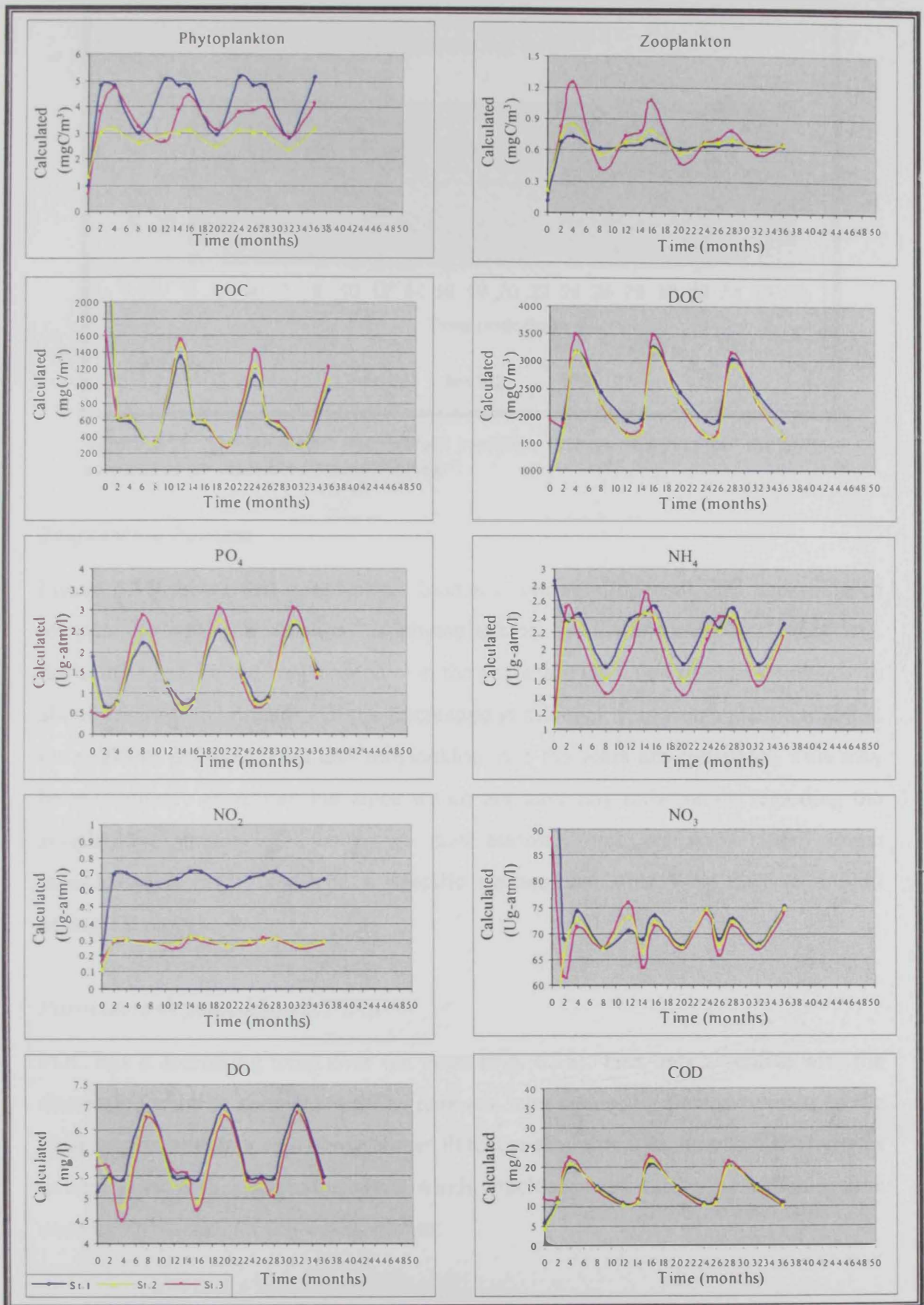
Figure 6.18: Compartment values for the base scenario (Q-Base) using approach 1 to create the boundary conditions and zero plankton in effluent loads. The results are at the three observation stations (St.1, St.2, and St.3).
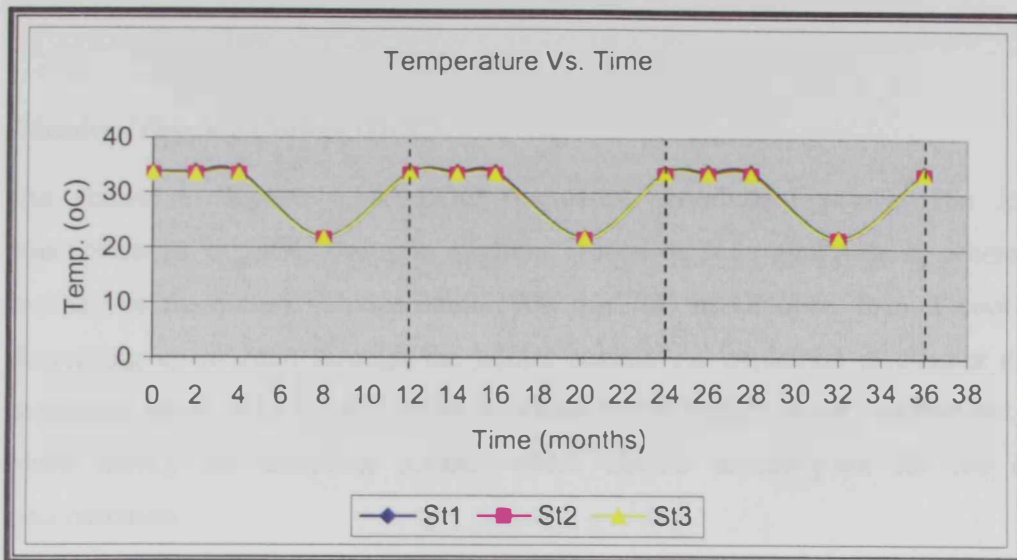
Figure 6.19: The simulated temperature variation through the year for the Q-Base scenario at the three observation stations

Zooplankton Biomass

Figure 6.18 shows that zooplankton biomass concentration oscillates according to temperature variation as same as phytoplankton. It is noticeable that there is a declining trend for the zooplankton over the years, but the value reaches ultimately to about 0.6 mgC/m3 after which the fluctuation is minimal. It is worth mentioning that the peaks of phytoplankton and zooplankton over the years are consistent. This may be ecologically abnormal; but since we do not have any information regarding the zooplankton grazing efficiency, we may attribute such result to either erratic measurements or it could be a specific phenomenon that may need a special biological survey.

Particulate Organic Matter (POC)

POC has a decreasing trend over the years (Fig. 6.18). This may associate with the decreasing trend of zooplankton. The dramatic increase during June may relate to the field measurements which show higher POC concentrations in June 2003. That was as mentioned earlier due to the strong winds which occurred during the sampling time causing turbulence for the water column.

Dissolved Organic Carbon (DOC)

As shown in Figure 6.18, DOC fluctuates periodically yearly. The lowest concentrations of DOC occur in summer season at June and August, whereas it reaches its maximum value around 3500 mgC/m^3 in October, then it continues decreasing up to June through the winter season. As explained in chapter 4, the maximum value of DOC in October is related to the rapture of oil pipeline that took place during the sampling period, which caused unreal peak for the DOC concentration.

Phosphate (PO$_4$)

As shown in Figure 6.18, PO$_4$ has a sinusoidal trend with constant amplitude over the years. It fluctuates between 0.5 to 3 μmol P/L. It has an inverse relation with the phytoplankton biomass concentration, where it drops to the lowest values in the summer when the phytoplankton reaches its maximum and rises to its maximum values at February when phytoplankton reaches its minimum concentration. This indicates that the phosphate may be controlling the phytoplankton biomass.

Ammonium (NH$_4$)

Ammonium variation is constant over the years (Fig. 6.18); that is almost similar to the phytoplankton trend. This indicates that the ammonium is not affected by the phytoplankton biomass concentration, and can't be regarded as a limiting nutrient for the phytoplankton growth.

Nitrite (NO$_2$)

As shown in Figure 6.18, nitrite has a constant trend over the years. Moreover, it fluctuates in a narrow range (i.e. less than 0.1 μmol /L). Its amounts in the Ruwais coastal water are very limited, so in the current scenario, it can not be classified as a limiting nutrient for the phytoplankton growth, because their values in all stations are less than the inhibition factor for the nitrogen nutrient uptake discussed earlier (considered as 1.462 μmol /L).

Nitrate (NO₃)

Nitrite has a constant trend over the years as shown in Figure 6.18 where it fluctuates between 65 to 75 μmol /L.

Dissolved Oxygen (DO)

Dissolved oxygen concentration has a typical cyclic trend over the simulated years (Fig. 6.18). It decreases in summer and increases in winter. The increase in winter is mostly due to the high currents taking place that increase the mixing process in the water column and hence increase the aeration. The other reason is related to higher saturation capacity of oxygen in the water during the winter of low temperature.

Chemical Oxygen Demand (COD)

As shown in Figure 6.18, COD has a symmetric trend over the years at all stations. In the current study, this trend is mostly corresponding to DOC concentrations. The high level of COD due to the oil spill incident increased the consumption of dissolved oxygen, hence the DO levels declined in October severely and COD increased dramatically.

20Q-All Scenario Using Approach 1

This scenario considers expansions of all the RIC facilities by 20 times. Figure 6.20 shows the results of simulation based on approach 1 considered to handle the boundary conditions of the expansion condition is addressed.

Phytoplankton Biomass

As shown in Figure 6.20, the phytoplankton trend does not change from the Q-Base scenario. The main difference is limited to the drop of phytoplankton biomass concentration at station 1 by 1 mgC/m³. The reason for such drop refers to the excessive effluents from the RIC facilities having zero plankton loads (phytoplankton and zooplankton) that tends to dilute the ambient phytoplankton concentration originally exists in the coastal water.

Zooplankton Biomass

As shown in Figure 6.20, the zooplankton trend at the expansion scenario does not change. The only change is limited again to drop of the zooplankton biomass concentration at station 1. This decreasing refers to the same reason mentioned with the phytoplankton case.

Particulate Organic Matter (POC)

POC does not suffer major changes due to expansion either in trend or values.

Dissolved Organic Carbon (DOC)

DOC has the same trend over the years, whereas, its value at station 1 is almost doubled due to extensive discharging effluents to reach up to 6000 mgC/m^3. It is clear that there is no any effect due to these discharging at either station 2 or station 3. This indicates that the effects of these effluents are limited to the discharging area.

Phosphate (PO$_4$)

The results show that PO$_4$ trend is not affected by the expansion of the facilities. In both stations 2 and 3, the PO$_4$ values are around their original values. Whereas, PO$_4$ values in summer periods rise to about 0.5 µmol /L. This increase is apparently due to the drop of phytoplankton biomass in these periods, so the consumption of PO$_4$ is reduced and its concentration is increased.

Ammonium (NH$_4$)

Ammonium trend remains unchanged over the years due to expansion. As the other compartments, its concentration at station 2 and station 3 does not suffer any change in the concentration values in either the summer or winter. At station 1, its concentration value is almost doubled to reach up to 5 µmol /L. This may be due to the increase of the nutrients loads because of the expansion.

Figure 6.20: Compartment values for the expansion scenario (20Q-All) using approach 1 to create the boundary conditions and zero plankton in effluent loads. The results are at the three observation stations (St.1, St.2, and St.3).

6-29

Nitrite (NO₂)

Nitrite (NO$_2$)

Nitrite trend does not change over the years too. However, station 1 experiences dramatic increase, where the concentration value increases up to 10 times to reach 7 μmol /L. This is related to extensive loads of nutrients from the different effluents that enrich the discharging area with nitrogen compounds, so NO$_2$ is largely influenced by such loads.

Nitrate (NO$_3$)

Nitrate concentration has a slight increase trend over the modeled years. Its concentration at station 1 increases to almost 5 μmol /L.

Dissolved Oxygen (DO)

DO trend remains the same as the base scenario over the modeled years. Moreover, the concentration values at station 2 and station 3 do not change but drops to 1.5 mg/L at station 1. This reduction is attributed to the large increasing of DOC that tends to more consumption of DO values associated with the bacterial decomposition activities

Chemical Oxygen Demand (COD)

COD trend does not change. Also, at station 2 and 3 its concentration values remain unchange. Whereas at station 1 its value is increased to 13 mg/L. This large increment and other fluctuations are synchronized with the DOC temporal change explained earlier.

Figure 6.21: Compartment values for the base scenario (Q-Base) using approach 2 to create the boundary conditions and zero plankton in effluent loads. The results are at the three observation stations (St.1, St.2, and St.3).

Q-Base Scenario Using Approach 2

The above time series results show repetitive trends for all the compartments over the modeled years. These trends can be attributed to use approach 1 that the previous year results to create the boundary conditions for the second and the third year as discussed in section 6.1.2. This process may give a misleading trend of the different compartment concentration values. So, approach that considers constant boundary conditions over the simulated period is investigated with the same previous simulations. The result values of the last simulated period are now used as initial and boundary condition of the next period. This allows avoiding the effect of the previous-year results on the next years' results, so the difference will start to appear after the first year simulation, whereas the results for the first year in both approaches 1 and 2 are identical. The results in this case are illustrated in Figure 6.21.

Comparison between approach 1 results (Fig. 6.18) and approach 2 results (Fig. 6.21) reveals that most of the nutrients have a declining trends and flatting-out for most of the compartments after the first year. This is with the exception of phytoplankton and dissolved oxygen that are both influenced by the temperature variation and keep displaying cyclic trends. Generally, these flatten-out trends are corresponding to constant boundary conditions used in the present case.

20Q-All Scenario Using Approach 2

Figure 6.22 shows the produced model values for the different compartments over 4-year simulation period, using approach 2 with an expansion scenario.

Comparing Figure 6.22 and 6.20 shows that phytoplankton, zooplankton, NO_2, and DO do not experience any change either in trend or values. Whereas, the rest of compartments are flattening-out after the second year.
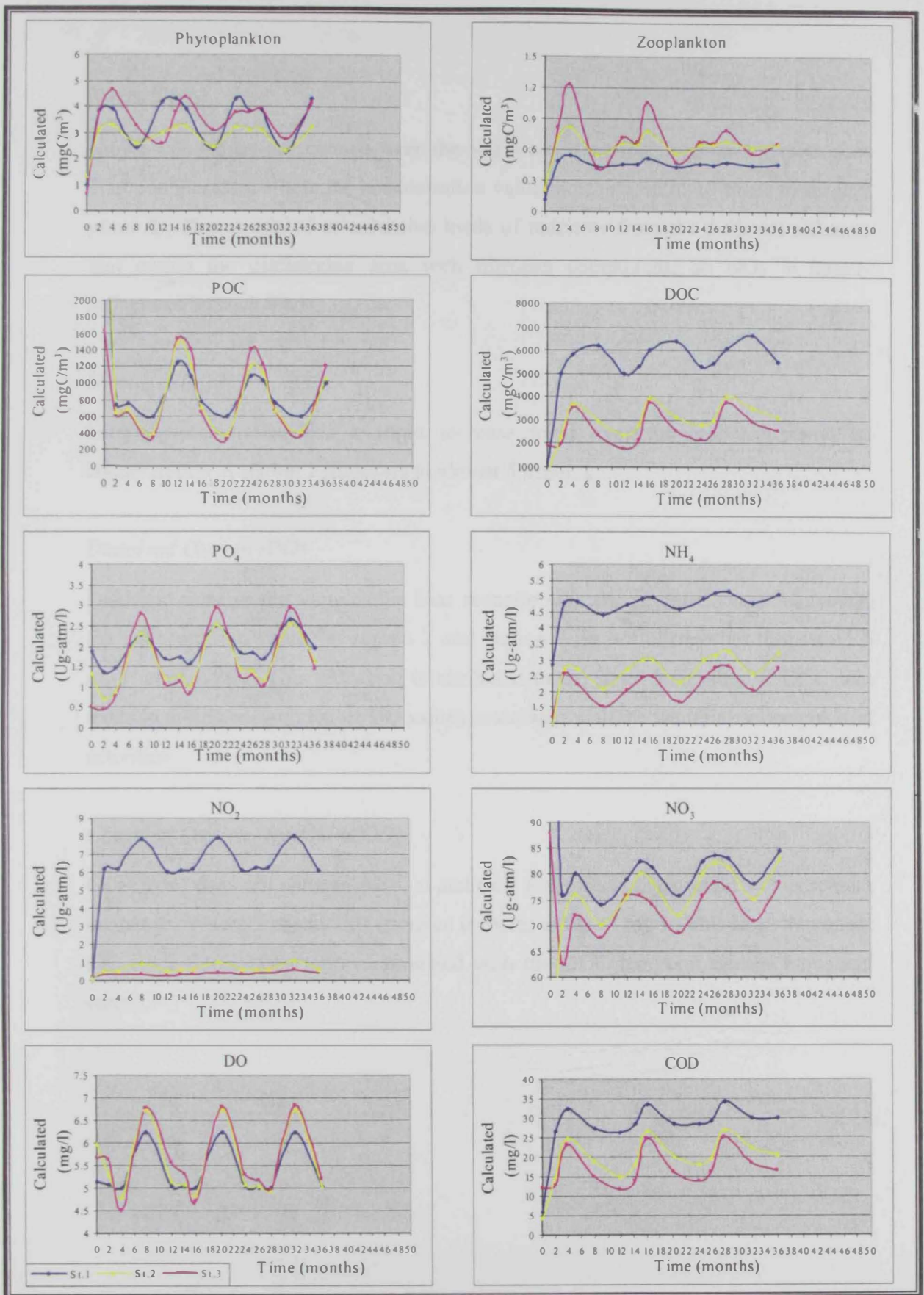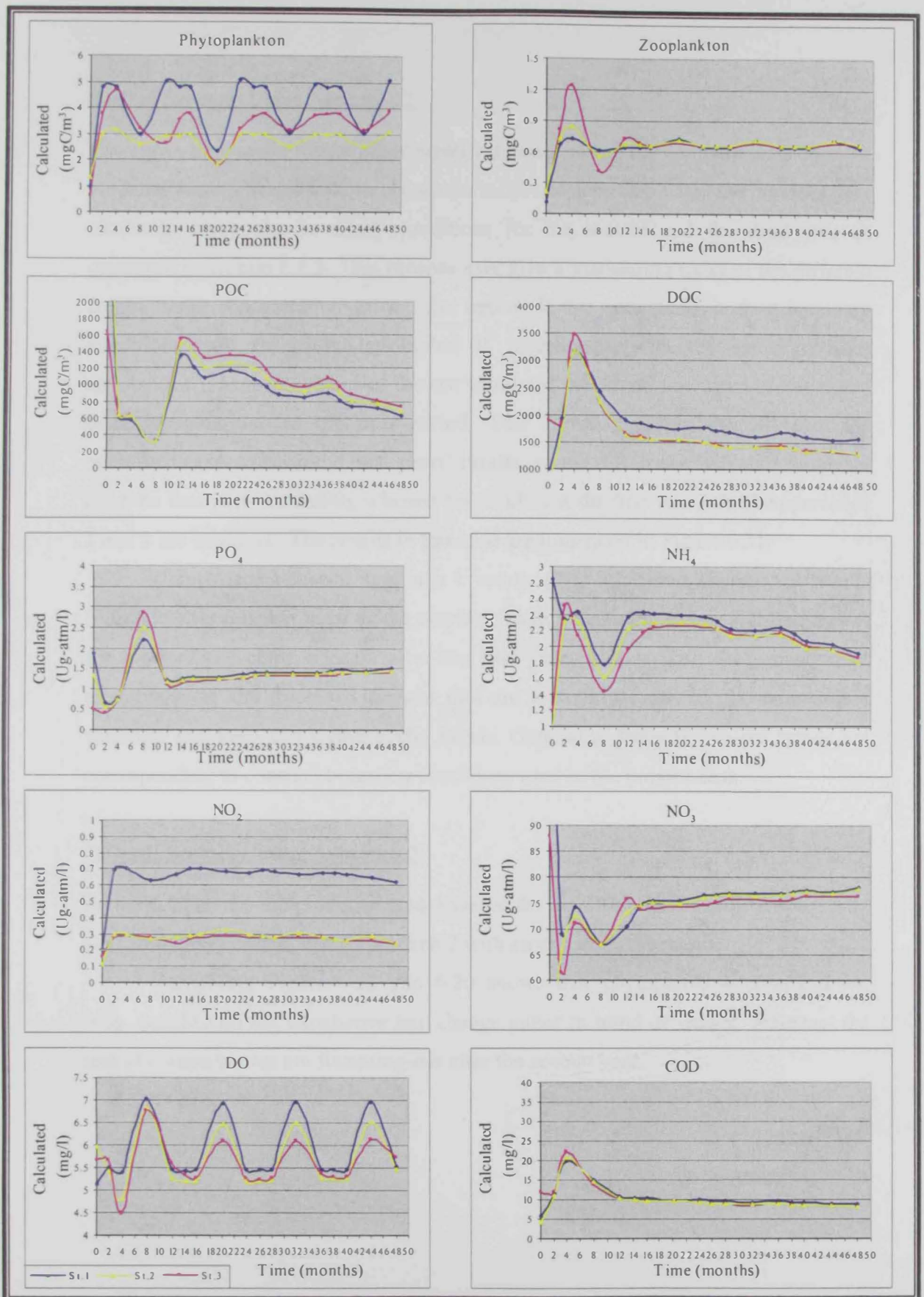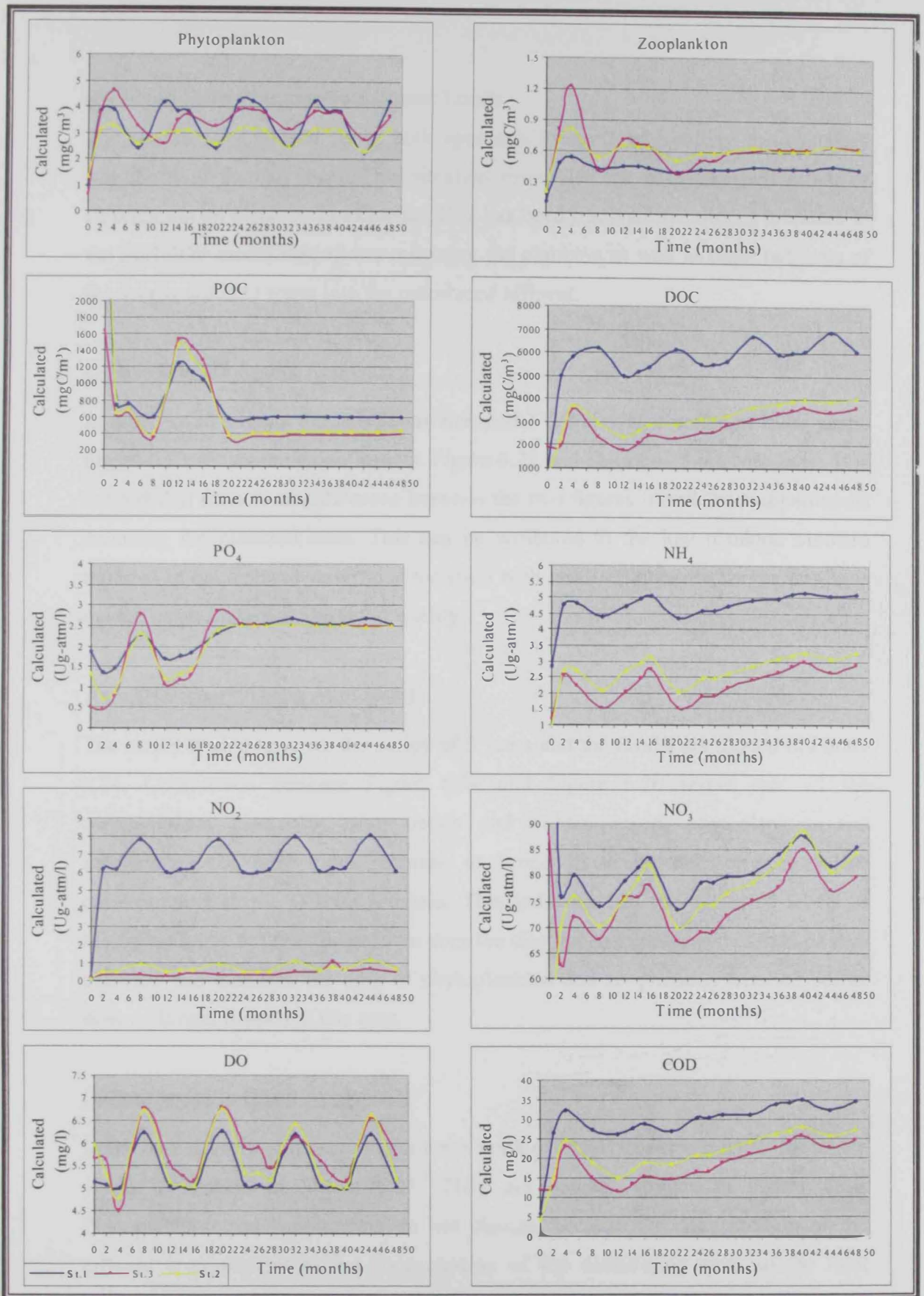
Figure 6.22: Compartment values for the expansion scenario (20-All) using approach 2 to create the boundary conditions and zero plankton in effluent loads. The results are at the three observation stations (St.1, St.2, and St.3).

6-33

6.4.2 Non-Zero Plankton in Effluent Loads

The results are obtained using both approach 1 and 2 in handling the boundary conditions of further years. This situation resembles the partial or null effect of chlorination on plankton in effluents. This has been resolved by utilizing a feature in the EUTROP model that allows mirroring the plankton as well as other nutrients of the nearby ambient water into the introduced effluent.

Q-Base Scenario Using Approach 1

In order to investigate the new setup, the model is run over a period of three years. Figure 6.23 shows the model results. Figure 6.23 and Figure 6.18 are compared. It is noticed that there is no difference between the two figures for all the compartments including the plankton ones. This can be attributed to the low plankton biomass reported in the ambient water in association with small effluent discharges that have overall small impact on the water quality.

20Q-All Scenario Using Approach 1

The model is also run over the period of 3 years and the results are plotted in Figure 6.24. Comparison between Figure 6.24 and Figure 6.20 shows that all the compartments have the same trends and values except phytoplankton and zooplankton, as they more increase to levels close to their original values corresponding to the Q-Base scenario. This indicates that the preserved levels of biological loads in the effluent loads does the dilution action repeated in case of zero plankton and therefore the drop of phytoplankton and zooplankton reported before does no longer happen in this case.

Q-Base Scenario Using Approach 2

In the base scenario, all the compartments remain at their trends and levels for all the years, as shown in Figure 6.25. They are exactly similar to Figure 6.21. Phytoplankton and zooplankton do not change, because the concentration of the effluent is equivalent to the concentration of the discharging area, so the final concentration of the area does not change.

20Q-All Scenario Using Approach 2

Figure 6.26 shows the results of the compartments for the expansion conditions. Comparing Figure 6.26 and Figure 6.22 shows that all the compartments have similar trends and values except the phytoplankton and zooplankton at station 1. Where, their values in Figure 6.22 are lower than their values in Figure 6.26. The phytoplankton and zooplankton concentrations in the current approach resumes to their concentrations in the base condition. Again the non zero levels of phytoplankton and zooplankton in the effluent loads explain that as before.

Figure 6.23: Compartment values for the base scenario (Q-Base) using approach 1 to create the boundary conditions and non-zero plankton in effluent loads. The results are at the three observation stations (St.1, St.2, and St.3).
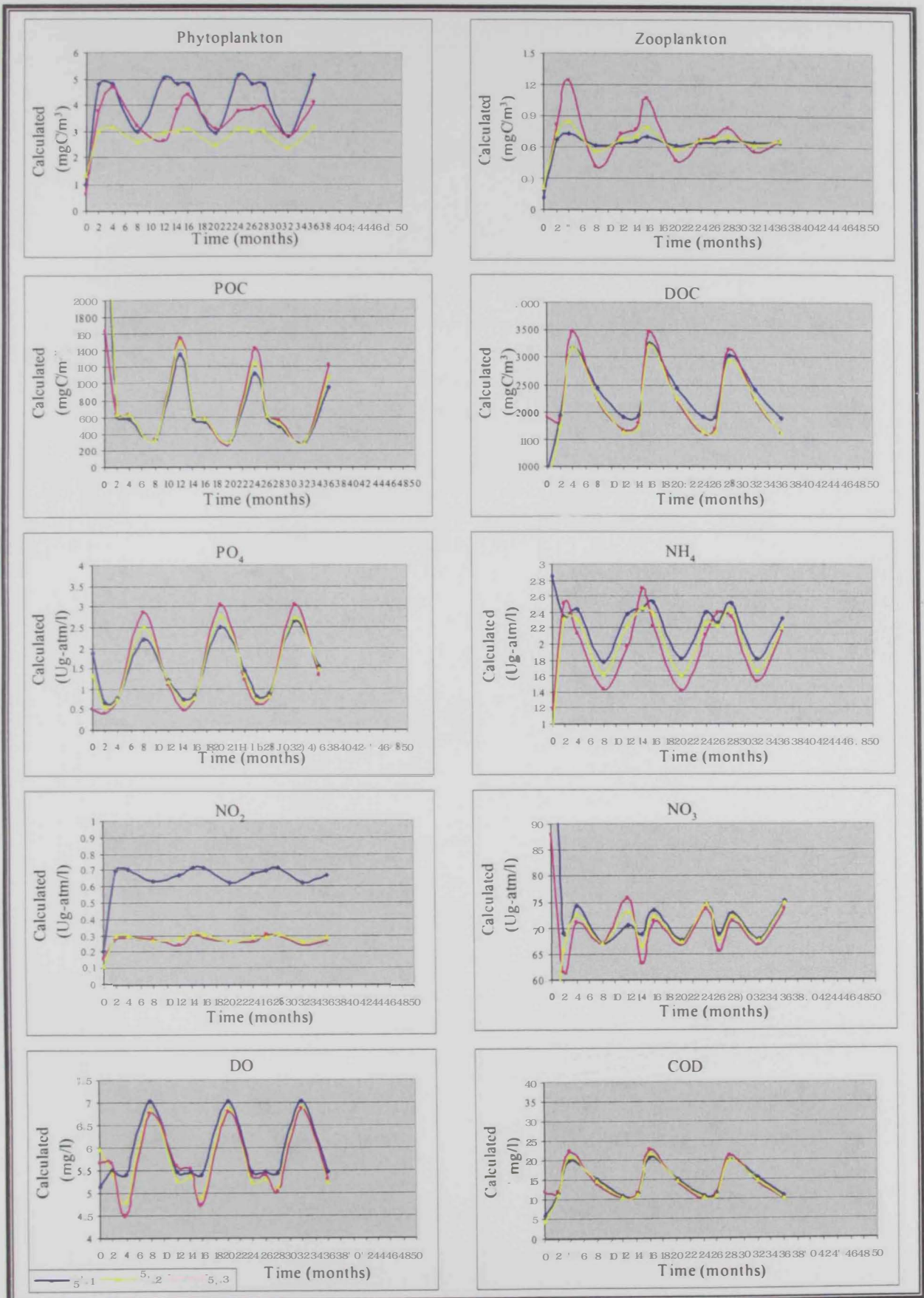
Figure 6.23: Compartment values for the base scenario (Q-Base) using approach 1 to create the boundary conditions and non-zero plankton in effluent loads. The results are at the three observation stations (St.1, St.2, and St.3).
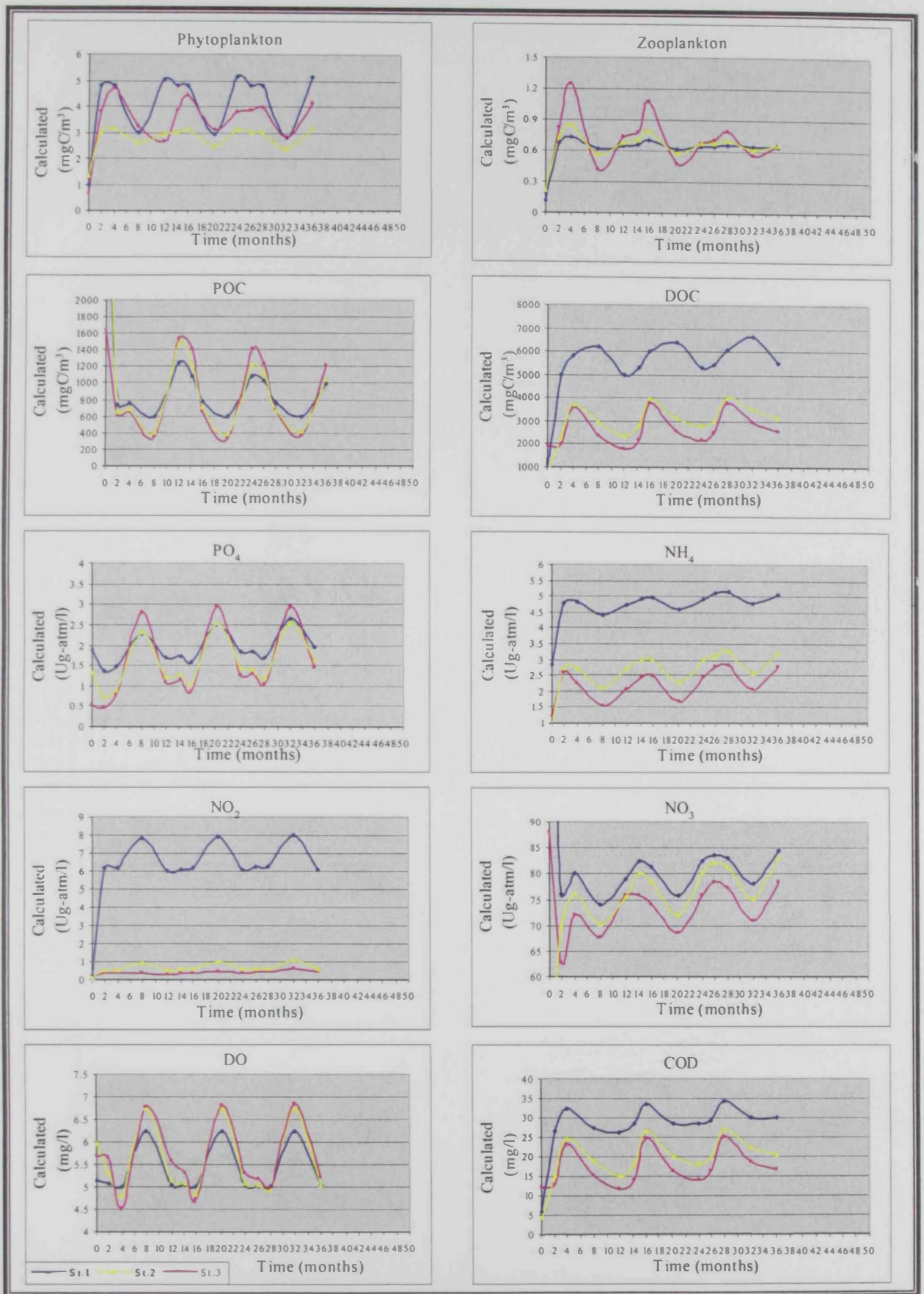
Figure 6.24: Compartment values for the expansion scenario (20Q-All) using approach 1 to create the boundary conditions and non-zero plankton in effluent loads. The results are at the three observation stations (St.1, St.2, and St.3).

Figure 6.25: Compartment values for the base scenario (Q-Base) using approach 2 to create the boundary conditions and non-zero plankton in effluent loads. The results are at the three observation stations (St.1, St.2, and St.3).
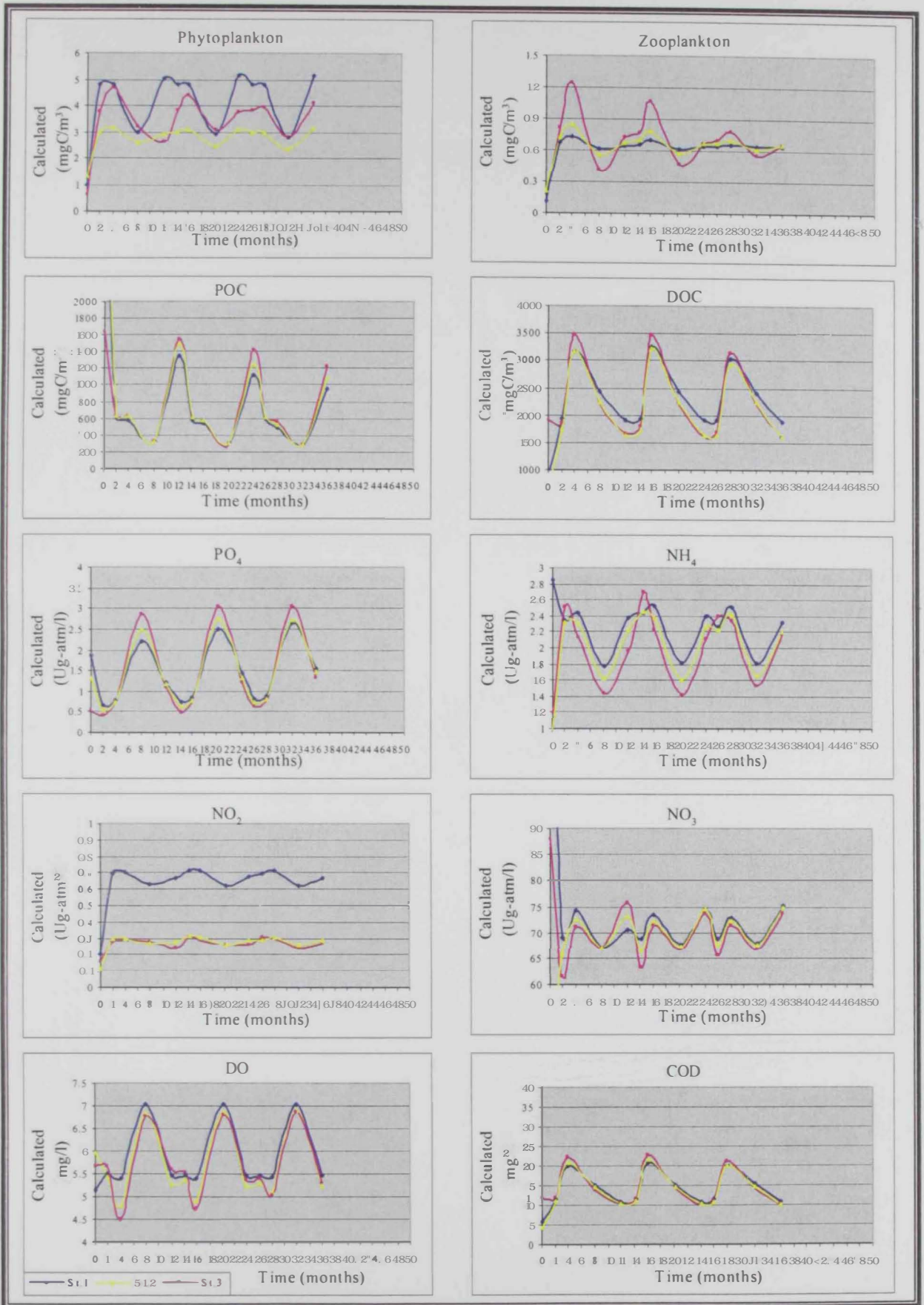
Figure 6.26: Compartment values for the expansion scenario (20-All) using approach 2 to create the boundary conditions and non-zero plankton in effluent loads. The results are at the three observation stations (St.1, St.2, and St.3).
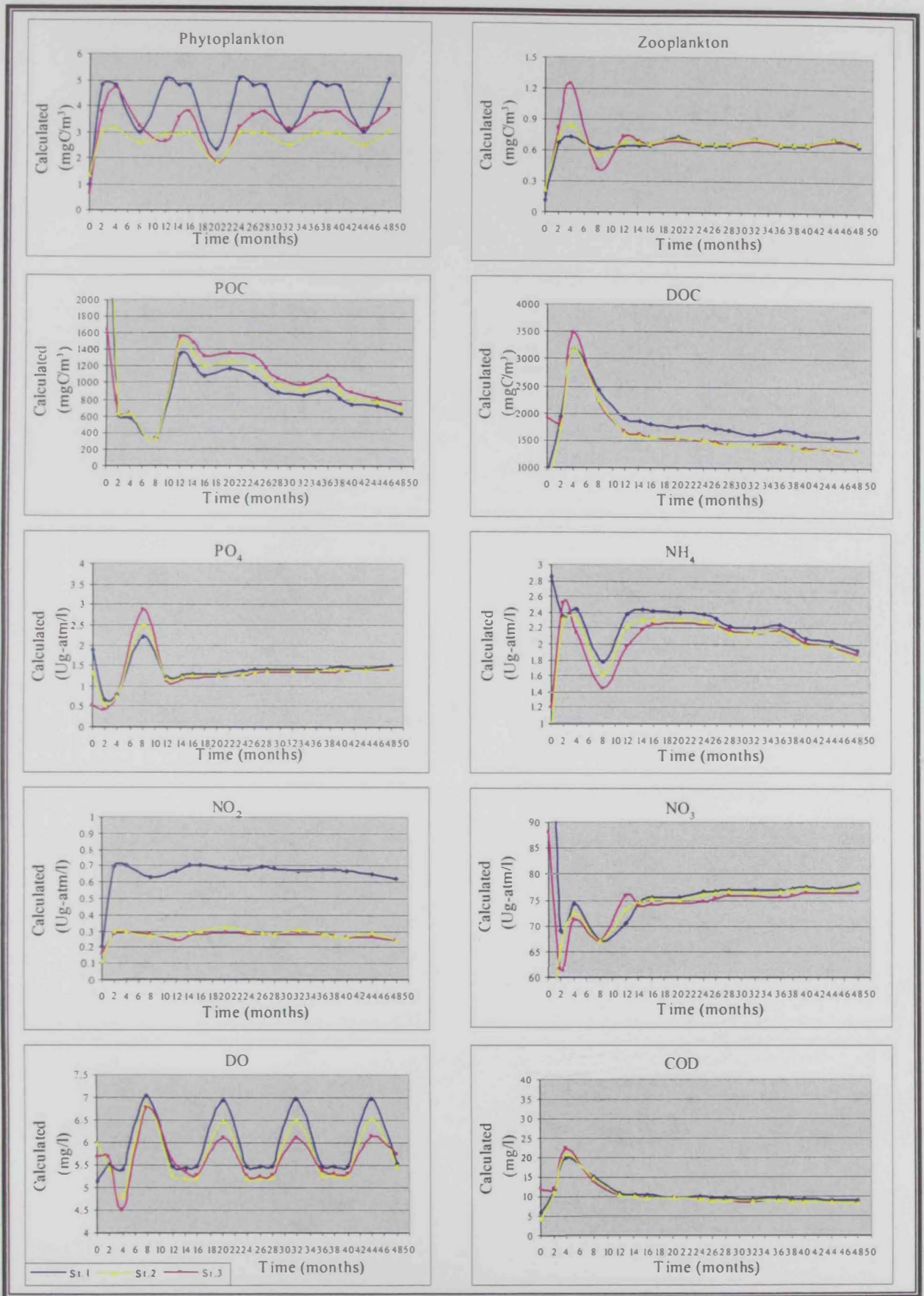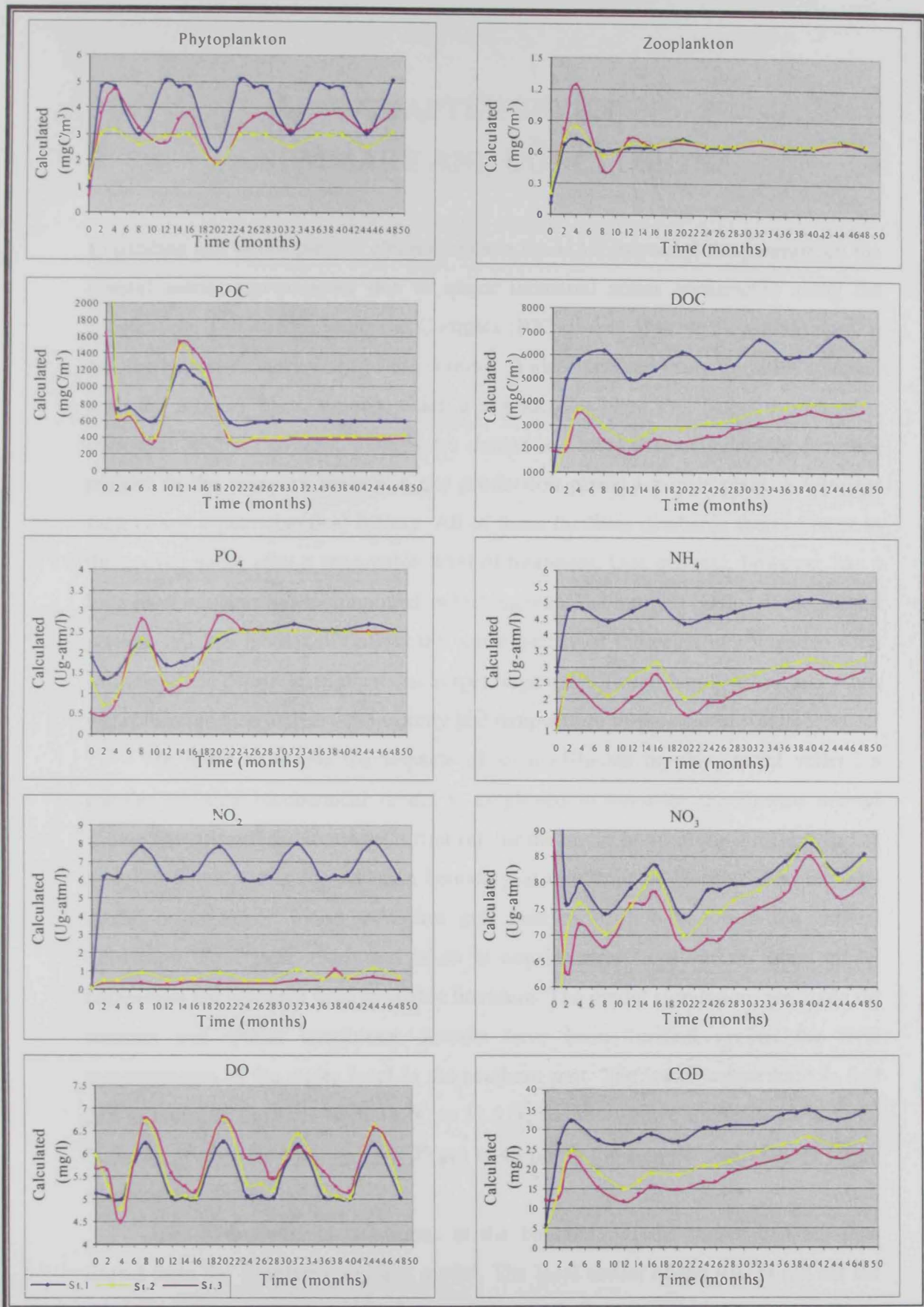
CHAPTER SEVEN
SUMMARY AND CONCLUSION

Expanding and developing of communities in the UAE increased the pressure on the coastal marine environment due to major industrial zones constructed along the coastal line. The Ruwais Industrial Complex (RIC) is one of these industrial zones. It has the largest refinery plant in the country. It also includes many facilities attached with the refinery plant, among which a desalination plant that caters to domestic, industrial, and agricultural fresh water demands. Other coastal industrial facilities present in the complex include a gas production plant, a power plant, a fertilizer factory and a petrochemical factory. All of these facilities discharge their effluent in the coastal water after a reasonable level of treatment. One effluent, however, has a high level of nitrogenous compounds which increase the nutrient budget of the coastal waters, and may potentially affect the water quality of the coast in a negative way. Moreover, the desalination plant discharges large quantities of highly saline and warm water that can also increase the salinity and temperature of the coastal waters.

In order to assess the impacts of such effluents on the coastal waters, a coupled physical-biochemical model is employed to simulate the Ruwais coastal water. The hydrodynamic model is first run for the entire basin of the Arabian Gulf as a regional model that has an open boundary at the Strait of Hormuz. The regional model is developed based on 5 km grid interval, with 6 layers in the vertical dimension. Four main rivers are taken in consideration, and various other model parameters are gathered from available literature. The model simulations are made for summer and winter conditions. Results have been verified against the field measurements of the water level in the southern part. The water temperature in that part is found to fluctuate from 31 °C to 32.5 °C in the summer and from 20 °C to 23 °C in the winter; the salinity from 39 ppt to 46 ppt in the summer and from 41 ppt to 46 ppt in the winter.

The hydrodynamic conditions at the boundary of the target area are then nested from the simulated regional model. The local model of the RIC is run for the whole year taking into consideration the effluents discharging from different facilities existing in the area. It is found that the water dynamics near the shore line are close to stagnant conditions as the mean currents rarely exceed 3 cm/s. The salinity in the

7-1

summer varies from 44.5 to 46.3 ppt and decreases offshore, whereas in winter it varies from 43.0 to 45.3 ppt and also decreases offshore. On the other hand, it is found that the water temperature has a wide variation between the summer and winter, varying in the summer from 31.5 °C to 33.4 °C, and in the winter from 21 to 22 °C. The basin thus has about 12 °C difference between the summer and winter water temperature and about 1.25 ppt difference in the salinity.

In terms of ecological characterization, the Ruwais marine water has been classified as HNLC (high nutrients and low chlorophyll/carbon) due to availability of nutrients and lack of biological production in the lower trophic level. That has been attributed to harsh environment conditions such as high temperature and salinity, in addition to the possible damaging effect of major chlorine spiking practiced at all facilities' intakes that potentially kill the marine biota to prevent them from entering the desalination plant and other facilities. The high potential for pollution in the area due to the oil related activities and accidental spills may also affect the zooplankton biomass in an adverse way.

The water quality model parameters have been reasonably calibrated for summer and winter conditions based on the field observed date.

Three scenarios (Q-Base, 20Q-Desal., and 20Q-All) are considered to represent the present and future loading conditions and to investigate their effects on the temperature and salinity of the Ruwais water. It is concluded that the expansion of the desalination plant only has no tangible effect upon the temperature of the whole area while the salinity is found to moderately increase (about 1.2 ppt) within a distance of about 4 km from the desalination plant. Expanding all the facilities (20Q-All scenario) produced larger effects on the temperature and salinity as the influence extends up to 10 km offshore. The temperature in the vicinity of the outfall increases of about 2.29 °C in summer and 3.18 °C in winter from the base scenario condition, while the salinity increases with 2.19 ppt in summer and 2.56 ppt in winter.

Since the scenario of future expansion in the desalination plant (20Q-Desal.) reflects tangible effects of salinity only while the salinity effects is not considered by the EUTROP model in different biochemical reactions, this scenario has been excluded from the long term water quality analysis. Hence, the long term simulation is conducted only for two scenarios; Q-Base and 20Q-All. Two approaches are conducted under each scenario. These approaches handle the boundary conditions for future years other than the first year, in different methods. The first method utilizes

the previous years observed data and therefore produce linearly interpolated B.C. over the simulated period. The second approach eliminates the effect of the previous records by considering constant B.C. over the simulated period.

Long term simulation is done over 3 to 4 years. It is noticed that the phytoplankton and zooplankton biomass decreases during the expansion scenario at station 1 by about 25% and 43%, respectively. This has been attributed to dilution effect that takes place in connection with disposing zero biological loads from the different facilities in the area. Zero loads of plankton represent the extreme condition of complete death of plankton due to the practice of disinfection at the influent waters. Taking these biological loads into consideration, it is noticed that the previous drop of phytoplankton and zooplankton biomasses is no longer reproduced in this case. Increasing trends are noticed for DOC, PO_4, NH_4, NO_2, NO_3, and COD due to expanding conditions; whereas, the other compartments (POC, DO) almost remain the same as in the original ranges.

In summary, extreme amplification of effluents discharged from other coastal facilities in the RIC only causes a moderate increase in the modeled temperature and salinity in the discharging area within a distance of 10 km from the shoreline. The water quality of the entire area and in particular near Sir Bani Yas Island does not experience major changes for the investigated expansion scenarios.

REFERENCES

1. Abdel-Moati A.R., 1990. Particulate organic matter in the subsurface chlorophyll maximum layer of the Southeastern Mediterranean Oceanological Acta. **13**: 307-315.

2. Abu-Hilal, A.H., Adam A., 1995. Sources, levels and distribution of nutrients and other pollution indicators in Dubai and Abu Dhabi Creeks and near shore waters (United Arab Emirates). J. Fac. Sci. U.A.E. Univ. **7(4)**: 56- 79.

3. Admiralty Tide Table (ATT), 2001.**Vol-3**, Hydrographer of the Navy, United Kingdom.

4. Ahmad, F., Sultan, S.A.R., 1991. Annual mean surface heat fluxes in the Arabian Gulf and the net heat transport through the Strait of Hormuz. Atmosphere Ocean. **29**: 54- 61.

5. Ahmad, M., Shayya, W.H., Hoey, D., Al-Handaly, J., 2001. Brine Disposal from Reverse Osmoses Desalination Plants in Oman and the United Arab Emirates. Desalination. **133**: 135- 147.

6. Aksnes, D.L. et al., 1995. Ecological modeling in coastal waters: towards predictive physical-chemical-biological simulation models. Ophelia. **41**: 5- 35.

7. Al-Hajri, K.R., 1990. The circulation of the Arabian (Persian) Gulf: A modeling study of its dynamics. Ph. Dissertation, 218, Catholic University of Am., Washington, D. C.

8. Allen, J.I. et al., 2001. A highly spatially resolved ecosystem model for the North West European Continental Shelf. Sarsia. **86**: 423- 440.

9. Altayran, A.M., Madany, I.M., 1992. Water Resources. **26**: 435.

10. Altman T., 2000. New Power and Water Co-generation Concept with Application of Reverse Osmosis (RO) Desalination, Salzgitter Anlagenbau GmbH.

11. Al-Weshah, R., 2002. The role of UNESCO in sustainable water resources management in the Arab World. Desalination. **152**: 1- 13.

12. Al-Yamani, F.Y., bishop, J., Al-Rifaei, K., Ismail, W., Al-Yaqout, A., Al-Omran, L., Kwarteng, A., Al-Ghadban, A., Sheppard C., 1997a. Assessment of effects of the Shatt al-Arab's altered discharge regimes on the ecology of the Northern Arabian Gulf. Final Report, Kuwait Institute of Scientific Research, Report No. KSIR 5174, Kuwait.

13. Al-Yamani, F.Y., Durvasula., R, Ismail, W., Al-Rifaei, K., Al-Saeed, T., Al-Yaqout, A., Al-Omran, L., 1997b. Oceanography of the Northwestern Waters of the Arabian Gulf: Ecological Significance of the Marine Food Web. Final Report, Kuwait Institute of Scientific Research, Report No. KSIR 5173 Kuwait.

14. ASCAD, 1997. Water resources and their uses in the Arab World. 2nd Symp. on Water Resources and Uses in the Arab World, Kuwait, 8- 1 0 March 1997.

15. Awerbuch, L. 1997. Dual Purpose Power Desalination/Hybrid Systems/Energy and Economics. IDA Desalination Seminar, Cairo, Egypt, September.

16. Azzam, M.H., Elshorbagy, W., Nakata K., 2004. Three Dimensional Modeling of the Ruwais Coastal Area of United Arab Emirates. Submitted to ASCE Journal of Waterway, Coastal and Ocean Engineering.

17. Banat, I.M, Hassan, E.S, Abu-Hilal, A.H, Adam, A.B, 1993. Microbial and nutrient pollution assessment of coastal and creek waters of northern U.A.E. Environment International. **19**: 569- 578.

18. Baretta, J.W., Ebenhoh, W., Ruardij, P., 1995. The European Regional Seas Ecosystem Model (ERSEM), a complex marine ecosystem model. Netherlands Journal of Sea Research. **33(3/4)**: 233- 246.

19. Baretta-Bekker, J.G., Baretta, J.W., Ebenhoh, W., 1997. Microbial dynamics in the marine ecosystem model ERSEM-II with decoupled carbon assimilation and nutrient uptake. Journal of Sea Research. **38**, 195- 211.

20. Basson, P. W., Burchard, J. E., Hardy, J. T., Price, A. G., 1977. Biotops of the western Arabian Gulf: Marine Life and Environments of Saudi Arabia. Aramco Ltd, Dhahran.

21. Blackford, J. C., 1997. An analysis of benthic biological dynamics in a North Sea ecosystem model. Journal of Sea Research. **38**, 213- 230.

22. Blain, C. A., 1998. Barotropic tidal and residual circulation in the Arabian Gulf, in Estuarine and Coastal Modeling. Proceedings of the 5th International Conference, M. L. Spaulding and A. F. Blumberg, eds., American Society of Civil Engineers, 166-180.

23. Blain, C.A., Preller, R.H., Rivera A.P., 2002. Tidal Prediction Using the Advanced Circulation Model (ADCIRC) and a relocatable PC-Based System. Oceanography. **15(1)**: 77- 87.

24. Brewer, P.G., Fleer A.P., Kadar S., Shafer D., Smith C.L., 1978. Chemical oceano-graphic data from the Persian Gulf and Gulf of Oman. WHOI Report No. 78- 37.

25. Britannica.com, 2001. The Tigris-Euphrates system. Online reference service.

26. Broekhuizen, N., Heath, M.R., Hay, S.J., Gurney, W.S.C., 1995. Modeling the dynamics of the North Sea's mesozooplankton. Netherlands Journal of Sea Research. **33(3-4)**: 381- 406.

27. CENSIS user guide, 2004. Chuden CTI, Japan.

28. Chao, T.W., Kao, Al-Hajri, K.R., 1992. A numerical investigation of circulation in the Arabian Gulf. Journal of Geophysical Research. **97**, 11219- 11236.

29. Cushing, D. H. 1958. Rapp. P-v Reun. Cons. Perm. Int. Explorer Mer. **144**: 32- 33

30. Dawes, C.J., 1998. Marine Botany. John Wiley & Sons.

31. Del Bane, J.V., Jirka, G., Largier, J., 1994. Ocean brine disposal. Desalination. **97**: 365- 372.

32. Dubai Municipality, 1996. Biological Characteristics of Dubai Marine Environment. EPSS, Dubai Municipality, 30 pp.

33. Ebenhoh, W., Baretta-Bekker, J.G., Baretta, J.W., 1997. The primary production module in the marine ecosystem model ERSEM-II, with emphasis on the light forcing. Journal of Sea Research. **38**, 173- 193.

34. Einav R., Hamssib K., Periyb D., 2002. The footprint of the desalination processes on the environment. Desalination. **152**: 141- 154.

35. Einav R., Lokiecb F., 2003. Environmental aspects of a desalination plant in Ashkelon. Desalination. **156**: 79- 85.

36. Elshorbagy, W., Azzam, M.H., Taguchi K., 2004a. Hydrodynamic characterization and modeling of the Arabian Gulf. Submitted to ASCE, Journal of Waterway, port, coastal and Ocean Engineering.

37. Elshorbagy, W., Azzam, M.H., Taguchi, K., Ichikawa, T., Terasawa, T., 2004b. Numerical simulation of the lower trophic level of Ruwais Coastal Industrial Area in the United Arab Emirates. Submitted to ASCE, Journal of Environmental Engineering.

38. Elshorbagy, W., Azzam M.H., Nakata K., 2004c. Temperature-salinity field of the shallow shelf of the western Arabian Gulf. Submitted to Continental Shelf Journal, Elsevier Science.

39. Elshorbagy, W., Azzam, M., Ichikawa T., 2004d. Temperature-Salinity Modeling for Ruwais Coast, UAE. Submitted to ASCE, Journal of Waterway, port, coastal and Ocean Engineering.

40. Elshorbagy, W., Mustafa, S., Azzam, M., Taguchi T., AlNahhal, S., 2004e. Ecological characterization of an industrial coastal basin in the UAE. Submitted to Elsevier, Journal of Water Resources.

41. Emara, H. I., 1998. Total organic carbon content in the waters of the Arabian Gulf. Environmental International. 24: 97- 103.

42. Emery, K.O., 1956. Sediments and water of Persian Gulf. Bull. Amer. Ass. Petrol. Geol. 40(10): 2354- 2383.

43. Emery, K.O., 1956. Sediments and water of the Persian Gulf, Bull. Amer. Assoc. Petrol. Geol. 40: 2354- 2383.

44. ESCWA, 1993.Water desalination: the experience of GCC countries, in: Regional symposium on water use and conservation. Report E/ESCWAINR/1993/ WG.1AVP.10, Amman.

45. ESCWA, 1999. Management of groundwater resources in ESCWA member states. Expert Group Meeting on Updating of Assessment of Water Resources in the ESCWA Member States, Beirut, Lebanon, 20-30 April 1999.

46. Estrada, M., 1985. Deep phytoplankton and chlorophyll maxima in the western Mediterranean. V. (eds.) Mediterranean marine ecosystems. Plenum Press, New York. 247- 277.

47. Galt, J.A., 1983. Trajectory analysis and simulation of oil spill movement in oceanographic modeling of the Kuwait Action Plan (KAP) Region (El-Sabh, M.I., ed.), 46- 54. UNISCO reports in Marine Science, 28. Paris.

48. Galt, J.A., Payton, D.L., Torgrimson, G.M., Watabayashi, G., 1983. Applications of Trajectory Analysis for the Nowruz oil spill. In Oceonographic Modeling of the Kuwait Action Plan (KAP) Region (El-Sabh, M.I., ed.), 55- 66. UNISCO reports in Marine Science, 28. Paris.

49. Hamza, W., Ennet, P., Tamsula, R. 2004. Simulation of the Egyptian coastal ecosystem functions. Marine Engineering. **157**: 23- 33.

50. Hastenrath, S., Lamb, P. J., 1979. Climatic Atlas of the Indian Ocean. Part II: The oceanic heat budget. The Univ. Wisconsin Press, 93 pp.

51. Hoepner T., 1999. A procedure for environmental impact assessments (EIA) for seawater desalination plants. Desalination. **124**, 1- 12.

52. Hoepner, T., Windelberg, J., 1996. Elements of environmental impact studies on coastal desalination plant. Desalination. **108**: 11- 18.

53. Horton, C., Clifford, M., Cole, D., Schmitz, J., Kantha, L., 1992. Operational modeling semi enclosed basin modeling at the Naval Oceanographic Office. Oceanography. **5(1)**: 69- 72.

54. Hughes, P., Hunter, J.R., 1979. Physical oceanography and numerical modeling of the Kuwait action plan region, Report MARINE, 278, UNESCO Division of Marine Sciences, 106 pp.

55. Hunter, J.R., 1983. Aspects of the hydrodynamics of the residual circulation of the Arabian Gulf. Coastal Oceanography. Plenum Press, 31- 42.

56. Ikushima, I., 1967. Ecological studies on the productivity of aquatic plant communities. Bot. Mag., Tokyo. **180**. 57- 67.

57. Johns, W.E. and D.B. Olson, 1998. Observation of seasonal exchange through the Strait of Hormuz, Oceanography. **11 (2)**: 58.

58. Ivlev V.S., 1945. The biological productivity of waters. Uspekhi Sovrem. Biol. **19**: 98- 120.

59. Khouri, I., 2002. Sustainable development and management of water resources in the Arab region. International conf. on water resources and integrated management in the third millennium, Dubai, UAE, 2-6 Feb. 2002.

60. Kimor B., Berman T., Schneller A., 1987. Phytoplankton assemblages in the deep chlorophyll maximum layers off the Mediterranean coast of Israel. J. Plankton Res. **9 (3)**: 433- 443.

61. King, G.R.D., 1998. Abu Dhabi Islands Archaeological Survey. Trident Press Ltd. 11- 12.

62. Lardner, R.W., Al-Rabeh, A.H., Gunay, N., Hossani, M., Reynolds, R.M., Lehr, W.J., 1993. Computation of the residual flow in the Gulf using the Mt Mitchell Data and KFUPM/RI Hydrodynamical models. Mar. Pollut. Bull. **27**: 61- 70.

63. Lardner, R.W., Belen, M.S. Cekirge, H.M., 1982. Finite difference model for tidal flows in the Arabian Gulf. Comp. and Math. with Appls. **8(6)**: 425- 444.

64. Lardner, R.W., Das, S.K., 1991. On the computation of flows driven by density gradient: Residual currents in the Arabian Gulf. App. Math. Modeling. **15**: 282- 294.

65. Lardner, R.W., Fraga, R.J., Lehr, W.J., Sarhan, M.A., 1988b. Residual circulation of the Arabian Gulf. II: Wind-driven flow. The Arabian Journal for Science and Engineering. **13(3)**: 411- 423.

66. Lardner, R.W., Lehr, W.J., Fraga, R.J., Sarhan, M.A., 1987. Residual circulation of the Arabian Gulf. I: Density-driven flow. The Arabian Journal for Science and Engineering. **12(3)**: 341- 354.

67. Lenhart, H..J., 1999. Eutrophierung im kontinentalen Kustenbereich der Nordsee, Reduktionsszenarien der Flubeintrage von Nahrstoffen mit dem kosystem-Modell ERSEM. Berichte aus dem Zentrum fur Meeres und Klimaforschung. Reihe B: Ozeanographie. **35**: 169.

68. Levinton, J.S., 1995. Marine Biology. Oxford University Press.

69. Maier-Reimer, E., Bacastow, R., 1990. Modelling of geochemical tracers in the ocean. In M. E. Schlesinger (Ed.), Climate-ocean interaction. Nederland: Kluwer Academic Publishers. 233- 267.

70. Meshal, A.H., Hassan, H.M., 1986. Evaporation from the coastal waters of the central part of the Gulf. Arab J. Sci. Res. **4(2)**: 649- 655.

71. Michel, H. B., Behbehani, M., Herring, D., Arar, M., Shoushani, M., Brakoniecki, T., 1986. Zooplankton diversity, distribution and abundance in Kuwait waters. Kuwait Bull. Mar. Sci. **8**: 37- 105.

72. Moll, A., 1995. Regionale Differenzierung der Primarproduktion in der Nordsee: Untersuchungen mit einem drei-dimensionalen Modell. Berichte aus dem Zentrum fur Meeres- und Klimaforschung. Reihe B: Ozeanographie. **19**: 151.

73. Moll, A., 2000. Assessment of three-dimensional physical-biological ECOHAM1 simulations by quantified validation for the North Sea with ICES and ERSEM data. Journal of Marine Sciences. **57(4)**: 1060- 1068.

74. Moll, A., Radach G., 2003. Review of three-dimensional ecological modeling related to the North Sea shelf system, Part 1: models and their results. Progress in Oceanography. **57**: 175- 217.

75. Morton, A.J., Callister, I.K., Wade, N.M., 1996. Environmental impacts of seawater distillation and reverse osmosis processes. Desalination. **108**: 1- 10.

76. Murty, T.S., El-Sabh, M.I., 1984. Storm tracks, storm surges, and sea state in the Arabian Gulf, Strait of Hormuz, and the Gulf of Oman. In: El-Sabh (Ed.), Oceanographic Modeling of the Kuwaiti Action (KAP) Region, 12-24. University of Petroleum and Minerals, UNESCO, Paris.

77. Mustafa, S., 1995. Ecology of plankton from Saltpans along the coastal Environment of Bombay, University of Bombay.

78. Nakata, K., Kishi, M., Taguchi, K., 1983. Eutrophication model in coastal bay estuary. Dev. Ecol. and Env. Quality. **2**: 357- 366.

79. Nakata, K., Taguchi, K., 1982. Numerical simulation of eutrophication process in coastal bay by eco-hydrodynamic model; 2nd Ecological modeling. Bull. Nat. Res. Inst. of Pollution and Resources. **12(3)**: 17- 36.

80. Nakata, K., Taguchi, K., Setoguchi, Y., 1985. Three-dimensional eco-hydrodynamic model for eutrophication process in the coastal bay. Proc. Int. Conference of modeling and simulation, 55- 59 pp.

81. NASA 1989. Goddard Earth Sciences Distributed Active Archive Center. http://www.geoinfo. amu.edu.pl/wpk/ocean/oss_126a.html

82. NOAA/EPA 1988. Strategic Assessment of Near Coastal Waters. Chapter 3, Susceptibility and Concentration Status of Northeast Estuaries to Nutrient Discharges.

83. Patsch, J., Radach, G., 1997. Long-term simulation of the eutrophication of the North Sea: Temporal development of nutrients, chlorophyll and primary production in comparison to observations. Journal of Sea Research. **38**: 275- 310.

84. Parsons, T.R, LeBrasseur, Fulton, J.D., 1967. Some observations on the dependence of zooplankton grazing on the cell size and concentration of phytoplankton blooms. J. Oceanogr. Soc., Japan. **23**: 10- 17.

85. Perrone, T.J., 1979. Winter shamal in the Persian Gulf, Naval Env. Prediction Res. Facility, Tech. Rept. 79- 06, Montery, 180.

86. Price, A.R.G, Sheppard, C.R.C., Roberts, C.M., 1993. The Gulf: Its biological setting. Mar. Pollut. Bull. **24**: 9- 15.

87. Privett, D.W., 1959. Monthly charts of evaporation from Indian Ocean (including the Red Sea and the Persian Gulf), Quarterly. Journal of Royal Metrological Society. **85**: 424- 428.

88. Proctor, R., Flather, R.A., Elliott, A.J., 1994. Modeling tides and surface drift in the Arabian Gulf: application to the Gulf oil spill. Continental Shelf Research. **14**: 531- 545

89. Radach, G., Pa¨tsch, J., 1997. Climatological annual cycles of nutrients and chlorophyll in the North Sea. Journal of Sea Research. **38**: 231- 248.

90. Raymont, J, E., 1983. Plankton and Productivity of the Ocean. Elsevier Science Ltd.

91. Reynolds, M.R. 1993. Physical Oceanography of the Gulf, Strait of Hormuz, and Gulf of Oman. Results from the Mt Mitchell Expedition. Marine Pollution Bulletin. **27**: 35- 39.

92. ROPME, 1999. Regional report of the state of the marine environment. Regional Organization for Protection of the Marine Environment. Kuwait. ROPME/GC-9/002.

93. Ross, D.A., Stoffers, P., 1978. Report C: General data on bottom sediments including concentration of various elements and hydrocarbons in the Persian Gulf and Gulf of Oman. Technical Report to National Science Foundation. Unpublished Manuscript. Woods Hole Oceanographic Institution, Woods Hole, Massachusetts.

94. RSMAS, 2000. Arabian Marginal Seas and Gulf. Technical Report, Rosenstiel School of Marine and Atmospheric Science, Miami.

95. Schott, G., 1918. Oceanographic and Klimatologie des Persischen Golfes und des Golfes von Oman, Ann. Hydrogr. Mar. Meteorol. **46**: 1- 46.

96. Semiat R., 2000. Desalination: Present and Future. Water International. **25 (1)**: 54- 65.

97. Shankar, N.J., Cheong, H.F., Chan, C.T., 1997. Boundary fitted grid models for tidal motions in Singapore coastal waters. Journal of Hydraulic Research. **35(1)**: 3- 19.

98. Sheppard C., Price A., Roberts C., 1992. Marine Ecology of the Arabian Region: Patterns and Processes in Extreme tropical environments. Academic press London.

99. Sheppard, C., 1993. Coral reef environmental science. Reef Encounter. **14**: 12- 13.

100. Sheppard, C.R.C., 1993. Physical environment of the Gulf relevant to marine pollution: an overview. Mar. Pollut. Bull. **27**: 3- 8.

101. Shriadah, M. and Al-Ghais, S., 1999. Environmental Characteristics of the United Arab Emirates water along the Arabian Gulf. Hydrographic survey and Nutrients slate. Indian Journals of Marine Science. **28**: 225- 232.

102. Skogen, M.D., 1993. A user's guide to NORWECOM: The NORWegian ECOlogical Model system. Technical Report of the Institute of Marine Research. 6: 1- 23.

103. Skogen, M.D., Aure, J., Danielssen, D., Svendsen, E., 1998. Natural fertilisation of the marine environment—modelling of the Glomma Flood 1995. Sarsia, 83: 361- 372.

104. Skogen, M.D., Eriksrod, G., Svendsen, E., 1997. Quantification of transports to Skagerrak. In E. zsoy, & A. Mikaelyan (Eds.), Sensitivity to change: Black Sea, Baltic Sea, North Sea. Amsterdam: Kluwer Academic Publishers. 327- 339.

105. Skogen, M.D., Svendsen, E., Berntsen, J., Aksnes, D.L., Ulvestad, K.B., 1995. Modeling the primary production in the North Sea using a coupled three-dimensional physical-chemical-biological ocean model. Estuarine, Coastal and Shelf Science. 41: 545- 565.

106. Sommariva, C., Syambabu, V.S.N., 2001. Increase in water production in UAE. Desalination. 138: 173- 179.

107. Sonu, C.J., 1979. Oceanographic study in the Strait of Hormuz and over the Iranian shelf in the Persian Gulf. Final report, contract N00014-76-C-0720, TC 3675, U.S. Off. Of Naval Res., Washington D.C.

108. Starikova, N. D., 1970. Vertical distribution patterns of dissolved organic carbon in seawater and interstitial. Oceanography. 10: 796- 807.

109. Steele, J.H., Henderson, E.W., 1992. The role of predation in plankton models. Journal of Plankton Res., 14, 157- 172.

110. Steele, J.H., 1962. Environmental control of photosynthesis in the sea. Limnol. Oceanogr. 7: 137- 150.

111. Sugden, W., 1972. The hydrography of the Persian Gulf and its significance in respect to evaporative deposition, Am. J. Sci., **261**: 741- 755.

112. Taguchi, K., Nakata, K., 1998. Analysis of water quality in Lake Hamana using a coupled physical and biochemical model. Special Issue: Modeling hydrodynamically dominated marine ecosystems. J. Mar. Sys. **16**: 107- 132.

113. Taguchi, K., Nakata, K., Ichikawa, T., 1999. A 3-D simulation of the lower trophic ecosystem in the Ise-Mikawa Bay estuary using a coupled physical and biochemical model. J. Adv. Mar. Sci. Tech. Soci. **5(1)**: 49- 62.

114. Takreer.com, 2004. The Abu Dhabi Oil Refining Company, (TAKREER). Online reference service.

115. Tamsalu R., Ennet, P. Ecosystem modeling in the Gulf of Finland. II. The aquatic ecosystem model FINEST. Estuarine and Coastal Shelf Science. **41**: 429- 458.

116. U.S. Hydrographic office, 1960. Sailing directions for the Persian Gulf, HO Publ., Washington D.C. **62**: 158.

117. Uriarte, I., Villate, F., 2004. Effects of pollution on zooplankton abundance and distribution in two estuaries of the Basque coast (Bay of Biscay). Marine Pollution Bulletin. **49**: 220- 228.

118. Varela, R.A., Cruzado, A., Gabaldon, J.E., 1995. Modeling primary production in the North Sea using the European regional seas ecosystem model. Netherlands Journal of Sea Research. **33(3/4)**: 337- 361.

119. Vine, P., 1999. Sir Bani Yas. Trident Press Ltd. **9**: 13.

120. Watt, W.D., 1966. Release of dissolved organic material from the cells of phytoplankton populations. Proc. Roy. Soc., London. **164**: 521- 551.

121. Williams, P. J., 1975. LeB. Biological and chemical aspects of dissolved organic matter in seawater. In: Riley, J. P.; Shirrow, G. eds. Chemical oceanography. London: Academic press. **2**: 301- 363.

122. Winston, W.S., Sirkar K., 1992. Membrane Handbook.

123. Wroblewski, J.S., 1977. A model of phytoplankton plume formation during variable Oregon upwelling. J. Mar. Res. **135**: 357- 394.

124. Zevenboom, W. 1994. Assessment of Eutrophication and its effects in marine waters. Deutsche Hydrographische Zeitschrift. **1**: 141- 170.

125. Zhang, Q.Y., Gin, K.Y.H., 2000. Three-dimensional numerical simulation for tidal motion in Singapore's coastal waters. Coastal Engineering. **39**: 71- 92.

ملخص الأطروحة

يعتبر الماء أساس الحياة على كوكب الأرض حيث قال الله تعالى "وجعلنا من الماء كل شيء حي أفلا يؤمنون" (الأنبياء- آية 30). لذلك يعد الحفاظ على موارد المياه من الأولويات التي لابد للإنسان أن يوليها جل اهتمامه. وجديرٌ بالذكر أن منطقة الخليج العربي تعد من المناطق الجافة التي يندر سقوط الأمطار بها، كما أن معظم بلدان الخليج تعتبر فقيرة من حيث موارد المياه الطبيعية العذبة.

تعتبّر دولة الإمارات العربية المتحدة من الدول التي تعاني من شح الموارد المائية، حيث أنها تمتلك قدراً ضئيلاً من المياه الجوفية التي لا تكاد تكفي لسد رمق القطاع الزراعي، لذا كان من البديهي أن تتجه مثل هذه الدولة الغنية بموارد الطاقة الطبيعية إلى اللجوء لتحلية مياه البحر واستخدامها كبديل للحصول على المياه العذبة التي تحتاجها في شتى مرافق الحياة. فنجد أن محطات التحلية تنتشر على طول الساحل المطل على الخليج العربي للدولة.

تعنى هذه الأطروحة بدراسة تأثير مخلفات محطة التحلية المقامة على شاطئ منطقة الرويس – غربي العاصمة أبو ظبي – على جودة ونوعية المياه البحرية في تلك المنطقة، حيث تتميز المياه المنصرفة من محطة التحلية بارتفاع في درجة الحرارة وكذلك نسبة الملوحة. وجديرٌ بالذكر أن هناك عدة منشآتٍ أخرى مقامة أيضا في منطقة الرويس ملحقة بمصفاة تكرير البترول هناك. حيث ينتج من هذه المنشآت بعض المخلفات التي تصرف أيضا إلى الخليج، وتتميز بوجود مركبات نيتروجينية وفوسفورية والتي تمثّل العناصر الغذائية الأولية لكائنات البحر الدقيقة.

ولدراسة الآثار المترتبة على تصريف المياه العادمة من محطة التحلية والمنشآت الأخرى، تم الاستعانة ببيانات متعلقة بنوعية المياه في منطقة الرويس الساحلية لتستخدم كمدخلات لبرنامجين حاسوبيين وهما COSMOS لدراسة حركة الأمواج والمد والجزر بالمنطقة بالإضافة إلى تتبع درجات الحرارة والملوحة الناتجة عن المخلفات المنصرفة، والبرنامج الثاني EUTROP لدراسة مدى تأثير هذه المخلفات على جودة المياه في المنطقة آخذاً بعين الاعتبار عدة متغيرات كيميائية وبيولوجية. وقد تم استخدام كلا البرنامجين لدراسة عدة سيناريوهات مختلفة منها الوضع الحالي لهذه المخلفات المنصرفة وكذلك الوضع المستقبلي في حال توسعة مثل هذه المنشآت وبالتالي زيادة كمية المياه المنصرفة إلى الخليج.

وقد وجد من خلال استخدام النمذجة الحسابية أن المخلفات المنصرفة من محطة التحلية والمنشآت الأخرى ليس لها آثار جانبية واضحة المعالم في الوقت الراهن سوى ارتفاع طفيف في ملوحة ودرجة حرارة المياه بالقرب من نقاط التصريف حيث تتلاشى هذه الظاهرة تدريجيا وتختفي بشكل نهائي على بعد 4 كم من منطقة التصريف. بينما وجد أن تأثير الارتفاع في ملوحة وحرارة مياه الخليج نتيجة لتصريف هذه المياه في حال توسعة المنشآت المختلفة في المستقبل قد يمتد إلى حوالي 10 كم وبالتالي فإنه لن يشكل ضررا حقيقيا على الحياة البحرية في المنطقة.

عنوان الأطروحة:	تقييم تأثير مخلفات عمليات التحلية على نوعية المياه البحرية بمنطقة الرويس- تطبيق نمذجة حسابية
المؤلف:	سامر جـودة النحــال
المشرف الرئيسي:	د. وليد الشوربجي – أستاذ مشارك – قسم الهندسة المدنية والبيئية – جامعة الإمارات العربية المتحدة
المشرف المساعد:	د. وليد حمزة – أستاذ مشارك – رئيس قسم علــوم الحيـاة – جامعة الإمارات العربية المتحدة
لجنة المناقشة:	د. وليد الشوربجي – أستاذ مشارك – قسم الهندسة المدنية والبيئية – جامعة الإمارات العربية المتحدة – إ. ع. م.
	أ. د. فيجي بانشانج – أستاذ – قسم هندسة الأنظمة البحرية – جامعة تكساس – الولايات المتحدة الأمريكية
	أ. د. عبد الرزاق زكري – أستاذ – قسم الهندسة الكيميائية والبترول – جامعة الإمارات العربية المتحدة – إ. ع. م.

جامعــة الإمــارات العربيــة المتـحدة
عمـادة الـدراسـات العليــا

تقييم تأثير مخلفات عمليات التحلية على نوعية المياه البحرية بمنطقة الرويس - تطبيق نمذجة حسابية

أطروحة مقدمة من الطالب

ســـامر جـــودة النحـــال

بكالوريوس هندسة مدنية
جامعــة بيـرزيت (2001)

استكمالا لمتطلبات الحصول على درجة الماجستير في
علوم موارد المياه